REPUBLIC OF IRAQ
MINISTRY OF HIGHER
EDUCATION AND SCIENTIFIC RESEARCH
UNIVERSITY OF BABYLON
FACULTY OF ENGINEERING
DEPARTEMENT OF CIVIL ENGINEERING

Dynamic Response of Sustainable Rubberized Reinforced Concrete Continuous Deep Beams

A DISSERTATION

SUBMITTED TO THE FACULTY OF ENGINEERING, UNIVERCITY OF BABYLON IN PARTIAL FULFILLMENT OF THE REQUIREMENT FOR DEGREE OF DOCTOR PHILOSOPHY IN CIVIL ENGINEERING (STRUCTUAL ENGINEERING)

BY

OLA MAZEN MAKKI ALI

(B.SC. IN CIVIL ENGINEERING 2015)

(M.SC. IN STRUCTURAL ENGINEERING 2019)

Supervises by: Prof. Dr. Hayder M.K. Al-Mutairee

JULY 2023

صدق الله العلي العظيم

سورة النساء (113)

Supervisor's Certificate

We certify that the preparation for this thesis dissertation "**Dynamic Response of Sustainable Rubberized Reinforced Concrete Continuous Deep Beams**" was prepared by "Ola Mazen Makki" under our supervision at the University of Babylon, Faculty of Engineering, as a partial fulfillment of requirements for the degree of doctor philosophy in civil engineering (structural engineering).

Signature:

Name: Prof. Dr. Hayder M.K. Al-Mutairee

Date: / / 2023

I certify that this thesis mentioned above has been completed in Civil Engineering in the College of Engineering / University of Babylon

Signature:

Name: Prof.Dr. Thair J. Mizhir Alfatlawi

Date: / / 2023

Examining Committee's Certificate

We certify as an examining committee that we have read the dissertation entitled "**Dynamic Response of Sustainable Rubberized Reinforced Concrete Continuous Deep Beams**" and examining the student Ola Mazen Makki in its content and in what is related to it. Our opinion it meets the standards of the dissertation for the degree of doctor philosophy of science in civil engineering (Structural engineering).

Signature: **Name: Prof. Dr.** Haitham H. Muteb (Chairman) **Date: / / 2023**	**Signature:** **Name:Prof. Dr. Saad** Khalaf Mohoisen **Date: / / 2023**
Signature: **Name: Asst. Prof. Dr.** Najlaa H. Al-Shareef **Date: / / 2023**	**Signature:** **Name: Asst. Prof. Dr.** Majid M.A. Kadhim **Date: / / 2023**
Signature: **Name: Asst. Prof. Dr.** Hayder M.J.A. AL-Khafaji **Date: / / 2023**	**Signature:** **Name: Prof. Dr.** Hayder M.K. Al-Mutairee **(Supervisor and Member)** **Date: / / 2023**

Approved by the head master of civil engineering department

Signature:

Name: Prof. Dr. Thair J. Mizhir *(Head of Civil Engineering Department)*

Date: / / 2023

Approved by the Dean of engineering facility – University of Babylon

Signature:

Name: Prof. Dr. Laith Ali Abdul-Rahaim *(Dean of the College of Engineering)*

Date: / / 2023

Dedication

To whom who will fill the earth with justice and peace

To whom who will calm dawn the muss of this world

To whom who is the hope of the painful generations

To Al-Imam Al-MAHDI

To mom, PROF. Dr. Zainb Hassan Radhie who is my life's sun

To mom, who supports me to keep going till I reach this top

To dad, PROF. Dr. Mazen Makki Ali, my intelligent manager, director and clever brain

To my lovely husband, my patient supporter PROF.Dr. Mezher Hamid

To my brother, ASST.PROF. Dr. Hayder Mazen, my soul mate

To my little sister, M.Sc. Tabarak Mazen, who looks after me till making me feel I am the little sister

To my little brother, Yaqeen Mazen, my small dream

To every Iraqi blood drops by oppression

To every mom tears

I decide this work

ACKNOWLEDGEMENTS

In the name of Allah, the most Gracious, the most Merciful

First of all, the great thanks for my Lord Allah for all his favor, kind, guidance, and for giving me the ability to complete this work.

I introduce my heartiest gratitude, my great respect and thank to my supervisor Prof. Dr. Hayder M.K. Al-Mutairee whom my success could not be turned to reality without his help. I really have the honor and the pleasure to work under his guidance and supervision. I thank him for his continual encouragements, patience, comments and very valuable advice.

Sincere thanks are expressed to the faculty of Engineering of the University of Babylon, my thanks also for the Civil Department at Al-Qadisyah University (especially the head of the Department Dr. Alaa Mahdi) for giving the permission to use the whole laboratories freely, thanks for all their appreciable assistance. My great thanks and gratitude for Prof. Dr. Haider Kadhim Ammash for his devices, time, discussions and patient, as well as Dr. Haider Kammona. My great thanks for Asst. Prof. Dr. Mohammed Shammel Abo Dhaheer for his great construction material advices, interest and time. I am so thankful also for Dr. Harith Ammer for using his own wonderful data logger. Finally, thanks to myself for her ambition and huge patient.

Ola Mazen Makki

Concluded Articles from this dissertation

	Title	Journal	Index	State
1	Rubberized Concrete Mix – Discussions for Literature Review	Journal of Physics: Conference Series	SCOPUS Q4	Published at 3/6/2021
2	Survey the behavior of impacted shallow and deep beams	Journal of Engineering Science and Technology Review	SCOPUS Q3	Published at 21/3/2023
3	Continuous Deep Beams Behavior under Static Loads: A Review Study	earth and environmental researches: Conference Series	SCOPUS Q4	Published at 11/1/2022
4	Response of Rubcrete Continuous Deep Beams under Sinusoidal Loads	International Journal of Engineering, Transactions A: Basics	SCOPUS Q2 Thomson Reuters & Clarivate	Published at 29/3/2022
5	Experimental Investigation for Sustainable Rubberized Concrete Mixes	AIP Conference Proceedings	SCOPUS Q4	Acceptance letter since 9/9/2022
6	Mechanical and Dynamical Properties of Structural Rubcrete Mixes	International Journal of Engineering Transactions C: Aspects	SCOPUS Q3 Thomson Reuters, and Clarivate	Published at 18/6/2022
7	Rubcrete Continuous Deep Beams under Cyclic Loadings	Practice Periodical on Structural Design and Construction	SCOPUS Q2	Under review since 23/1/2023
8	Rubberized Continuous Deep Beams Subjected to Impact Loads	Journal of King Saud University - Engineering Sciences	SCOPUS Q1	Under review since 15/3/2023
9	Rubberized Continuous Deep Beams capacity under a High Velocity Impact Hit	International Journal of Impact Engineering	SCOPUS Q1	Under review since 10/3/2023
10	Impact Load Exposed on Rubcrete Continuous Deep Beams	International Journal of Engineering, Transactions A: Basics	SCOPUS Q2 Thomson Reuters & Clarivate	Under review since 22/6/2023
11	Experimental and Statistical Capacity of Rubberized Continuous Deep Beams under Repeated Load	IOP Conference Series: Earth and environmental	SCOPUS Q4	Acceptance letter at 19/1/2023

To view the published articles, please visit [Ola Mazen | ResearchGate]

Abstract

The behavior of rubberized Continuous deep beams (CDBs) under dynamic loads were investigated in this dissertation. It is an essential topic since the CDBs are highly exposed to dynamic loads and to increase the concrete's ductility by adding rubber. Especially the wastes of scraped tire rubber form a real environmental trouble and the engineers nowadays working on recycling the rubber in the constructions.

The volumetric replacement was corresponded to cast the beams. The adopted mix was of 10, 20, and 30% of the crumb was replaced by sand, as well as the same percentages for chip versus gravel. 21 continuous deep beams (CDBs) were casted and classified into three groups. The first group contains 7 beams tested under a monotonic load to discuss their ultimate strength. The second group consisting of 11 specimens tested using two dropping weight of 30 and 40 kg at single span only. This group have been retested after impact using static load. The last group of the experimental work considering by 3 beams tested by repeated load. Numerical solution by FEM adopted by using ANSYS V.15.0 and modified to apply a reverse repeated load. The final part of the dissertation involves developing Timoshenko beam theory to represent the harmonic load and comparing the results with numerical 2D model.

As a conclusion, converting the rubcrete compressive strength from 100*200 cylinder to 150*300 cylinder ranged from (0.86 to 0.94) for 10%, 20% and 30 rubber replacement. Also, the CDBs under impacts still behave in accordance to the STM method. STM found to be more suitable for solving rubcrete beams than the conventional CDBs.

The most effective crack due to hit viewed at the struts position, the positive cracks at the upper of middle support also appeared, so as the cumber cracks at

mid span of the upper face of the un-impacted span. Retesting the impacted beams by static load shows that, the impacted cracks develop and merged till cause the final failure. It has been concluded that, the reference CDBs loss a strength equals 23.8% and 36.5% from them total capacity after hitting by 30 kg and 40 kg respectively.

For repeated loads, the CDBs after repeated loads lost about 14%, 8% and 9% for conventional beam, gravel and sand replacement beams respectively, which means that, the presence of rubber enhances the beam capacity for repeated load. The numerical analysis of repeated load shows a good agreement with the experimental results.

List of Contents

List of Figures

List of Plates

List of Tables

Notations

A_b: cross sectional area (mm^2)

A_o: initial amplitude

A_n: amplitude after n number of cycles

a: Beam shear span (mm)

b: beam width (mm)

c': Upper concrete cover (mm)

c: Lower concrete cover(mm)

c: damping coefficient

C_b: longitudinal wave velocity (mm/s)

Cu: Copper material

E: modulus of elasticity (MPa)

E_p: Secent modulus of elasticity (MPa)

Eb: energy in the form of bending deformation (MPa)

Em: membrane component

Es: shear deformation

Ec: indentation effect when the projectile rebounds from the beam

Ek: beam kinetic energy (jole)

F1: Interior struts loading capacities

FE: Exterior struts loading capacities

$F(t)$: applied dynamic load (kN)

F_{dp}: Impact force load

$f'c$: failure concrete compressive strength (MPa)

G_d: Dynamic modulus of rigidity (MPa)

g: Gravity acceleration (m/s^2)

h: Total beam depth (mm)

H: Dropping height (mm)

I: Moment of inertia (mm^4)

K: structure stiffness matrix

l: Beam length (mm)

m: member mass (kg)

M: the dropping weight mass (kg)

Mp: is the hogging moment (kN.m)

$\frac{m_2}{m_1}$: impactor mass to beam mass

Pt: total calculated load (kN)

t: duration of wave (s)

ü: Acceleration (m/s^2)

u̇: Velocity (m/s)

u: Displacement (mm)

v: Concrete effectiveness factor

v: poisons ratio

V1, V2: the initial and residual impactor velocity (mm/s)

Vs: volume of specimens

v_o: Impactor velocity

v_d: Dynamic poisson' s ratio

W: Applied Load (kN)

Wu: Ultimate Load (kN)

W1S: Interior width of strut (mm)

WES: Widths of exterior concrete compressive struts (mm)

WEst : The upper exterior strut widths (mm)

WESb: Lower exterior strut widths (mm)

W1St: Upper interior strut width (mm)

W1Sb: The lower interior strut width (mm)

Wtn: Upper tie depth which equal to 2c` (mm)

Wbn : Lower tie depth which equal to 2c (mm)

y: distance from neutral axis to the top face of the beam (mm)

ω : Natural frequency of the continuous beam deformation mode (Hz)

ω_1: Natural frequency of the continuous beam first mode of deformation (Hz)

ω_2: Natural frequency of the continuous beam second mode of deformation (Hz)

ω_3: Natural frequency of the continuous beam third mode of deformation (Hz)

ω_4: Natural frequency of the continuous beam forth mode of deformation (Hz)

Ω: Ohm (Resistance unit)

ε': strain at f'c

ε_I: strain generated by indent wave

ε_r: reflected wave

ε_t: incident wave

ϕ, k: coefficient of linear equation

ρ_{ma}: the modified material parameter at the ascending branch

ρ_{md}: the modified material parameter at the descending branch

Δ: Static deflection (mm)

Abbreviations

CDBs: Continuous deep beams

DIF: dynamic increase factor

SDBs: Simply supported deep beams

SEA: specific energy absorption

STM: strut – tie method

CHAPTER ONE: INTRODUCTION

1.1. General

Deep beams are one of the most important members in constructions. It could be found usually in bridge support, pile caps, and high rise buildings [1], as shown in Plate 1.1. The geometric difference between shallow and deep beams is that, for ACI 318 -19 [2], the clear span of deep beams to its depth (L/D) does not exceed 4 for simply supported beam and 2.5 for continuous beams. The ACI-318 code gives another condition to consider the beam as deep, which is the load location condition. If the Concentrated load is at a distance does not exceed 2h from support then the beam also considers as deep [3]. The American code defines continuous deep beams depending on shear behavior, while European code definition (L/D is not greater than 1.15) based on flexural behavior [4] [5].

The failure mode is one of the most significant difference between shallow and deep beams. Shallow beams may fail by flexural besides diagonal shear, while in deep beams the control failure is diagonal shear failure, in which the cracks started from support into the point of loading [5].

Plate 1.1 Continous deep beams

1.2. Dynamic loads and dynamic response of continuous beams

Dynamic loads usually formed by multi different ways in accordance to the applied load exposed on it as explained in Table 1.1.

Generally, the response of a construction to the dynamic is given by the equation

$$M * \ddot{u} + C * \dot{u} + K * u = F(t) \quad (1\text{-}1)$$

Table 1.1: Dynamic loads definitions [6]

Load type	Causes
Impact load	crash or hammer blows
Seismic loads	Earthquake or blast (spectrum analysis)
Vibration	rotating machine
Transient load	It is the initial dynamic load without damping effect
Model analysis	Explains the magnitude of vibration of a structure
Harmonic loads	Rotating machines exert steady, alternating forces on bearings and support structures. These forces cause different deflections and stresses depending on the speed of rotation.
Random vibrations of varying frequencies	caused due to rocket launch, road transport

The dissertation focuses on the impact, harmonic and cyclic loadings. Impact loads may be subjected on constructions due to vehicle collisions, terrorist attacks, falling rocks in mountain regions, industrial accidents, explosions, pedestrian blocks, roadside barriers landslides and impulsive loads which are caused by failing objects [7]–[13], as shown in Figure 1.1. It causes a large inertial force which accelerates the member. If the member is ductile, the acceleration can be ignored because the failure happened after member accelerated and the

oscillations inertia fades away [14]. Impact load is usually higher than the static load capacity of brittle beams. The impact load is usually applied on a very small region, sometimes concentrates in a point (in case of spherical shape impactor), this concentrate caused a spalling, punching, or may be drilling [15]. The impact region is an area where the impactor inertia released on and the failure becomes worse when the impacted region is small [16].

a. pedestrian bridge [17]

b. Vehicle crashes into a structure [18]

c. Rock fall over a tunnel [19]

Figure 1.1. Some types of impacts applied on structural members

Repeated loads are exposed on a structure may vary in the magnitude, direction and the applied time. In which, usually, the construction weakens due to fatigue

strain and failure by a stress smaller than its ultimate load. Repeated load may occur with all positive load or with both positive and negative (which named by reverse loading). Reverse loading may be subjected on CDBs due to the earthquake loading wave [20].

As Biggs introduced [21], the dynamic response of the continuous deep beams is a very complex matter to be understanding because it has several natural modes with frequencies, each one of them may contribute the mechanism of failure. The modes are shown in Figure 1.2, Figure 1.3 and Figure 1.4.

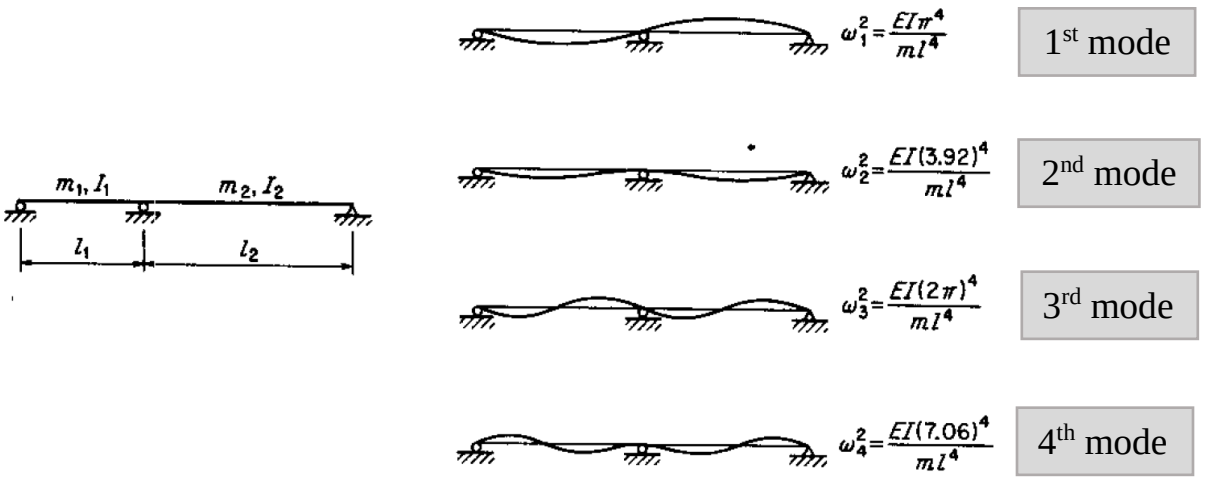

Figure 1.2. Natural modes of identical two spans [21]

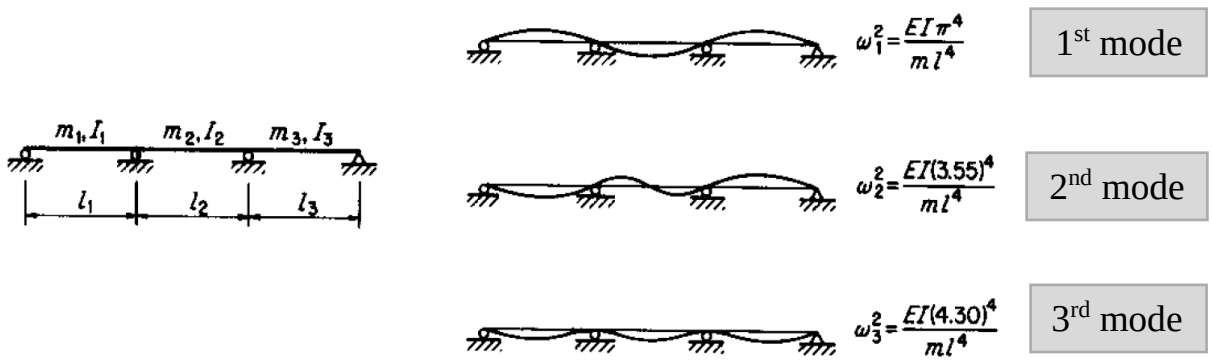

Figure 1.3. Natural modes of three identical spans [21]

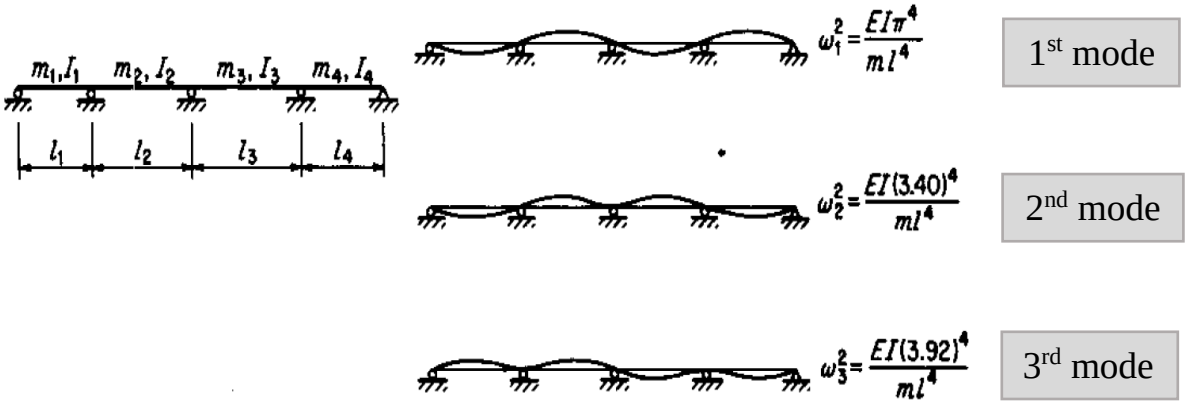

Figure 1.4. Natural modes of failure of four continuous beam [21]

1.3. Damping factor

The damping factor can be defined as the ability of the structure to energy absorption which exposed from vibration or (it is the way that the structure tries to dissipate the vibration energy applied on). This property found naturally in all structures but its magnitude varying from type to type in accordance to some factors like [6]:

- Material type
- Motion velocity
- Frequency of vibration.

Damping factor is classified into three categories which are (Viscous damping, hysteresis or solid damping and Coulomb or dry-friction damping). This study focuses on solid damping because it involves solids in dynamics, in contract to viscous damping which deals with bodies moving into a fluid and dry friction damping which caused due to sliding between two solids [6].

Solid damping (structural damping, hysteretic damping) involves the internal vibrations occurs in material during motion. The frictional forces imbed into the material matrix associated with the slipping between particles and its revelation to each other during motion. Structural damping independent on member frequency but its approximately has a proportional to member deformed elastic body amplitudes [22]. Structural damping is working on reducing the member

amplitude with respect to the area of hysteresis loop. For rubbers, the hysteresis loop (as explained in Figure 1.5) has much more area larger than metallic materials, for that reason, rubber used usually as dampers [22].

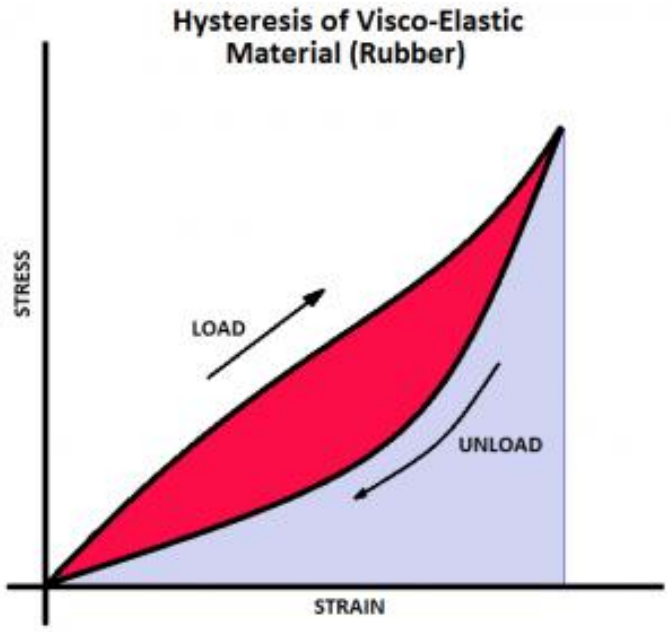

Figure 1.5. Stress strain curve of rubber material [22]

Usually, the coefficient of structural damping ignored for safety and because its small enough to be ignored [22]. For concrete structures, damping factor ranged from (7-10)% [23]. Damping factor can be estimated from the response data of an experimental dynamic loads subjected on member. Estimating method depending on the type of load applied, where each load gets its own method of calculating.

1.4. Rubbers as a waste material

Environment pollution is one of the most problems that researchers working on it to minimize its effect. The world, in general, is going towards recycling the human waste especially the not easy biodegradable wastes such as plastics and rubber. The world products millions tons of scraped tire in a year (303 million tire each year at united states [24]). The most biggest landfill of waste tires lies at Kuwait

in Arhyyah [25]. It is named as tires graveyard and it can be seen from satellites. Google map GPS showed it clearly (Plate 1.2).

In some civil engineering constructions, there is a great necessity to get a concrete with low unit weight concrete, high toughness, and high impact load resistance. In order to control that, developing mechanical elastic properties is the first step. For this purpose, researchers nowadays direct to add the waste tires concrete mix in aspecified percentages. The new concrete forming (rubcrete) has significant properties like: light weight, energy absorption, sound and heat isolation, erosion control, high toughness and ductility, high deformable under post failure load, high fatigue, impact load resistance and etc. [26][27]. But on the other hand, replacing aggregate by rubber has some avoidable negative effects such as compressive strength drop. That may be get rid of it by using any mineral or chemical additives to rise the strength. Especially the rubber is a chemically inert substance i.e. it will not react with any another chemical additives.

Plate 1.2. Arhyyah waste tires graveyard

During applying external load on rubcrete member, rubber particles resist a smaller amount of load than the surrounding aggregates. That will generate stress construction on the surrounding particles and causes to reduce the overall member flexural bearing capacity. Rubber particles is working on delaying forming cracks by behaving as a small micro imbedded spring units thereby enhance the flexural deformation capacity of rubcrete members [28]. Lengthy studies in literature investigated the replacement and its effect on concrete mix properties.

Tires (such as a lot of another pollutant) may be recycled in structural engineering constructions by adding crashed cleaned tiers into the concrete mix. Table 1.2 [24] shows the recycling tire percentages of different countries in civil engineering applications.

Table 1.2 Tire recycling in civil engineering [24]

Countries	Recycling (%)	Civil engineering (%)	Energy recovery (%)	Export (%)	Total recovery (%)	Disposal (%)
United States[a]	17	15	55	2	89	11
Europe[b]	43	—	47	5	94	6
Japan[c]	9	—	64	17	91	9
Mexico[d]	90	90	—	—	90	10
South Korea[d]	16	16	77	—	—	—
Canada[d]	75	75	20	—	95	5
New Zealand[d]	15	15	—	—	15	85
Australia (total)	10	6	<1	18	34	66
Australia (ex OTR)	17	8	1	29	55	45

Tires cleaned then crashed into small particles in special machines (Plate **1.3** from Abbaj alkut factory at Al-Diwahniya for tire recycling). Essentially, rubber crashed till reaches the general sizes of sand and gravel particle sizes. Recycling factories also product rubberized floors for electrical isolation Plate **1.4**). Rubber as an aggregate can be classified into four categories in accordance with its size, which are: shredded/chips (2-20mm), crumb (0.4- 4.75mm), ground (passing through sieve 0.4mm) and shredded fibers [29], [30].

Plate 1.3. Hashing machine

Plate 1.4. Rubberized floor units and crashing machine

1.5. Aim of Study

For environmental sustainability and structural necessity of getting members has a high energy absorption, rubberized continuous deep beams under dynamic loads has to be investigated especially after the noticeable poor information in literature about it. So, this dissertation involves the following axes:

1. Doing trail mixes to estimate the suitable properties for rubcrete, using weight and volume replacement, also study the case of sand or gravel replacement.
2. Experimental tests for continuous deep beams with different percentages of rubber replacement under static loading, impact load under different loading cases and repeated loading.
3. Numerical modelling for the repeated load and then simulated the cyclic reverse load for the same model using ANSYS APDL (V.15.0) software.
4. Find a theoretical solution for the conventional CDBs exposed to sinusoidal load and changing the properties for matching the rubcrete.

1.6. Dissertation Layout

- First chapter introduces a general information about the overall dissertation title expressions meanings, discusses the research importance, and shows the study program.
- Second chapter investigates clearly and deeply the progress in literature for this subject, explains the main theories of continuous deep beams, the effect of rubber on concrete properties and identifies the literature gap in information which allows the researcher to experiment this scientific point.
- Chapter three involves the details of overall experimental tests, method of testing, rubcrete mixes details and results, and manufacturing devices systems.
- Fourth chapter comprises all experimental work results and its discussions.
- Chapter five shows the numerical simulation for the member under repeated and reverse loading.

- Chapter six introduces a theoretical and numerical study for rubcrete CDBs under the effect of harmonic loads.
- Chapter seven denoted to discuss the results conclusions and recommendations for future works.

CHAPTER TWO: LITERATURE REVIEW

2.1. Overview

Continuous deep beams are an essential member in bridges, pile caps, foundation walls [5] and multi-story buildings. It may exposed to dynamic loads furthermore a static ones. Dynamic loads may be generated from machines vibrations (harmonic loads) earthquakes (harmonic loads), explosion (impulse loads), car accident (impact loads), human moving (transient loads), and etc. The behavior of structural members differs depending on the type of load applied. Dynamic loads (especially impact and impulse loads) causes a very high rate of straining on the material particles and caused a rapid damage.

On the other side, reinforced concrete members are brittle material, has no or little ability to absorb energy. In order to partially convert the concrete behavior from brittle to ductile, rubber may be added to the mix as a percentage replacement from aggregate in order to increase energy absorption and controlling the high rate of straining.

The following sections in this chapter describe the philosophy of deep beams, continuous beams, reviewing the influence of adding scraped tire rubber to concrete mix, dynamic and impact loads effect of rubberized deep beams and every comparable significant research in literature to this dissertation title. Furthermore, a small layout highlights the gap in information literature about this dissertation title.

2.2. Rubberized Concrete Material Properties

Usually, the material has a density equals to (480 kg/m^3 for crumb and 500 kg/m^3 for the chip) [31], no water absorption, and low thermal conductivity (0.14 W/m K). Rubcrete is expected to produce a high deformation capacity during post-

failure load stages, lower unit weight, high impact resistance, high damping properties, and high dynamic modulus [29]. The main unfavorable property is the dropping in compressive and tensile strength and the plastic state of workability.

2.2.1. Unit Weight

Logically, a slight dropping in unit weight occurs due to rubber-aggregate replacement. The reduction in unit weight is a result of less rubber density than aggregate, where the density of sand (1450 kg/m3), gravel (1650 kg/m3), and natural rubber (500 kg/m3). Literature paper results (shown in Table 2.1) indicate that the unit weight of concrete mix reduced concerning replacement percentages. From the result, almost, there is no significant difference in unit weight between using sand or gravel replacement. The right column in Table 2.1 shows the percentage of dropping with respect to the normal mix of each reference.

Table 2.1 Rubcrete unit weight results in the literature

Ref.	Replacement type (volume or weight)	Replacement percentages	Unit weight drop (%)
[32]	Gravel (NA)	5-10-15	⇓(8.8- 17.6- 23-36)
[33]	Sand (Cement repl.)	1-2-3-4-5	⇓(14.7- 3.3- 2.5- 6.4- 8.6)
	Gravel (Cement repl.)	1-2-3-4-5	⇓ (11.2- 4.2- 7.4- 2.1- 4.5)
[34]	Sand (weight repl.)	3-6	⇓(1.7-3.8)
[31]	Sand (Volume repl.)	5-10-15-20	⇓(1.2-2.3- 3.5-4.6)
	Gravel (Volume repl.)	5-10-15-20	⇓(1.2- 2.4- 3.6- 4.8)
[35]	Sand (Additive.)	5-10-20	⇓(3.3- 5- 10.7)
[36]	Sand (Volume repl.)	50	⇓5
	Gravel (Volume repl.)	50	⇓9
	Both (Volume repl.)	25-50-75-100	⇓14- 25.5- 37- 44.7

2.2.2. Workability

The slump test gives the an indication about workability. In literature, adding rubber to concrete mix sometimes decreases workability and sometimes increases it. Many researchers (as listed in Table 2.2) observed an incremease in a slump. Since the rubber particles have a hydrophobic surface, water particles do not stick

on, contrary to aggregate particles which have an absorption capacity[31]. Emam [34] investigated that, water covers rubber particles which lead to decrease the friction between concrete mix.

The concrete mix becomes more workable, pump, flow, and compact when adding graded rubber as a percentage of sand replacement [37]. References [34], [38] witnesses an opposite behavior against rubber adding. In such cases, the increment was due to the use of angular (mechanical grinding) which provides less fluidity in contract with rounded rubber aggregate [38].

Table 2.2. Influence of multi rubber replacement percentages on the slump

Ref.	Replacement type	Percentages	Slump (%)
[39]	Coarse sand (Volume repl.)	10-20-30	⇓(13.4-19-40)
[36]	Sand (Volume repl.)	50	⇓10.3
	Gravel (Volume repl.)	50	⇓24.7
	Both (Volume repl.)	25-50-75-100	⇓(10- 35- 64-71)
[40]	Sand (Volume repl.)	20-40-60-80-100	⇓(19-52-76-86-93)

2.2.3. Compressive Strength

Logically, rubber replacement (either by sand or gravel) leads to decrease concrete compressive strength in percentages depending on the amount and the way of replacement. When replacing one sieve of aggregate with the equivalent sieve of rubber, concrete strength will drop fairly. But when replacing a percent of the overall graded aggregate by full graded to aggregate a high drop in strength occurs because load pursued weak paths in the cube to flow within. Finding the rubber in different sizes in the mix will multiple the weakness paths in the cube. Thus, the drop is a common behavior but the way of replacement restricts the situation. In literature results (Table 2.3) most results refer to the occurrence of drop in strength. Each researcher explains their discussion for that decreasing. The poor bond between cement paste and rubber is the first achieved cause [41]–[45]. The loss of bond happened due to the larger difference between the modulus of

elasticity of rubber and cement paste [29]. Some researchers showed that reduction in concrete compressive strength may be due to rubber deformability which create cracks between cement paste and rubber just like air voids cracks [40], [43]. Reduction in compressive strength was happened due to the drop in mix density after replacement [43]. As shown in Table 2.3, some results give a slight increase in compressive strength, which is may be due to, increase compressive strength when adding rubber because of better stress dissipation causes better damaged tolerance [37], chemical agents which enhance bond, crumb ability to absorbed more energy and ductile behavior before failure [34]. Perhaps the presence of the steel wires and beads in edger chips tended to increase slightly the tensile strength of the tested cylinders [38]. From the view of the authors, rubber enhanced stress distribution and energy absorption and may lead to a slight rise in the strength if it is well distributed in the mortar and worked as a filling material to the air voids replacing gravel caused more decreasing in strength than sand replacement [42]. From table results, sand replacement by 15% almost causes to decrease compressive strength in about 30% for sand and 50% for gravel. While 10% replacement of sand causes a decrease in compressive strength ranged from (20%-40%). The rubberized specimen is capable to resist 20%-40% of the ultimate compression load for 2-3 min without full disintegration [38], [42].

Table 2.3. Effect of adding rubber on concrete compressive strength

Ref.	Replacement type	Percentages of replacement	Compressive strength reduction (%)
[39]	Coarse sand (Volume repl.)	10-20-30	⇓ (31.5- 45.2- 62.5)
[41]	Sand (Volume repl.)	5-10-15	⇓(3.3-10-15)
[32]	Gravel (NA)	5-10-15	⇓(23- 33- 50)
[33]	Sand (Cement repl.)	1-2-3-4-5	⇓(14.7- 3.3- 2.5- 6.4- 8.6)
	Gravel (Cement repl.)	1-2-3-4-5	⇓(11.2- 4.2- 7.4- 2.1- 4.5)
[34]	Sand (Weight repl.)	3-6	⇓(2- 1)

[31]	Sand (Volume repl.)	5-10-15-20	⇓ (15.3- 19.1 -31.3- 40)
	Gravel (Volume repl.)	5-10-15-20	⇓ (11.79- 16.92- 29- 37)
[35]	Sand (Additives)	5-10-20	⇓(30- 46- 68)
[36]	Sand (Volume repl.)	50	⇓78
	Gravel (Volume repl.)	50	⇓85
	Both (Volume repl.)	25-50-75-100	⇓(86- 88- 91- 90.5)
[37]	Sand (Weight repl.)	7.5-15	⇑ (5.9- 0)
[46]	Sand (Weight repl.)	2.5- 5-7.5	⇓(6- 16- 30)
[40]	Sand (Volume repl.)	20-40-60-80-100	⇓(25-51.5-68-82-90)
[47]	Sand (NA)	0.5-1-1.5-2	⇓(0-0-12- 21.8)
[42]	Sand (Volume repl.)	15-30-45	⇓(36- 42- 56)
	Gravel (Volume repl.)	15-30-45	⇓(50- 69- 81)
[43]	Sand (Volume repl.)	5-10-15	⇓(12.5- 21.6- 34.8)
[44]	Sand (Weight repl.)	4-4.5-5-5.5	⇓(3.7- 11.6- 15- 17.7)
[48]	Gravel (NA)	15-30	⇓ (54 – 70)
[49]	Sand (Volume repl.)	20-40-60-80-100	⇓(58- 66- 73- 87- 94)

- Continued

2.2.4. Splitting Indirect Tensile Strength

Every scientific reason mentioned in compressive strength matched with the tensile strength. Rubcrete in tensile shows a high capacity of absorbing energy [42]. The specimen resists post failure load and undergoing noticeable displacement [42], i.e. concrete mass able to resist loads even when cracked, due to its capability to undergo a large elastic deformation before failure [50]. From previous results of literature as noting in Table 2.4, it can be noticed that the tensile strength after 15% fine replacement decreases approximately from 20%-40%. While 5% of fine replacement leads to minimize tensile strength in a range that varies from 5%-15%. Course replacement by15% leads to minimize strength from 20%-50%.

Table 2.4. Rubcrete splitting strength

Ref.	Replacement type	Replacement Percentages	Tensile strength (%)
[39]	Coarse sand (Volume repl.)	10-20-30	⇓ (24.2-25.5-37.6)
[41]	Sand (Volume repl.)	5-10-15	⇓(14- 27- 43)
[32]	Gravel (NA)	5-10-15	⇓ (17.17-24.6-39.06)
[34]	Sand (Weight repl.)	3-6	⇓(19-33)
[31]	Sand (Volume repl.)	5-10-15-20	⇓ (11-14.8- 24- 34)
	Gravel (Volume repl.)	5-10-15-20	⇓ (8- 11-21- 31.3)
[37]	Sand (Weight repl.)	7.5- 15	⇓(19- 32)
[40]	Sand (Volume repl.)	20-40-60-80-100	⇓(15.6-47.8-66-81-92)
[47]	Sand (NA)	0.5-1-1.5-2	⇓(0-0-15- 20)
[42]	Sand (Volume repl.)	15-30-45	⇓(32-52-64)
	Gravel (Volume repl.)	15-30-45	⇓(53-67-74)
[43]	Sand (Volume repl.)	5-10-15	⇓(5.4-8.9-17.8)

2.2.5. Flexural Strength

The reduction in flexural strength which is observed in Table 2.5 may occur due to a drop of overall mix strength after replacement, furthermore, the line of failure perhaps passed through rubber particles. 15% of fine replacement causes to decrease the flexural strength from 14-23%.

Table 2.5. Effect of different percentages of replacement on the flexural strength

Ref.	Replacement type	Percentages	Flexural Strength
[39]	Coarse sand (Volume repl.)	10-20-30	⇓ (24- 24- 37)
[33]	Sand (Cement repl.)	1-3-5	⇓(7-21-32)
	Gravel (Cement repl.)	1-3-5	⇓(5.7-14-31)
[31]	Sand (Volume repl.)	5-10-15-20	⇓ (5- 12-23- 35)
	Gravel (Volume repl.)	5-10-15-20	⇓ (5- 10-22- 32)
[47]	Sand (NA)	0.5-1-1.5-2	⇓(0-0-14- 19)
[37]	Sand (Weight repl.)	7.5- 15	⇓(10- 14)

2.2.6. Modulus Of Elasticity

It is an indication of material stiffness. It is the ratio between stress and reversible strain (usually varies between 14000-40000 MPa) [51]. The modulus of elasticity

represents the slope of the stress-strain curve. Logically, dropping concrete compressive strength leads to minimize modulus of elasticity and that can be observed in the literature. Reference [37] shows a slight rise in compressive strength (discussed before) and it leads to raise elasticity too.

Table 2.6. Modulus of elasticity of rubcrete

Ref.	Replacement type	Percentages	Elastic modulus
[37]	Sand (Weight repl.)	7.5-15	⇓10- ⇑11.4
[49]	Sand (Volume repl.)	20-40-60-80-100	⇓(11- 14.7- 74- 88- 94)

2.2.7. Ductility

The ductility of concrete logically increases after adding rubber [40], [52]. Since ductility is the opposite property of brittleness, researchers studied brittleness to get an indication for ductility. Zheng et al. [52] investigate brittleness behavior using hysteresis loops of specimens.Figure 2.1 illustrates the brittleness index in which the lower brittleness indexes the higher ductility index. Typically, for compressive tests specimen, the inelastic strain noticeable at fracture on the order of 0.002 [53]. Normal concrete strain at failure load equals 0.0015, while for 7.5% replacing sand by crumb the failure occurs at 0.002 strain (to at 15% replacement) [37].

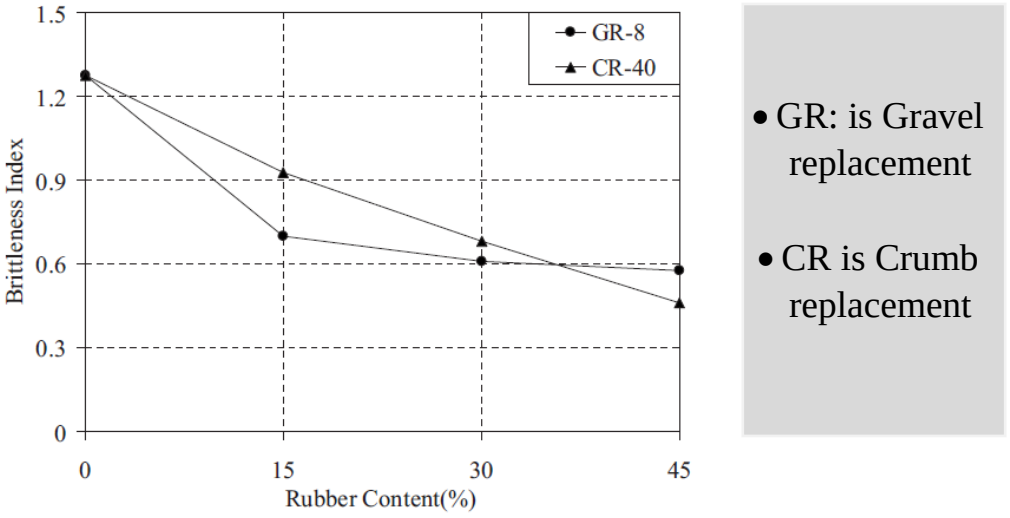

Figure 2.1. Brittleness index [52]

2.2.8. Water Absorption

Almost all references indicate that water absorption of rubcrete mix increases with the increment of rubber replacement when comparing with conventional concrete. Ganjian et al. [54] investigated that, replacing 10% of course aggregate with rubbers, leaded to raise water absorption but replacing ground rubber (range 0.075–0.475 mm) from cement caused dropping in water absorption. Adding 5% rubber replacement may cause an increment in absorption by (40-90%) proportion to rubber shape. Rubber addition working on restricting water propagation and reducing water absorption [55].

Table 2.7. Water absorption of rubcrete mix in literature results

Ref.	Replacement type	Percentages	Water absorption
[46]	Sand (Weight repl.)	2.5-5-7.5	⇑(42- 90.82- 547)
[35]	Sand (Additives)	5-10-20	⇑(14- 30- 41.8)
[44]	Sand (Weight repl.)	4-4.5-5-5.5	⇑(12.5- 26- 41.8- 68)

2.2.9. Dry Shrinkage

Dry shrinkage rises by 43% after 15% of rubber replacement [52]. The shape of rubber particles showed no effect on shrinkage as concluded by reference [56]. An increment in shrinkage in conventional concrete occurs as a result of low aggregate stiffness, and consequent reduction in “internal restraint’ which leads to strain capacity enhancement [27]. While, for rubber, the softness of rubber particles leads to reduce dry shrinkage [57]. Figure 2.2 shows shrinkage values for different rubcrete mixes.

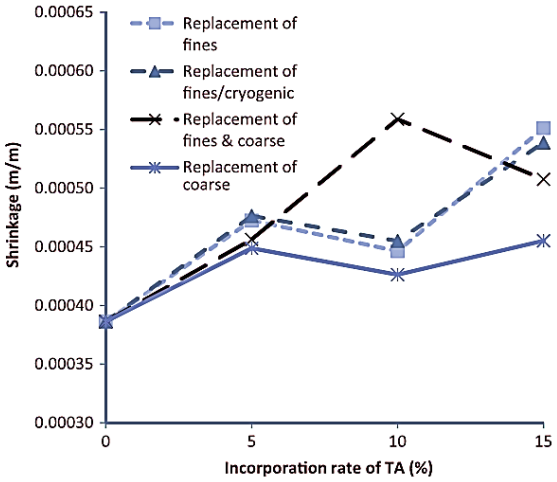

Figure 2.2. Shrinkage values for different replacement percentages[58]

2.2.10. Freeze and Thawing

Rubber aggregate replacement improves the resistance to freeze and thawing of concrete [59]. The amount of increment depends firstly on replacement percentage and secondly on rubber particle size. The larger rubber size causes dropping in the freezing resistance [60]. Richardson et al. [61] studied the optimum particle size which introduces maximum freezing resistance and minimum compressive strength dropping. It was found that particles less than 0.5mm provide the higher freezing resistance and compressive strength dropping equals 5.24% only. (10%, 15%, 20%) sand replacement enhances freezing resistance by (3.2, 3.1% 2.1%) respectively [62].

2.2.11. Thermal Conductivity

It is the capacity of the material to absorb heat, i.e. the temperature flux in a material. Concrete conductivity depends on its composition. In the case of saturated concrete, conductivity varies from 1.4 to 3.6 joule/meter square per second. Since weight can be reduced by using rubber replacement and thermal conductivity improves, so it can be a better option in the partition wall and the exterior wall which is exposed to sunlight [13]. Shah et al. [32] replaced gravel by (5%, 10%, and 15%). It was concluded that there is a rising in thermal conductivity by (4.4% -8% -11.7%) respectively.

2.2.12. Fatigue Resistance

The importance of fatigue strength is an essential property for structures exposed to repeated or cyclic loads. For concrete structure design in practice fatigue stress level (S) must be less than 0.50. In conventional concrete mixes, the fatigue life could be more than 2*106 cycles at a fatigue stress level of 0.55 [63]. Reference [28], tested normal concrete by 5–25% of rubber content replacement and got an increment in fatigue life within the range of 5–10%. References [64], [65] concluded that adding 60 kg of rubber particles in 1m3 of the concrete unit can increase the fatigue life up to 10 times. In general, it can be said that rubcrete has a fatigue strength up to 15%, more than normal concrete, and may increase more by more rubber adding. Reference [43] replaced sand by rubber by (5%, 10%, and 15%) which causes a dropping in fatigue strength equals (45.7%, 46.3% , 46.6%) respectively.

2.2.13. Stress-Strain Curve

Normal concrete strain at failure load equal to 0.0015, while for 7.5% replacing sand by crumb the failure occurs at 0.002 (to at 15% replacement) [37]. Figure 2.3 and Figure 2.4 show a typical stress-strain curves of rubcrete for two different groups of rubber replacement. The author noticed that the average strain of rubcrete equals two to three times that of conventional concrete [38] which is due to rubcrete ductility.

In [42], the normal concrete mix reached the maximum strain at 0.002. Similar behavior is observed for normal concrete and CR-15 (coarse aggregate replacement by 15%). From Figure 2.4, it is clear to notice that, adding rubber increases the maximum strain in a range that varies between 0.003-0.005. Stress-strain curve of rubber concrete behaves more non-linearly than conventional concrete. The non-linearity occurs due to the lower compressive strength of rubcrete [24].

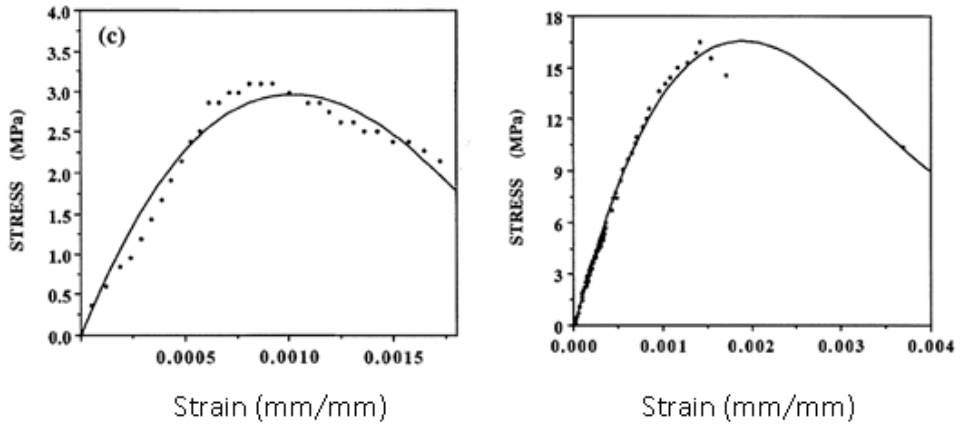

Figure 2.3. Typical stress- strain curve of rubberized concrete [38]

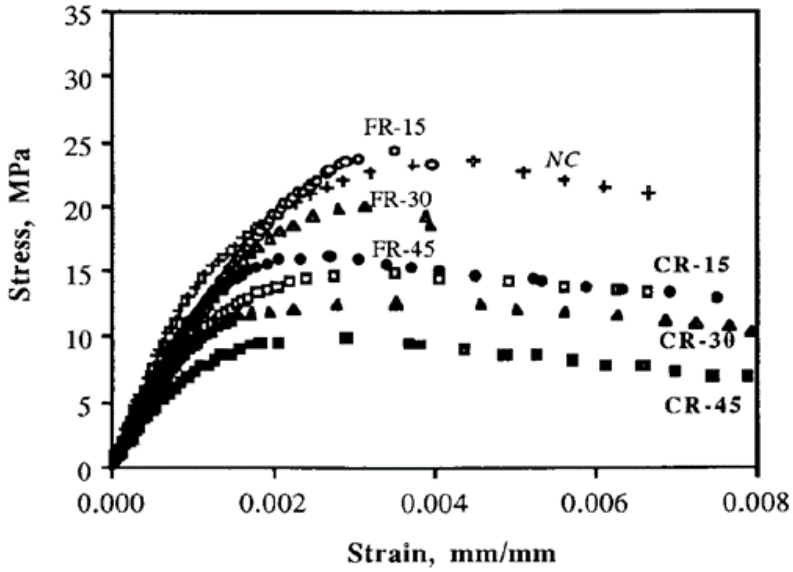

Figure 2.4. Stress- strain curve for NC, sand (FR) and gravel (CR) replacing [24]

2.2.14. Impact Resistance

The most important properties of concrete are rigidity and brittleness. Previous researchers noticed that adding rubber enhanced the deformability and ductility of the concrete members [66]. Thus, rubcrete may cast in places where deformability and toughness are more important than strength, such as in seismic areas. Rubber particles delay the forming of new cracks and act as multi distributed springs diffused in between cement paste [28]. From Table 2.8, adding rubber increases the overall impact resistance by more than 100% for different used percentages. Sand has a property of energy absorption contrariwise with

gravel. So, for reference [32], gravel replacement shows a significant increase in impact resistance than sand.

Table 2.8. Impact resistance tests result from the literature

Ref.	Replacement type	Percentages	Impact energy
[31]	Sand (Volume repl.)	5-10-15-20	⇑(138-185-300-396)
	Gravel (Volume repl.)	5-10-15-20	⇑(150-204-326-426)
[49]	Sand (Volume repl.)	20-40-60-80-100	⇑(90.8-112-141-165-160)

2.3. Impact Loads

Concrete structures response under impact load differs from static one due to two reasons. Firstly, the wave propagation effect [8], [67], in which the stress transformation within the loaded structure differs in local and global, which caused a difference in the negative bending moment and reaction force [68]–[70]. The second is the stain rate effect [71], [72]. Members under impact loading exposed to a very high strain rate loading, in such matter, the structure responses to the load rapidly from zero to peak external stress applied. The internal work develops also rapidly to balance the external one [73]. There are many ways to test concrete under high strain rate like, free fall bodies, explosive tests, hopkinsin's split bar test, charpy/ Izod test and fracture machines tests [73]. In the case of impact load, the structural member exposed to either compressive stresses- strains or tensile stresses-strains [15].

The impact load accelerates the concrete beam and attack its inertial force [74], [75]. Due to beam large acceleration under the impact load, its inertial force has the most significant effect under dynamic loadings [76] especially in the first milliseconds of impacting when the beam resist the hit by its inertia only and before reaching the load to support [77], [78]. Ignoring inertial force leads to an error in calculating reinforced concrete beam fracture if designers equals the exposed impact load to the bending load carried by beam [79].

The structural response of the member depends on some parameters like impact energy, the member stiffness, contact rigidity, and material mechanical properties [15], [80]–[83].

In laboratories, an impact load can be provide easily using several methods –as a branch of dropping bodies- like: dropping weight, swimming pendulum and rotating flywheel. Dropping weight also may be classified into a single blow, repeated blow with a constant value and repeated blows with an increment magnitude. There is no effect for the striking face of steel impactor on the dynamic response [84].

2.3.1. Shallow Beam Behavior under Impact Loads

The duration of impact wave depends in the first degree on velocity of impact. For higher ones, the duration may become 6 times the slow impacts [85]. The peak point of impact load occurs at the point of time of zero deflection [85]. When a stress wave generates due to impact load, the wave flows inside the concrete shallow beam till reach to its surface at sides (near support) then the wave reflect back as a tensile stress. The generated compressive stress wave intersect with the reflected tensile one, that minimize the compressive stress wave and increases the tensile amplitude. The concrete beam may be cracked due to this tensile stress. This process may be repeated until the resultant stress wave becomes lower than the dynamic tensile concrete strength [78], [86].

Dynamic loads especially impulsive ones, transported within the member by stress wave separation into the solid body particles vertically and laterally. So, every discontinuity in beam (caused by opens and shear or flexural cracks) obstructs the stress wave and the vibrations to extent the support beam side. This matter cause weakens in receiving all real response data at support during failing objects impact experimentally tests [87].

Shallow beams exposed to statically one point load show a positive flexural cracks under loading point, while for impact ones, a negative and positive moment cracks generated. The negative ones appears at the top surface of beam besides supports [15],[88], [89] as shown in Figure 2.5. Researchers are divided into three opinions when discussing the reason behind these cracks. The first, It is due to the beam local negative curvature resulting in tensile strength [90]. The second, it is due to supporting conditions (i.e. the upper roller support which is very essential to prevent the beam from uplifting) [8]. While the third, said it is due to beam hogging [91].

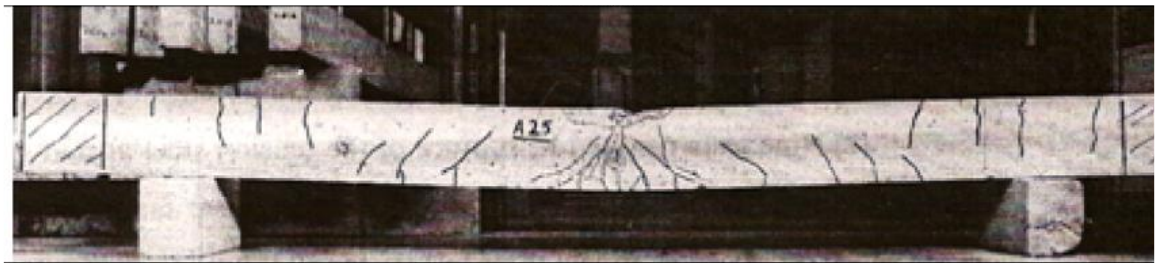

Figure 2.5. Cracked beam due to an impact load [88]

Furthermore, the simply supported reactions under impact loads started downward, shear and moment diagram differs compacting with the static point load as explained in Figure 2.6. It can be also noticed that, the impacted beam exposed to negative moment as a result of hogging due to the inertial force of beam [91].

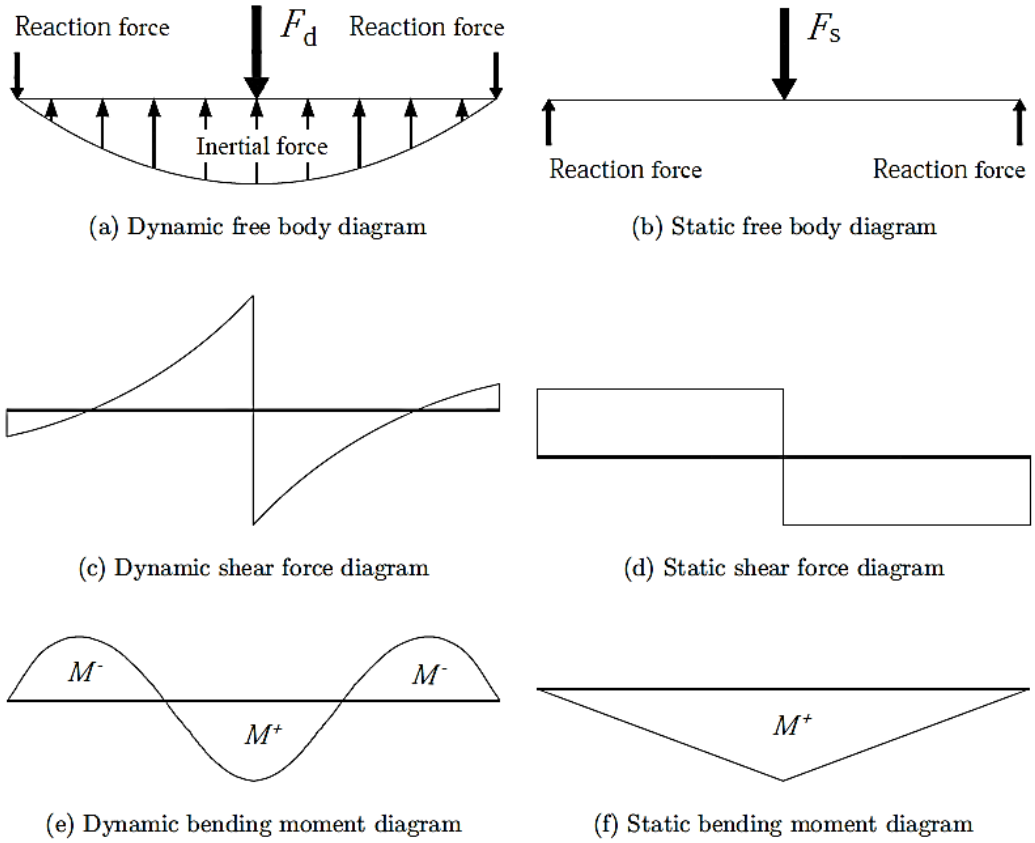

Figure 2.6. Shear force and bending moment diagrams for static and impacted simply supported beams [91]

Peak impact force can be calculated by an empirical equations concluded from other researchers. Like [92]–[94]:

$$F_{dp} = (12.6\, v_0 - 0.0079 v_0^3) * 9.8 \quad (2\text{-}1)$$

$$F_{dp} = 980 \sqrt{\frac{m_2}{1000}} * \frac{v_0}{8} \quad (2\text{-}2)$$

$$F_{dp} = 880 \sqrt{\frac{m_2}{1000}} * \left(\frac{v_0}{8}\right)^{\frac{2}{3}} \quad (2\text{-}3)$$

The previous equations shows that, concrete beam mass has no effect on the peak impact force, but Guo [75] offers an opposite opinion:

$$F_{dp} = (52.5 v_0 + 30.8)\left(0.19\, ln\left(\frac{m_2}{m_1}\right) + 1\right) \quad (2\text{-}4)$$

The impact load resisted by supporting and beam inertia [95]. From reference [96], it can be noticed that, only 17.5% of the impact load reached to the support and the remain 82.5% resisted by beam inertia. This percent is not general but depends on concrete beam inertia properties. From Figure 2.7, it can be noted that, the beam in the first phase (transient load) resist impact load by its inertia only while for the second phase (free vibration) the reactions accompanied slightly.

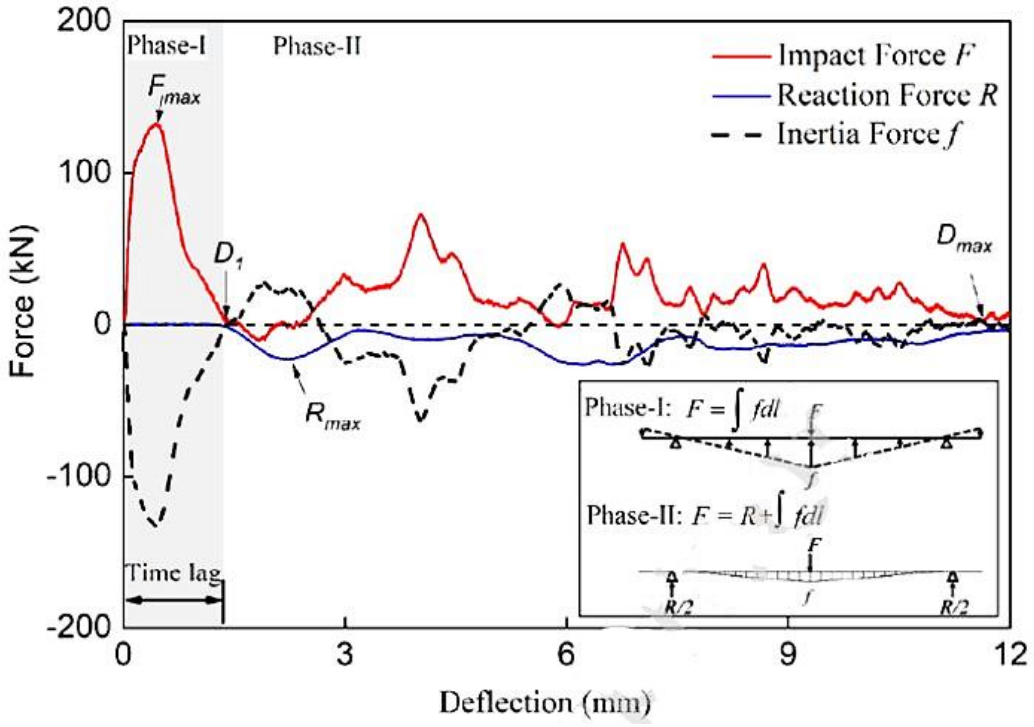

Figure 2.7. Forced and free vibration for beam resist impact by inertia and supporting [97]

To design the beam to impact load, it may be designed as static load with amplification factor n, static displacement has to be indicated under the same weight, thereby finding the maximum stress and displacement from the following formulas [15], [98]:

$$\Delta_{max} = \Delta * n = \Delta * \left[1 + \sqrt{1 + \frac{2h\eta}{\Delta}}\right] \quad (2\text{-}5)$$

Where η is the efficiency of the kinetic energy converting the moving mass, equals 1 for collision 100% efficient. If h=0 then n=2. If the mass travels horizontally then n calculated from equation (2-6).

$$n = \sqrt{\frac{\eta v^2}{g\Delta}} \tag{2-6}$$

$$\sigma_{max} = \frac{w * l * y}{4 * I} \tag{2-7}$$

Kishi et al. [85] discovered that, the impact shear capacity of RC beam without shear rebar equals 1.5 the static one.

During impacting, the beam deflects downward and getting away from the dropping weight (i.e. Impactor), which leads to impact force decreasing due to descends of interaction between the beam and impactor, then impactor rebounds and contact disappear.

Generally, it can be concluded from past researches [77], [78], [85], [95], [97] that, the crack behavior of shallow beam under impact load classified into three categories in accordance to dropping weight velocity. Firstly, if the velocity is relatively low, the concrete beam fails in flexural bending cracks, in another word, the slow drop weight acts as static load. This response appears also in references [90], [87],[9],[99]. Flexural crack width depends also on the impactor velocity[85], [87]. The crack width is not affected by the subsequent blows [77]. The beam collapse due to bending when the residual displacement reaches 1.1% of the clear span length [100].

Secondly, diagonal shear failure accrued at high velocity rate, and shear plug ,at higher, impactor velocities [101]. It is a diagonal collapse happened in beam exactly under the impact force point in a very short direction. This ball shape collapse may occur also under low velocities of dropping weight if the magnitude of transversal reinforcement increases [77].

The philosophy of shear plug can be explained as the following: when the dropping weight hits the beam, the travelling stress passes through the beam at a velocity equals v. Immediately at the first part of second of impact, an infinitesimally little section at the center of the beam will accelerate corresponding to the applied velocity [102]. The neighboring points stills at rest. Duwez et al. [103] illustrated that, the bottom of the V there is a stationary one plastic hinge, while at the top there are two moving plastic hinge travelling away from the V center, which effect on the shear plug enlarging.

The third shape occurred in relatively high speed impactor, in which the cracks start diagonally then becomes parallel to the main longitudinal bars. The latter may expand or short in accordance to speed. The RC beams collapsed under shear failure due to the flexural cracks connecting [85].

Pham speed Figure 2.8 shows typically experimental beams under shear and flexural failure. It is worth to mention that, if the high ratio longitudinal reinforcement bars forced the beam to fail in shear even when the velocity was low [78],[9]. On context, the little or no shear reinforcement cause converting the behavior of low velocity impacted shallow beam from flexural behavior to shear blog(bell shaped form [86]) [77].

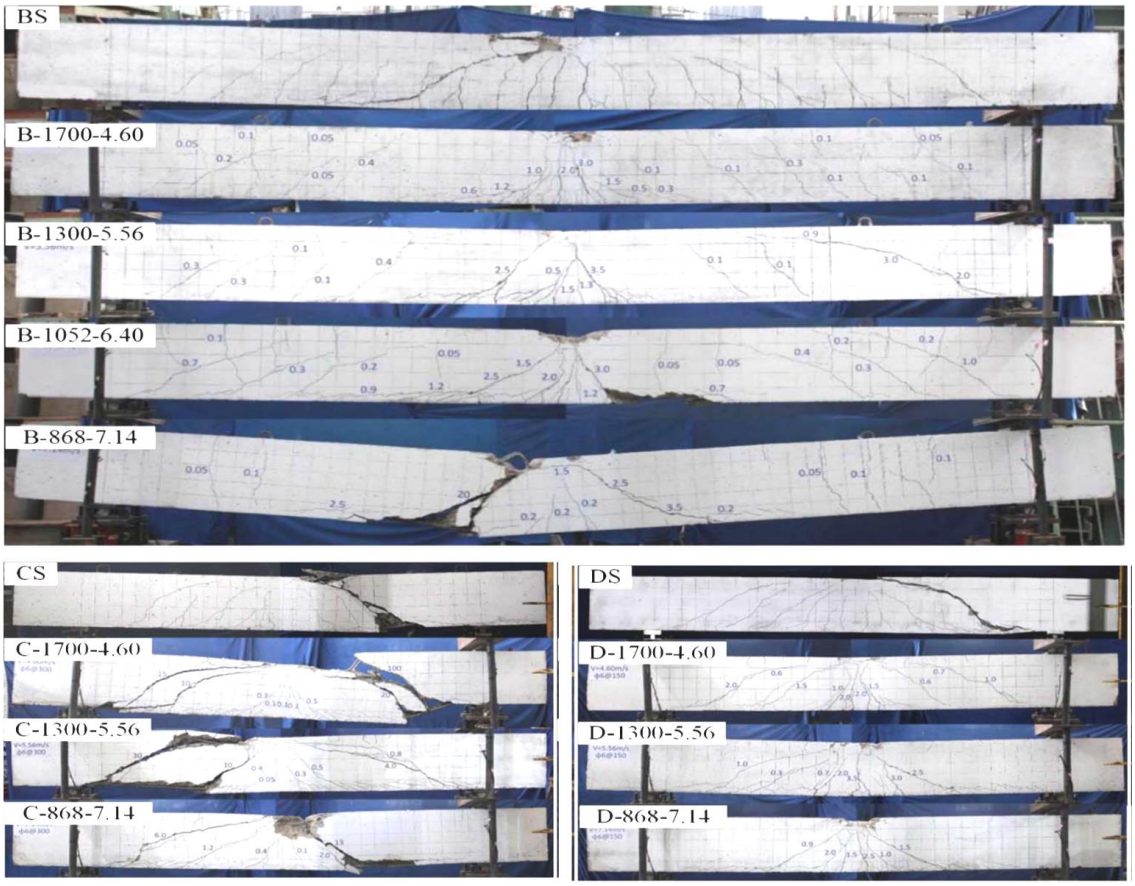

Figure 2.8. Beams crack under impact load [34]

Fu et al. [97] provided an indication for the high and low speed classification, the impactor velocity between 6.9 and 8.4 m/s is a critical speed converts the beams behavior from flexural to shear, but the behavior does not depend on the velocity only so these numbers cannot be generalized,. Adhikary et al. [104] suggested that, the slow loading rate equals 0.04 m/s, medium 0.4 m/s and the high one equals 2 m/s.

Kishi et al [85] suggested that, when the shear-capacity ratio (static shear capacity/static bending capacity) is less than one, the shear behavior currents in beam. In contrast, if the ratio is larger than one, the flexural behavior shows but conditioned by the drop weight velocity.

Impacting velocity has another significant effect on shallow beams which is bended span length $L_{effective}$. When the velocity is slow, the beam completely has

the enough time to resist the load and bend, while for higher velocities (but still within the flexural failure) the bended span minimized till reach a small part below the impact point. Regarding to that, the concrete beam deflection under high drop velocities has less effected by the beam span than the flexural beams failure [95]. This behavior could be understood from reference [21,22] failure. Due to this behavior, the support condition changes from hinge to both ends fixed.

Time lag or time delay (which is the delay of responding the support to the applied weight) have to be measured by researchers to get an indication for stress wave propagation influence [95]. It seems to be related only on the beam span [95]. The reason behind time delay expressed in reference [96], beam initial rising period amplitude is very small to provide the sufficient deformation, that leads to generate variations in the contact resistance, and therefore, the signal off the reaction load disappears a sensible vibrations. 1 ms has been indicated for time lag for Fujikake [9] beams.

A phenomenon observed in past researches worth to be mentioned and discussed, which is the amount of reaction load at high velocity impactor is smaller than the lower one. This phenomenon may be generated due to two reasons [86]:

The damaged beam associated with the cracking of concrete and steel yielding due to stress wave absorption. The short duration of loading process and time delay.

Few researches investigated the hogging occurs in concrete beam during impact hit. Hogging moment changes the expected mechanism of cracked beam [77], [86]. The peak value of hogging is proportional linearly with the impactor force [75]. Hogging moment for simply supported beam can be calculated from the following equation [75]:

$$\left|M_p^-\right| = 0.12\, F_{dp} + 6.84 \qquad (2\text{-}8)$$

Where F_{dp} represents the peak impact force.

The impact energy is reflected back into the rebound in an ideally elastic impact while a portion of the impact energy is transformed in elastic deformation and remaining part of the impact energy is consumed in the plastic deformation and failure in real impacts [105]. The energy balanced method can be used to verify the input kinetic energy and the component energies in a beam. The energy-balanced equation can be expressed as follows:

$$\frac{1}{2}M(V_1^2 - V_2^2) = E_b + E_s + E_m + E_c + E_k \quad (2\text{-}9)$$

Studies like [106]–[108] matched with this theory quietly well. The concrete beam after impact hit, loss some of its ductility due to the impact cracks. The magnitude of losing depends on the impactor energy. Dok et al. [87] found that, for low impact weight the beam lost 24.6%, for medium weight it lost 31.9% and for higher one 44%.

The absorbed energy of impacted beam increases with dropping weight velocity increment irrespective to beam type [85]. The deformation energy W of simply supported beams may be calculated by an equation offered by [9] so as the energy loss during impact E_R:

$$\frac{m_2 v_{ib}^2}{2} - E_R + (m_1 + m_2)g\delta_{max} = W \quad (2\text{-}10)$$

$$E_R = \frac{m_1 m_2}{2(m_1+m_2)} v_{ib}^2 \quad (2\text{-}11)$$

Where: m_1 is the equivalent mass of beams, m_2 weight of impactor, and v_{ib} impactor velocity. The experimental results of Zhao et al. [95] where verified with the pervious equations. It has been found that, for flexural behavior beams, there are 10% underestimated caused by neglecting deformation energy strain. While for shear behavior beams, a large difference observed reached even to 100%

because of the difference between the estimated failure shape and the actual displayed one.

2.3.2. Impact Force History

The generated shape of impact load – displacement curve is approximately triangular, so as the reaction – deflection one. A second peak appears in impact history resulting from steel reinforcement re-bearing after the concrete cracked[85], but it may occur also due to the impactor reflect after first hit (Zhao et al [95] explained the multi peaks for the same reason) , which causes another hit per single drop (as shown in Figure 2.9).

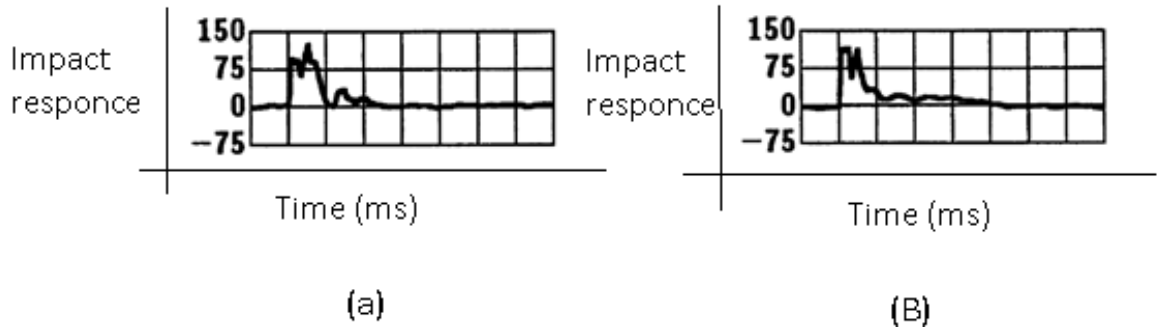

Figure 2.9. Load - Time impact wave (A. at 3m/s impactor velocity and B. at 5m/s dropping velocity) [85]

The triangular shape of impact load force versus time curve has been appeared at the numerical model proposed by [101] and the experimental test of [85]. The analytical solutions are better from experimental ones to get the exact triangle and the overall behavior [86], [101].

The higher impact load leads also to higher plastic deformation capacity due to the positive effect of the diagonal shear cracks nearby the impacting point. Thus, a large part of steel reinforcement may reach the yielding point, consequently, the length of plastic hinge increases and the plastic hinge gets larger [90].

Impacted structures behaves in two phases, firstly, the impact load phase which holds just few milliseconds (10ms) and the free-vibration phase which may reaches to 100 ms [78].

The beam under impact load has two shapes of displacement depends on the dropping weight velocity, the first is a wave fluctuates faintly accompanying by drift after the impact loads drops to zero. This phenomenon means that, the main steel bars only resist the impact force, free vibration period, after diagonal cracks growth [85]. The second is for faster impactor velocities, the deflection wave rises from zero then moves within a constant value (Figure 2.10). Impactor velocity effects on the beam deflection, where the deflection minimized when applying a high loading velocity because the time required to reach the peak displacement minimized [95].

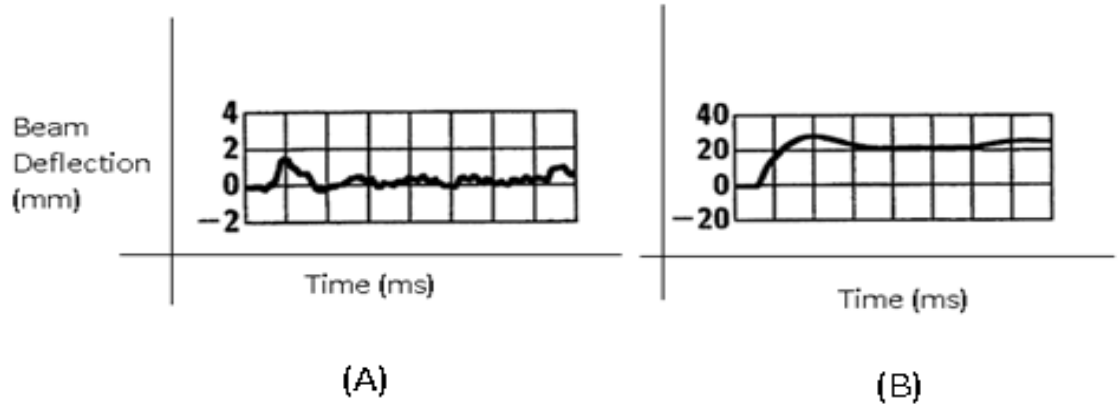

Figure 2.10. Deflection- Time wave of beam under dropping weight (A and B are at 3&5 m/s impactor velocity respectively) [85]

2.3.3.Deep Beams under Impact Loads

The shallow beam behavior may develop from flexural to shear when supplying the impact load nearby the support which may satisfy the second condition of deep beam specification in ACI- code (the impact weight applied at a distance equals 2h from support) [87]. As mentioned before, failure mode in static load is always shear failure, for deep beams, it has been noticed that, for impact load and for any

loading rate, the failure under impact load occurs also at strut as crashing. Strut crashing combined with diagonal splitting for low impactor velocity, bearing at medium speed, and massive spalling of concrete at high impact loading rate [104], as explain in Figure 2.11

Low velocity of impact

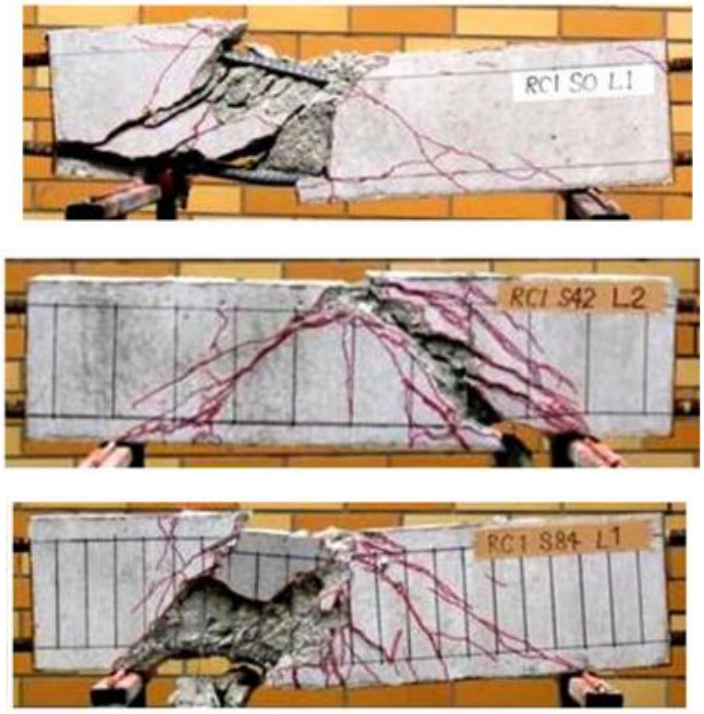

Without web reinforcement

0.42% web reinforcement

0.84% web reinforcement

Figure 2.11. Followed

Medium velocity of impact

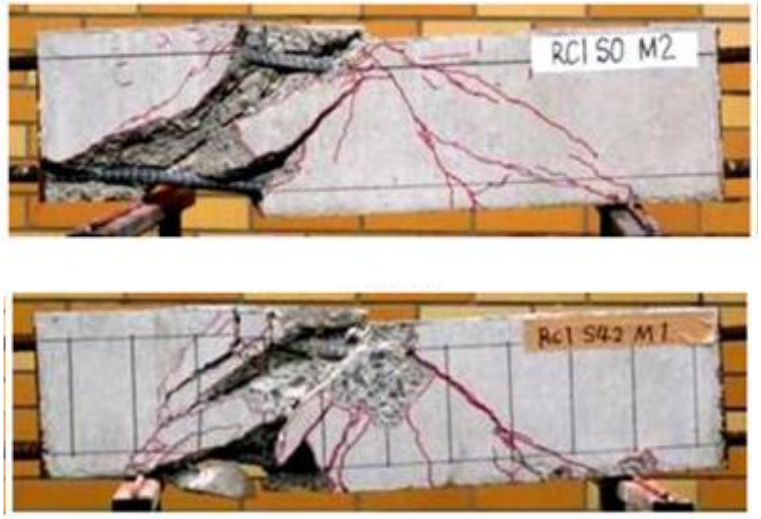

Without web reinforcement

0.42% web reinforcement

0.84% web reinforcement

Without web reinforcement

High velocity of impact

0.42% web reinforcement

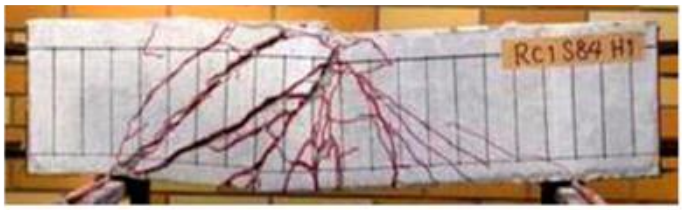

0.84% web reinforcement

Figure 2.11. Strut failure of impacted deep beams [104]

ACI- code 318 [2]provides an equation to calculate shear resistance strut without shear reinforcement but there is no guidelines for those with stirrups [109]. The shear reinforcement enhanced deep beam capacity by 25% of equation A-4 in ACI 318-14 code. It has been found that from reference [104] increasing shear reinforcement caused to increment the ultimate shear resistance of beam for low, medium and high rate of straining. The load versus deflection curves of deep beams under (low, medium and high) impacts has a delay indentation before reaching the peak value due to cracking development. Beams (without shear stirrups) stiffness increases when raising loading rate and the existence of shear

reinforcement has no effect on stiffness [104]. Yielding stress of ties rises when increasing load rating.

If the ultimate shear strength of deep beams is little (due to no or few transversal reinforcement) so as longitudinal reinforcement rate, the increment of ultimate load carrying capacity is higher when comparing with deep beams has high amount of main reinforcement. There is a mathematical model to calculate DIF suggested in the same reference for impact load depending on (a/d) ratio and it gets a good accuracy with its experimental work for static, low, medium and high loading rates as shown in Figure 2.12 [104].

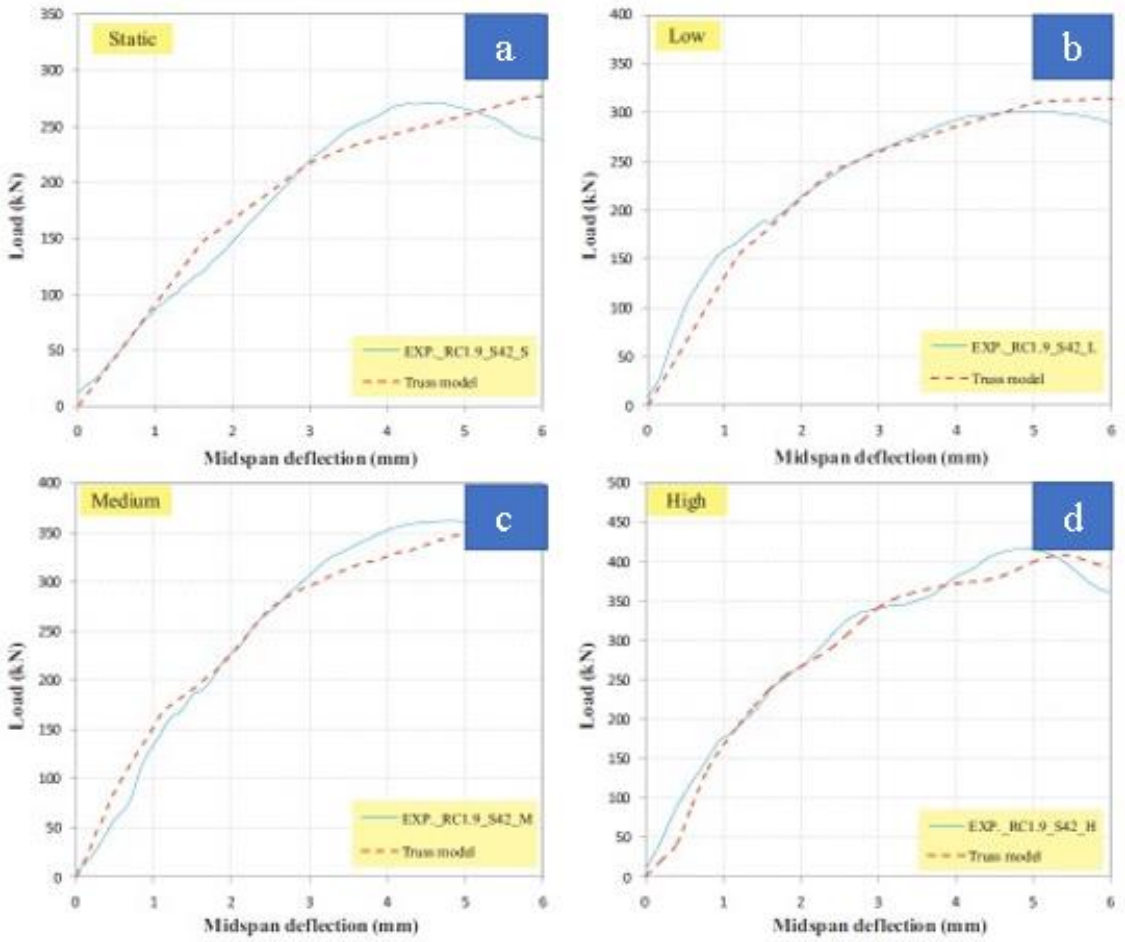

Figure *2.12*. Truss model results versus experimental lab data under different loading stages (a. static, b. low impact, c. medium impact, d. high impact) [104]

The empirical equation of DIF factor of deep beams without stirrups is given below

$$DIF = \left[0.45 + 0.09\rho_g + 0.48\left(\frac{a}{d}\right)\right] e^{\left[0.3-0.05\rho_g-0.05\left(\frac{a}{d}\right)\right]\delta} \quad (2\text{-}12)$$

If the deep beam has a transversal reinforcement, then the DIF equals:

$$DIF = \left[1.25 - 0.04\rho_g - 0.04\rho_v + 0.05\left(\frac{a}{d}\right)\right] e^{\left[0.22-0.03\rho_g-0.03\rho_v+0.03\left(\frac{a}{d}\right)\right]\delta} \quad (2\text{-}13)$$

Where ρ_g and ρ_v are main and shear steel reinforcement percentages, $\left(\frac{a}{d}\right)$ is the shear to span depth and δ is the static deflection.

2.3.4. Improve Concrete Properties Against Dynamic Loads

In order to earn concrete enhancement dynamical properties, it has to provide a better energy absorption to the mix. Improving the concrete energy absorption is by replacing rubber by specific percentages of aggregate (even sand or gravel). The generated mix (rubcrete) has a special improvement energy absorption [110]–[112] (higher impact energy by 10-18% for 15-30% rubber content [78]) but a lower mechanical properties due to replacement [31], [33], [35], [36], [40], [42], [46], [66], [113]. Rubber in concrete mixes behaves like a small impeded springs working on energy absorption. So, it has been evident that, for 15% and 30% rubber replacement leads to reduce stress wave velocity by 5% and 26% respectively [78].

2.4. Continuous Deep Beams under Static Loads

wide researches in literature involved the topic of CDBs made from rubcrete [5], [114]. There are many difference in behavior between Simply and continuous deep beams[115], [116], as an example:

(1) The both spans failure mechanism forms at the CDBs but not at the simply supported beam (SDB).

(2) large shear and negative moment occurs at middle interior support of CDB while can not be found at the simply supported.

(3) Supporting settlement may occurs in the Continuous beam only [117].

(4) the CDB strut has a great degree of deterioration than SDB at the same parameters and specimen details [118].

The diagonal cracks in CDB occurred in higher degree of deterioration and lower effected by compressive strength of concrete comparing with SDB of the same parameters [118]. The strut tie method provides by ACI 318-14 code showed less safety for CDB than SDB [118]. CDB failure amount and type is not warranted due to two reasons: the first one is the capability of differential settlement accruement and the second, the inflecting point formed nearby the critical shear failure zone of strut, so that the empirical equations of the ACI 318-14 code may be more accurate foe SDB [5]. The most effective factors on CDB shear ultimate capacity are the shear span to depth ratio and the compressive strength of strut [119]. The moment at the central support has been found equals 1.17 times the moment under the loaded point [120]. This paper involves understanding the behaviour of CDB by reviewing the few and limited past researches.

2.4.1. Web Reinforcement Effect

Shear reinforcement in deep beams represented by longitudinal and horizontal web reinforcement. The improvement in beams shear capacity due to such reinforcement depends on bars area and the spacing between the stirrups. It has been found that, for continuous deep beams, adding both types of web reinforcement enhanced shear capacity of beams in a magnitude depends on the steel amount. But, the vertical web reinforcement provides more significant strength than the horizontal one (because of the contribution of this reinforcement

with concrete to resist the shear stresses) and allows the beam to show more deflection. In contrast with the horizontal reinforcement which reduces the beam displacement (due to confinement effect) [121], [122]. Reducing beam deflection pushes the beam to fail by diagonal shear faster. Noting that, the effect of increasing horizontal shear reinforcement has no significant effect on beam strength when a/h ratio is more than 1, while for a/h less than 0.6, beam shear capacity increases with horizontal shear reinforcement increment [123].

In simply supported deep beams, the horizontal web reinforcement has the significant effect on beam strength. Casting continuous deep beams without vertical web reinforcement makes the beam collapse as a brittle and in every increment in vertical web reinforcement the beam became more and more ductile [122], [124].

2.4.2. Shear Span To Depth Ratio

CDB behavior approaches to be flexural with the smaller a/h ratio, and its shear strength capacity increased linearly with reduction a/h [115]. The smaller a/h ratio shows less deformation capacity of CDB also ductility and beam load capacity [124]. Beams tested with the same a/h but with different (a) and (d) values and increasing amounts of main steel reinforcement has no impact effect on beam stiffness [125]. The crack pattern is affected at the first degree by a/h ratio, for the same steel ratio amounts,. The larger a/h the earlier flexural cracks formatting and less visible diagonal shear cracks [124]. Both compression and shear stress at the strut increases when decreasing the beam depth [126].

2.4.3. Main Reinforcement Impact

The percentage of main reinforcement has effects on CDB behavior. Rodiguez et al.[127] introduced a load capacity versus main reinforcement percentage Figure 2.13 lists below for different diameters of steel stirrups to study beam behaviour affected. It can be noting that, increasing the amount of main-reinforcement greater than 1% leads to steady the failure load, curves tend to be asymptotic, in

another word, for high amounts of steel main reinforcement, the failure is limited by strut strength capacity[123], [127]. It has been also noted that, for main reinforcement amounts less than 0.6%, the structural failure is conditioned by the tie. Also, it can be noting that, the load capacity increase when stirrups diameter increases.

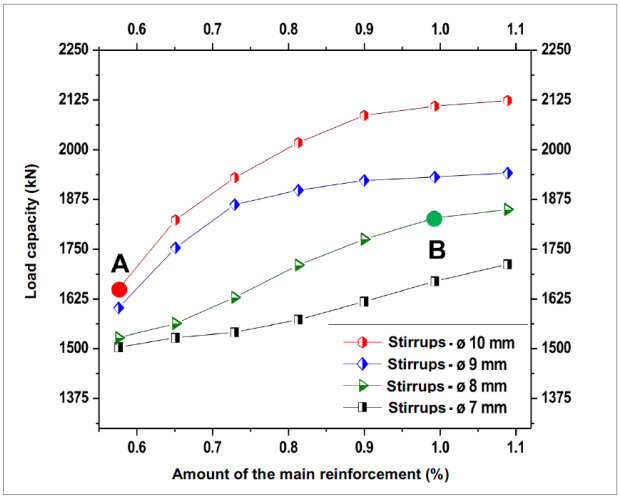

Figure 2.13. Main steel reinforcement ratio effect on loading capacity [127]

2.4.4. Cracking Patterns

At the final stages of loading, the crack patterns at both sides going to be symmetric at final failure load [128] as shown in Figure 2.14, but unsymmetrical for beams without shear reinforcement [125]. The number and width of cracks minimized when increasing beam depth (h) due to the increment of energy releasing rate and expansion of crack width which causes a brittle failure. The shear failure dominates the collapse types in deep beams [125], [129]. The shear failure is brittle which decreases the beam ductility and decreases the structural member strength [129]. The diagonal shear exterior span cracks forming suddenly just when approaching to the final failure load [124], [125]. After the first diagonal crack, at the middle support, the amount of load transfers to the external support becomes higher [125]. If a/h ratio is very small, no flexural cracks appeared till failure load neither in sagging nor hogging regions [130].

Figure 2.14**.** Typical shear cracks of CDB [23]

Since the CDB failure dominates by shear, then the flexural positive cracks has little effect on beam stiffness while the diagonal ones have the most effective impact [128]. Table 2.9 shows the amount of loading at first visible cracks for the pervious researches, it can be concluded that, shear cracks may appear at (33-40)% of the failure load for beams without any shear reinforcement and this variation depends on a/h ratio and main steel reinforcement amount. For beams with a/h ratio=1, first diagonal crack occurs at about (23-49%) of the overall beam capacity relenting on main and shear steel reinforcement amounts and concrete compressive strength.

Table 2.9. loading stages of apperance shear and flexural cracks for CDB

Ref.	a/d	ρ_e (%)	ρ_v	ρ_h	$f'c$	*1st +ve crack %	** 1st –ve cracks	*** 1st shear crack
[121]	1	2.13	0.25	0.34	36	20-23	80	Larger than 23
[129]	1.4	1.29			25	22	33	26
[124]	1	4.2	0.33	0.33	25	25	80	30
[125]	0.5	0.1	0	0	32.4	After 40	80	40
[131]	1	1.8	0.56	0.56	35	0	0	32
	0.5	1.3	0.56	0.56	40	0	0	46
	0.33	0.9	0.56	0.56	38	0	0	43
[132]	1	0.89	0.22	0.22	30	---	---	48.5
[133]	1.67	1.53	0	0	38.1	13	13	33
	1.33	1.53	0	0	38.7	14	14	34

* Load percentage at first positive flexural visible crack (%)

** Load percentage at first negative flexural visible crack (%)

*** Load percentage at first shear visible crack (%)

2.4.5. Concrete Strain

It is worth to mention that, the surface strain at first loading stages and before cracking, shows a linear relation, but after cracking the behavior transfers to the nonlinearity with a significant large and rapid amounts of straining [121]. The straining rate increases when the beam is a horizontal web reinforced [121]. The maximum compression straining at diagonal strut is about 0.002 at reference [129]. Before first cracking, both top and bottom steel reinforcement shows a compressive straining, which soon convert into a tensile one after the appearance of the first diagonal crack due to tie arch action [125].

2.4.6. Reinforcement bond

CDB easily to loss the bonding of longitudinal reinforcement and concrete when exposed to the same rotational bending moment at the two sequenced spans [126].

2.4.7. Influence Of Concrete Properties

Incrementing concrete compressive strength offered more brittle behaviour and showed larger load carrying capacity so as stiffness, also rises the ultimate load of the CDB due to strut compressing [123], [131]. Doubling concrete compressive strength increases CDB capacity in a range 6-21% [128].

The aggregate interlock across shear cracks shows an impact effect on CDB and SDB mechanisms, because the shear stress transferred by frictional effect and aggregate interlocking [134]. 50% of the transferring shear stress is carried by aggregate interlock at slender beams [135] but the contribution of aggregate interlocking in transferring shear stresses increases as the a/h ratio decreases as a result of the steeper angle of diagonal cracks [136]. The contribution certainly depends on aggregate specifications like: size, shape, aggregate strength and concrete compressive strength [137]. The aggregate size incrementally proportional with the ultimate shear capacity of shallow beams[138]. While inversely proportion has been found between the smoother aggregates and the beam capacity [139]. Increasing beam size without increasing aggregate size

causes to minimize the aggregate interlock and thereby the overall shear strength of beams [140].

Some few researches studying the impact of adding scraped cramped rubber into concrete mixes of CDB for dynamic absorption purposes [31], [141], [142]. It has been found that, adding rubber as a gravel replacement leads to dropping the compressive strength as well as the overall ultimate load of continuous deep beams [31], [141] (replacing 10 and 15% of sand by rubber decreases the ultimate load failure by 33 and 45% respectively, so it's not recommended to be replaced by more than 10% [141]).

2.4.8. Shear Failure Carrying Capacity

The most effective factors effects on the shear capacity of section are: ratio of flange width to gross width, span/depth ratio and the compressive strength of the concrete [143]. Experimental work tests showed that, the design equation provides by ACI -318 code (so as EC2-2004 [144]) are a lower bound theory. i.e. the failure load showed in experimental tests more than the theoretically calculated using the equations [118], [124], [129], [142], [145]. Verification factor has been calculated to discuss the difference between experimental tests and empirical design equations (of ACI 318-19 and EC2-2004) and found to be 1.004 and 1.158 % respectively [142]. EC2 is more conservative for CDB [131]. The underestimation occurred because the fact that the CDB equations derived from SDB tests [124].

2.4.9. Continuous Deep Beams Capacity Calculation

Elastic analysis for SDB or even for CDB provides us by an elastic ultimate load in an acceptable degree of accuracy but it is not suitable for nonlinear analysing due to the deep beam nonlinearity and the contra-flexure point of the CDB. For analysing the CDB many methods may be used like: finite element analysis, ACI -318 code equations (STM), Kong Robins and sharp and truss model [5]. The artificial neural network (ANN) and multi linear regression also used for

estimating the ultimate load and deflection of concrete CDB. When calculating the capacity of 75 CDB tested experimentally with the ANN method, getting a 99.13% degree of correlation and a 81.16% for the multi linear regression[146].

STM depends is a lower bound theory based on material ultimate strength and forces equilibrium conditions [125]. For low and medium concrete compressive strength, the strut and tie method introduced a good agreement with a different design codes procedures [147].

There are more than one mode of strut and tie shape per one loading case for CDB in contract to SDB (see Figure 2.15). Mode estimation governs a significant effect on the failure load calculation, and that one of the reasons which made a difference between experimental results of beam and the theoretical calculations. Usually, that model is the best in which the loads follow the path with the least force and the least deformation [116].

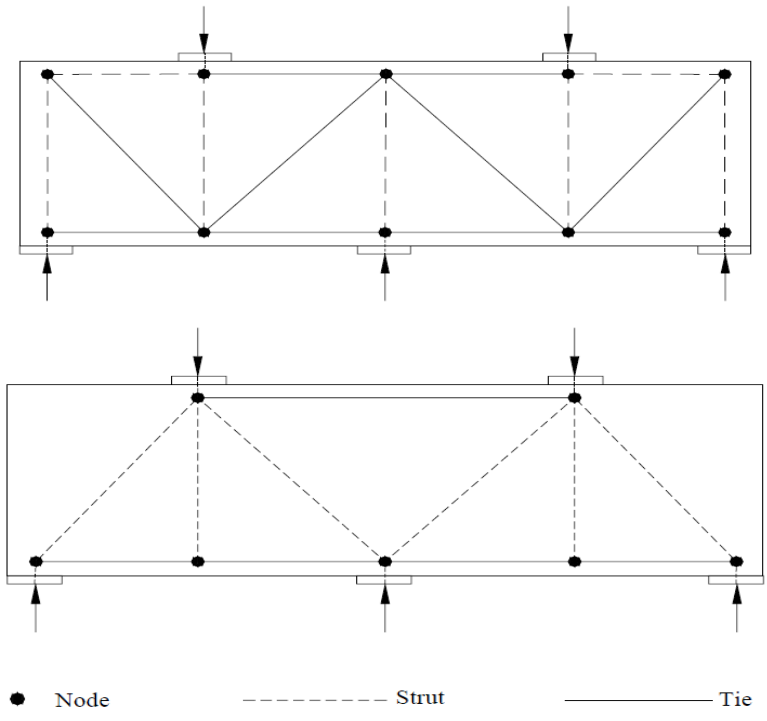

Figure 2.15. CDB Strut and tie models [115]

Estimating CDB capacity may determine using strut and tie method STM, in which it depends on the plastic theory, balance theory and yielding state theory [116]. The discontinuous regions considers as a truss where tension and compression forces transfer to support by struts and ties as shown in Figure 2.16. The nodes collect struts and ties. The CDB shear capacity represented by both internal and external reactions (VE & VI) and it can be determined as the following:

$$F_E = v\, f'c\, b\, W_{ES} \quad (2\text{-}14)$$

$$V_E = F_E \sin\theta \quad (2\text{-}15)$$

$$F_1 = v f'c\, b\, W_{1S} \quad (2\text{-}16)$$

$$V_1 = F_1 \sin\theta \quad (2\text{-}17)$$

$$\theta = tan^{-1}(\frac{h-c-c`}{a}) \quad (2\text{-}18)$$

As ACI-318 recommendations, the angle θ must not to be more than 25˚. The failure load of beam can be determined by evaluating the average of lower and upper strut width:

$$W_{ES} = \frac{W_{ES_t}+W_{ES_b}}{2} \quad (2\text{-}19)$$

$$W_{1S} = \frac{W_{1S_t} + W_{1S_b}}{2} \quad (2\text{-}20)$$

The effective width of the strut can be estimated from the following equations. It's clear to note that it depends on bearing plate's width, depth of ties, and angle degree.

$$W_{ES_t} = 0.5LLP\ sin\theta + Wtn\cos\theta \quad (2\text{-}21)$$

$$W_{ES_b} = LEP \sin\theta + Wbn\cos\theta \quad (2\text{-}22)$$

$$W_{1S_t} = 0.5LLP\ sin\theta + Wtn\ cos\theta \quad (2\text{-}23)$$

$$W_{1S_b} = 0.5\ LIP \sin\theta + Wbn\cos\theta \quad (2\text{-}24)$$

$$P_t = 2(V_1 + V_E) \quad (2\text{-}25)$$

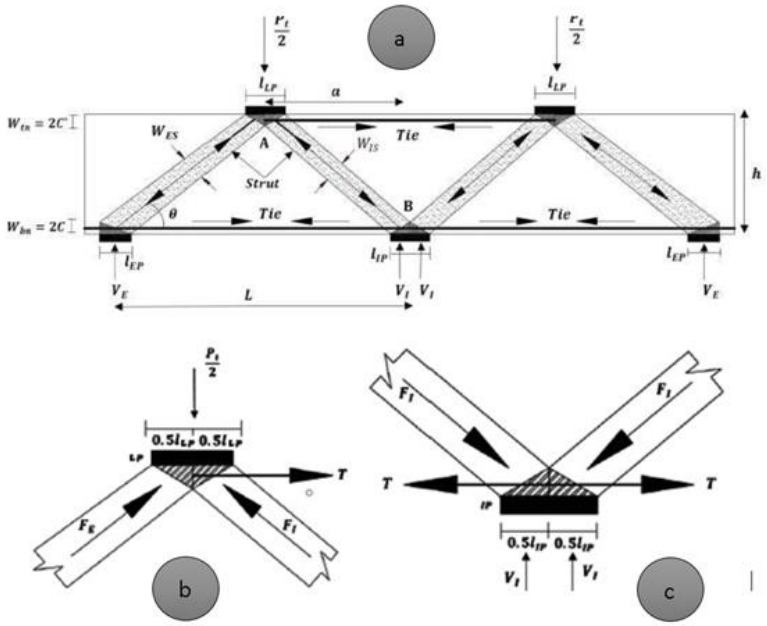

Figure 2.16. STM of CDB, a-Truss model, b-loading joints, c-intermediate supporting joint [142]

2.5. CDBs Harmonic Load

Generally, the response of continuous concrete deep beams has not investigated by the past researches especially for rubcrete mixes. Mahdi [148] investigated experimentally the response of two way bubbled slab under harmonic loads. Numerical solutions by different software programs has been interested with the reinforced concrete beams [149]. There are also some theoretical studies about concrete beams which exposed to harmonic loads [150]–[154] and plate foundation with regarding to Winkler model of subgrade reaction [155]–[157]. Through reference [152], the cracked and un-cracked concrete cantilever beam was investigated under the effect of harmonic load. It was found that, crack existing near to the fixed end support of the cantilever beam decreases the natural frequency compared with crack existing away from the fixed support. Also, displacement will be more for cracked beam compared to unloaded beam because of reduction in stiffness. Chen et al.[154] introduced a theoretical study for solving deep beams which are exposed to distribute harmonic load. Finite element

(FE) method (coded by Mathlab software [158]) has been used for certificating the theoretical solution. It is noticed an excellent matching between the derived equation and the FE results. CDBs have been studied in many articles with static load [1], [131], [159], [160], repeated and cyclic loads on simply supported deep beams [160], [161], rubberized continuous deep beams statically tested [141], [142], and rubberized deep beams under static loads [30] but not investigated under the effect of harmonic loads. So, solving the CDBs under the effect of harmonic loads has not been studied yet.

2.6. Repeated and Cyclic Loading

The behavior of deep beams in the first cycles matches with the monotonic loads. The cracks opened with loading and closed when unloading. The ultimate load decreases during repeated load by 8% and the beam deflection also decreases by 25% [162].

For cyclic loading, there are three types of failure mechanisms of fixed ended deep beams (i.e., continuous deep beams) depend on four factors (the magnitude of top and bottom steel reinforcement, concrete compressive strength, a/d ratio and load position and overall beam geometry)[163]. The failure mode are:

a. Flexure-shear failure: occurs when the top steel reinforcement equals 0.002 bd. Both diagonal and vertical flexural cracks formed on beam.
b. Shear failure: occurs after the appearance of the initial vertical bending cracks, it forms diagonally till causing spalling and crashing at concrete edges.
c. Bearing failure: Bearing local failure occurs in CDBs when using small bearing plate.

The failure pattern of CDBs under cyclic loads differ when comparing with the monotonic static loads. The diagonal cracks orthogonally crossed together as shown in Figure 2.17. This phenomenon minimizes the beam capacity by about

18% compared with the static load [164]. This is because of the cyclic load effects on the beam top and bottom by sequence in positive and negative series of forces, each force (positive and negative) has its own struts.

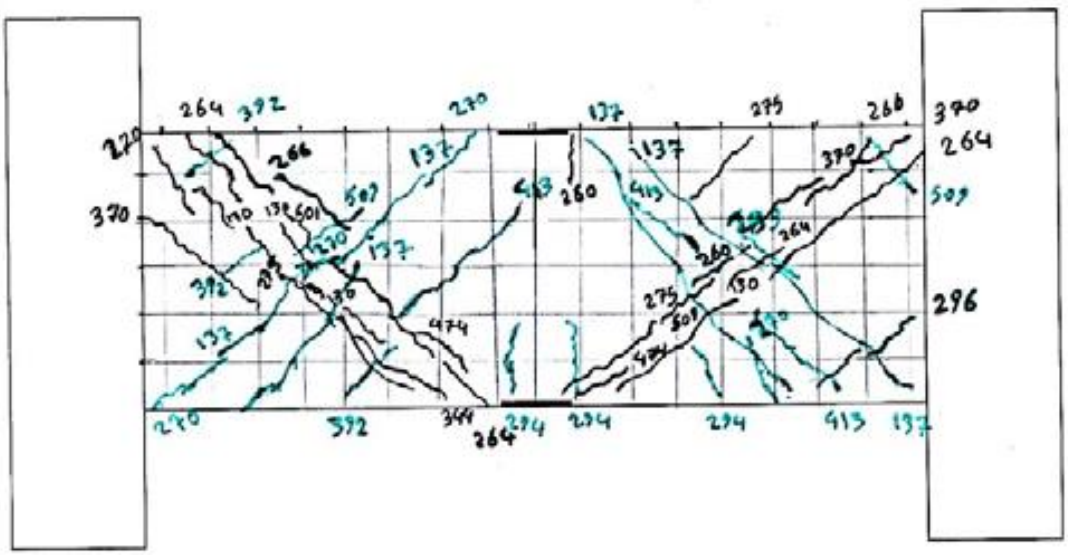

Figure 2.17 CDBs crack pattern [164]

2.7. Concluded Remarks

From the previous researches, CDBs investigated under static loads and repeated loads, but have not been studied ever against any type of dynamics. So the dissertation devotes on rubberized CDBs under impact, repeated, cyclic and sinusoidal loading. The presence of rubber enhance the dynamic properties of beams. As well as it is focusing on finding the degree of deterioration of impacted CDBs and identifying the capacity loss after the impact.

CHAPTER THREE: MATERIAL PROPERTIES, EXPERIMENTAL PROGRAM AND BEAM'S PREPARATIONS

3.1. General

The importance of investigating the response of CDB under dynamic loads has been well explained in the previous chapter. The details of rubcrete mixes, mix properties' results, methodology of experimental work, manufacturing devices preparation, beams details and molds have been listed and discussed at the present chapter.

3.2. Rubcrete Mixes and Steel Reinforcement Properties

Two totally different rubcrete mixes have been investigated. The first one is a weight replacement of (1:1.5:3) which is listed at **Appendix A**, while the second is a volumetric replacement of (1:1.4:2). The second mix details, preparing, mixing, curing and type of tests are listed below.

Seven mixes were casted to investigate the effect of rubber-aggregate replacing. 10, 20 and 30% replacements are investigated for sand and gravel separately volumetric replacement, the last mix is a normal concrete to be used as a reference. All mixes were prepared with (1:1.4:2) percentages and of w/c ratio equals 0.365. Supperplasticsizer GLENIUM G54 also utilized with properties shown in Table 3.5 and **Appendix B**. Plate 3.1 and Plate 3.2 illustrate the mixing processes, casting, curing, and specimens before tests. A rotating mixer of 250 Kg total capacity was utilized. Specimens was cured by sinking into water for 28 days. Mixes percentages per one cubic meter were listed in Table 3.1. Mixes were prepared using a full graded replacement for 14 mm maximum gravel-chip size which are matched with the ASTM C33-78, so as for sand crumb replacement.

Chemical and physical properties for rubber, sand, gravel, supper-plasticizer and cement are listed in Table 3.2 to Table 3.6.

Its worth to mension that, the sand versus crumb replacement denoted by **S** letter and followed by the percentage of replacement, while the gravel-chips replacement denoted by the letter **G**.

Table 3.1. Mixes weights (kg/m^3)

Mixes	Cement	Sand	Gravel	Rubber	water	GLENIUM G54
NC	475	760	1119	0	173.3	2.33
S10	475	684	1119	34.2	173.3	2.33
S20	475	608	1119	68.4	173.3	2.33
S30	475	532	1119	102.6	173.3	2.33
G10	475	760	1008	44.1	173.3	2.33
G20	475	760	896	88.2	173.3	2.33
G30	475	760	784	132.3	173.3	2.33

Table 3.2. Chemical and physical properties of rubber

Composition	Value
Chip density	650 kg/m^3
Crumb density	720 Kg/m^3
Carbon black	20%
steel	4 %
Water absorption	0.01
Specific gravity	1.09

Table 3.3. Chemical and physical properties of fine aggregate

Properties Test results Limits of	magnitude
Sulfate content (SO3)	0.01 %
Specific gravity	2.65
Fineness modulus	3.19
absorption	0.1
Unit weight	1600 Kg/m^3

Table 3.4. Chemical and physical properties of course aggregates

Properties	**Magnitude**
Sulfate content (SO3)	0.08 %
Specific gravity	2.6
absorption	0.15
Unit weight	1650 Kg/m^3

Table 3.5. Supper-plasticizer properties [165]

Chemical name	Glenium 54
Chemical composition	Sulphonated melamine and naphthaline formaldehyde condensates
Appearance	Whitish to straw colored liquid
Relative density	1.07 gm/cm^3 at 20 ℃
Chloride content	Nil.
PH	5-8
Storage	Should be stored in original containers and at above 5 ℃
Transport	Not classified as dangerous
Labeling	Not hazard label required
Alkali content (as NaO_2) equivalent	0.26%

Table 3.6. Cement properties (mass- Basian type)

Test	Result	ASTM C150/ASTM C150M-17
Standard texture test	w/c=0.25	------
Initial setting time	168 min	45 min (Minmum)
Final stetting time	3.15 hr	6:15 hrs (max)
Cement density	1450 kg/m^3	-----
Finenness	96.2 %	-----
Mortar compressive strength in 3 days Area=2500 mm^2	1st sample =86.01 kN 2nd sample= 79.48 kN 3rd sample= 84.15 kN Average 84.21 kN f'c=33 MPa	12 MPa (Minimum)

Plate 3.1. Specimens before test

a. Cylinder sample excluding

b. Applying air pressure for excluding samples

c. Rotating mixer

d. Sinking samples curing

Plate 3.2. Mixing, excluding specimens from molds and curing

In this investigation, the steel reinforcing deformed bars of Ukrainian producer were employed. Steel reinforcements of 12 mm and 8 mm are used for longitudinal reinforcement and transverse reinforcement, respectively. According to the American standard (ASTM A615 / A615M-16, 2016) [166], the yield and ultimate strengths are shown in Table 3.7. Material testing at Al-Mussaib Technical Institute is carried out in its material laboratory, and the tested samples were subjected to a computerized tensile testing equipment until they ruptured, as shown in Plate 3.3.

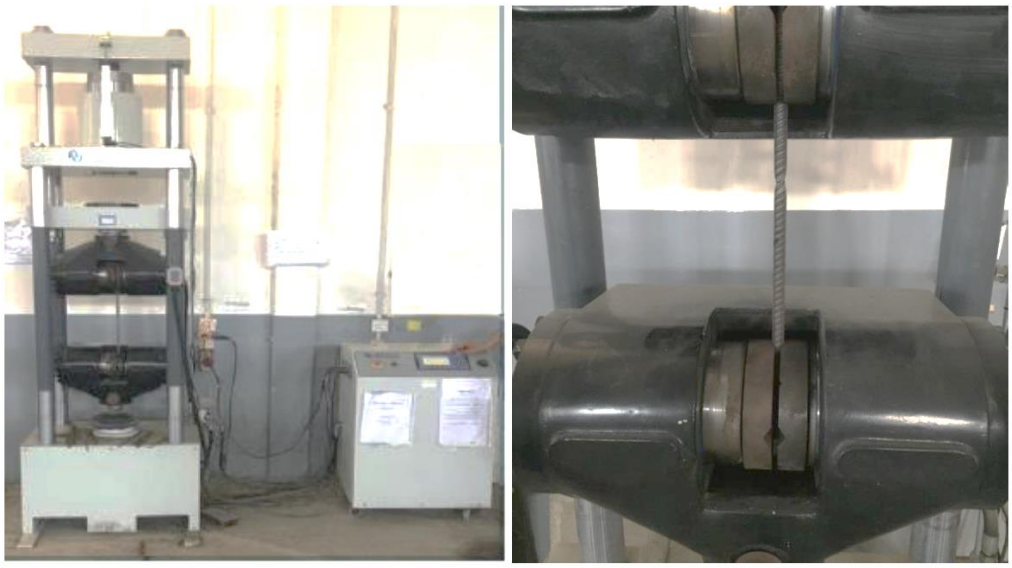

Plate 3.3. Steel tensile test

Table 3.7. Steel bars tensile stresses

Steel bar diameter (mm)	fy (MPa)	Fu (MPa)
8	432	635.1
12	570.8	718.1

3.3. Material Mix Testing Procedures

In accordance to the ASTM standards specifications, the concrete mixes were tested to investigate some on its' properties like: concrete compressive strength for 100 and 150 mm cubes, splitting test, rupture strength, stress-strain curves, ultrasonic test in addition to the workability and unit weight (as explain in Plate

3.4 to Plate 3.8). It's worth to mention that, the surface of each cylinder was smoothed before each stress-strain testing, as explained in Plate 3.9.

Plate 3.4. Compressive strength test

Plate 3.5. Splitting strength test

Plate 3.6. Rupture test

Plate 3.7. Greasing samples

Plate 3.8. Sample preparing for ultra-sonic test

Plate 3.9. Smoothing rubcrete mixes' cylinders with different replacement percentages

3.4. Material Mixes Results and Discussions

3.4.1. Workability

The workability of concrete mixes were investigated using slump test in accordance to the ASTM 143M-12 [167]. It can be concluded from Figure 3.1,

which shows the results of slump test, the replacement working on decreasing concrete workability in amounts depend on replacement percentages. It can be also noting that, the mix has a good workability for civil engineering works. The unrounded rubber particles (in comparing with the aggregate) will bound the water particles into their irregular shapes, that what causes the low slumps for rubcrete. Slump shapes for all mixes are shown in Plate 3.10.

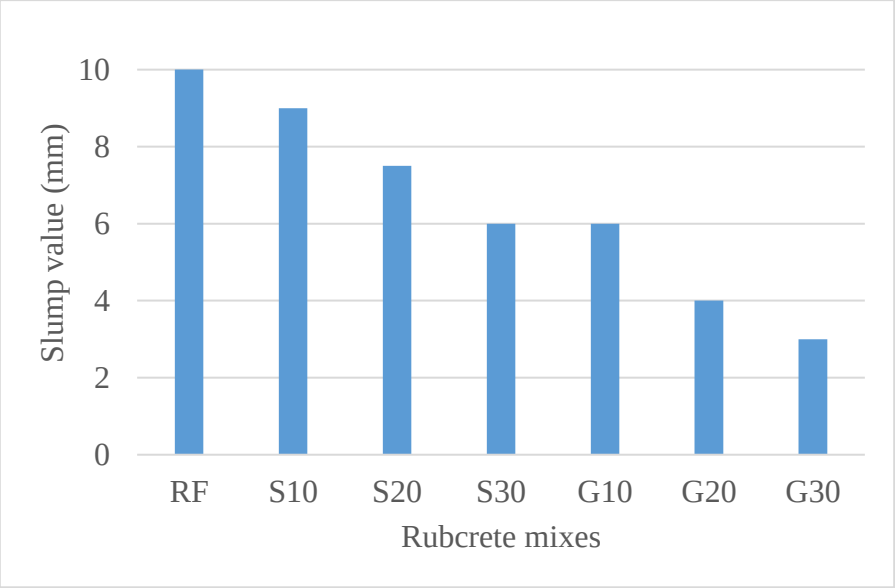

Figure 3.1. Slump test values

Plate 3.10. Workability test

3.4.2. Unit Weight

Logically, the unit weight of rubcrete is lower than concrete due to replace the heavier aggregate by the lighter rubber, and that what proved as literature in Table 2.1, and experimentally at Table 3.8. The results based on the mean of three samples for each single mix. The unit weight of rubcrete decreases for each incrementing in rubber percentages for both sand and gravel replacement. Sand replacement specimens heavier than the gravel for the same replacing percentages. It is due to that, the unit weight of gravel is greater than that of sand.

3.4.3. Water absorption

It is the ability of material to absorb water. It can be stated that, replacement increases water absorption of concrete mixes since rubber is a hydrophobic material. All results are listed in Table 3.9. and such result matched with references [35], [44], [46].

Table 3.8. Rubcrete unit weight of specimens 150 mm cubes (All weight in kg)

Mix	Sp.1	Sp. 2	Sp.3	Mean	Redaction %
RF	8.03	8.025	8.034	8.030	-------
S10	7.670	7.665	7.625	7.653	4.69
S20	7.445	7.393	7.375	7.403	7.80
S30	7.090	7.065	7.16	7.105	11.5
G10	7.905	7.870	7.850	7.875	1.93
G20	7.705	7.705	7.660	7.690	4.23
G30	7.325	7.31	7.345	7.327	8.76

Table 3.9. Water absorption details

Mix	Water absorption (%)	Increment (%)
RF	0.0245	-------
S10	0.0273	11.43
S20	0.0377	53.88
S30	0.0416	69.80
G10	0.0277	13.06
G20	0.0305	24.49
G30	0.0338	37.96

3.4.4. Compressive strength

The average of three cubes of 150 mm size is tested in 28 day age to get the British compressive strength F_{cu}. Furthermore, the average of three cylinders of 150*300 mm (diameter * height) is also tested to get the American compressive strength $f'c$. The converting factor from British to American compressive strength is also checked out for rubcrete. Table 3.10 shows the results of the three cubes specimens, the means of them, and the difference in accordance to reference mix and the converting factor from cylinder to cube. It can be noted that, compressive strength drops for each incrementing in rubber percent but still structural for this suggested rubcrete mix, such result matches with the literature researches listed in Table 2.3. Also, since the replacement is from the volume of aggregates, the weight of rubber in cubic meter is more than the gravel, that which made the gravel replacement specimens stronger than the sand replacing. The failure of the RF mix is as a fully sudden explosion due to its strength in contrast to other rubcrete mixes. Relenting on the results, the converting factor (CF) from cubes to cylinders was found to be ranged from 0.82 to 0.76 which is matched with the normal converting factor, and it is recommended to be used for rubcrete.

Table 3.10. Cubes compressive strength

Mix	Mean F_{cu} (MPa)	$f'c$ (MPa)	Redaction Depending on F_{cu} results (%)	$CF = F_{cu}/f'c$
RF	53.06	43.20	------	1.22
S10	34.35	26.60	35.25	1.29
S20	25.97	19.90	51.06	1.30
S30	22.74	18.11	57.14	1.25
G10	37.92	29.00	28.53	1.30
G20	34.30	26.04	35.36	1.31
G30	27.48	21.00	48.21	1.30

To discuss the converting factor from 100*200 mm cylinder into a 150*300 mm specimen, an average of 3 specimens are tested and compared with the bigger cylinders results. All details are listed in Table 3.11. It can be concluded that, the reconverting factor from bigger to smaller cylinder is ranged from 0.8 to 0.94 for rubcrete mixes.

Table 3.11. Cylinders compressive strength

Mix	$f'c$ (MPa) 100*200	$f'c$ (MPa) 150*300	$CF = \frac{f'c\ of\ (100 * 200)}{f'c\ of\ (150 * 300)}$
RF	34.76	43.20	0.80
S10	22.88	26.60	0.86
S20	18.29	19.90	0.91
S30	15.70	18.11	0.86
G10	26.08	29.00	0.89
G20	24.53	26.04	0.94
G30	18.60	21.00	0.88

3.4.5. Stress Strain Curve

Stress versus strain curves are one of the best behavior viewers to the concrete mixes. It shows the linear, and nonlinear stages under loading conditions. It was tested through evaluating the average of three cylinders of 100*200 mm (diameter * height) for all seven mixes. From Plate 3.11, one may conclude that, rubcrete mixes have a strain values much more than the conventional concrete mixes due to its elasticity under loading with lower compressive strengths. The type of failure of cylinders is columnar vertical cracking through both ends. The intensity of this behavior becomes more visible at high replacement rates. The brittle exploded failure of the reference mix was less gradually after every incrementing in rubber percentages and becomes as a ductile failure. All cylinders failed within the standard expected failure types listed in ASTM VC39/C39M − 15a [168]

specification for type 3 (i.e. columnar vertical cracks from both ends) as shown in Figure 3.2 which illustrated the failure mode of three different mixes.

Plate 3.11. Failure mode of cylinders

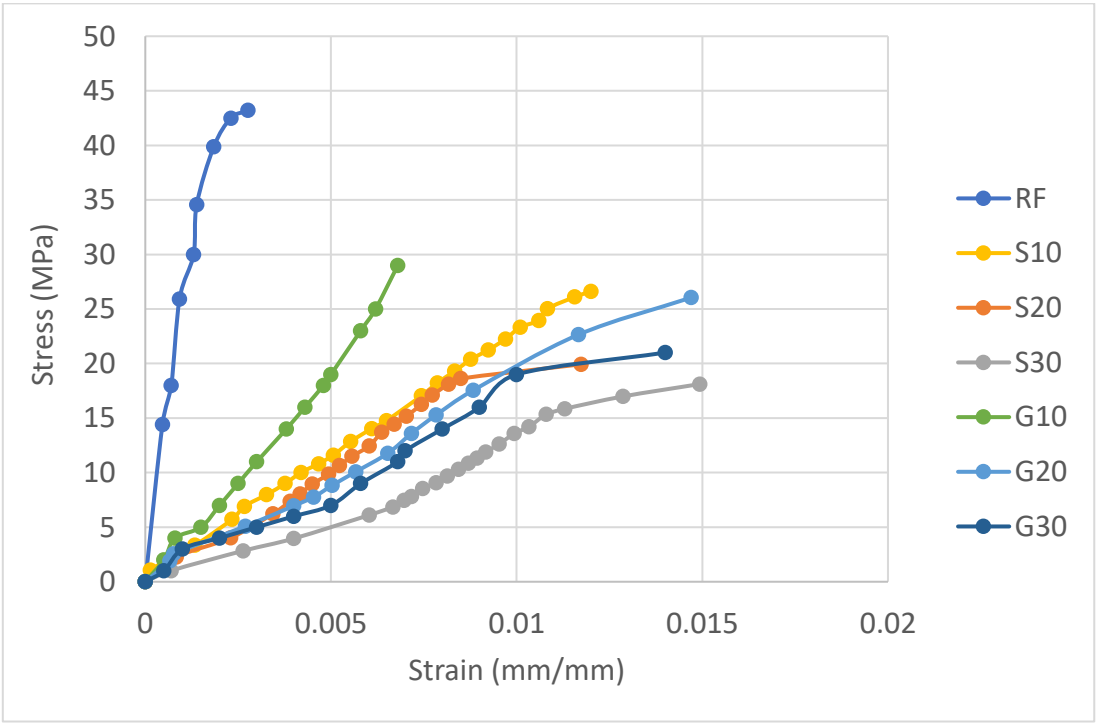

Figure 3.2. Stress - strain curves for all mixes, cylinder (300mm*150mm)

3.4.6. Tensile Strength

Three samples of 100*200 mm cylinders are tested to investigate the splitting tensile strength of the seven mixes in accordance to the ASTM C469-11 specifications [169] . Table 3.12 lists the tensile strengths in which deduced that, the tensile strength of rubcrete decreases for every rising in replacement amount due to loss of bonding, less density of rubcrete and/or due to the micro cracks of mortar which multiples due to the difference between the rubber elastic modulus and the mortar. Specimens after failure can be seen in Plate 3.12.

Table 3.12. Tensile splitting test details, recorded load

Mix	Sp.1 (kN)	Sp. 2 (kN)	Sp. 3 (kN)	Ft=2* Mean load/($\pi * L * D$) (MPa)	Redaction (%)
RF	344.8	242.61	341.12	10.98	------
S10	220.86	222.8	224.78	7.88	28.20
S20	200.24	203.68	200.88	6.42	41.54
S30	163.78	164.52	162.74	5.21	52.54
G10	262.30	257.60	260.94	8.28	24.52
G20	209.70	208.60	211.6	6.68	39.12
G30	182.55	183.94	185.08	5.85	46.68

Plate 3.12. Failure splitting plane

3.4.7. Rupture Strength

A prisms of (100*100*300 mm) dimensions were casted for the seven mixes to test the modulus of rupture at 28 days in accordance to the ASTM C133-97 [170]. The tested specimens' results were clarified at Figure 3.3, and accordingly the rupture strength of rubcrete reduced due to the reduction in bending strength. It possible to conclude that, a dropping in fr noted since the flexural strength effected in the first degree on compressive strength as well as the bonding strength between mortar and rubber particles, which matches with Table 2.4. Results also show that, the flexural strengths of sand replacement are slightly higher than the gravel replacement, which is due to the sand replacement provides higher ductility than gravel replacing. Rupture test for rubcrete also investigated widely at reference [171]. Failure shape of all specimens was similar so one specimen was considered as to show the failure (Plate 3.13).

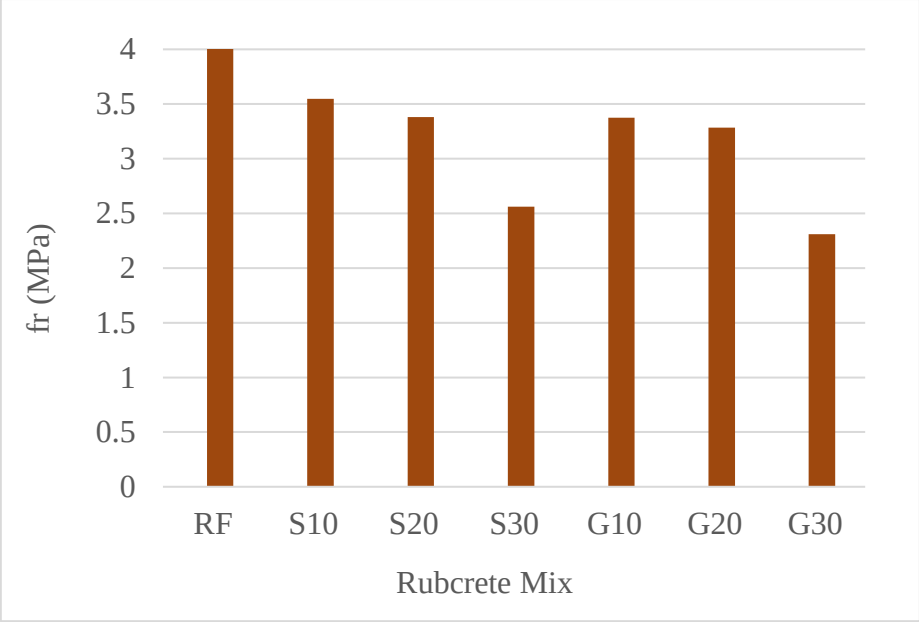

Figure 3.3. Flexural strength results

Plate 3.13. Flexural failure of specimen G10

3.4.8. Ultrasonic Test

It is used for investigating the velocity of passing sound waves through concrete mixes to show its deterioration against loads and its cracks. It can also view how the sound wave effected by aggregates-scraped rubbers replacements. A non-destructive test was made for disk specimens (65*152 mm (diameter * length)) for the seven concrete mixes. The specimens' centers were identified in order to achieve the extremely direct wave path passing through them. From results which are shown in Table 3.13 it can be noting that, the replacements slowed down the sound wave which crossed within due to the high energy absorb of rubber. Gravel replacement showed more slowly velocity when compared with the same percent of replacement of sand due to the larger rubber particles.

Table 3.13. Sound velocities through rubcrete

Mixes	Velocity (m/s)	Decrement (%)
RF	5191	------
S10	4928	5.066
S20	4304	17.09
S30	4224	18.63
G10	4444	14.39
G20	4201	19.07
G30	4172	19.63

3.4.9. Impact Test

In accordance to ACI committee 544 [172], the impact resistance of concrete may be gotten by casting a cylindrical specimens of 65*152 mm (diameter * length) and applying a drop weight simulated of 4.54 kg. Number of hits which caused the first crack were recorded besides the total number of hits at final failure. The impact test showed that, replacing causes a higher impact resistance for rubcrete mixes comparing with normal concrete as detailed in Table 3.14. Gravel replacement mixes shows more impact resistance when comparing with sand replacement. The reason was visible and sensible during the test, it is due to that, the chips particles bigger than sand which will collect the cracks and prevent them to be developed during the test. Failure shapes of the mixes were listed in Plate 3.14. It is worth to mention that, all the failure modes were local and global expect the control mix in which the failure was global only.

Table 3.14. Impact test results

No.	Number of hits till 1st crack	Number of hits till failure	energy at first crack = $N_1 mgh$	energy at failure = $N_2 mgh$	Increment of impact resistance due to rubber replacement%
RF	6	8	122.1	162.8	--------
S10	4	17	81.41	346.0	112.5
S20	7	35	142.4	712.3	337.5
S30	12	61	244.2	1241.5	662.5
G10	5	24	101.7	488.4	200
G20	8	38	162.8	773.4	375
G30	15	116	305.3	2361	1350

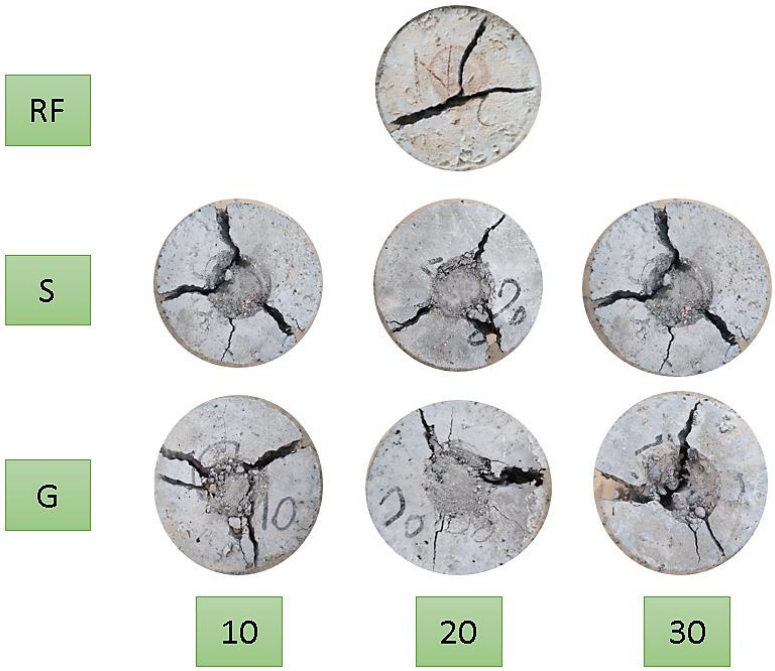

Plate 3.14. Specimens after failure due to impact load

3.5. Experimental CDBs Program

The selected experimental work was chosen to fill the scientific gap at literature that involved the CDBs. By ignoring rubberized concrete temporarily during scanning the researches, there is neither an indication about the behavior of CDBs under the effect of repeated and cyclic loads nor the response of CDBs exposed to an impact load. So, this dissertation deals with impact load effect on CDBs and also the repeated load. Beams deterioration and ductility after a single impact was also discussed by retesting the hitted beams statically and comparing their results with the ultimate capacity of pure statically loading of similar beams.

3.5.1. Tested Beams Details

Three percentages (10, 20 and 30%) of rubber replacement have been selected. The replacement is of sand or gravel for the single mix. The total number of mixes are seven. One mix without any replacement and the others of the mentioned percentages and properties which explains before at section 3.4. The total concrete beams are 21 specimen and it is divided into three groups. The first group which are 7 beams, tested by statically loading to obtain the ultimate load capacity of

rubberized CDBs. The second group (11 beams, one of them is a simply supported, to show the effect of continuity) is for beams which hitted by dropping weights (two weights are used, 30 and 40 kg both drop from 1.86 meters). Finally, the last group consists of three beams which are exposed to repeated load. The following Table 3.15 sums all details while Figure 3.4 shows the beams sketching. The design procedure is illustrated in **Appendix C**.

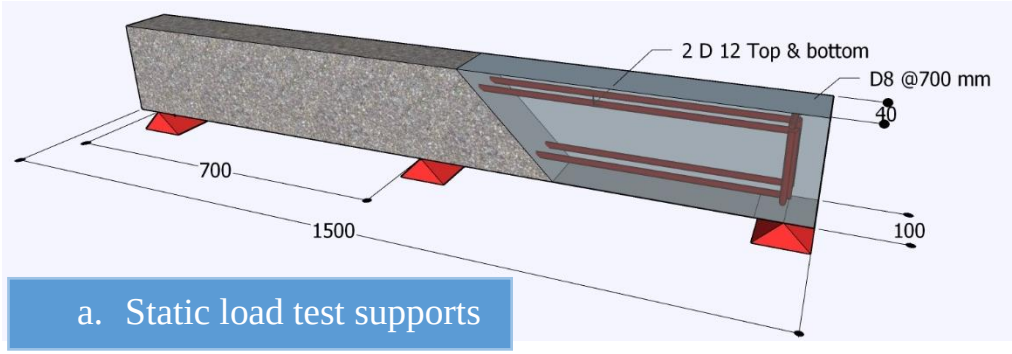

a. Static load test supports

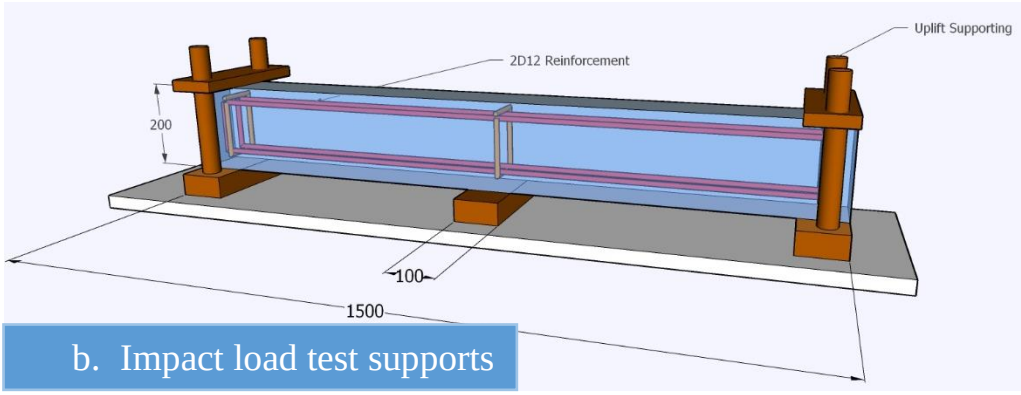

b. Impact load test supports

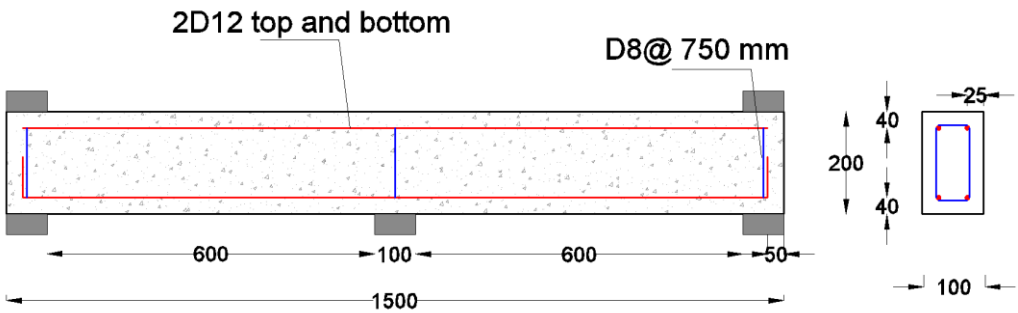

c. Beam reinforcement details

Figure 3.4. CDB dimensions and reinforcement, (all dimensions are in mm)

The first letter of beam sampling refers to the load type which may be **St**atic, **I**mpact or **R**epeated, noting that in the case of impact load it followed by the mass

of impactor. The second part defines the replacement method (**S**and or **G**ravel) and finally the replacement percentage. **SS** sample is an abbreviated for **s**imply **s**upported beam.

Table 3.15. Specimens' details

No.	Beam sample	Load type	Beams dimensions
1	ST	Monotonic load	200*100*1500
2	ST.S10		200*100*1500
3	ST.S20		200*100*1500
4	ST.S30		200*100*1500
5	ST.G10		200*100*1500
6	ST.G20		200*100*1500
7	ST.G30		200*100*1500
8	I30	Impact weight = 30Kg	200*100*1500
9	I30.S10		200*100*1500
10	I30.S20		200*100*1500
11	I30.S30		200*100*1500
12	I30.G10		200*100*1500
13	I30.G20		200*100*1500
14	I30.G30		200*100*1500
15	I30.G30.SS		200*100*750
16	I40	Impact weight = 40 Kg	200*100*1500
17	I40.S30		200*100*1500
18	I40.G30		200*100*1500
19	R	Repeated load	200*100*1500
20	R.S10		200*100*1500
21	R.G10		200*100*1500

3.5.2. Beams Casting and Curing

The concrete mixes were casted within two sequence days in the same weather conditions. All construction materials are saturated surface dry. Crumb and chip used were shown in Plate 3.15 and Plate 3.16. Water used was without salt, fit for human use. Wooden molds were made to get the specified beams dimensions (as clarified in Plate 3.17). Steel mesh was tied and placed within the molds at the exact covering lengths using spacers (as presented in Plate 3.18). A mixer of 250 Kg total weight was used (as exhibited in Plate 3.19). At the beginning, the mixer operated to mix the dry materials (gravel, sand, rubber, and then cement) only for one minute for unified their colors. Supper-plasticizer was added to the water and mixed well then applied on the mixer dry contents and mixed for one minute. Fresh concrete applied into molds and vibrated for compacting the mix into the molds in order to insure arriving the concrete for corners and underneath the steel bars. Beams' surfaces were smoothed and leaved one day to dry then cured by sinking into water for the ruled 28 days (as revealed in Plate 3.20). After curing, specimens were painted by white color to enhance observed small cracks.

Plate 3.15. Crumb rubber

Plate 3.16. Rubber chips

Plate 3.17. Beams wooden molds

Plate 3.18. Used steel reinforcement mesh and Molds preparing

Plate 3.19. Dry mixing

Plate 3.20. Casting fresh concrete into molds

3.6. Testing Systems

3.6.1. Static and Repeated Device

CDBs was tested using static universal press system load device as shown in Figure 3.5 and Plate 3.21. The device records the load versus deflection automatically using LVDTs. For more certainty, digital dial-gages of 25 mm capacity were also used as illustrated in Plate 3.22. The DIC technology was certificated by the experimental static results. Beams were stippled using black spry. The DIC technology based on following the movement of these black points to find its displacements.

With regard to supporting, a rigid steel girder was used with two roller supports and one stiff pin. The two point loads were gotten by using a rigid load distributer girder.

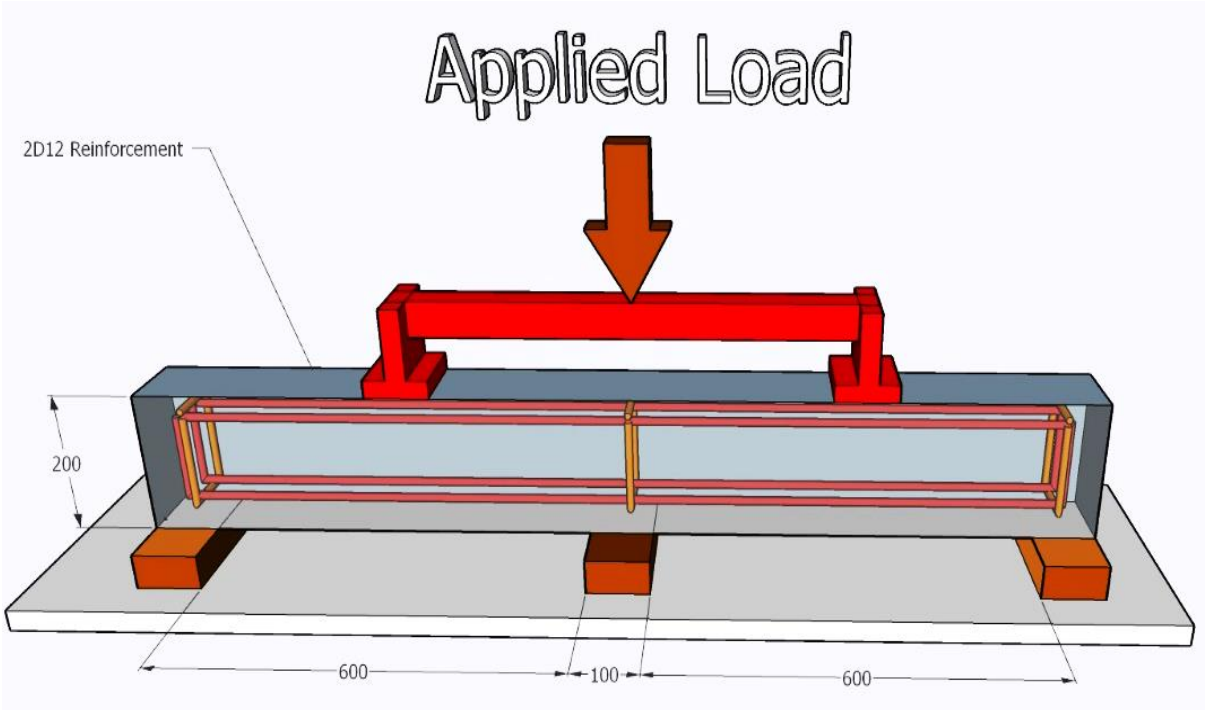

Figure 3.5. Static load test for CDBs (all dimensions are in mm)

Plate 3.21. Static universal press system, supports and load distributer

Plate 3.22. Used dial gages

3.6.2. DIC Technology

The technics gives the difficulties of experimental works encountered by experimental mechanicians during the postprocessing of photographically recorded measurement data, and the growth of image processing methods in the

vision community, it was natural for researchers to employ the recent progress in digital imaging technology [173].

A continuous deep beam was prepared to the Video image correlation, in which it requires speckling the beam by regular black points and videoing the beam under the stepped loading from near distance with a high accuracy camera.

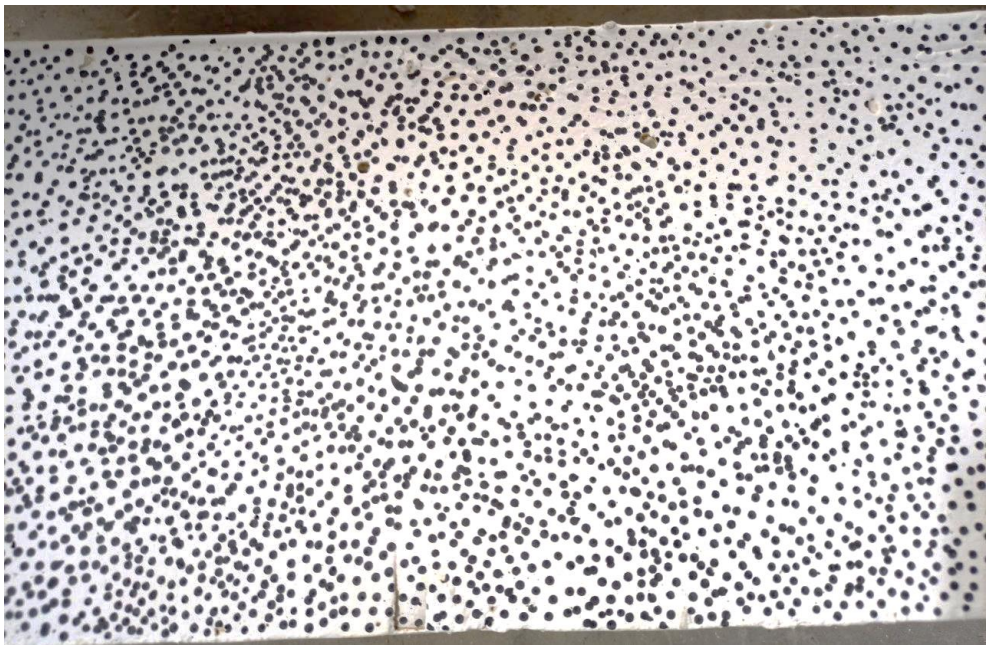

Plate 3.23. Beam speckling

3.6.3. Impact Loading

The easiest way to obtain impact loads in laboratory is by the falling mass object, see Figure 3.6. A steel spherical surface mass of 30 or 40 kg was dropped from 1.86m on the CDBs so as to be impacted s shown in Plate 3.24 and Plate 3.25. The beam during impact millisecond, uplifted due to the hit and it have to be prevented, so uplift supports at both ends were provided as explained in Plate 3.26 and Plate 3.27. These supports were fixed into the floor by casted them within the earth and then crossed over the beam then locked it by steel upper plates. All supports were of 100 mm width (as explained in Plate 3.26 and Plate 3.27).

Six strain sensors were fixed on each beam in order to collect beams' responses due to hits. The sensors placed in the most sensitive and effective points of CDBs

as shown in Figure 3.7. Strains were fixed at the middle line of struts or even ties zones. The Strut and ties were drawn accurately at the side face of beam Plate 3.28. Strains G1 and G6 used for calculating the exterior strut strains while G3 and G5 for the interiors. G2 and G4 strains necessary for investigating the tie strains. The left portion of all beams is selected as the impacted span.

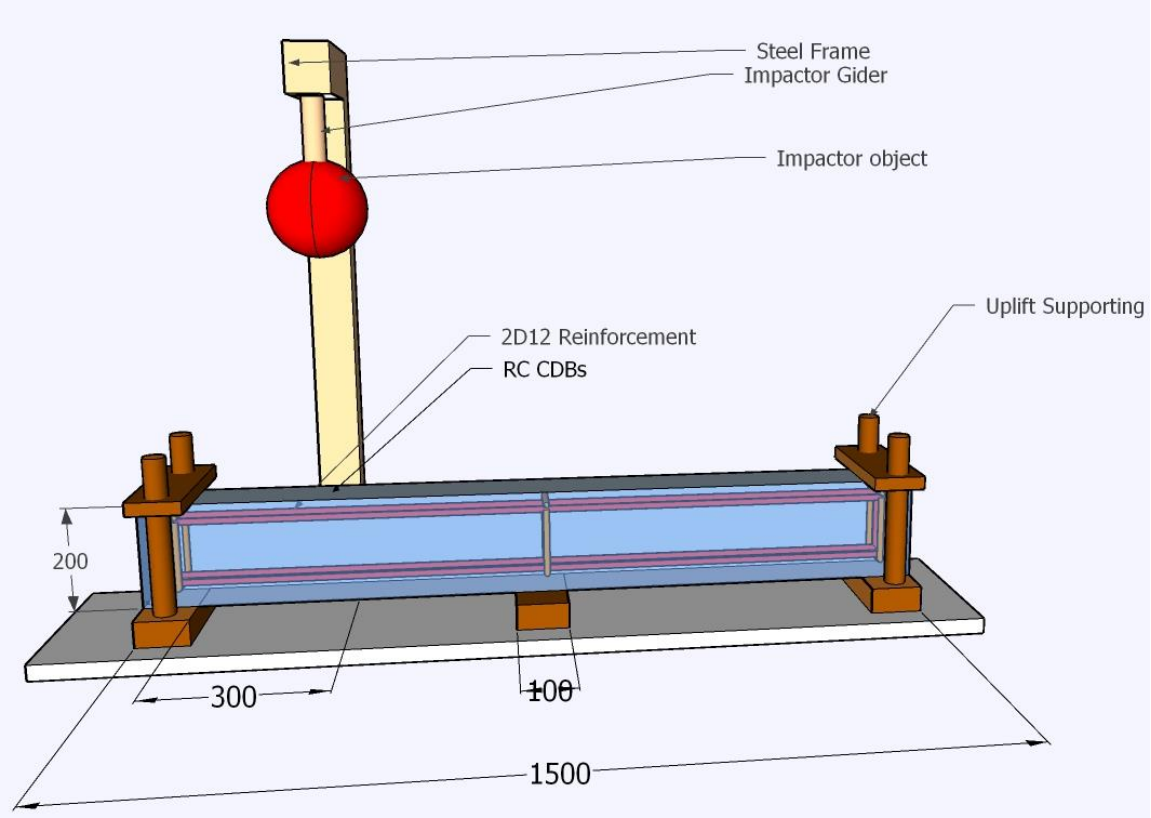

Figure 3.6. Sketching CDB under impact load (all dimensions are in mm)

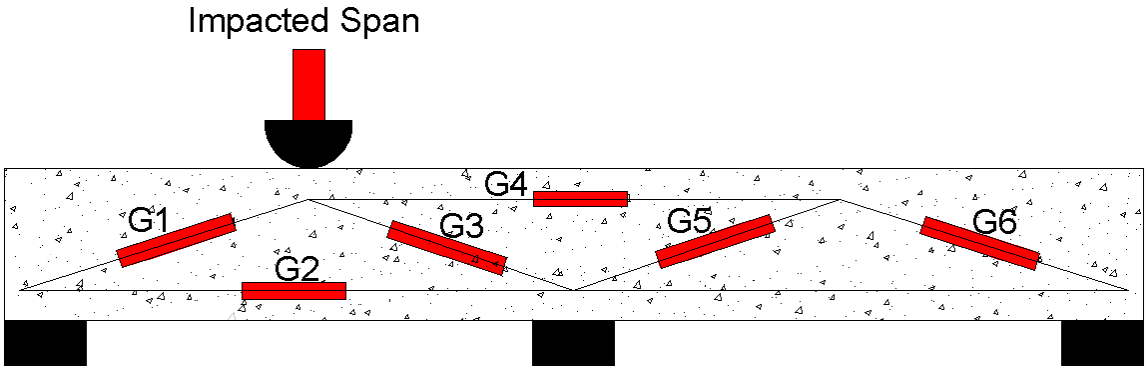

Figure 3.7. Strain gages' positions and numbering

Plate 3.24. Impact system

Plate 3.25. Dropping weight

Plate 3.26. Steel support

Plate 3.27. Uplift preventing hooks

A uniaxial strain resistance (foil) strain gages of 30 mm size and 120 Ω resistance were used (as explained in chapter one and **Appendix D**). A recommended adhesive (CN-E and CN-Y) used for fixing the gages into specimens. All the strain gauges were connected using quarter bridge circuit. Three processes have to be done to put the gages on specimens, which are:

- Sketching the strut and tie positions on beams to ensure the right exact sites, see Plate 3.28 and Plate 3.29.
- Scraping the strain position by glass-paper to softening it as shown in Plate 3.30, then washing the position by thinner liquid.
- Mixing the adhesive and applying it on the specified position then fixing the gage on it as explained in Plate 3.31.

After completing all strains, the beams left to dry for one day before testing Plate 3.32.

Plate 3.28. Strain gauge positions indicating

Plate 3.29. Identifying the exact position of the strain gages centers

Plate 3.30. Scraping the strain position

Plate 3.31. Fixing the gage

Plate 3.32. Beams after strains' instillation

The test program of this research is based on measuring the strain, using the NI 9235 quarter Bridge strain gauge and data logger as shown in Plate 3.33. NI 9235 and 9236 quarter_bridge strain gauge modules are designed for higher_channel_count, dynamic strain measurement systems based on NI Compact DAQ, Compact RIO, or other compatible C-Series hardware, with eight simultaneous channels per module. 44 Simultaneous sampling is important for higher-speed acquisitions where it is necessary to compare results from different locations at a particular instant in time, such as impact tests. Table 3.16 lists more details about the used data logger.

Plate 3.33. Data logger details

Table 3.16. Impact data logger details [174]

Number of channels	8 analog input channels
Quarter_bridge completion	120 Ω, 10 ppm/°C max
ADC resolution	24 bits
Type of ADC	Delta-Sigma (with analog profiteering)
Sampling mode	Simultaneous
Frequency	12.8 MHz
Accuracy	±100 ppm max
Data rate range using internal master time base fs	Minimum 794 S/s Maximum 10 kS/s
Data rate range using external master time base fs	Minimum 195.3125 S/s Maximum 10.547 kS/s
Full_scale range	±29.4 mV/V (+62,500 με/–55,500 με)
Scaling coefficient	3.5062 nV/V per LSB
Overvoltage protection between any two terminals	±30 V

3.6.4. Strain Gauges Properties

The instrument is a foil strain gauge of a polyester resin backing working in accordance the principle of the P series (where P-series is a series where the common exponent p is a positive real constant number). The gauge maybe found in three different lengths which are 10, 20 and 30mm, so it is suited mainly to strain measurement on concrete or mortar [175]. Figure 3.8 shows a sketch for the strain used.

Table 3.17. PFL-30-11-3LJC-F strain sensor properties [175], [176]

Resistance	120Ω
Applicable specimen	Metal, Concrete, Mortar
Backing	Polyester
Operational temp. (C°)	-20~ +80°C
Element	Cu-Ni
Bonding adhesive	CN-E, RP-2, PS
Kind:	Single element, for steel, concrete and mortar use

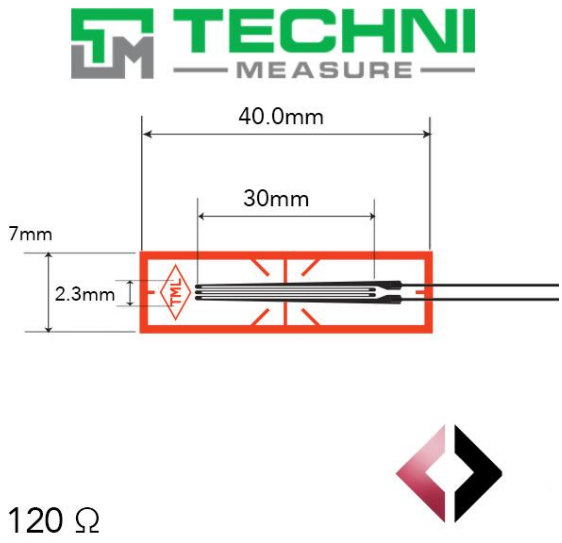

Figure 3.8. Strain sensor geometric properties [175]

CHAPTER FOUR: EXPERIMENTAL RESULTS AND DISCUSSIONS

4.1. Introduction:

After applying all mixing and curing processes, the CDBs have been tested under different loading types. This chapter views the results and their discussions for statically, repeated and impact loads loaded beams.

4.2. Monotonic Beams Results

After applying monotonic loads which mentioned previously, CDBs results were recorded and listed in Figure 4.1 to Figure 4.7. It can be concluded that, sustainable rubberized CDBs results supported the literature conclusions especially which involved to the STM, where the experimental load is larger than the theoretical one which approves that the STM is a lower bound theorem.

From figures Figure 4.1 to Figure 4.7, it can be found that, The CDBs lose some of its ultimate capacity due to the dropping of concrete compressive strength after aggregate-rubber replacement, while an increment in the deflection could be seen due to the higher deformability of the rubcrete mix i.e. the concrete gained some flexibility after replacing. From Table 4.1, It can be also noted that, 39%, 52% and 56% of the concrete conventional beam capacity decreases after replacing 10%, 20% and 30% of gravel respectively, While the decrement in ultimate strength was observed for 10%, 20% and 30% of sand replacement by 30.1%, 39.1% and 52.38% respectively. One can conclude that, gravel replacement is better than the sand replacement according to the ultimate strength.

The failure load mechanism was pure shear for all specimens. The cracks start to form in bending zones then the behavior converts towards the shear failure as observed previously in the literature researches [5].

Table 4.1. Ultimate load capacities and displacements for static loads group

Sample	Ultimate Load (kN)	Ultimate right span deflection (mm)	Ultimate left span deflection (mm)	Reduction for ult. load (%)
ST	378	5.20	6.55	------
ST.S10	230	1.92	2.30	39.16
ST.S20	180	2.90	3.70	52.38
ST.S30	165	3.50	3.90	56.35
ST.G10	264	1.60	1.92	30.15
ST.G20	230	6.00	5.10	39.16
ST.G30	180	7.50	8.15	52.38

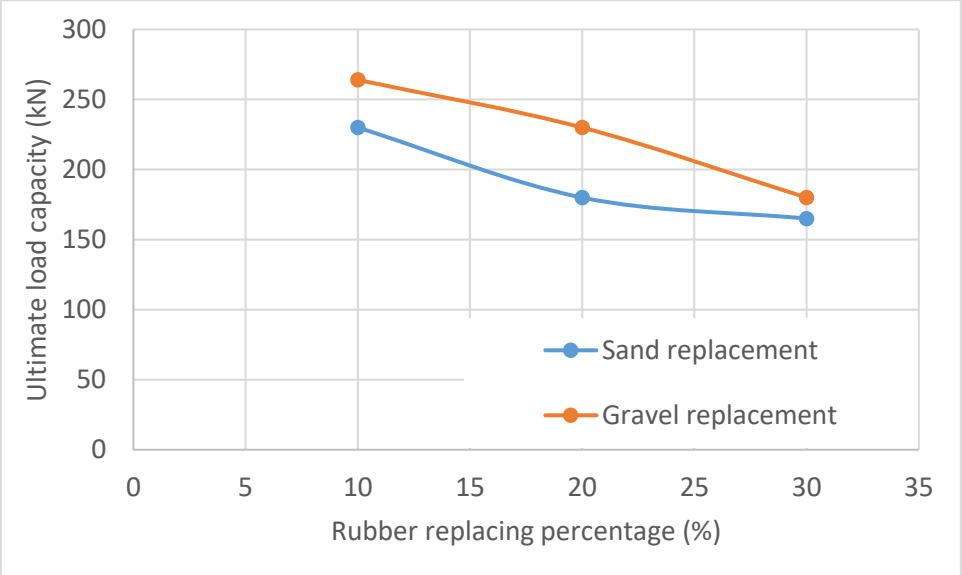

Figure 4.1. Ultimate load capacity for specimen under monotonic load

For sand sample replacement, at 165 kN, left span, the deflection for 10%, 20% and 30% equals 1.25 mm, 3 mm, and 3.5 mm respectively. Also, for the gravel replacement samples, at a fair load like 165 kN, the deflection for the same percentages of replacements was 0.65 mm, 4.2 mm, 4.3 mm respectively. That's means the increment in rubber amount rises the ability of beams to deflect under the same level of loading due to increase their flexibility after replacement. Also,

it appears that the gravel replacement has flexibility greater than the sand replacement.

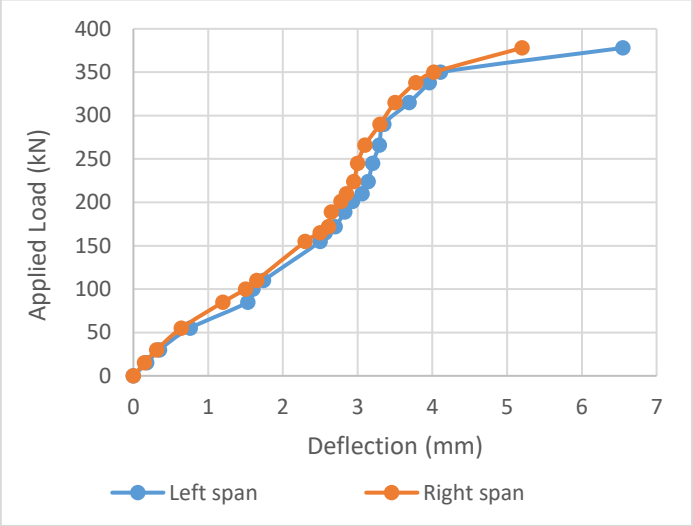

Figure 4.2. Load vs deflection curve for ST sample

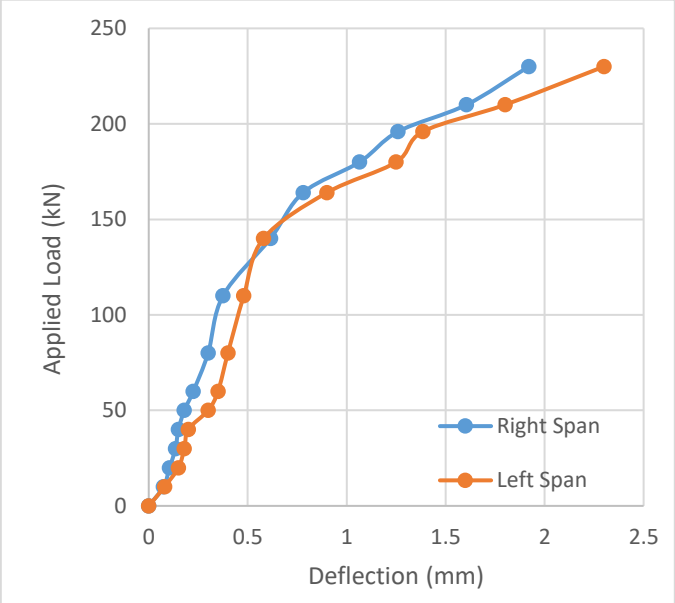

Figure 4.3. Load-deflection curves for ST.S10 specimen

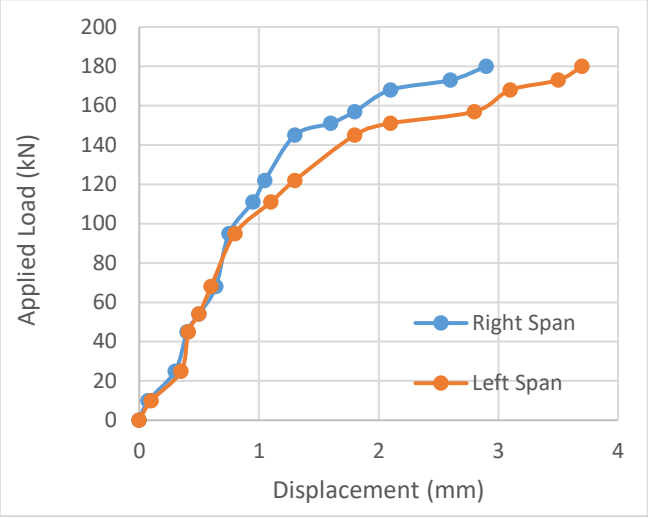

Figure 4.4. ST.S20 Rubcrete beam statically loading results

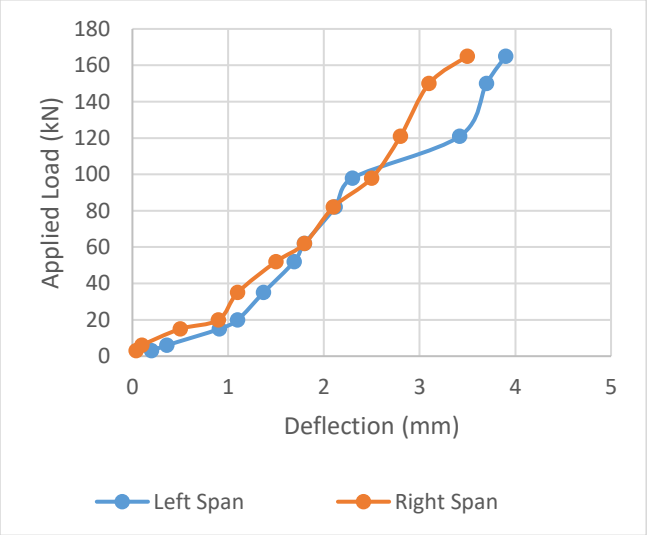

Figure 4.5. ST.S30 Rubberized CDB results monotonically loaded

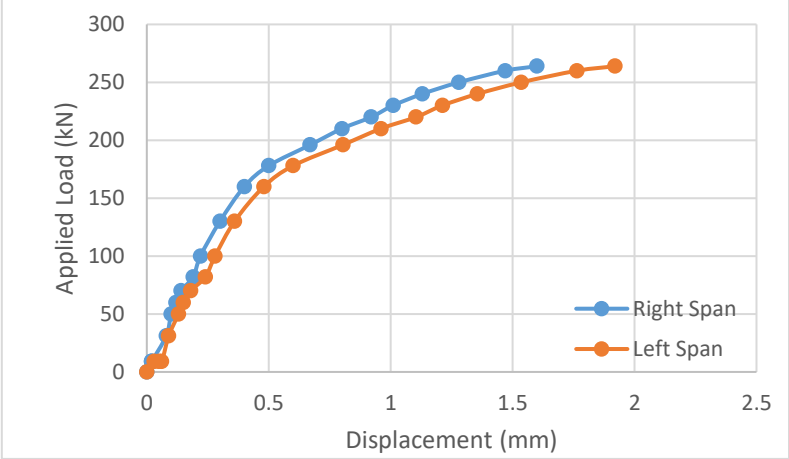

Figure 4.6. Statically loading ST.G10 beam

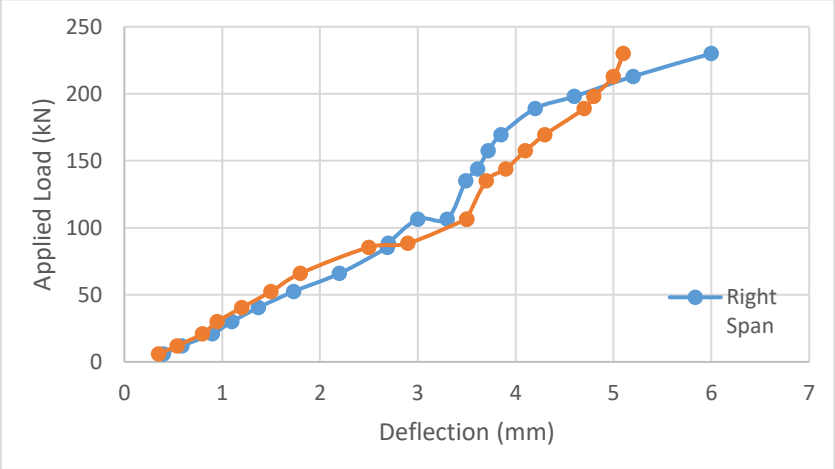

Figure 4.7. Load deflection curve for ST.G20 member

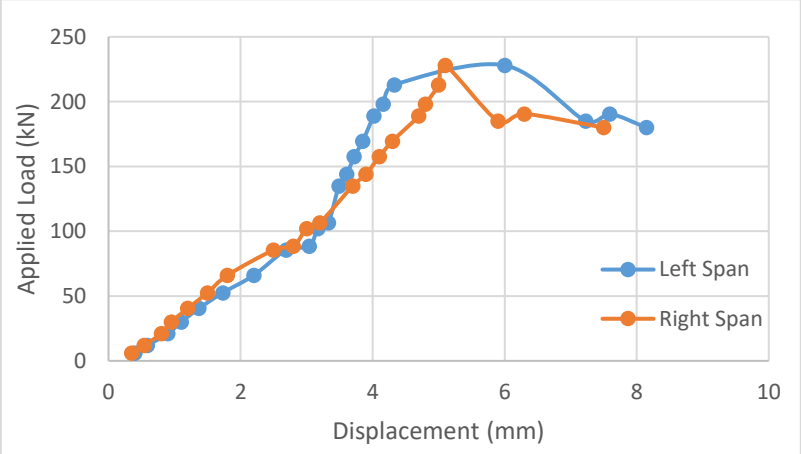

Figure 4.8. ST.G30 static load results

Plate 4.1. Statically test for conventional beam

Plate 4.2. ST.S10 specimen crack patern

Plate 4.3. ST.S20 cracked beam

Plate 4.4. ST.G30 monotonic failure mechanism

Plate 4.5. Failure shape of ST.G10

Plate 4.6. ST.G20 failure mode

Plate 4.7. Failure mechanism of sample ST.G30

DIC technology views the strain energy which appears on the side of 2D face of beam, which it also indicats strain transfer and generating during the test. Beam

defflection at any point may also gain from this technic. The DIC results for the tested beam (ST. G10) were slightly approched to the Dial-gage results (as shown in Table 4.2) , the slight difference is because of the farness of camera which could not track beam point movement accurately and the camera quality. For the first stages of loading, the stress generated along the beam as a red random irregular areas (Figure 4.9.a), then the interior strut starts to be appeared at the left span (Figure 4.9.b), continued the loading, all over other struts generated during high loading as well as the positive bending stress also cleared (Figure 4.9.c), and finally, the collapse at the left strut viewed at the collapse load of the member.

Table 4.2. LVDT and DIC deflections for every load step of ST.G10

Applied load (kN)	LVDT right span deflection (mm)	DIC right span deflection (mm)
0	0	0
9.1	0.02	0.042
9.1	0.02	0.06
9.1	0.02	0.08
31.2	0.08	0.12
50	0.1	0.13
60	0.12	0.18
70	0.14	0.19
82	0.19	0.24
100	0.22	0.31
130	0.3	0.38
160	0.4	0.52
178	0.5	0.682
196	0.67	0.856
210	0.8	0.88
220	0.92	0.99
230	1.01	1.08
240	1.13	1.21
250	1.28	1.26
260	1.47	1.53
263.9	1.6	1.92

(a)

100 kN

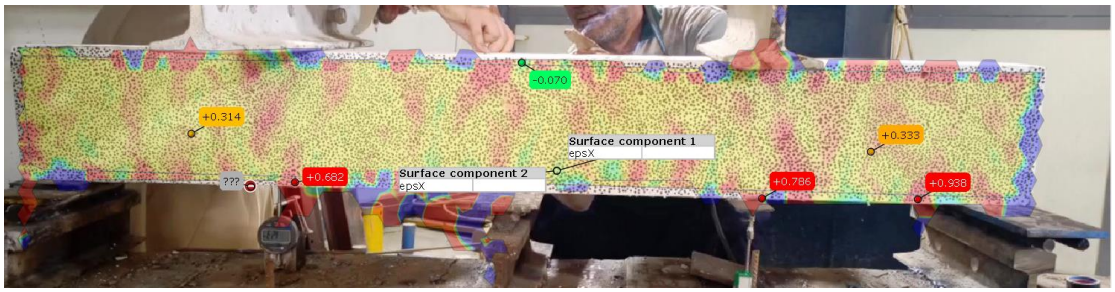

(b)

160 kN

(c)

210 kN

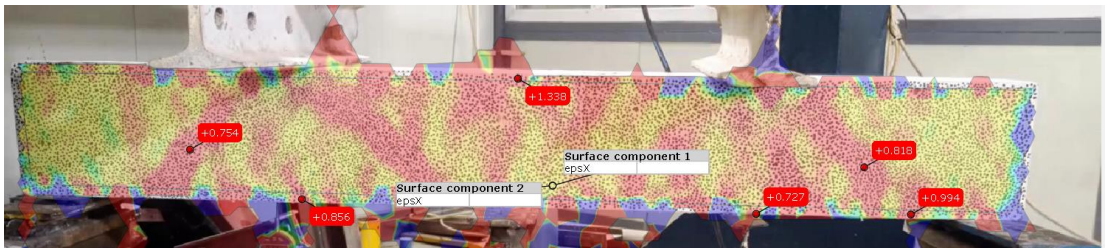

Figure 4.9. DIC deflection development

ST.G30 specimen was randomly chosen to investigate the monotonic load versus strain, the data-logger contain two channels for the strain data. At the external and internal strut, six strain gages were instilled but just two of them could be tested which are inside the red circles G1 and G3 (Plate 4.8). Strain results were listed at Figure 4.10. The internal points strains larger than the external because of the internal stress which develops to form the other span. The data after this stage of loading point were lost because the beam starts to be cracked at the strains instillation points.

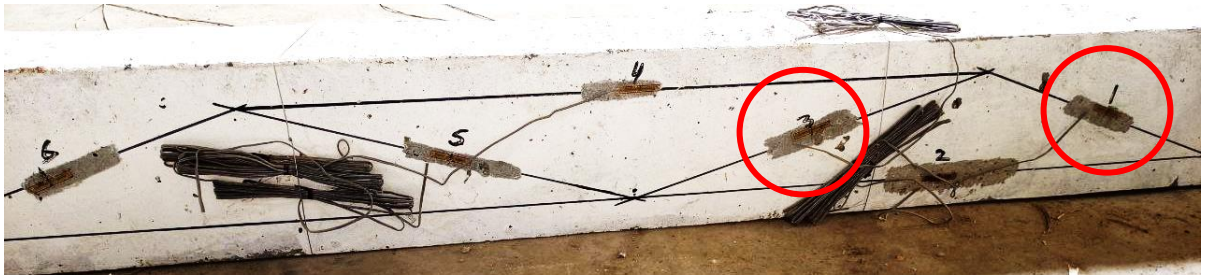

Plate 4.8. ST.G30 strain gages

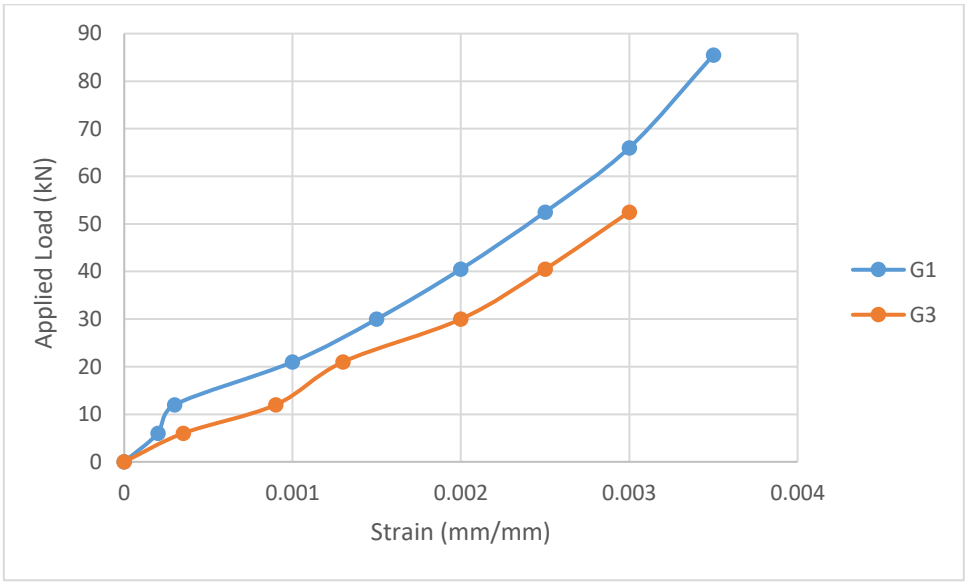

Figure 4.10. Strain versus load curve for the ST.G30 beam

4.3. Impact Load Results

After testing device preparing and instillation, the dropping weights were subjected on the specimens and the response were recorded using the strain gages. All results and discussions were listed in this section.

4.3.1. Specimen I30

From Figure 4.11, it can be noted that, the CDB deformed in a manner matches with the STM. The impacted panel struts compressed (G1,G3) while the tie in between undergoes to tensile strain during the hit. The other span match the first natural mode of continuous beams (which mentioned at chapter one), in which the unloaded span cumbered during the hit and it causes a tensile strain at its struts. G6 is slightly higher than G5 and approached to be equal. The little difference in

strain due to the uplifting pressure which concentrated at the external supports. G6 is nearer to this stress concentration zone than G5. It is worth to mention that, the strain values still the same for full 10 second. The maximum strain value for this sample is a tensile strain equals 0.003 for the impacted bending point, followed by the negative impacted strut which reads -0.00276 which for G1. The crack pattern which shows for such sample viewed a strut cracks at the impacted span, negative crack moment, uplifting crack at the farer support and a bending cracks at the un-impacted span (Plate 4.9).

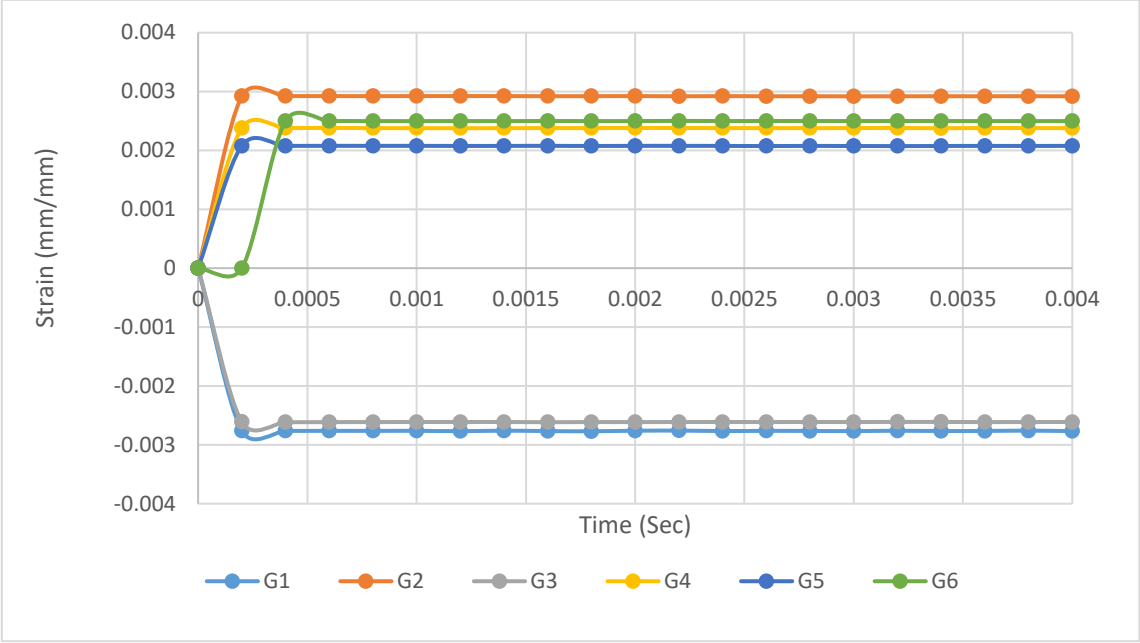

Figure 4.11. Strain-time results of I30 member

Plate 4.9. Impacted I30 specimen cracks

4.3.2. Specimen I30.G10

Adding rubber gained the result some fluctuates when comparing with I30 as viewed in Figure 4.12. G3 point shows rising strain from zero to a maximum negative strain -0.001875 then suddenly reflect to a maximum positive value equals 0.001811, followed by some another positive strains and then reflected again to the negative zone and steady there. An approach opposite wave is observed from the strut curves at the un-hitted span G6. The impacted span seems to be affected by a reverse wave from the right span at the time 0.0002 to 0.002 seconds, G1 shows the slighter affectivity by the reflecting. G1 dominates the higher negative strain value which equals -0.0022545, while the higher positive strain was obtained from G6 which equals 0.0029445.

G6 dominates the higher strain value for this specimen due to the uplifting stress. It is effected also by a straight vertical crack occurred due to uplift at exactly the middle distance of the farer support. The beam sample bent with hit but cambered at the second span due to the continuity till getting small visible crack at the top of the un-hit span as illustrated in Plate 4.10.

Adding 10% of chip replacement decreases the negative strains G1 and G3 by 21% and 28% respectively and 29% decrement for the impacted tie zone (G2).

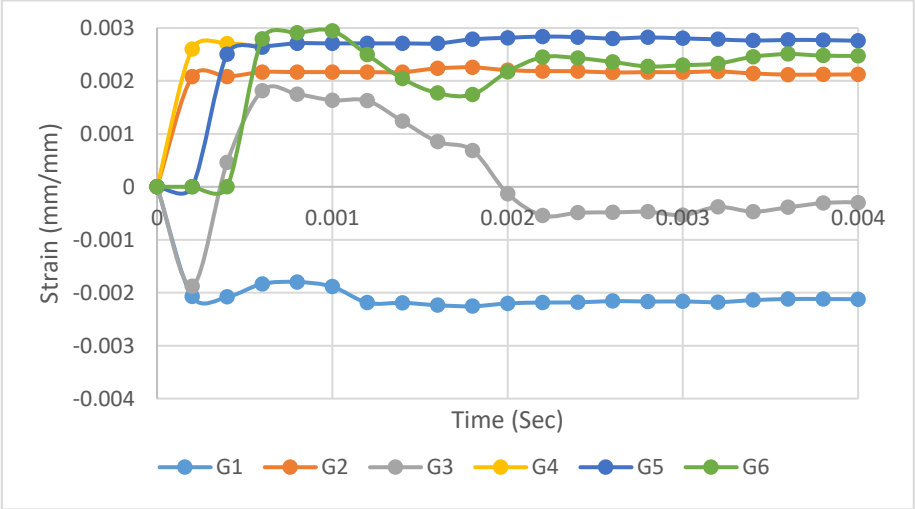

Figure 4.12. Strain-time curves of sample I30.G10

Plate 4.10. I30.G10 cracks after impact

4.3.3. Specimen I30.G20

The same behavior for CDB is observed for I30.G20 in comparing with the I30.G10 (Figure 4.13). G3 affected by a reverse strain traveled from the un-impacted span which cause the curve to bend towards the positive axis noting that G5 showed the same opposite behavior. The uplifting pressure dominates the higher positive strain values (G6). G6 and G5 were the more sensitive to the hit, at the same time the G3 suffers from effective cracks at its strut. G1 also introduces higher strain values, by referring to the beam crack pattern, a vertical crack observed at the nearby middle support which affects the strain of G1. Negative and camber vertical cracks also seen at this sample as shown in Plate 4.11.

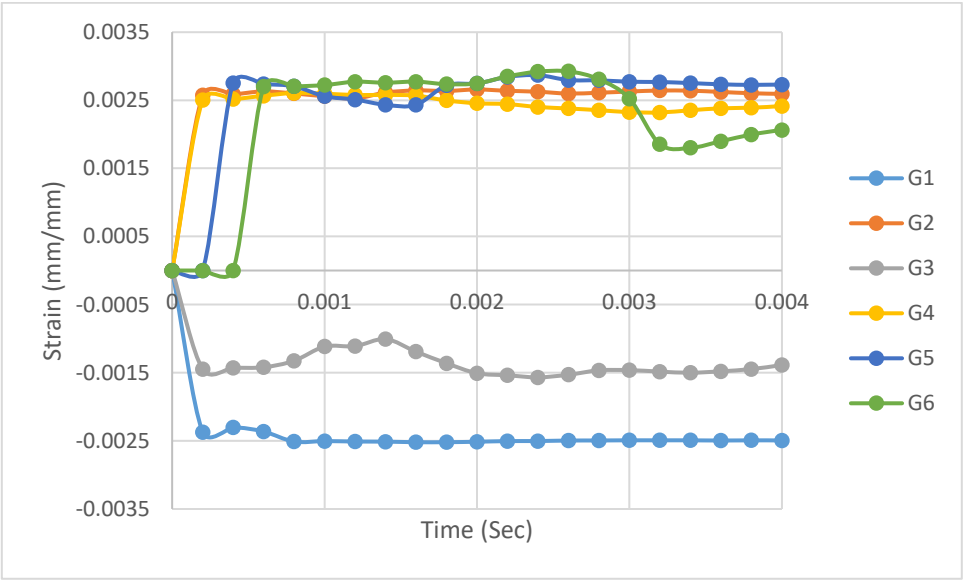

Figure 4.13. Strain-time curves for I30.G20 specimen

Plate 4.11. Effect of impact on I30.G20 member

4.3.4. Specimen I30.G30

Figure 4.14 introduced that, the sample reflected slightly after the hit (This could be noticed by observing G3 strain values decrementing at 0.0004 sec to 0.0018 sec, as well as the opposite wave of G5. This behavior appears at this specimen due to the high flexibility of G30 rubcrete mix. G2 controlled the higher positive moment values with G1 dominate the higher negative strains as usual. Visible cracks were noticed at G1 and G3 (see Plate 4.12Plate 4.27). The free vibration of G6 settles at 0.4 seconds, G3 and G4 calm down after 0.93 seconds, and G1 and G2 rest at 0.0068 seconds.

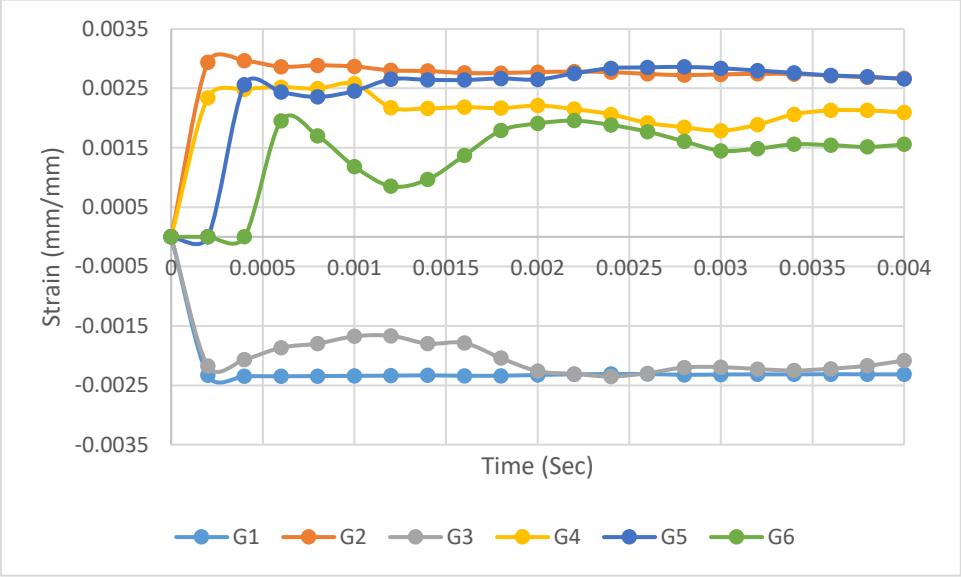

Figure 4.14. I30.G30 Strain-time curves

Plate 4.12. Impacted I30.G30 sample

4.3.5. Specimen I30.G30.SS

The difference between continuous and simply supported deep beam is the focused on goal for this sample. Figure 4.15 shows the large differences, i.e. the simply beam resist the impact by bending while the struts opposite the bending strain as an attempt to equilibrium the stresses on beam. Such behavior seen at I30.G30 due to its high ability to bend due to its flexibility. It may be changed at the lower percentages of rubber replacement. The behavior may depend on shear wider. Shear visible cracks at struts are observed as shown in Plate 4.13. As expected, the positive moment strain for the simply supported specimen is larger than the continuous, due to the present of the tie which activates the second span. The maximum positive moment observed at the second 0.0008 which was 0.0035, while the maximum compressive strains were 0.00210 and 0.00223 for G1 and G3 respectively.

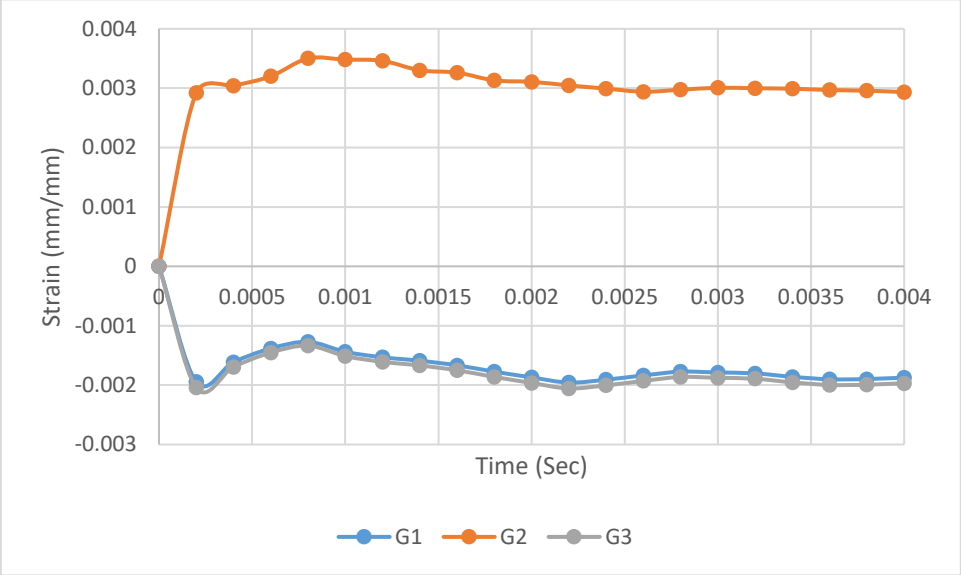

Figure 4.15. Strain-time results of simply supported beam

Plate 4.13. Simply supported I30.G30 crack pattern

4.3.6. Specimen I30.S10

Effective cracks at G3 and G6 can be identified when observing the results of I30.S10 specimen at Figure 4.16. G3 suffers from more fluctuates and settles after 0.4 sec while G6 rests after 0.234 sec. G4 works as a bridge travel the load to the un-impacted span. G2 dominates the higher positive strain value of 0.00303 while G1 dominates the higher negative strain of -0.002642. G4 convert the load into the second span at an approximately constant strain equals 0.00267. From crack pattern shown in Plate 4.14 and Plate 4.22. The specimen suffered from strut cracks at impacted span and flexural cumber cracks at the other span.

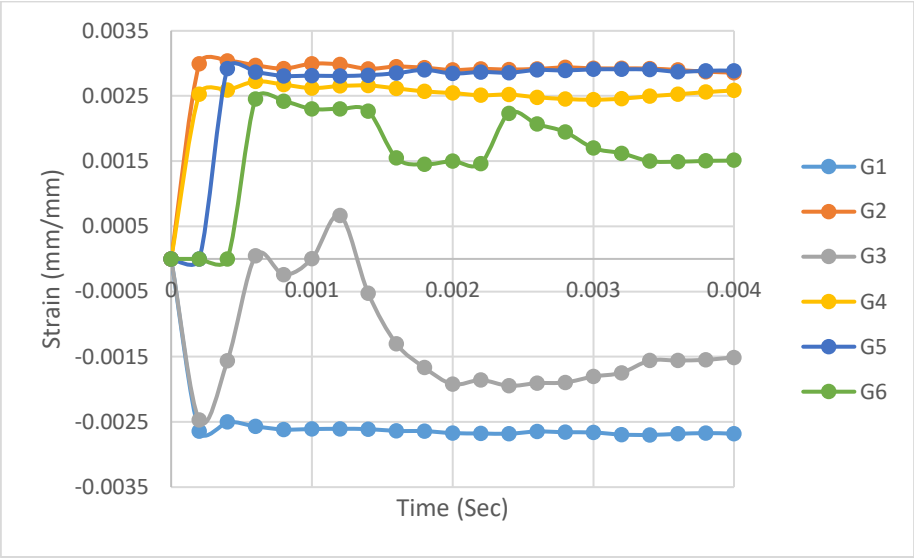

Figure 4.16. Strain-time results of I30.S10 specimen

Plate 4.14. Crack pattern of impacted I30.S10

4.3.7. Specimen I30.S20

G3 compressed during the hit as well as G1. G1 controls the higher compression strain of 0.002348 and still steady to the end of the free vibration. While G3 waved during the hit and settles down after 0.04 sec. G2, G4 and G6 vibrate reversely with G3 and so effected by it. All rest after 0.01 sec from the impact. For such specimen, the concrete compressive strength and the percentage of rubber allow to the beam to still waved totally. The bending strain at G2 shows an effective values due to the higher bending capacity of rubcrete beams (0.003278). Diagonal strut cracks appears at the impacted span, negative moment vertical cracks and a vertical crack at the middle of farer support as shown in Plate 4.15.

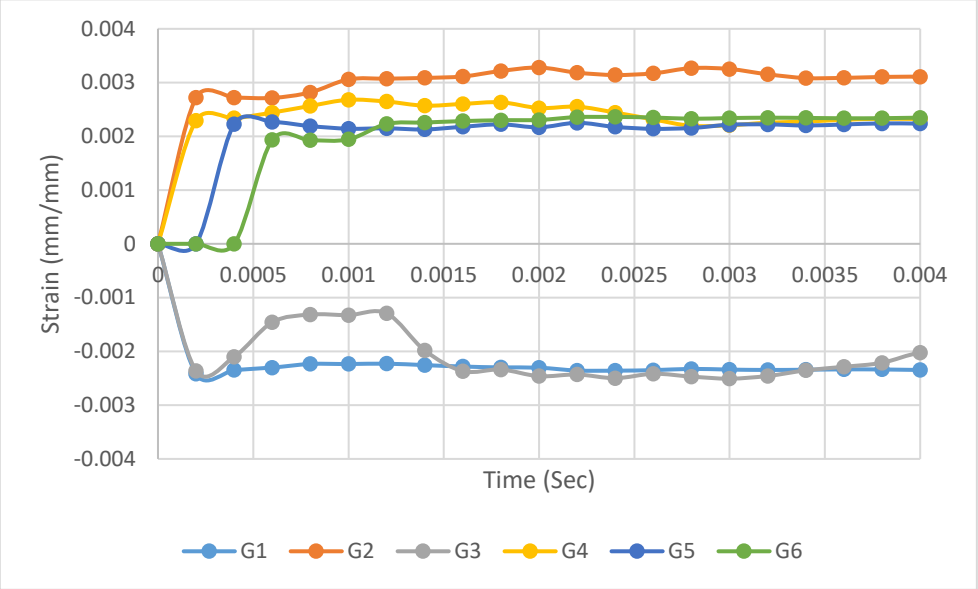

Figure 4.17. Strain-time curves for I30.S20 member

Plate 4.15. I30.S20 failure mode due to impact

4.3.8. Specimen I30.S30

The strength of this sample as well as the amount of rubber allowed the beam to vibrate totally with the hit. G1 and G3 compressed in the same behavior and the same magnitude of negative strain. G6 strained positively but at the opposite of them. G4 opposite the behavior of G6 in spite of they are both in tension. Flexural strength of rubcrete mix affects the behavior of CDB by incrementing the strain value at the bending zone G2. Asymptotic results can be noticed at G4 which is dominates the higher positive strain values of 0.00376 at 0.001 sec. As well as I30.S20, G3 and G6 show the same fluctuated (vibrated harmony) till 0.005 sec then reversed. G1 strains equals G3 as shown in Figure 4.18 as a one line. G5 introduce the same value (0.002167) all over the period. Both of the hit strut,

negative moment zone and at the half of the upper un-impacted span as explained in Plate 4.16 and Plate 4.24.

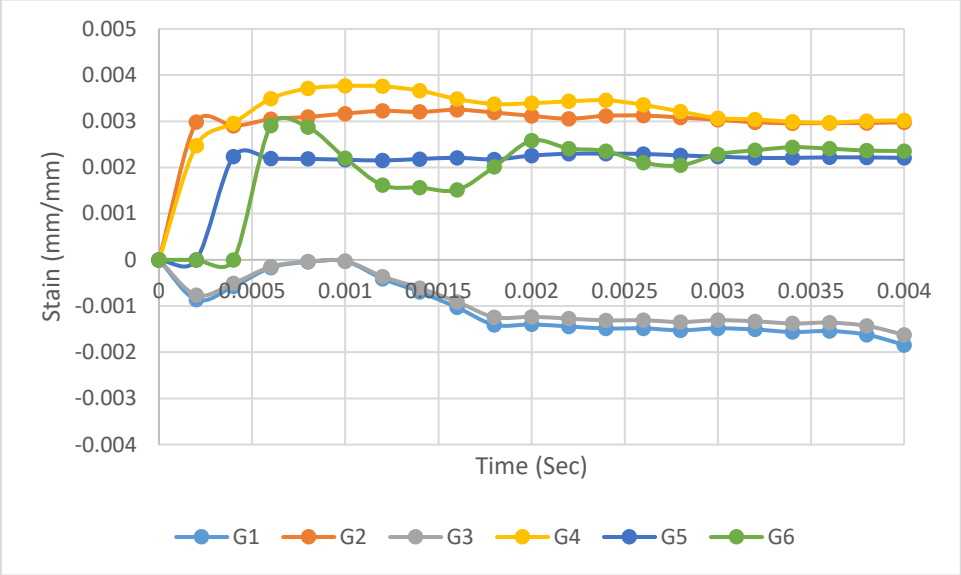

Figure 4.18. Strain-time results of I30.S30

Plate 4.16. I30.S30 crack mode after impact

4.3.9. Specimen I40

Logically, the same behavior which presented by I30 is also presented by the specimen I40. Approximately, a constant value of strains appear from G2, G5 and G6 while there are some fluctuates at the other strains' results. G1 and G3 seem to vibrate together between 0.004 sec to 0.0024 sec. G4 fluctuates reversely at the same period, as explain in Figure 4.19. The maximum strain value is recorded by G2 (equals 0.0031) and it is logical results for conventional concrete mix. But it appears higher than I30, due to increase the dropping weight. Both impacted struts

were cracked due to the hit, upper face of middle support as well us cumber cracks at the un-impacted span (Plate 4.17). All vibrations settle after approximately 0.00068 sec.

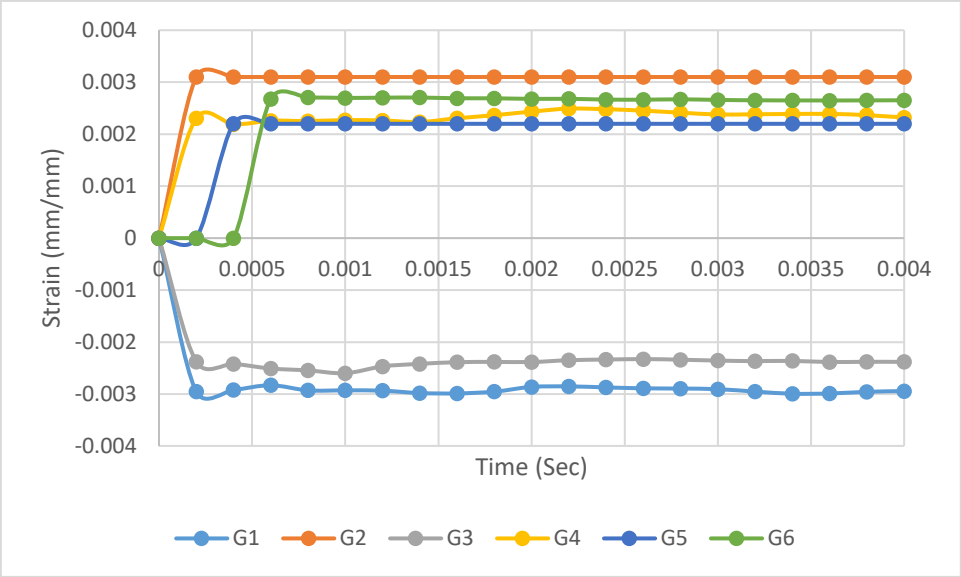

Figure 4.19. Strain versus time results of the beam I40

Plate 4.17. Cracks of I40 after impact

4.3.10. Specimen I40.G30

G2, G5 and also G4 introduce the same constant value of straining at the hit as listed in Figure 4.20. G3 introduce irregular pleats, the strain values drops to the negative zone then recovered into the positive, returns back into the negative zone and fluctuated there till rest at 0.08 sec. G1 shows a similar tiny behavior but without converting to the positive strain zone. G1 and G3 values meet at 0.003 sec but diverge after that, G1 steady on its higher compression strain (-0.002045) and G3 fluctuates above it as explained in Figure 4.21. For G3, many pleats

formed along the curve then undergoes the free vibration and rests after 0.1 sec as explained in Figure 4.21.

A vertical crack formed at the external un-impacted support center, vertical negative moment camber cracks, in addition to the diagonal strut shear cracks were formed at that sample (as explained in red lines at Plate 4.18) .

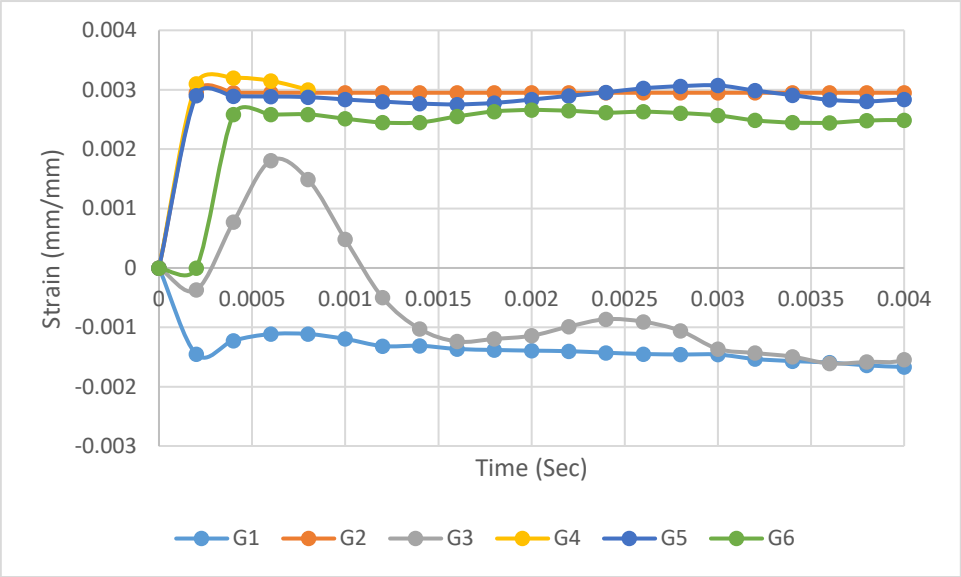

Figure 4.20.Strain versus time results of I40.G30 specimen for 0.004 sec

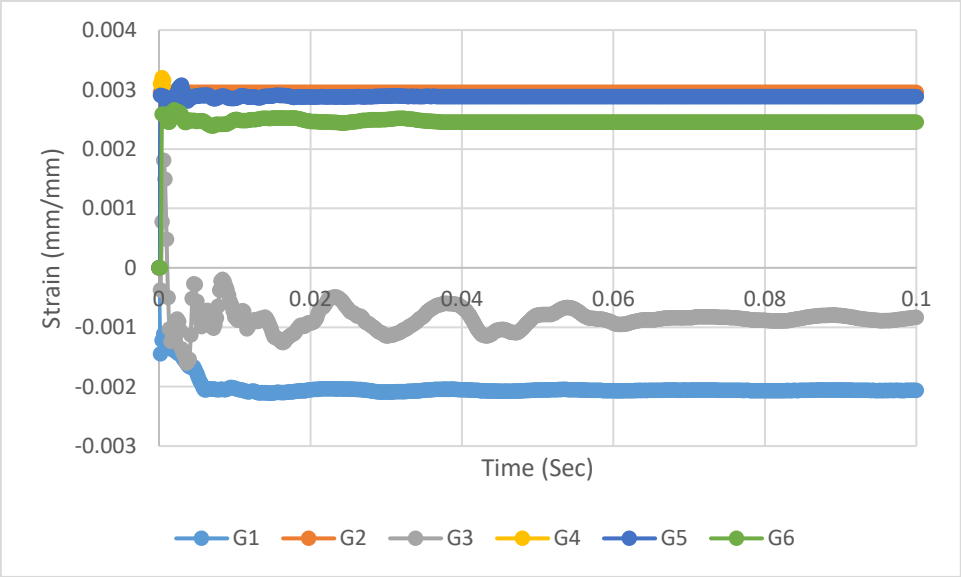

Figure 4.21. Strain versus time curves for I40.G30 till 0.1 sec

Plate 4.18. Crack mode of I40.G30

4.3.11. Specimen I40.S30

G1 and G3 are deformed compressively, G3 dominates the higher strain value (-0.0028) and keep its top for small period of time (till 0.001 sec) then it strain minimized and G1 steady at the higher compressive strain which equals 0.0024, so appears at Figure 4.22, the same behavior was noticed at I40.G30. A sharp drop is investigated due to forming and effective cracks nearby their zones. An opposite behavior can be investigated from G4, which means that, it moves the load widely to the other span. As well as, G2 and G5 identify the same constant straining rate (0.00302) against the hit. G6 and G4 deform at the same period of the other struts then descended to constant values 0.00202 and 0.00245 respectively. The cracks form at both impacted strut, cumber cracks and also cracks halved the external un-impacted support, as explained in Plate 4.19.

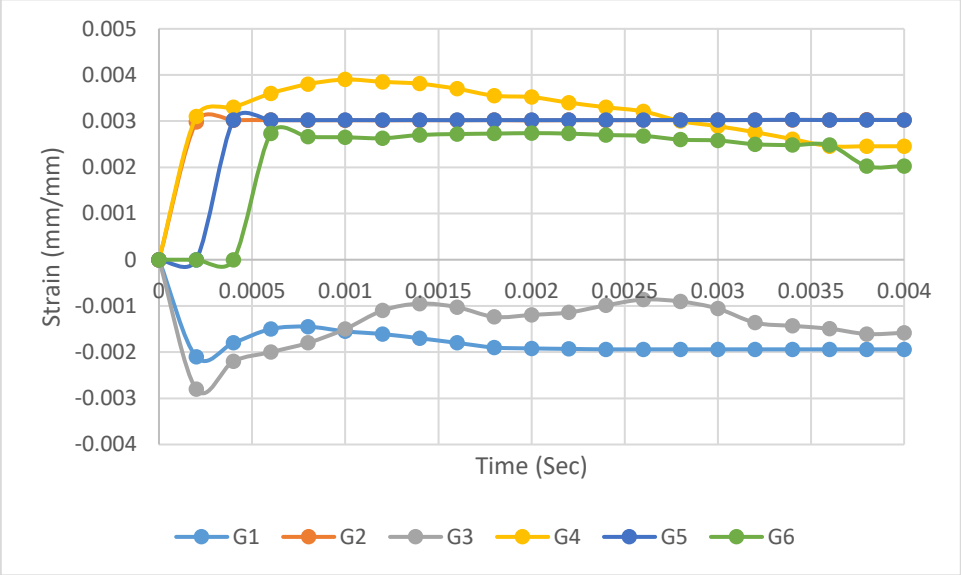

Figure 4.22. Strain-time curves of I40.S30 sample

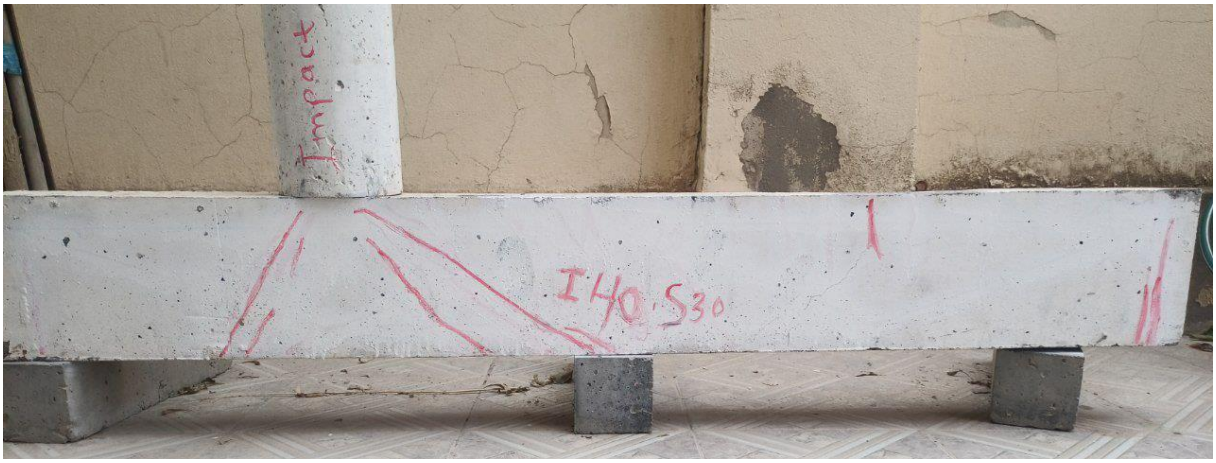

Plate 4.19. Crack pattern of I40.S30 specimen

4.4. Comparisons between Struts and Ties of Beams

The maximum absolute value of negative or positive strain for each beam and for every strain position were listed in the Table 4.3.

It can be concluded that, the higher strain value of G1 position observed at I40 due to the higher hit intensity when comparing with I30. Increasing the impact intensity by 33.34% on the reference beams leads to increase the strain by 7.04% at G1, %.5.8% for G2, 0.0 % for G3, 6.7 for G5 and 7.4% for G6, while decreasing G4 by 4.8%.

For the 30kg beams, replacing sand versus crumb by 10%, 20% and 30% leads to rising all G2 strains by 2.3%, 10.7% and 10.97% respectively, while decreasing G3 strains by 25.6%, 4.2% and 63.1% respectively.

The variation between such results is not graduated. The strains behave as a one body and convert the deformation between each other, so it cannot get an exact behavior, besides the fact that, the data in Table 4.3 built up on the maximum absolute maximum strain along the hit, which may happen at different times between the beams.

G6 Competes with G2 on the maximum tensile strain value. It can be noted that, the impacted tensile strain (G2) in all members is greater than the uplifting strain value except at I30.G10 and I30.G20 beams. It's due to that, these two beams may resist the load by uplifting larger than to be bent.

When discuss the effect of discontinuity of the beams (I30.G30 and I30.G30.SS), it can be said that, the simply supported beam prefers to bent to overcome the load by shear, G2 is larger for simply by 15% than the continuous beam.

Table 4.3. Maximum strain values for each specimen

Specimen	G1	*G2	G3	*G4	*G5	*G6
I30	0.00277	0.00292	0.00261	0.00238	0.00207	0.00250
I30.S10	0.00277	0.00299	0.00194	0.002722	0.00290	0.00245
I30.S20	0.00251	0.00327	0.00250	0.00255	0.00225	0.00235
I30.S30	0.00281	0.00328	0.00253	0.0037563	0.00229	0.00290
I30.G10	0.00225	0.00225	0.00150	0.00270	0.00283	0.00279
I30.G20	0.00251	0.00265	0.00156	0.00260	0.00286	0.00292
I30.G30	0.00234	0.00296	0.00225	0.00257	0.00286	0.00195
I30.G30.SS	0.00210	0.0035	0.00223	------	------	------
I40	0.00298	0.00310	0.00261	0.00227	0.00222	0.00270
I40.S30	0.00194	0.00302	0.00160	0.00385	0.00302	0.00274
I40.G30	0.00210	0.00295	0.00160	0.00320	0.00307	0.00284

* Tensile strain

4.4.1. Impacted Left Strut (G1)

Under such hit situation, G1 suffer from compression strains their values were shown in Figure 4.23 for 0.004 sec. It can be noted that, the strain maximum value of reference models (I30 and I40) don't accede the conventional concrete straining point which is 0.003. I40 specimen shows a strain larger than I30 due to its higher stress. Replacing gravel by chips leads to rising the strain values for the same magnitude of impact due to the dropping in concrete compressive strength and the higher strain for rubcrete mixes. Approximately, at the same period of time, G1 curves have fluctuated after 0.0002 sec, after a peak negative value, and then rest after a while of time depending on rubcrete mix details.

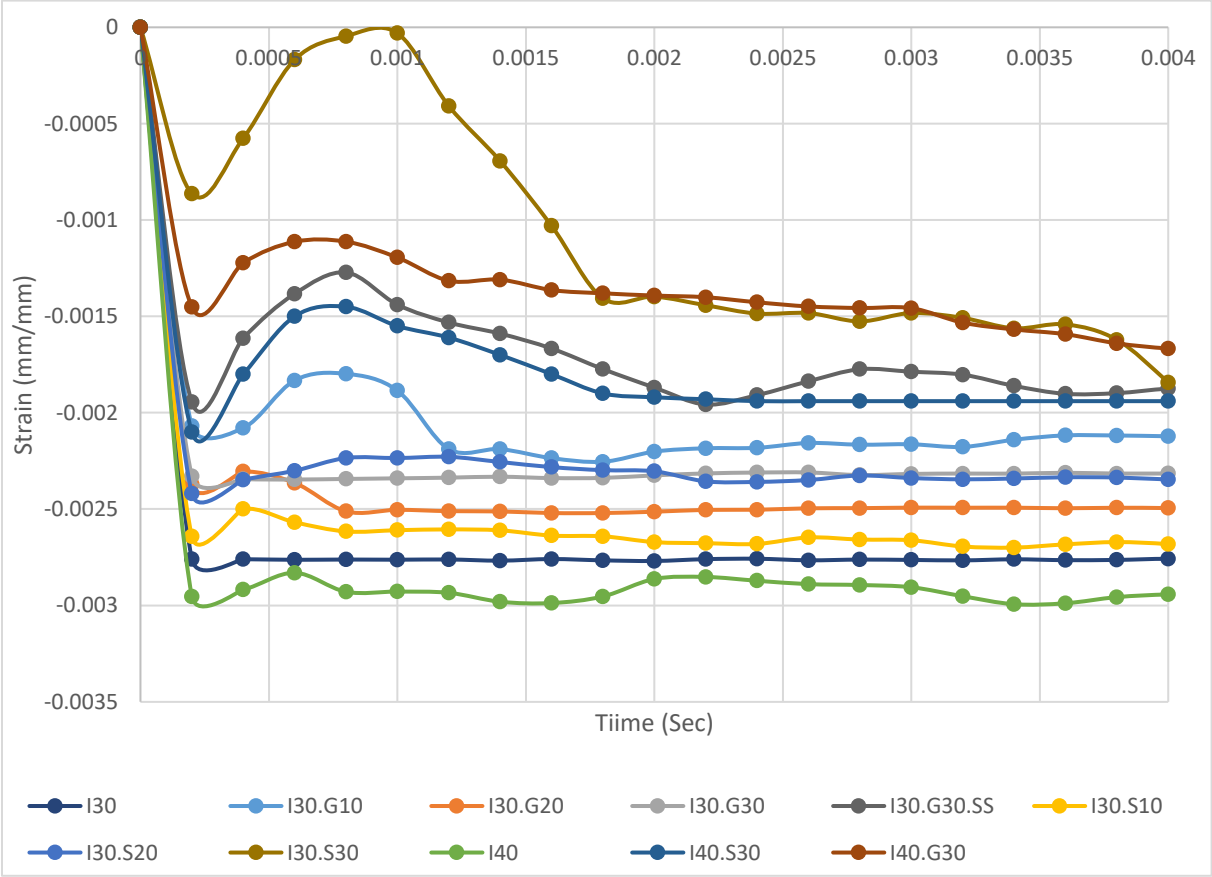

Figure 4.23. Strain-time curves at all G1 points

Figure 4.24 shows that, the free vibration period generated after the impact interval for all specimens which is so logical state. The strain values at free vibration period have some fluctuates but settle down after few parts of seconds.

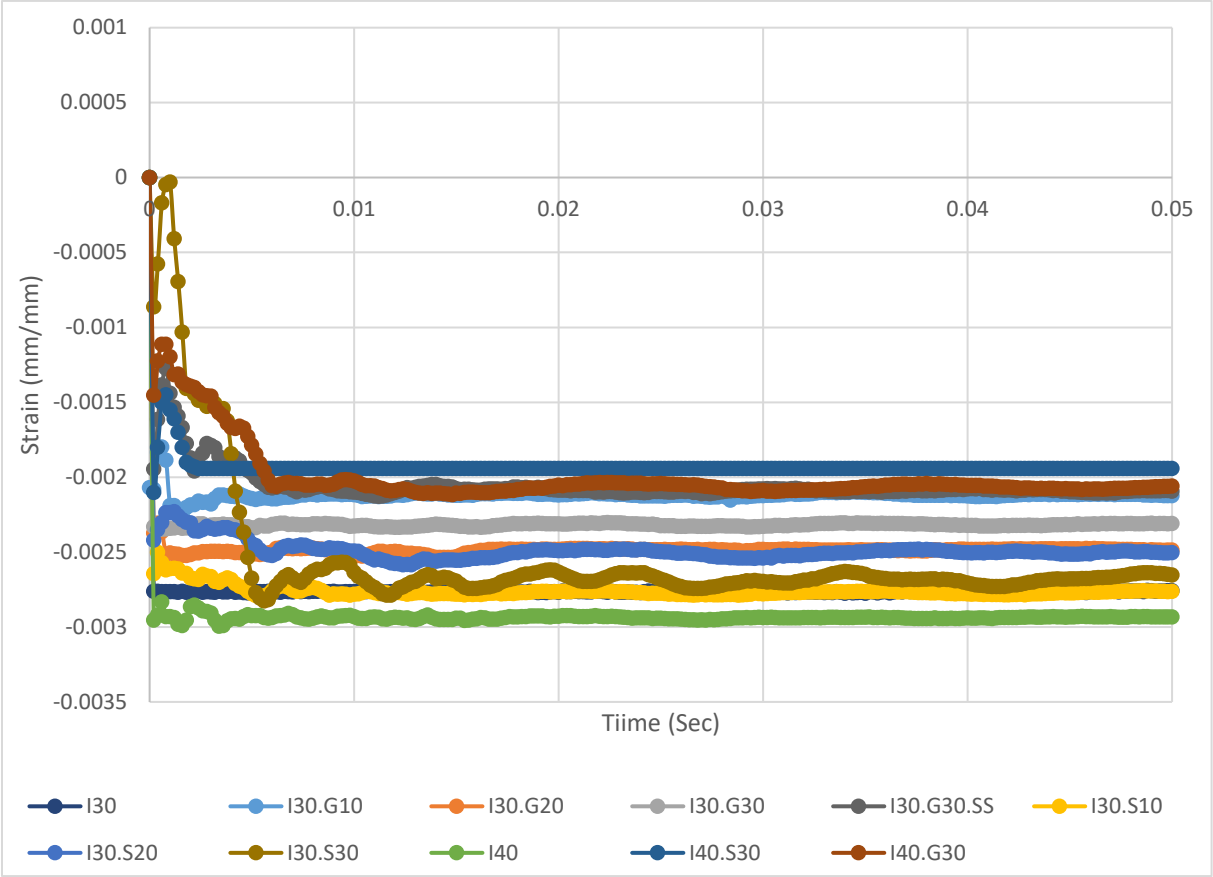

Figure 4.24. Strain-time curves for all G1 for 0.1 sec

4.4.2. Impacted tie moment (G2)

Since the beam is governed (as a design geometry – appendix A) by shear strut failure, then the curves shown at Figure 4.25 approximately do not show many fluctuates, which means that, the CDBs accede the impact using strut strength not using the bending strength of the beam. From Figure 4.26, which showed the bending strain at 0.05 sec, the waving settling down defers from specimen to another. All of them settles within 0.003 sec, expect I30.S20 which settles after 0.008 sec.

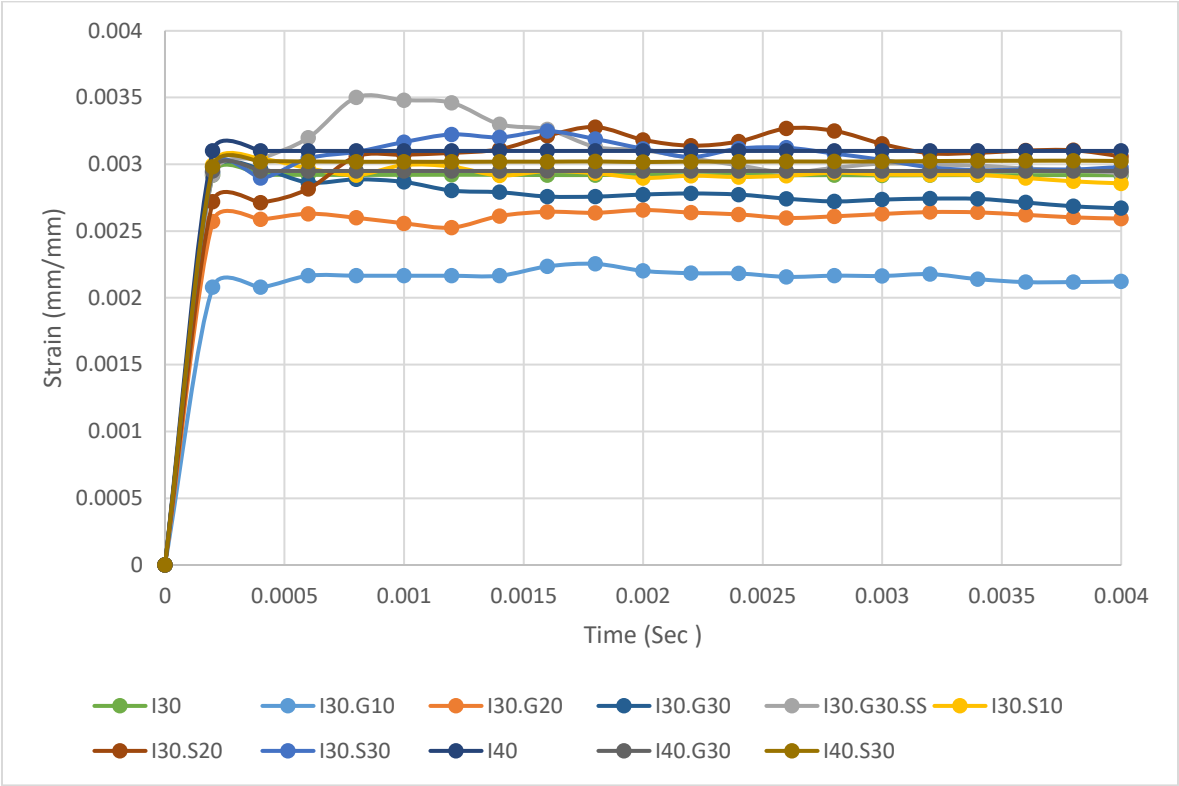

Figure 4.25. Strain-time curves for all G2 points

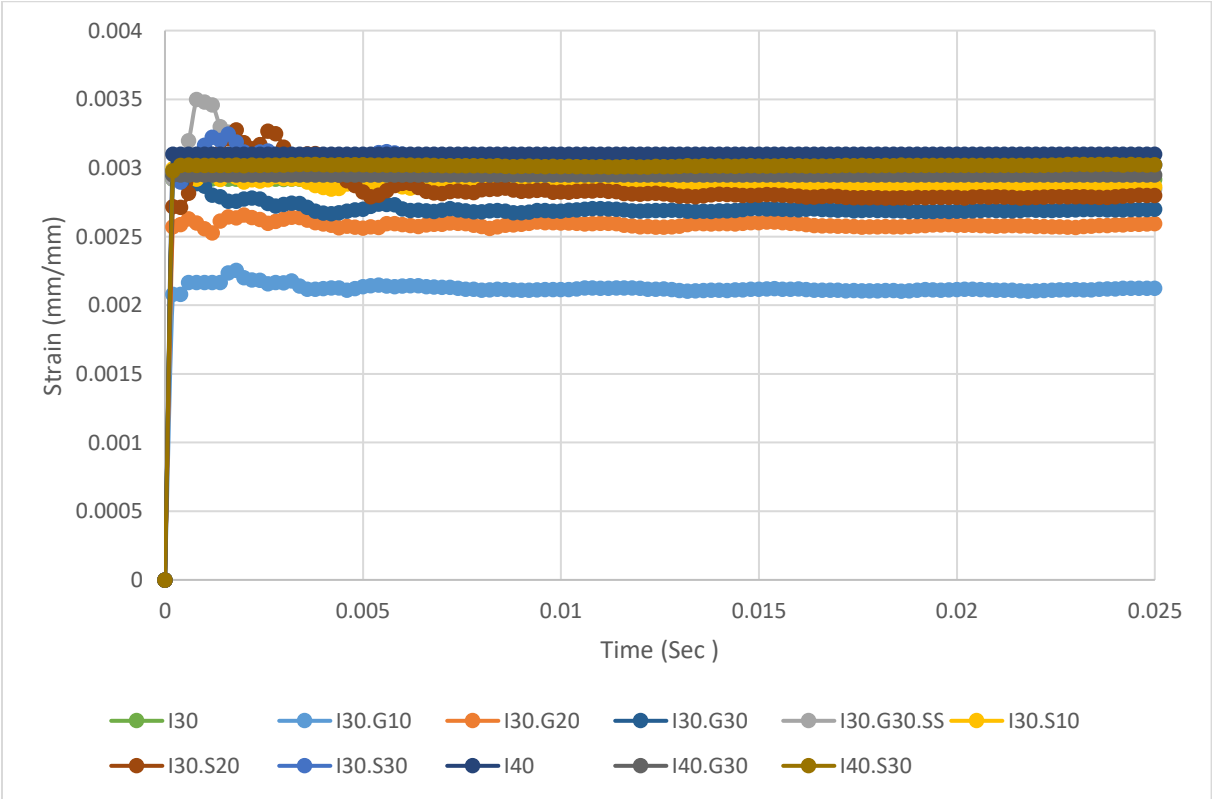

Figure 4.26. Strain versus time curves for G2 for 0.025 sec

4.4.3. Impacted Right Strut (G3)

The reference beams (I30 and I40) show the higher constant strain value along the load interval due to their high rigidity (as explained in Figure 4.27).

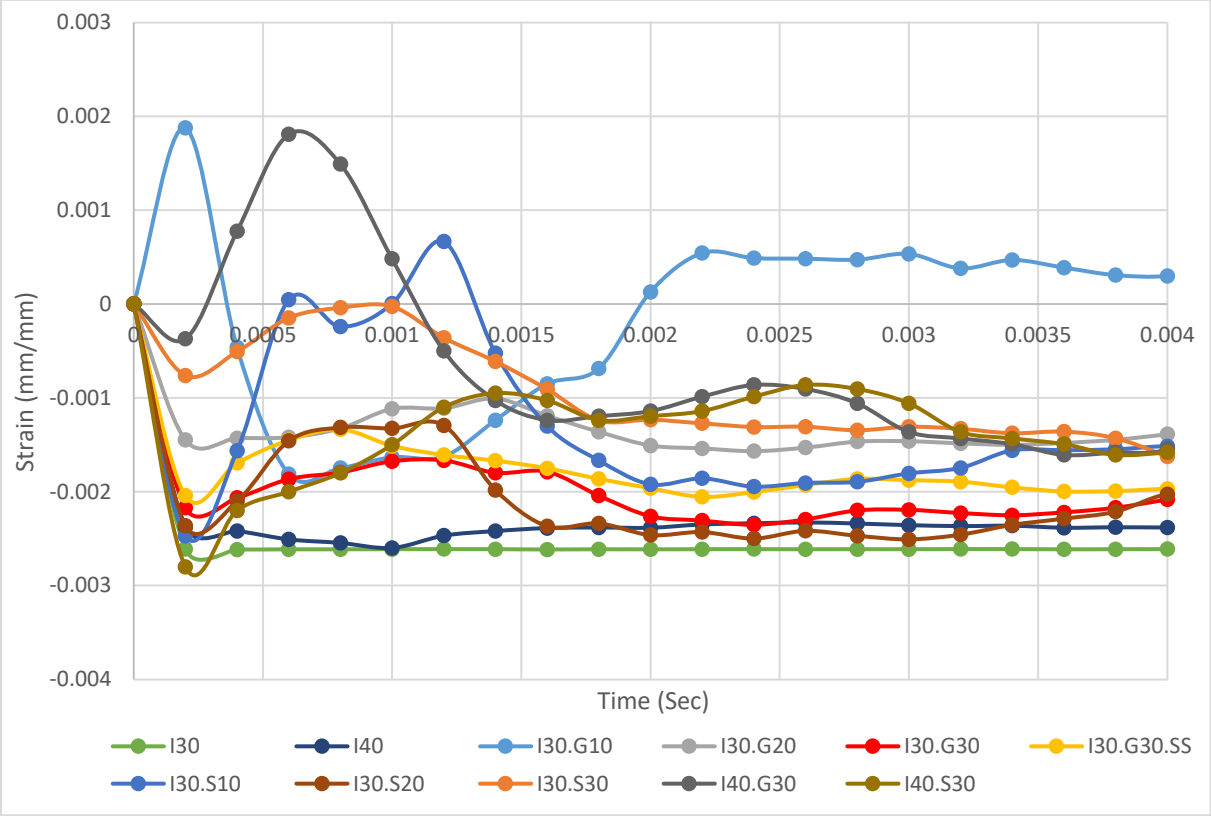

Figure 4.27. Strain versus time curves for G3 position

For more visibility, Figure 4.27 shows the strain-time curves for the gravel replacement only. It is clear that, the rubberized CDBs deform largely under the effect of hit especially for the higher impact weight. The strain values rise suddenly from zero to significant points then drops sharply to small values. Specimen I40.G30 was the higher fluctuated when comparing with the other gravel replacement, and it has significant vibration under the 40 KG dropping weight. Simply supported beam deforms under the impact at a manner similar to the continuous beams but not at the same values of strain, i.e. I30.G30.SS shows higher sensitivity due to its discontinuity which avoid the beam to overlapping a load to the Un-impacted span.

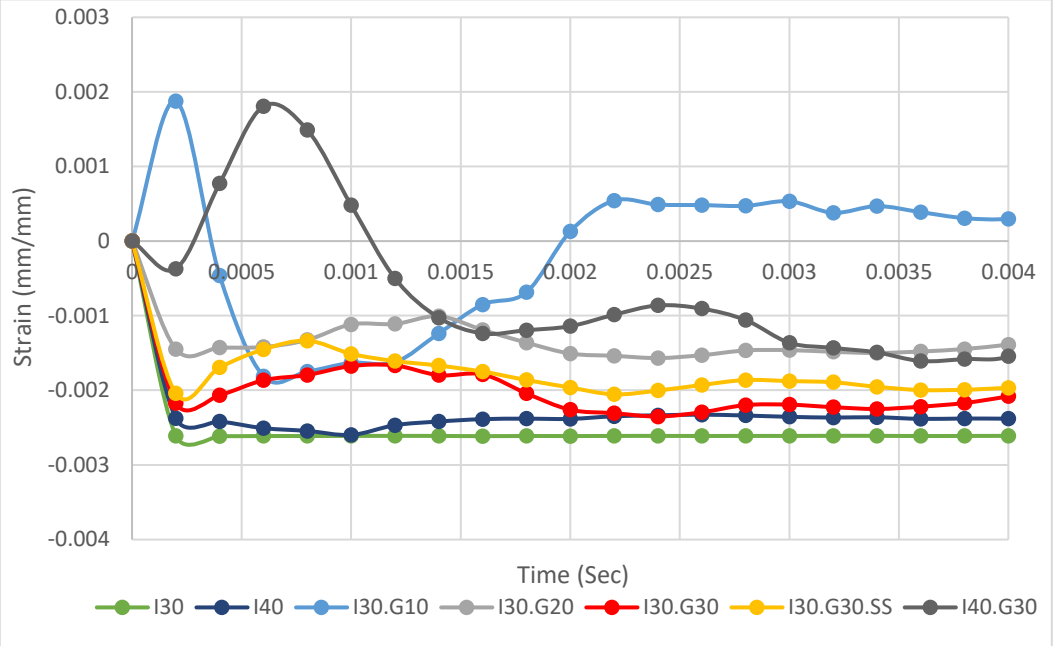

Figure 4.28. Strain- time curves for G3 position for gravel replacement

For sand- crumb replacement, the beams view more chaotic under loading due to the higher amount of rubber used into the mixes (Figure 4.29). The beams overcome the dropping weights and strained in a manner which guarantees gaining the flexibility under stresses as illustrated in Figure 4.30. All specimens get rid of free vibration after 30 milliseconds expect I30.S10 and I40.G30 in which the fluctuated rest after 50 Milliseconds (see Figure 4.30)

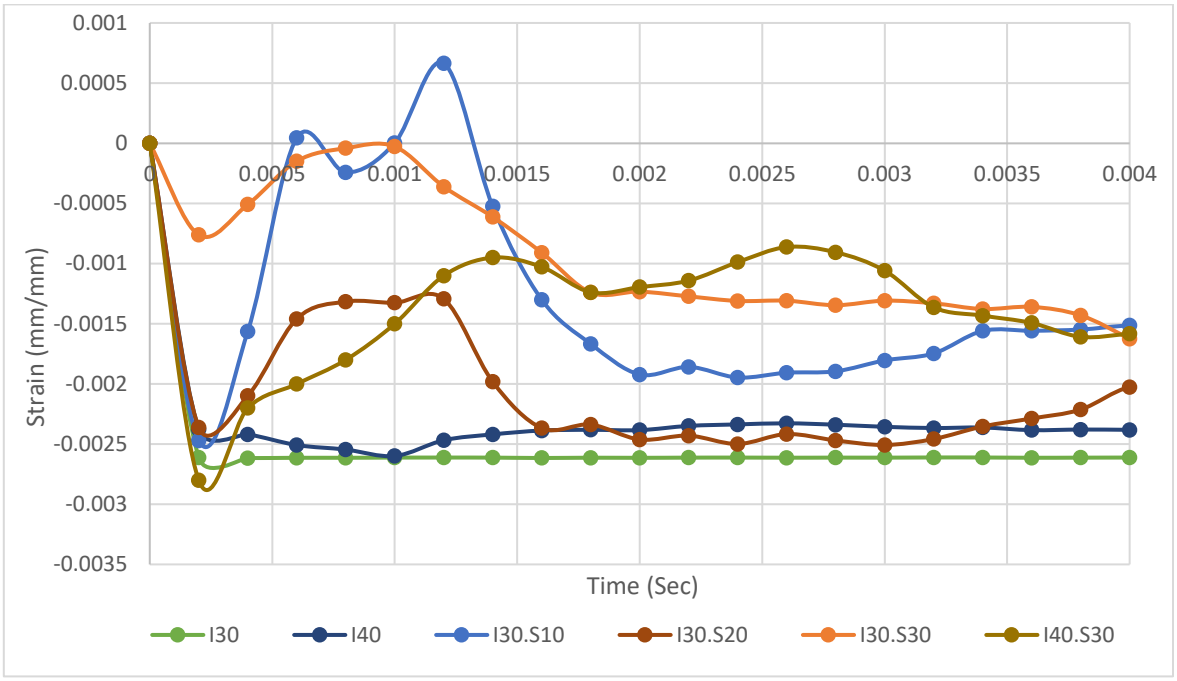

Figure 4.29. Strain-time curves of sand replacement for G3 for 0.004 seconds

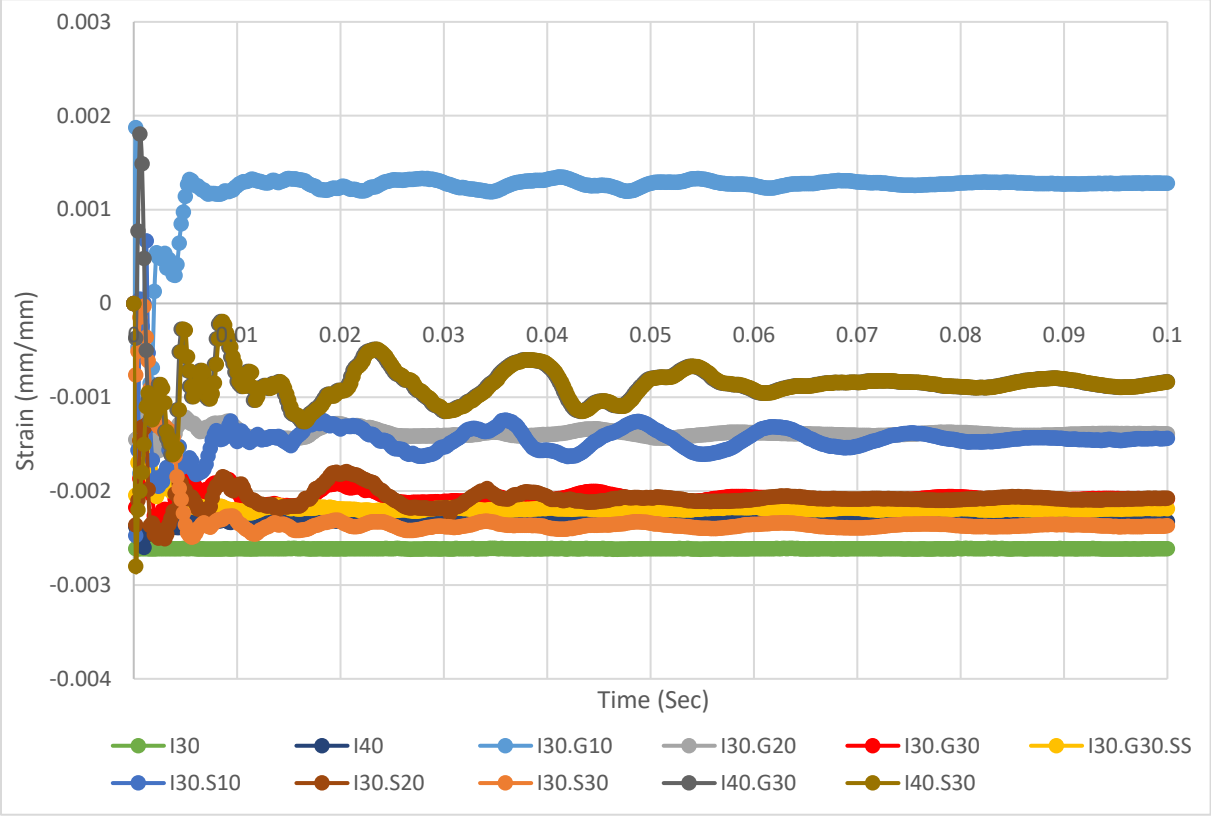

Figure 4.30. Strain versus time curves of G3 results for 0.1 sec

4.4.4. Positive Moment Strain (G4)

Figure 4.31, shows the value of conventional concrete strains (I30 and I40) that do not accede the logical strain 0.003, the difference between them values is due to the load intensity variation. Unfortunately, the data of specimens I30.G10 and I40.G30 were lost due to strain gages damaged during the test (see Figure 4.32 for more clearness). Specimens I30.S30 and I40.S30 showed the larger tensile strain which accede the conventional point of straining due to the high strain for rubcrete mixes. A variation in the curves can be observed for the remaining specimens depending on it concrete compressive strength and the strain behavior for the rubcrete mix itself. Figure 4.33 shows the sand replacement in more legibility.

Figure 4.34 describes the G4 wave within 0.1 seconds. All specimens approximately settles after 30 Milliseconds except I30.G30 and I30.S30 were rests after 50 milliseconds.

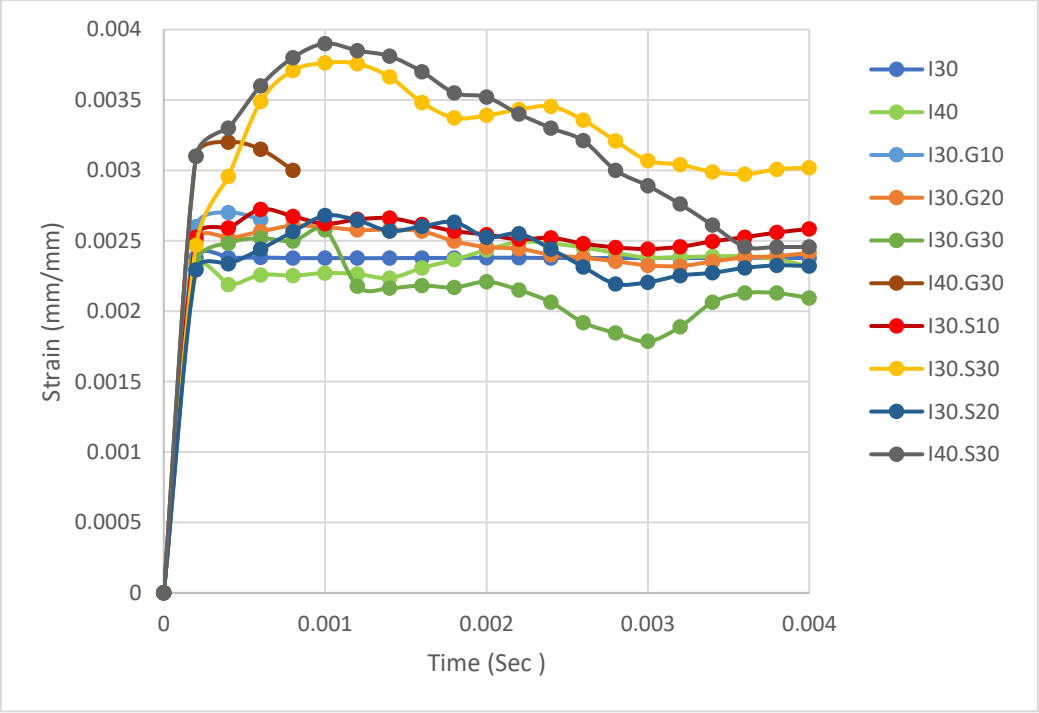

Figure 4.31. Strain-time curves for G4 points for all beams

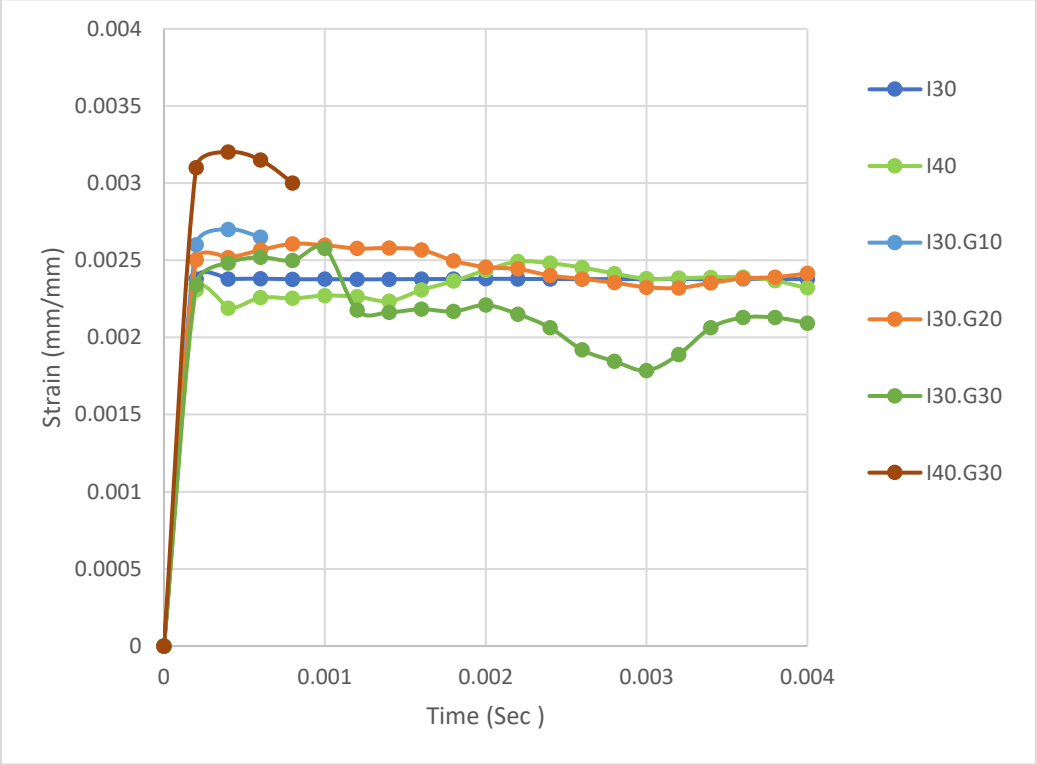

Figure 4.32. Strain vs time curves for gravel replacement for G4

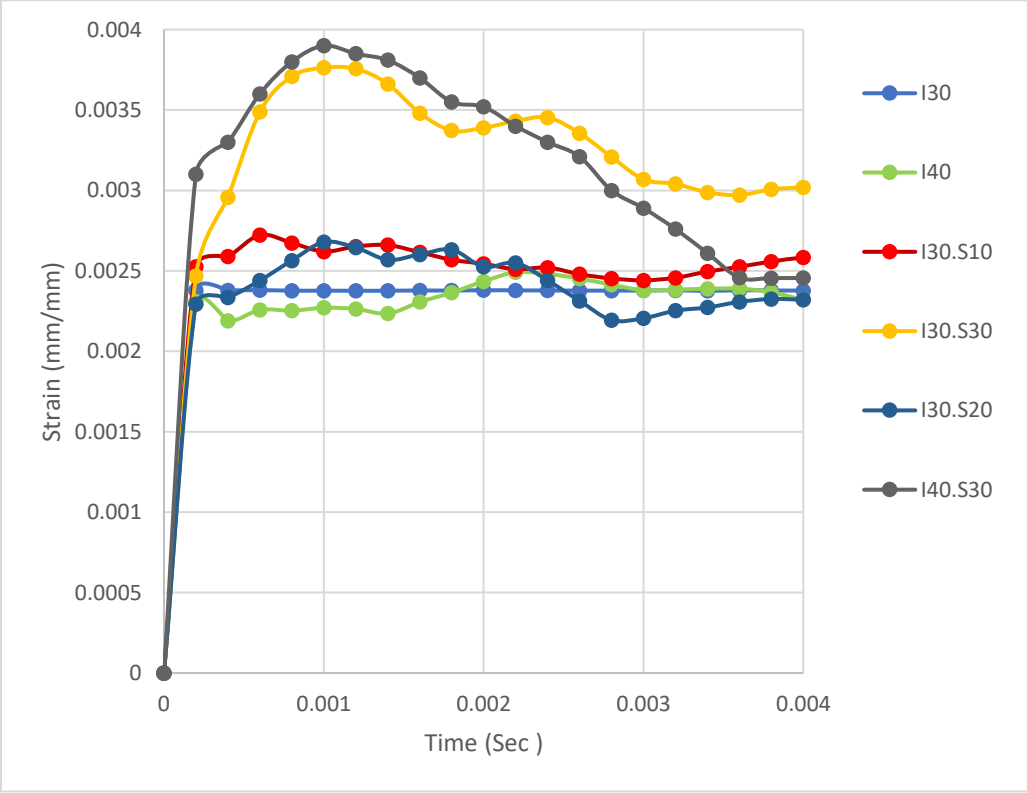

Figure 4.33. Strain-time curves for sand replacement for G4

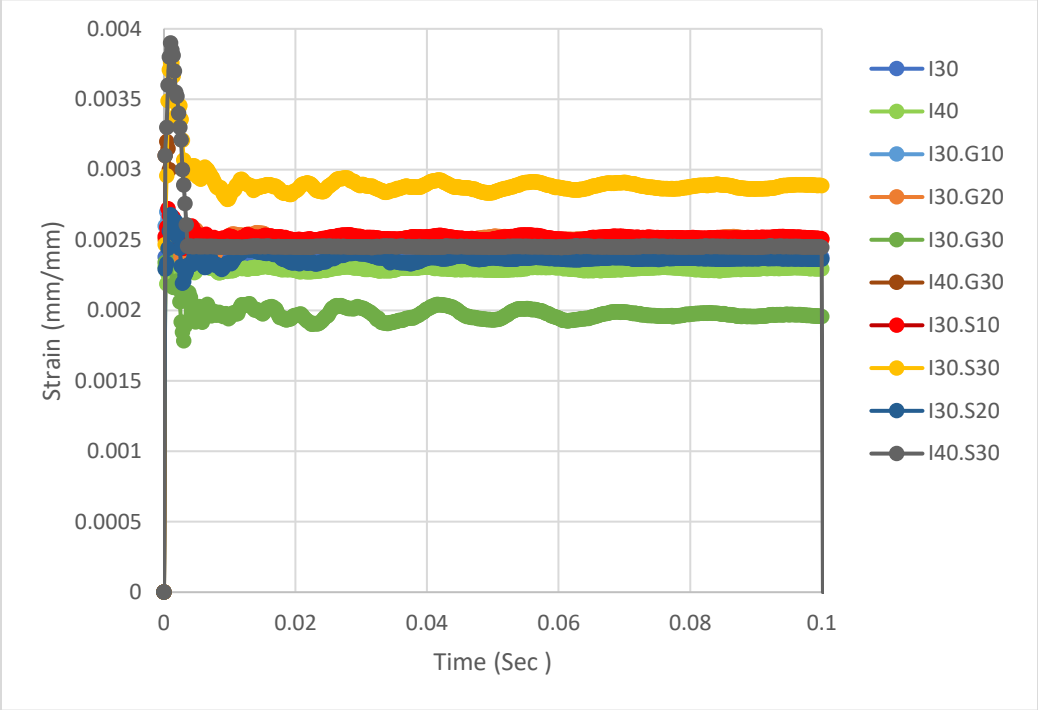

Figure 4.34. Strain-time curves for 0.1 sec for G4

4.4.5. Right Un-Impacted Strut (G5)

As shown in Figure 4.35 strains values' for all specimens approximately appear in a constant value without or with slightly fluctuating as illustrated in specimens I30.G30, I40.G30, I30.S30 and I30.S10. Such constant values indicated that, little stresses overcome by this portion of CDB. Conventional concrete mixes show the lower strain values due to the little energy absorption capacity by the member, while for rubcrete beams, the strains growing up independent on the load intensity, rubcrete compressive strength and rubberized mix strain. All over CDBs rest from vibration after passing 0.035 seconds as explained in Figure 4.36.

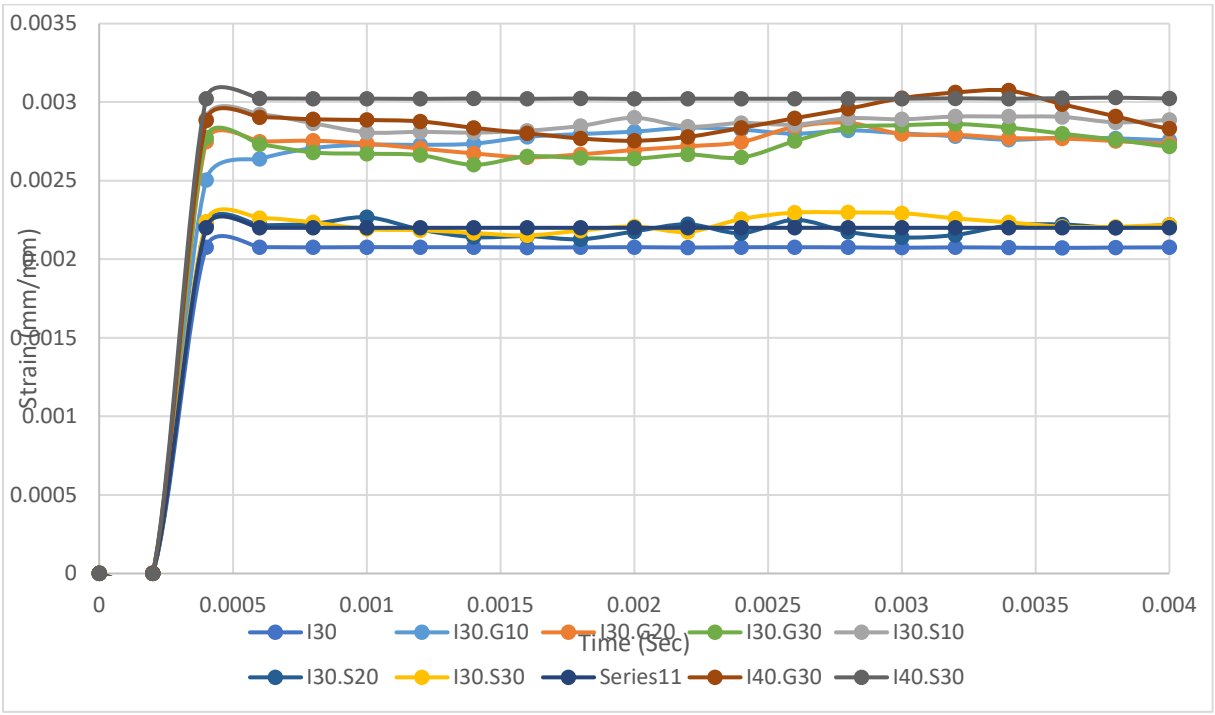

Figure 4.35. Strain-time curves for G5 for 0.004 second

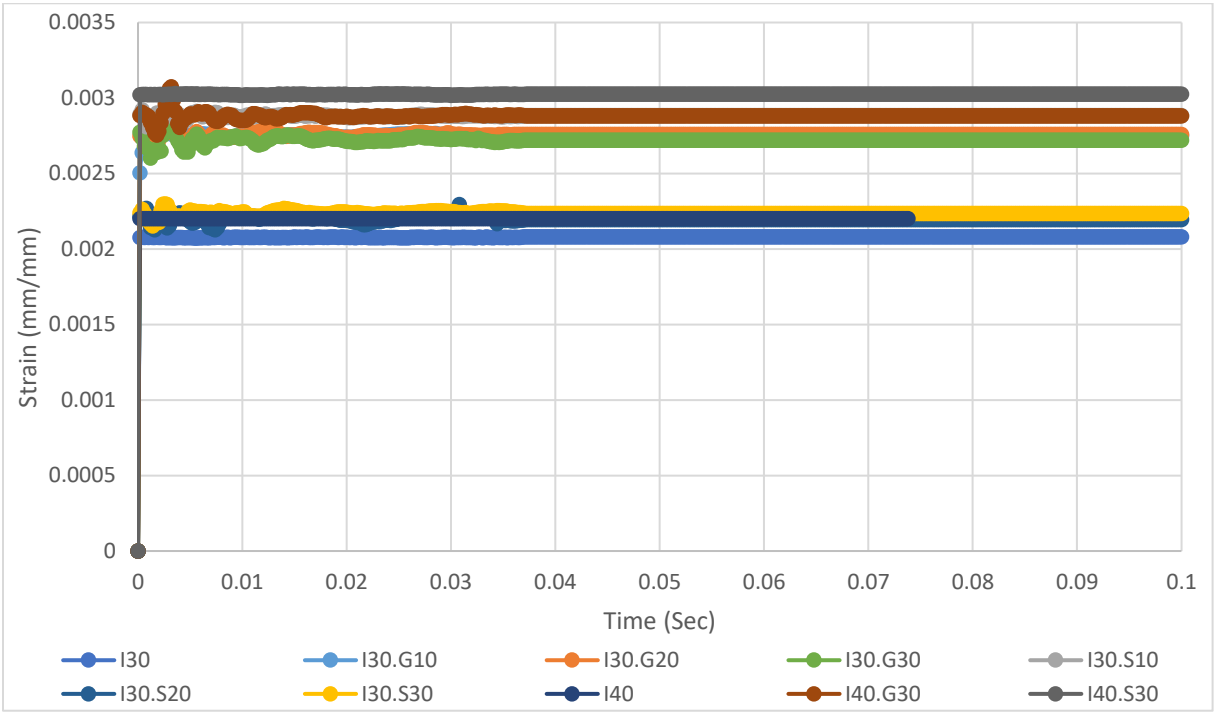

Figure 4.36. Strain versus time curves for 0.1 sec for G5

4.4.6. Left Un-Impacted Strut (G6)

CDBs fluctuate at the final end strut due to the uplifting stresses. All beams approximately suffer from the uplifting wave in which causes the final un-impacted strut to be sensitive to the applied load on the other span. Figure 4.37 shows the results for all beams, while Figure 4.38 and Figure 4.39 detaile the gravel and sand replacement respectively.

Since this strain is located nearby the far end of beams, it suffers from the uplifting stress wider and larger than any other point, so it shows higher activations toward impact then G5. The period of free vibration is also affected for the same reason. It clear to inform that, the interval of free vibration continued to 1.3 sec. Another pulse is shown in the curves which is due to impactor rebounding (Figure 4.40).

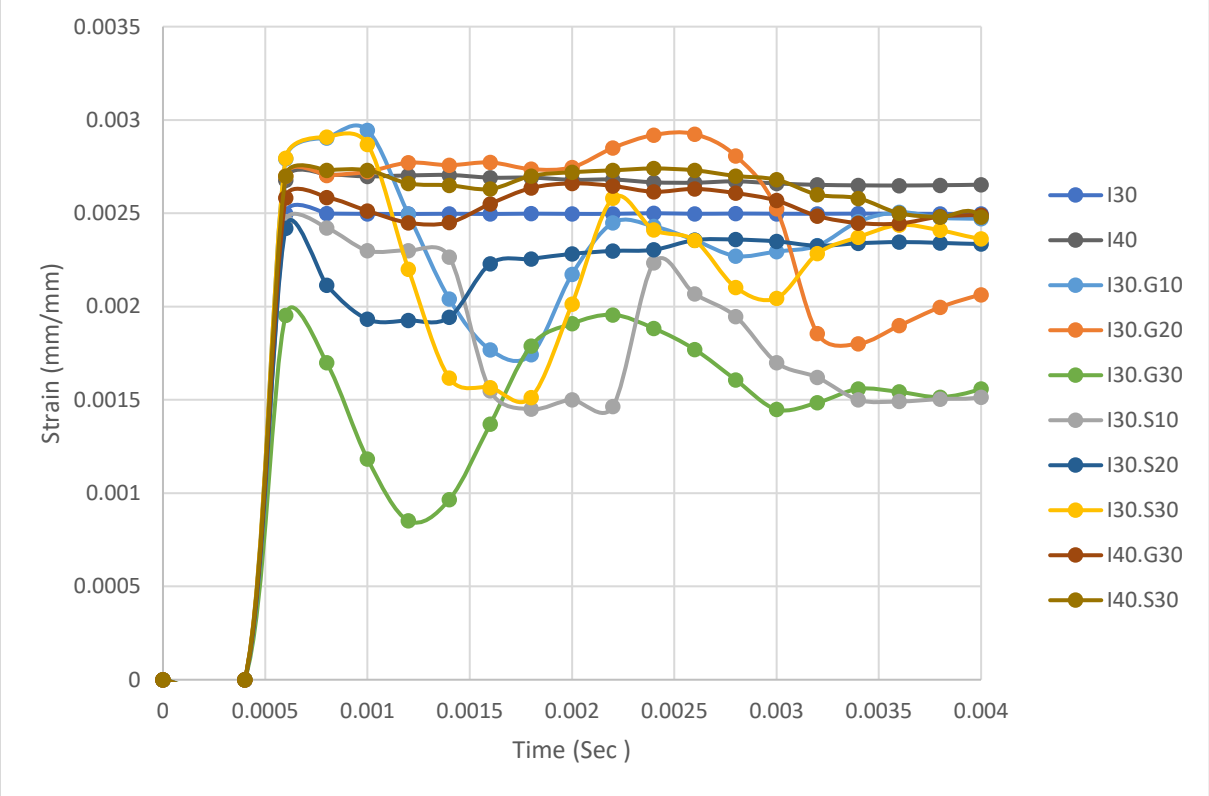

Figure 4.37. Strain versus time curves for G6 for all samples

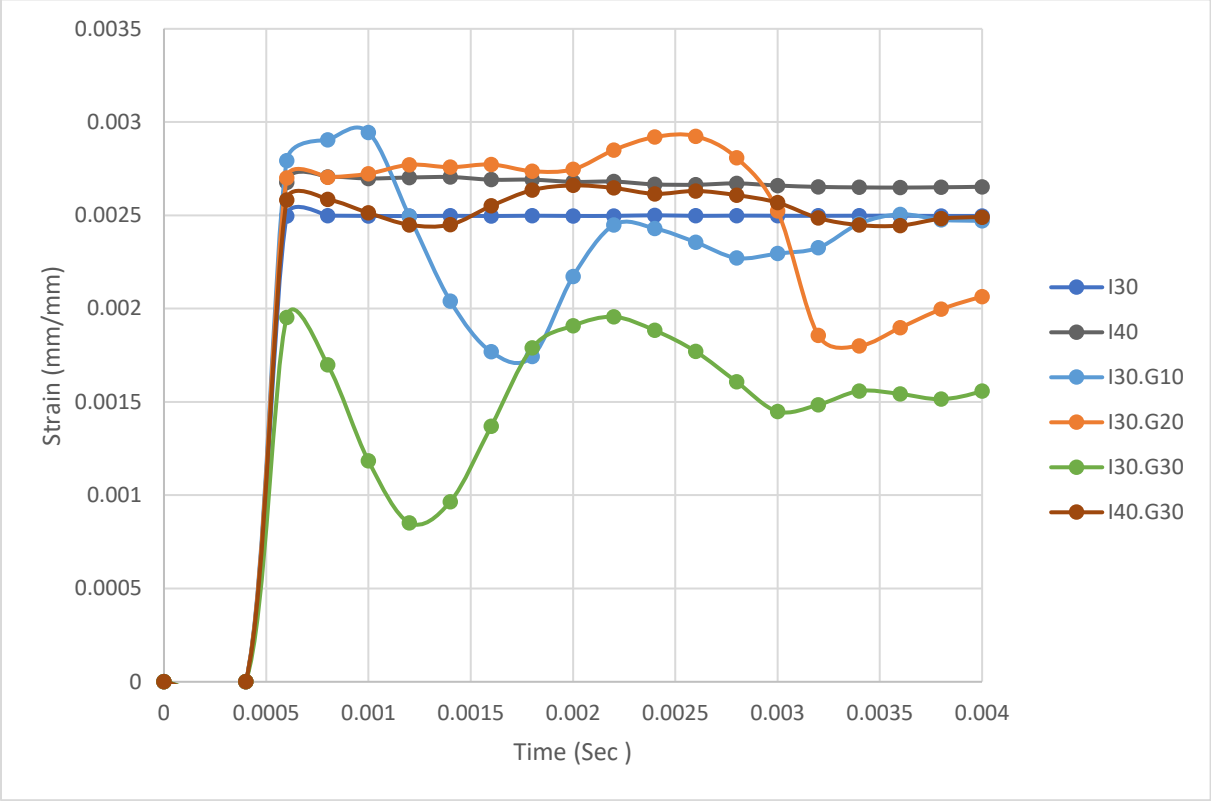

/Figure 4.38. Strain-time curves for gravel versus chip replacement G6

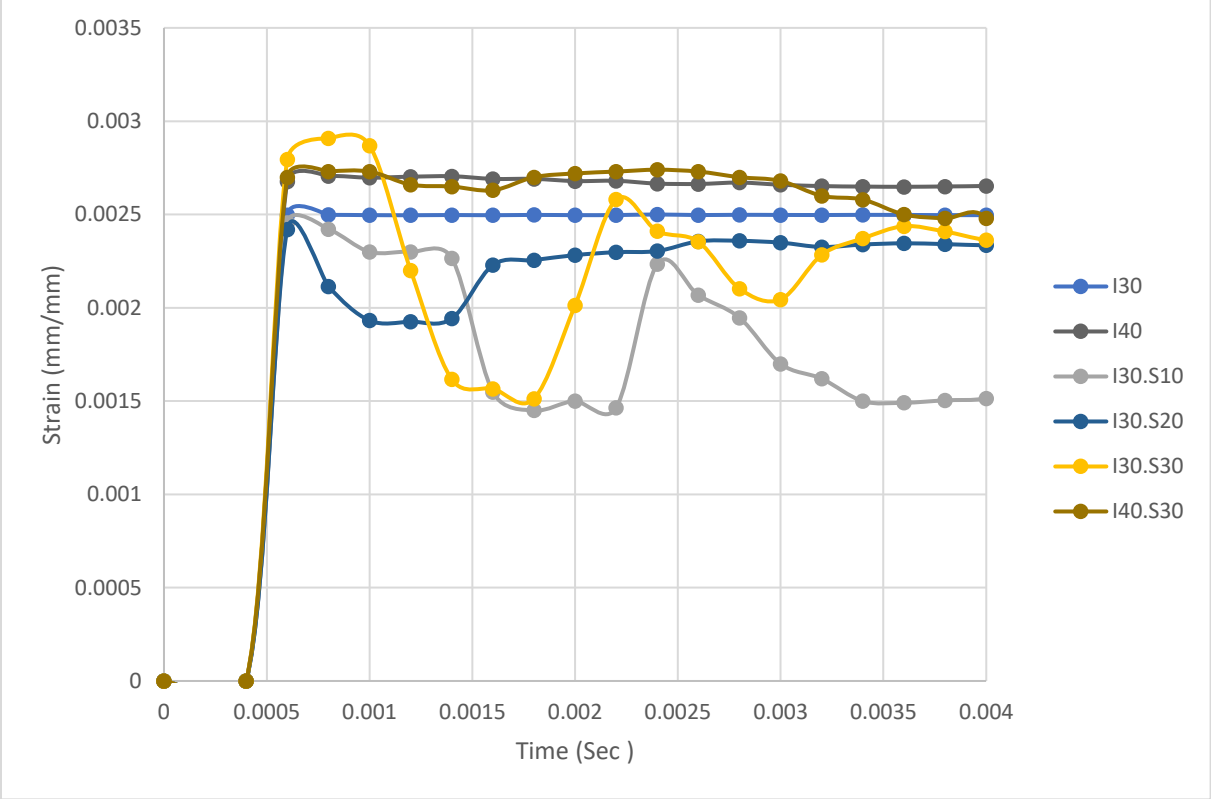

Figure 4.39. Strain versus time curves for G6 sand replacement

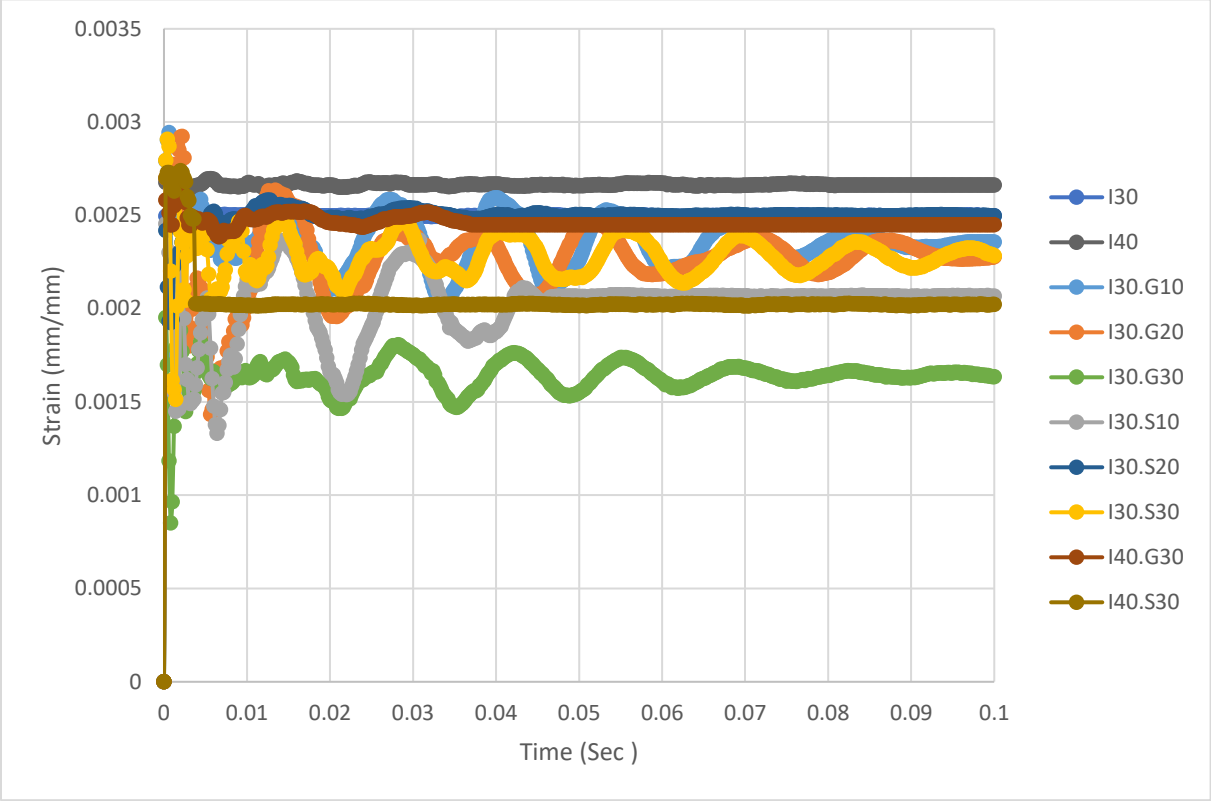

Figure 4.40. Strain-time curves for G6 full vibration interval for all rubcrete mixes

4.5. Retesting CDBs Result

Residual impact deflection was identified using dial-gages placed under the mid-spans before impact. The gages measure the deflection of beam after impact for each specimen as explained in Table 4.4 and Plate 4.20. To calculate the equivalent static load, kinetic energy was equaled to the potential energy of beam and forming equation: $mgh = \frac{1}{2}mv^2$, noting that, dropping velocity is computed by $v = \sqrt{2gh}$ [177]. The forces for each member were listed in Table 4.4.

From Figure 4.41, its noted that, the increment in rubber percentage (what ever was the type of replacement) leads to increase the deflection due to the more flexibility of the rubberized beams.

Plate 4.20. Deflection measuring after impact

Table 4.4. Residual deflection and load after impact

Beam sample	Deflection for impacted span (mm)	Percentage of positive deflection increment (%)	Deflection of un-impacted span (mm)	Percentage of negative deflection increment (%)	Applied impact load equivalent to monotonic (kN)
I30	0.33	----	-0.13	-----	55
I30.G10	0.35	6.06	-0.15	15.38	55
I30.G20	0.38	15.15	-0.18	38.46	55
I30.G30	0.42	21.40	-0.21	61.53	55
I30.S10	0.37	12.12	-0.25	92.3	55
I30.S20	0.41	24.24	-0.22	69.23	55
I30.S30	0.45	36.36	-0.26	100	55
I40	0.54	63.63	-0.3	130.7	73
I40.G30	0.72	33.40	-0.42	40.00	73
I40.S30	0.81	50.00	-0.51	70.00	73

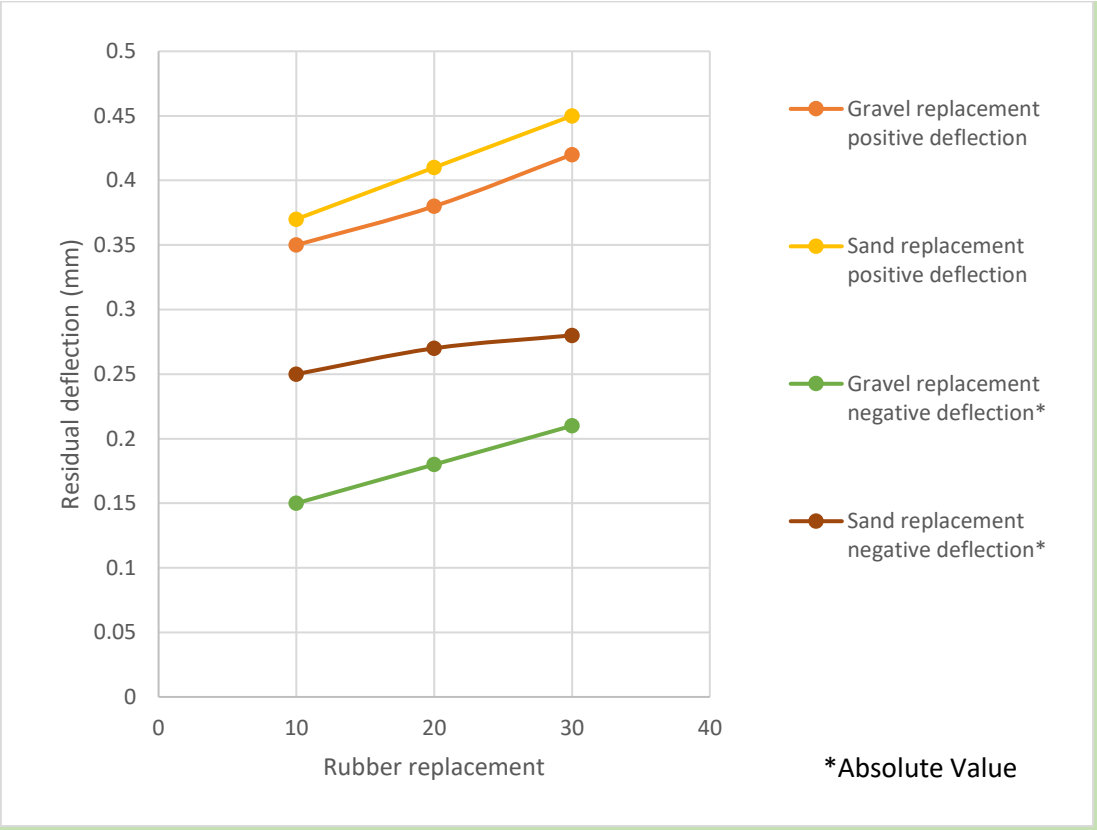

Figure 4.41. Residual deflection versus rubber percentages curves

After testing the CDBs by dropping weights, the beams were retested statically in order to view the capacity deterioration causing by the impact. The failure loads for beams were listed in Table 4.5.

Its noted that, the STM greatly identify the ultimate load capacity of the rubcrete continuous deep beams in a percentage ranged from 1.008 till 1.095. As well as, A+B approximately equals the monotonic experimental load which refers that, the equivalence impact to static equation gives an approximated logical value to static load. In addition, there is little loses in load can be noticed from the Table 4.5.

Table 4.5. Static load capacity of CDBs with or without impact

Specimen	* STM results (kN)	Ultimate static load (kN) (Table 4.1)	STM to Exp. %	Equivalent Impact load (A)	static after hits (B)	A+ B	Load losing (%)
I30	345	378	1.095	55	288	343	9.25
I30.S10	228	230	1.008	55	167	222	3.47
I30.S20	168	180	1.071	55	113	168	6.66
I30.S30	152	165	1.085	55	106.5	161.5	2.12
I30.G10	243.6	264	1.083	55	180.4	235.4	10.83
I30.G20	222	230	1.036	55	155	210	8.69
I30.G30	175.7	180	1.024	55	120	175	2.77
I40	345	378	1.095	73	263	336	12.5
I40.S30	152	165	1.085	73	88	161	2.424
I40.G30	175.7	180	1.024	73	101	174	3.33

*Solves at **Appendix E**.

Figure 4.42 introduces the monotonic results for I30 sample after the impact. Very large deflection is observed for the impacted span due to unify the impact cracks under static loads. From Plate 4.21, which shows the crack pattern of the sample I30, it can be noted that the impacted span develops the cracks during static load and a strut cracks in the other span is also generated. This means that, such hit (30 kg from 1.86 m) does not weakens the impacted span enough, so the tie success to develop the load into the other span, and the beam go on bearing the load by STM. In addition, it can be seen that, all impacted crack is doubled after static loads. For all plates from Plate 4.21 to Plate 4.30, the red color is for the impact

cracks while the black is for the static test cracks. The ultimate load of the reference beam decreases by 23.8% due to hit and the deflection of the impacted span rises to 25.2 %.

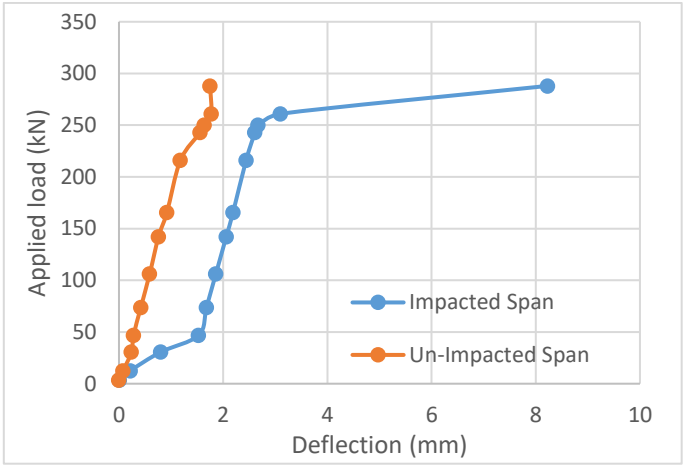

Figure 4.42. I30 Specimen

Plate 4.21. I30 Impacted-Monotonic tests crack pattern

I30.S10 sample also suffers from large deflection for the impacted span during static load, due to the past cracks development. The same behavior of converting the load of I30 sample is observed for I30.S10, which refers to, the impacted span still strong enough to convert the load into the un-impacted span. Negative crack moment and strut shear cracks appears at the other span as shown in Plate 4.22. Due to the hit, the ultimate load of the specimen dropped by 27.4% while the impacted span deflection rises to 56.5%.

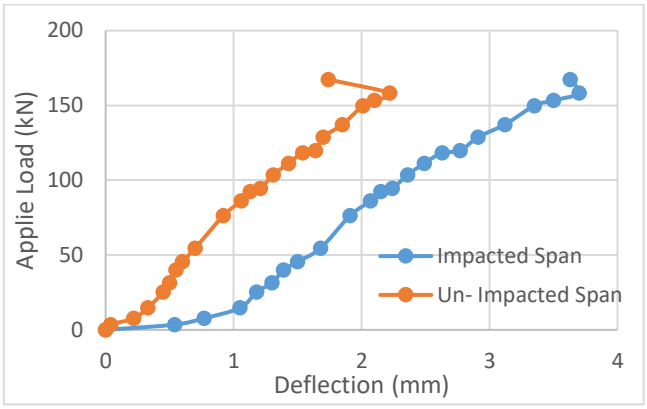

Figure 4.43. I30.S10 load- displacement curve

Plate 4.22. Crack mode of specimen I30.S10

I30.S20, which can see its results at Figure 4.44, coverts the load professionally into the other un-impacted span till the final failure cracks appears in the un-impacted span. The final failure is clarified at Plate 4.23. The ultimate beam load after the hit dropped to 37.22% as well as the deflection drops by 77.8%.

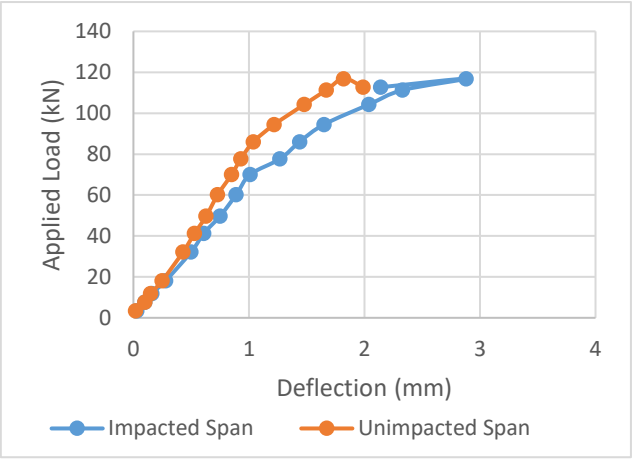

Figure 4.44. I30.S20 CDB results

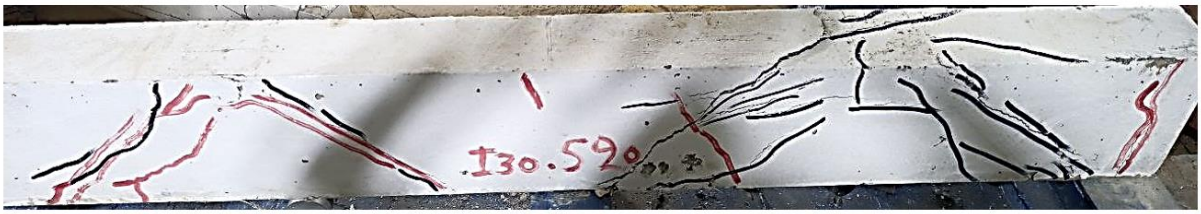

Plate 4.23. Sample I30.S20 crack mode

Plate 4.24 and Figure 4.45 discuss the behavior of the impacted I30.S30 and then monotonically testing results, the sample also is strong sufficiently to overlap the load into the un-impacted span but the final failure load stills at the impacted span. It is due to the ductility and the rubcrete compressive strength difference between the two specimens. The ultimate load capacity of the beam decreases to 35.45% while the deflection of the impact span increases to 62%.

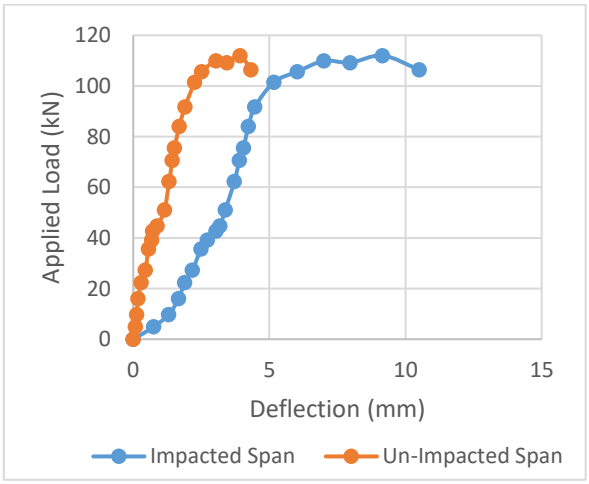

Figure 4.45. Load-deflection curves of I30.S30

Plate 4.24. Failure mode of I30.S30

I30.G10 (Figure 4.46) shows a huge different in displacement value when comparing between the impacted and un-impacted span, but anyway it stills converting the load into the other span in spite of the hit and finally the failure appears at the impacted span (as illustrated in Plate 4.25). Strut cracks at both spans were generated as well as a few negative and positive moment cracks. The ultimate load of this specimen decreases by 31.6% while the deflection rises by 30.2%.

The same behavior can be also noticed for I30.G20 (which results are shown in Figure 4.47) but it cracked more than I30.G10 and vertical cracks at middle both external supports is shown (Plate 4.27). The ultimate load of I30.G20 is dropped to the 32.6% while the deflection decreases by 45.68%, the same behavior is observed at I30.S20.

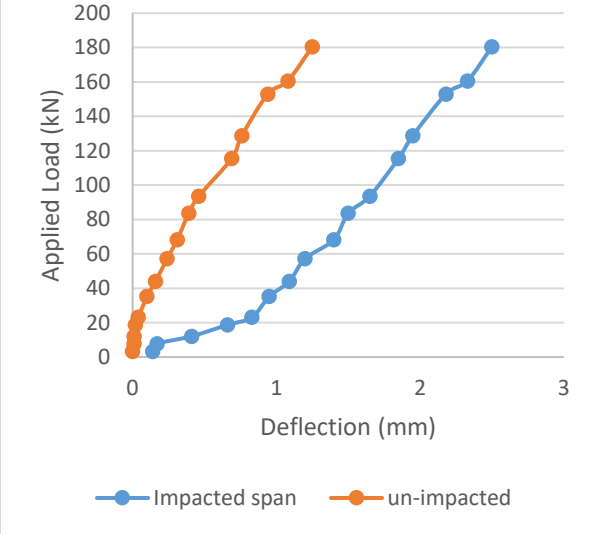

Figure 4.46. Load-deflection curves of I30.G10

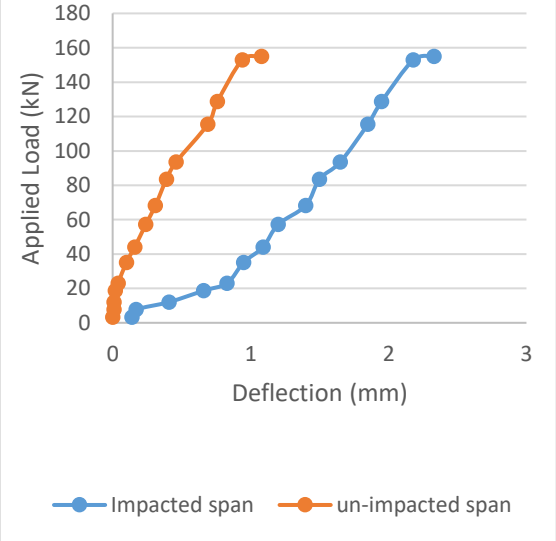

Figure 4.47. Load-displacement curves of I30.G20

Plate 4.25. Crack pattern for I30.G10

Plate 4.26. I30.G20 failure shape

I30.G30 sample in spite of the hit, stills able to convert the load into the other span but with larger displacement for the impacted span. Strut cracks developed at the impacted span and generated in the un-impacted span. The ultimate load of beam decreased by 33.34% as well as the deflection dropped to 64.29%.

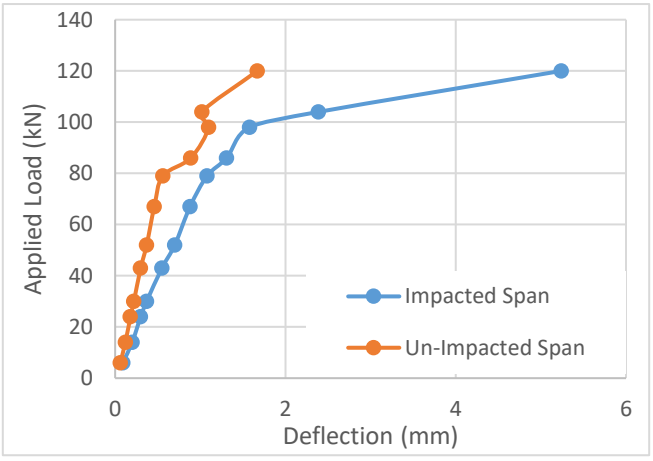

Figure 4.48. Monotonic load deflection curves for I30.G30

Plate 4.27. Failure mode of I30.G30

For the same load intensity (30 Kg impact), comparing between the group of sand replacement and the gravel replacement group, it can be found that, the CDBs strength of sand replacements dropped by 42%, 60%, 63% when comparing with the conventional concrete, while the group of gravel replacement decreases by 37%, 46% and 58% respectively. Which means that, the gravel replacement keeps the capacity of the beam from higher dropping.

I40 suffers from cracks more than I30 due to the higher energy of the impactor. Logically, the impacted span shows a deflection larger than other span. All struts are cracked even the un-impacted, positive moment at the impacted span, negative moment at the upper of middle support and uplifting cracks at the external supports could be observed at Plate 4.28.

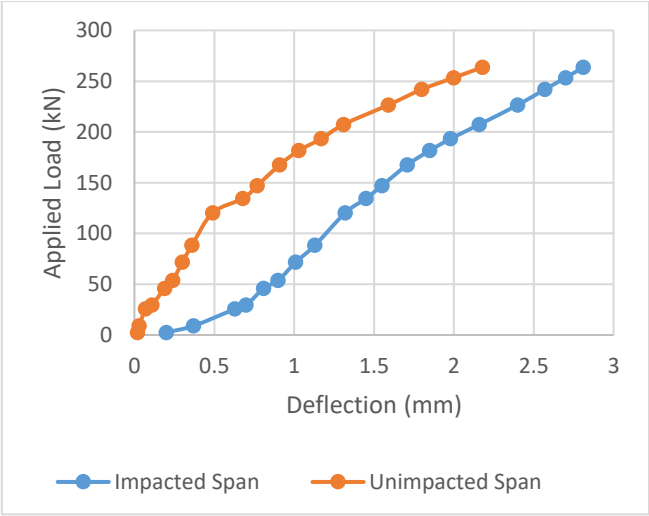

Figure 4.49. Statically result of I40 sample

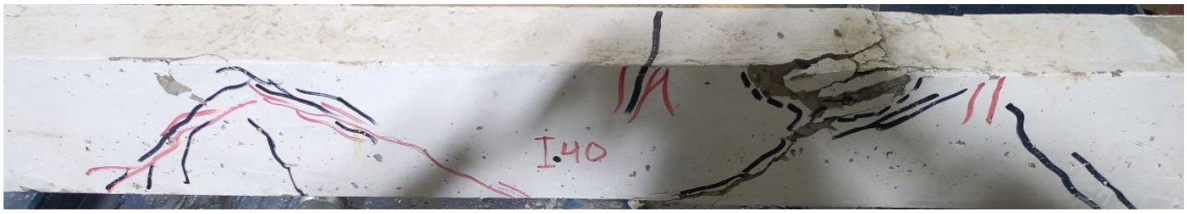

Plate 4.28. Impact and monotonic cracks of I40 specimen

The total loss in energy for I30 equals 9.25% While equals 17.20% for I40, which is due to the higher energy. The deflection also larger at I40 specimen, i.e. for the same load value (let use the 250 kN), the deflection of I40 is higher than I30 due to the higher stress intensity.

I40.G30 and I40.S30 show the same crack pattern, all strut are cracked, cumber cracks, uplifting cracks and a simple negative moment at the head of the middle support (as illustrated in Plate 4.29 and Plate 4.30). The static load develop the impact cracks till reach the failure at the impacted span for the samples both. When comparing between these two specimens with them past two twins (I30.S30 and I30.G30), ones can be concluded that, losses increase slightly when developing the dropping weight. The losses of I30.S30 is 2.12% and I40.S30 equals 2.42%, while I30.G30 and I40.G30 equal 2.77% and 3.33% respectively.

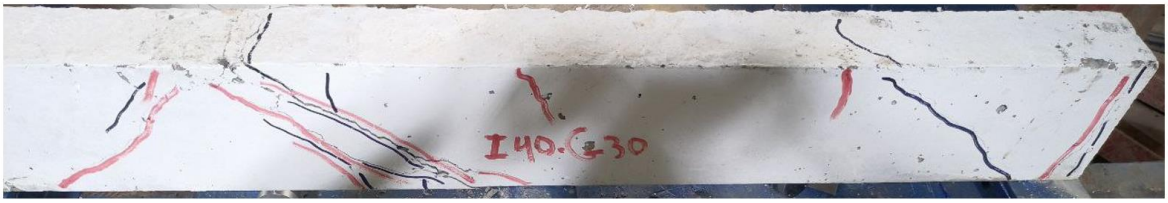

Plate 4.29. Failure mode of I40.G30

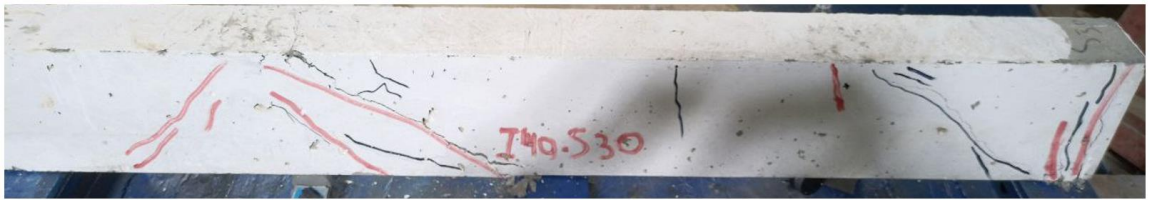

Plate 4.30. Failure pattern of specimen I40.S30

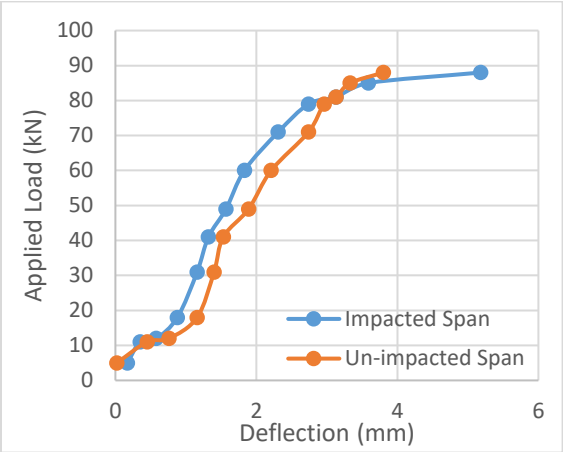

Figure 4.50. Load-deflection curves for I40.S30 specimen

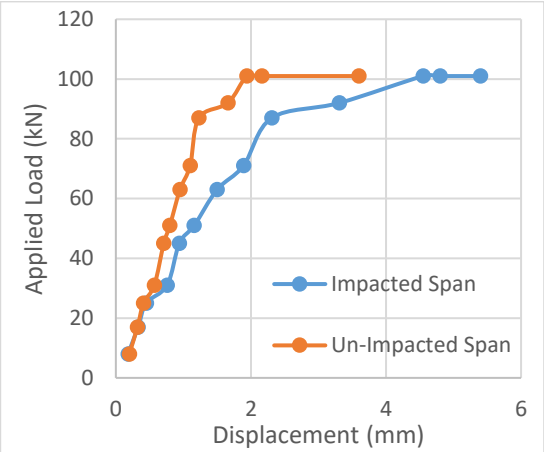

Figure 4.51. Load-displacement curve for I40.G30

When comparing between the totally static tested beams and the impacted-static beams, it can be noted that, the CDBs loss a capacity gradually with every rubber increment. Taking into account that, the gravel replacement specimens dropping is more graduated than the sand replacement as explained in Table 4.6. For higher load intensity, I40 losses about 36% while I30 lost 23.8%. For I30.S30 the losing capacity is 35% while it is 46% for I40.S30. For I30.G30 and I40.G30, the losing capacity for the same specimen is 33% and 43% respectively.

Table 4.6. Comparison between static loads for hitted and un-hitted beams

Specimen	Static capacity (kN)	Specimen	static after impact (kN)	Dropping % due to impacting
ST.0	378	I30	288	23.81
ST.S10	230	I30.S10	167	27.39
ST.S20	180	I30.S20	113	37.22
ST.S30	165	I30.S30	106.5	35.45
ST.G10	264	I30.G10	180.4	31.67
ST.G20	230	I30.G20	155	32.61
ST.G30	180	I30.G30	120	33.33
ST.0	378	I40	263	43.72
ST.S30	165	I40.S30	88	46.67
ST.G30	180	I40.G30	101	43.89

4.6. Experimental Repeated Load Results

The repeated load series which applied experimentally on the three CDBs, the experimental results are illustrated in Figure 4.52. A reference beam, 10% gravel replacement and 10% sand replacement are tested, the ultimate loads of the three beams respectively are 309.8kN, 243 kN and 220.9 kN. Due to the repeated cycles of loading, the ultimate strength of the beams decreases when comparing with the static loads by 18%, 8% and 4% for conventional beam, gravel and sand replacement beams respectively. One can conclude that, the rubcrete is more suitable for repeated loads, as well as the sand replacement is better than the gravel replacement according to the repeated load results. The ultimate deflection increases by 6.4% and 12.12% for gravel and sand replacement respectively.

Ultimate load capacity of R.G10 larger than R.S10 due to the higher compressive strength of the first, while deflection values for sand replacing beam are slightly larger than the R.G10 due the higher flexural capacity of S.R.10 itself as investigated in reference [178]. It can be noted that, from Figure 4.52 and Table 4.7, the residual deflection at the end of each cycle increases gradually due to crack developing after each cycle.

For G10 impacted and repeated beams, (I30.G10 and R.G10), it can be noting that, the beam losses about 10.83% of its capacity due to the hit, while 18% due to the repeated loads which exposed on it. Also, for S10 beams (I30.S10 and R.S10) the CDB lost 3.47% due to impact and 4% as a result of the repeated load.

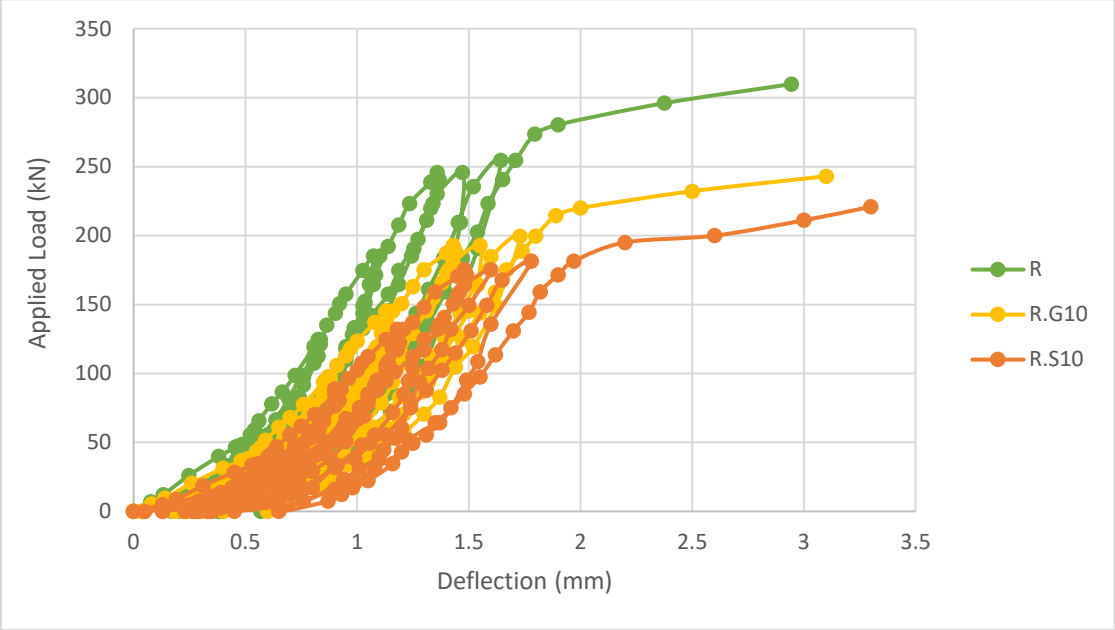

Figure 4.52. Experimental load-deflection curves of repeated specimens

Table 4.7. Residual deflection at the end of each cycle for R, R.G10 and R.S10 specimens (All values in mm)

Cycle number	R	R.G10	R.S10
1st cycle	0	0	0
2nd cycle	0.03	0.04	0.05
3rd cycle	0.06	0.08	0.14
4th cycle	0.13	0.18	0.25
5th cycle	0.19	0.22	0.29
6th cycle	0.21	0.24	0.31
7th cycle	0.24	0.28	0.36
8th cycle	0.27	0.3	0.4
9th cycle	0.39	0.4	0.45
10th cycle	0.53	0.6	0.67
Final loading	2.9	3.1	3.3

Plate 4.31. Repeated tested rubcrete beams

CHAPTER FIVE: NUMERICAL INVESTIGATION FOR REPEATED AND REVERSE LOADINGS

5.1. General

Numerical and experimental investigation were studied to discuss the CDBs under different repeated loads. Three CDBs specimens have been tested under repeated load experimentally and then simulated using ANSYS software in order to get the validation percentages in accordance to the experimentally work. The simulation model was used for representing cyclic reverse load.

The following sections show the details of this work, taking into consideration that, the numerical results gives more smooth results and usually higher members' capacities due to the ideal conditions of computer programs. In another word, the real beams contain certainly many of dry shrinkage pores which may join by the applied load, that cannot to be found at all numerical simulation program which allows the higher members capacities for numerical simulations.

5.2. Model Simulation

The concrete simulated as Solid 65 which is an eight node isotropic brick element (hexahedral brick element). Each node contained three usual degrees of freedom [179]. It is suitable for concrete because provides the plastic deformation, creep and crash of concrete besides the capability of cracking in the three directions.

Many element sizes were investigated to get the best results matching. The best suitable size is (10*10*20) mm after many trial models (as shown in Table 5.1). Supports have been simulated as steel plates and considered as ALL DOF fixed at external ends while roller support at the middle support as shown in Figure 5.1. Steel reinforcement represented by link 180, which is two nodded line element may undergo the yield which is necessary for the imbedded steel (Figure 5.2).

Max number of iterations was 100, load increment steps were used, tolerance at displacement analysis was considered and equals 0.03. The applied load was every 5 kN for maximum load step and 1 kN for minimum load step. All inputs details were listed in Table 5.2.

Table 5.1. Convergence study for R.G10 beam

Meshing size	Experimental load (kN)	Experimental deflection (mm)	Simulation load (kN)	Simulation deflection (mm)
20*20*20	266	1.63	232.7	0.88
15*15*20			245.5	1.2
10*10*20			263.9	1.6
10*10*10			263.9	1.6

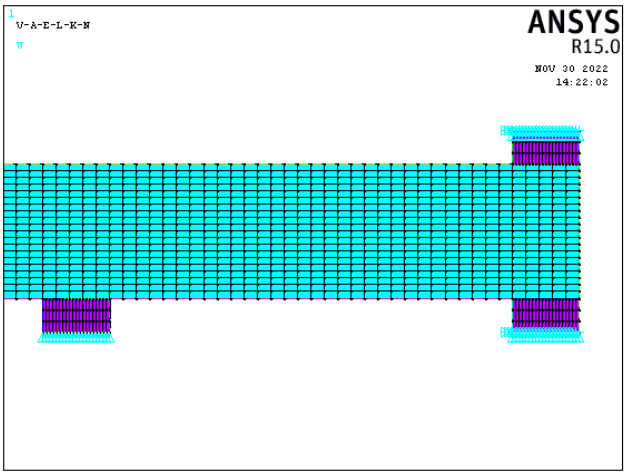

Figure 5.1. Meshed beam and supports

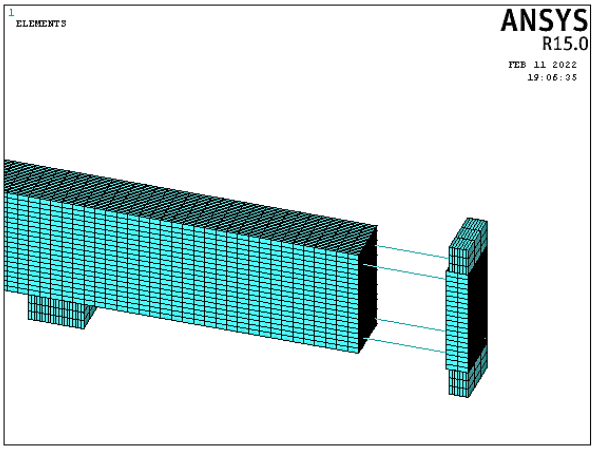

Figure 5.2. Steel bars simulation

Table 5.2. ANSYS input data

Material model number	Element type	Materials properties (MPa)	
1 (For concrete)	SOLID 65	Linear isotropic behavior	
		Ex	Defers from mix to another
		υ (PRXY)	Defers from mix to another
		Multi-linear isotropic properties	
		Expressed by the stress versus strain curves which were tested and listed at the third chapter for each rubcrete mix.	
		Concrete properties	
		Open shear coef.	0.2
		Close shear coef.	0.6
		Uniaxial cracking str.	Depending on the mix properties
		Uniaxial crashing str.	Depending on the mix properties
2 (For bearing plate)	SOLID 185	Linear isotropic	
		Ex	210000
		υ (PRXY)	0.25
3 (For steel bars)	LINK 180	Linear isotropic	
		EX(MPa)	210000
		υ (PRXY)	0.25
		Fy (MPa)	570.8
		Fu (MPa)	718.1

5.3. Monotonic Repeated and Reverse Loading

Repeated and reverse loads have been inserted into the program using the option of adding file. The rainfall style of loading (Figure 5.3) was used for repeated load and then converted numerically into reverse cyclic load. Noting that, the load is

applied at repeated and reverse as Ps which refers to 70% of the ultimate load capacity of monotonically loaded beam.

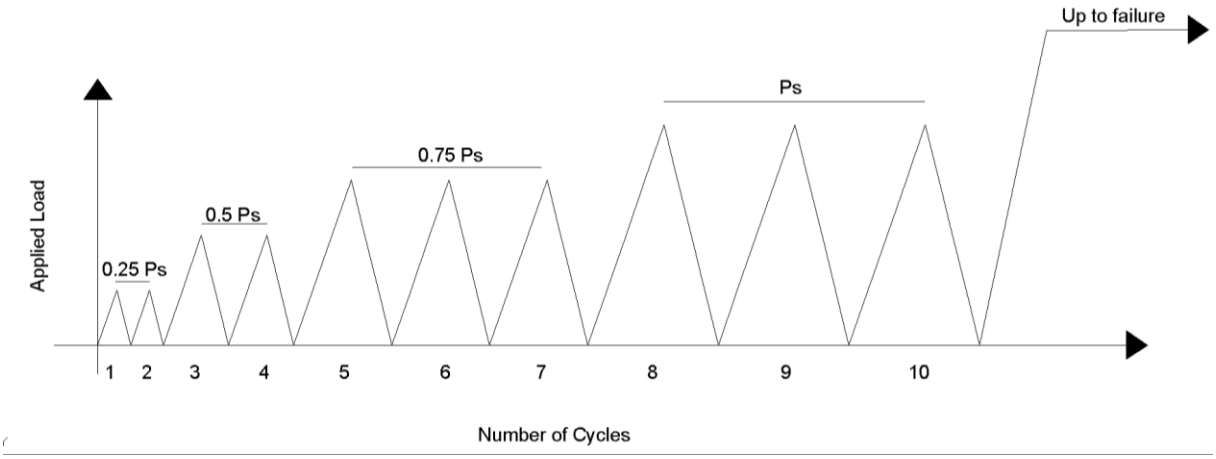

Figure 5.3. Repeated rainfall style loading

5.4. Static Load Simulating Results

After applying all material properties as input at ANSYS software, a good matching obtained from it (as could be seen at Figure 5.4 and Figure 5.5). Numerical analysis always produces results higher than the experimental work due to the exemplary condition of the concrete and even steel in the software. In which there are no creep and shrinkage cracks which exist at the realistic beam and develops during test and may cause earlier failure.

The beams show bending crack at positive and negative moment portions and the strut. As expected, the failure mode happened due to shear at strut as can be seen in Figure 5.6. First cracks appear firstly at the positive moment then the negative bending portions and finally the shear cracks which dominate the failure, other details illustrated in **Appendix F**.

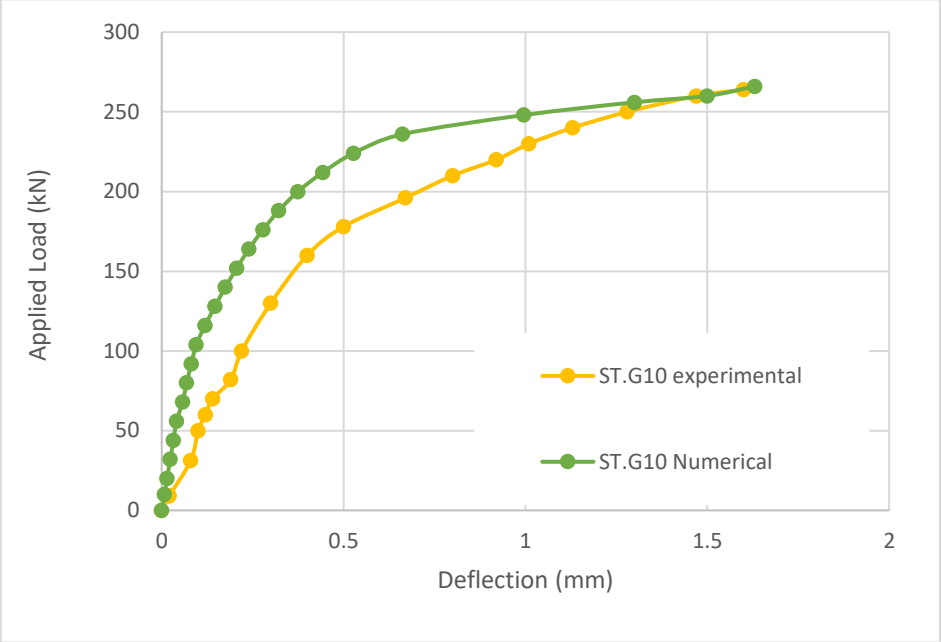

Figure 5.4. Experimental and numerical load deflection curves for ST.G10, right span

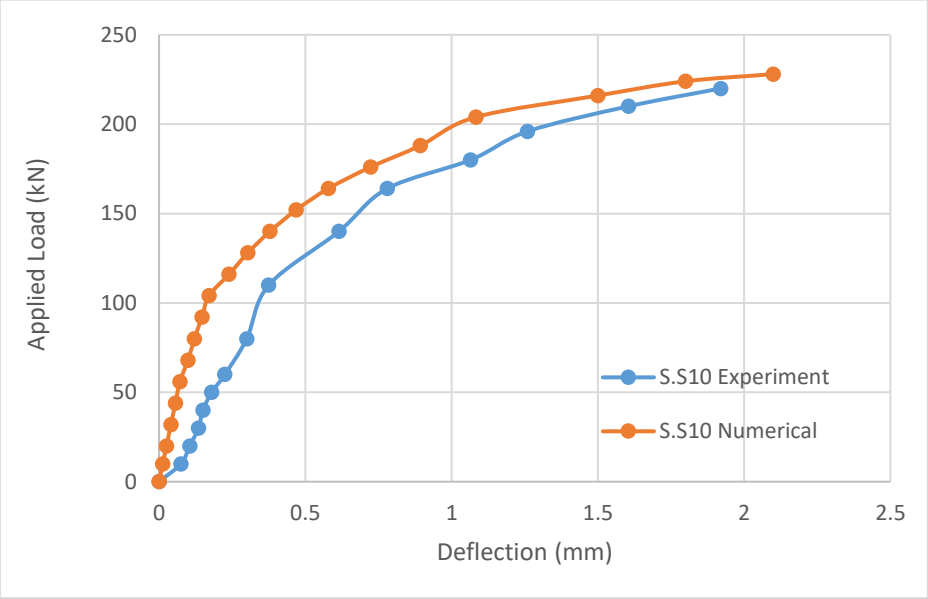

Figure 5.5. Experimental and numerical load deflection curves for ST.S10, right span

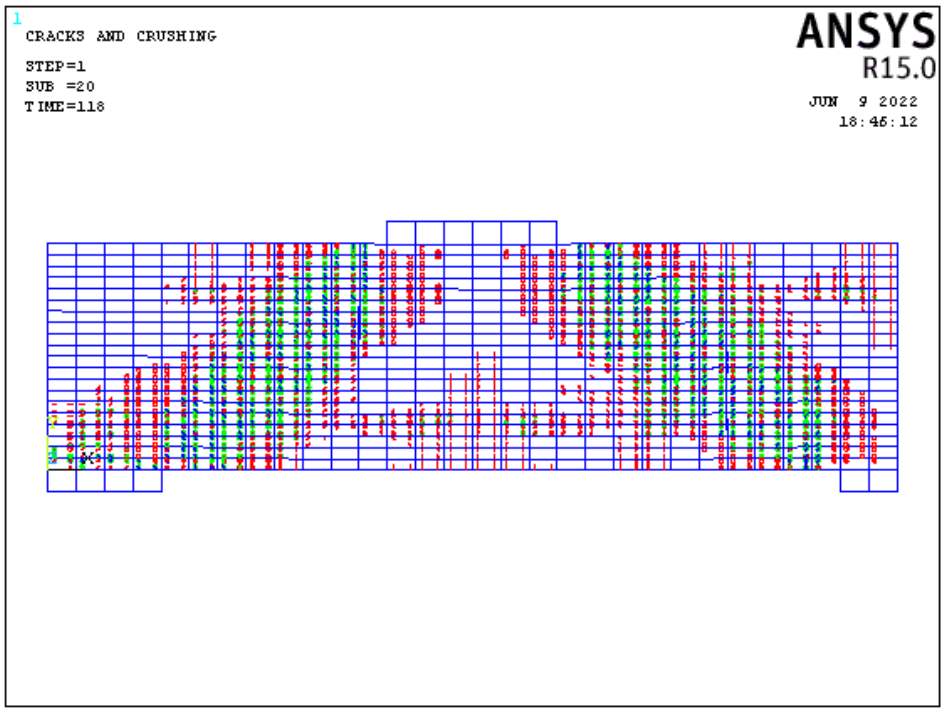

Sign of the flexural crack.

Sign of the compressive crack.

Sign of the diagonal tensile crack.

Sign of two cracks (the diagonal tensile crack is the first crack and the compressive crack that appears in the green circle outline is the second crack).

Sign of three cracks (the diagonal tensile cracks are the first and second cracks and the compressive crack that appears as blue circle outline is the third crack). [179]

Figure 5.6. Numerical failure mode for ST.G10 (for left span)

5.5. Repeated Load Simulating Results

The final loading stage were listed for more visibility at Figure 5.7. It can be noting that, there is a matching in behavior between experimental and numerical results for the both mixes. There is a slight difference between them caused by the material properties simulating and the high ideality of the numerical analysis simulant. The difference between numerical and experimental for gravel and sand specimens were 3% and 7% respectively. Crack pattern failure is listed in Figure 5.8.

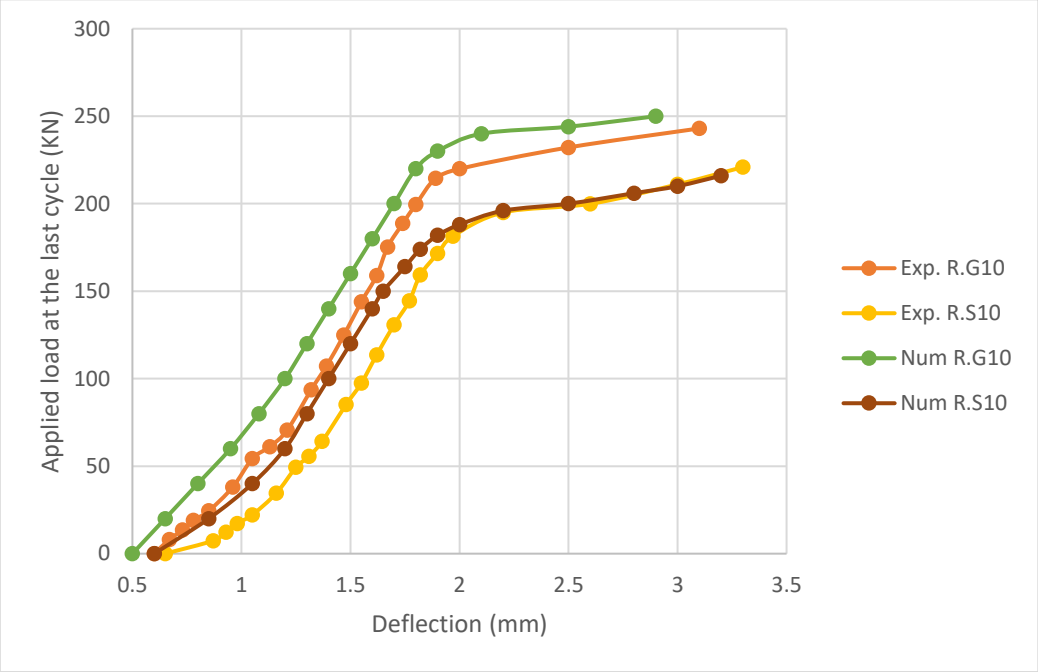

Figure 5.7. Experimental and numerical curves for R.G10 and R.S10 specimens

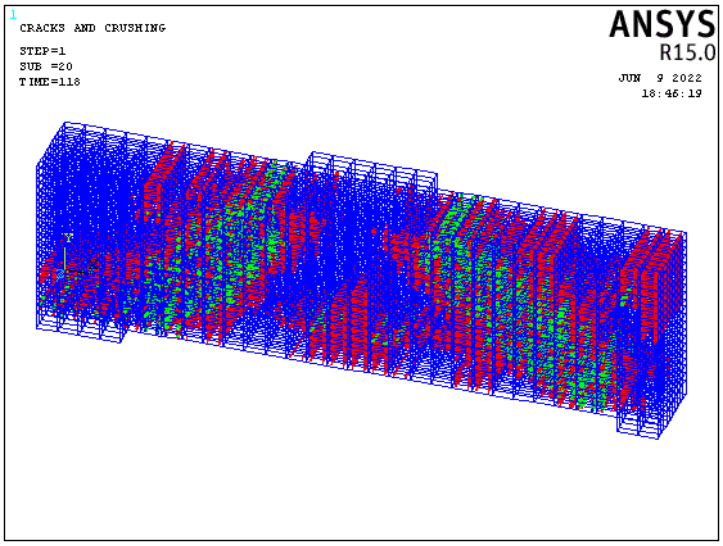

Figure 5.8. Cracks pattern for samples under repeated load

5.6. Reverse Loading

The same loading process of repeated rainfall style depends on to simulate the reverse wave using ANSYS solution control options. All modelling data involves the static and repeated samples are successfully worked on the reverse cyclic loading. The same behavior of failure observed for all specimens modelling

results. The CDBs forms upward and downward struts crossed at the N.A. which made a point of high stress intensity due to the negative and positive cracks. The presence of rubber plays a significant effect on the cyclically loaded beam's deflection. The amount of deflection increases gradually by rising the weight of rubber in the mix.

The ultimate load capacity of each sample is affected by the concrete compressive strength in the first degree, and secondly be the amount of cracks in the beam (increasing rubber leads to higher micro cracks inside the concrete mix, and that is because of leaking bond between cement paste and the rubber particles). Figure 5.9 to Figure 5.15 list the behavior of conventional and rubberized CDBs under reverse cyclic loading. Noting that, each sample was named initially by the letter **C** which denotes to Cyclic load and then followed by the replacement way and its percentage.

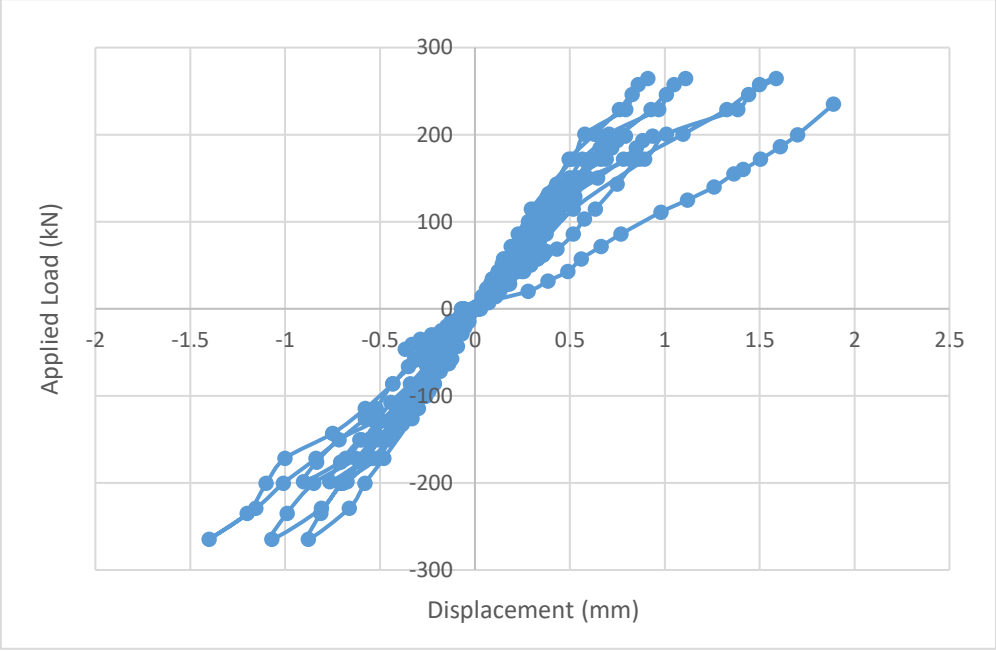

Figure 5.9. Load-deflection curve of conventional CDB under cyclic load

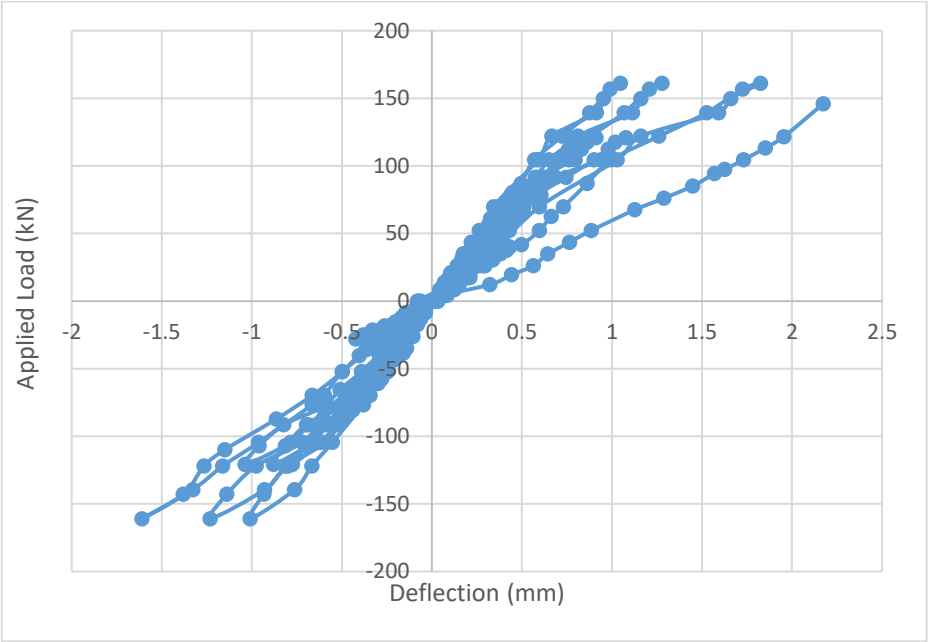

Figure 5.10. Load versus deflection curve for C.S10

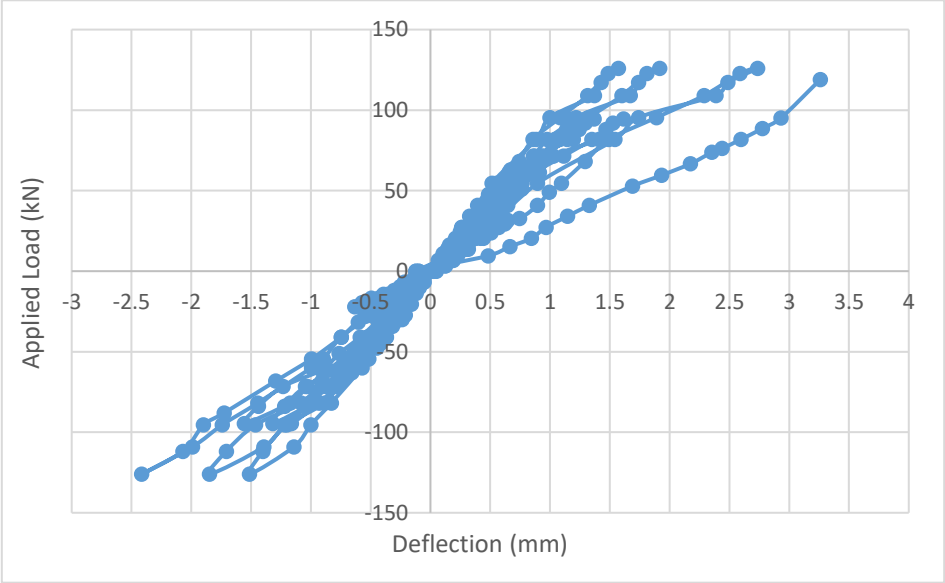

Figure 5.11. Load-displacement curve for C.S20

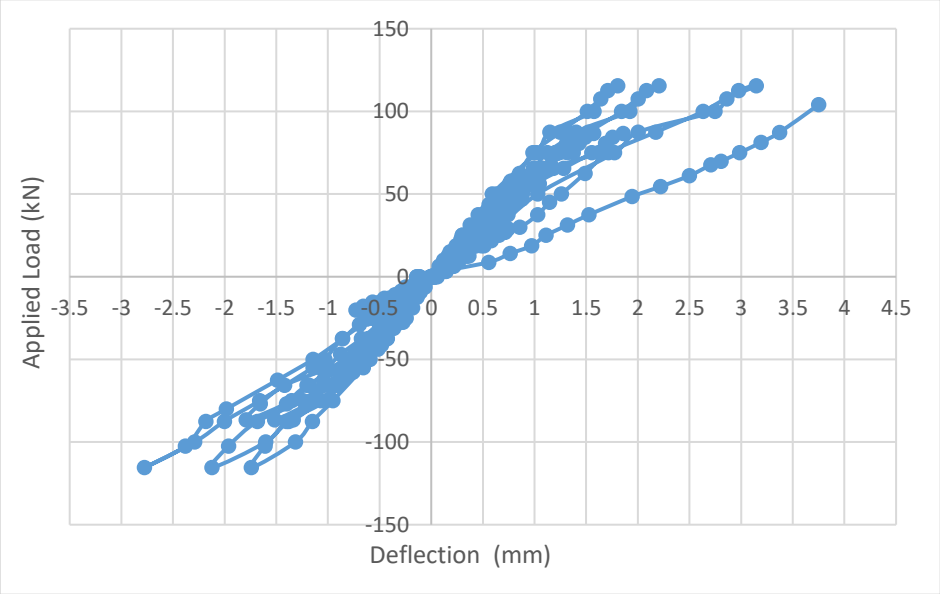

Figure 5.12. Cyclic load-deflection curve of C.S30

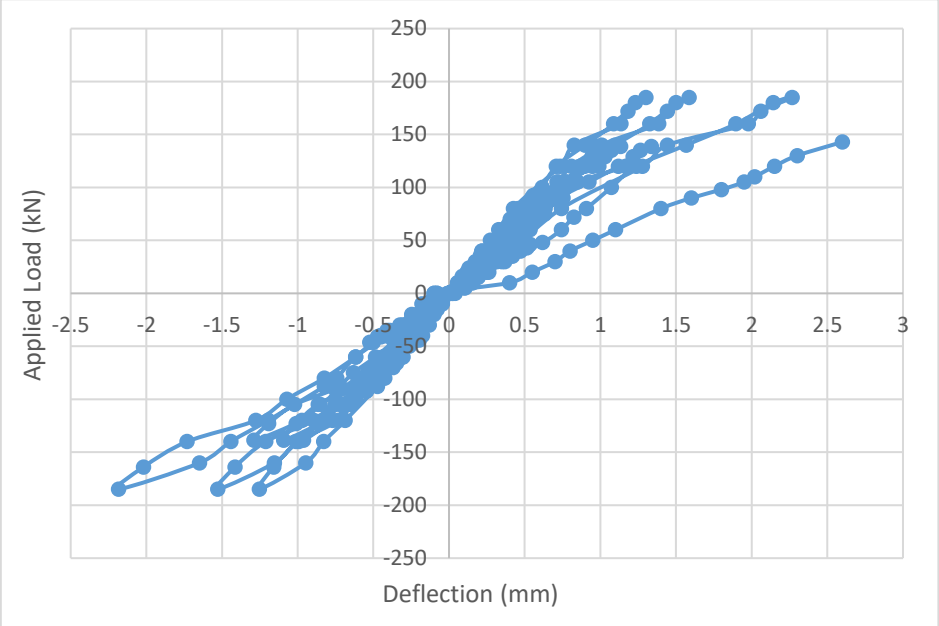

Figure 5.13. Cyclic load versus deflection curve of C.G10

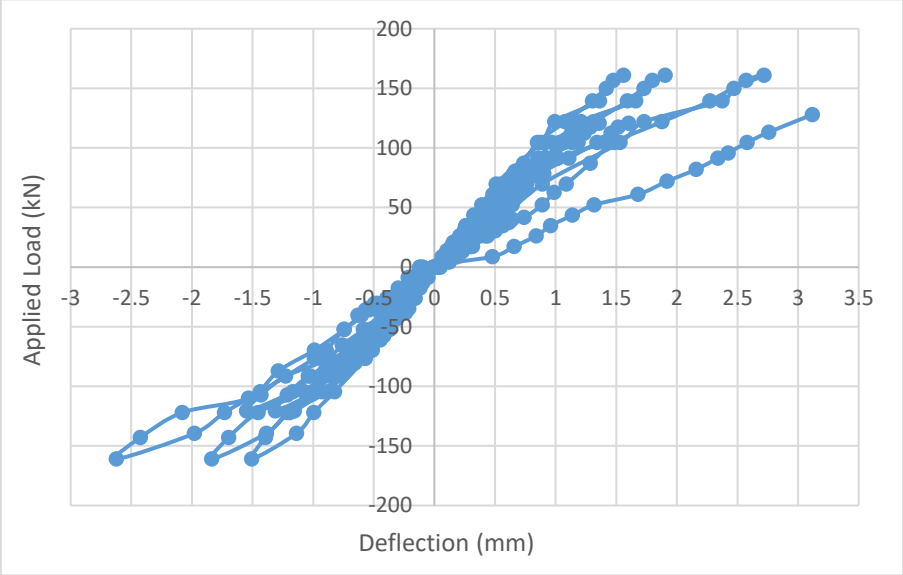

Figure 5.14. Applied cyclic loading on C.G20 sample

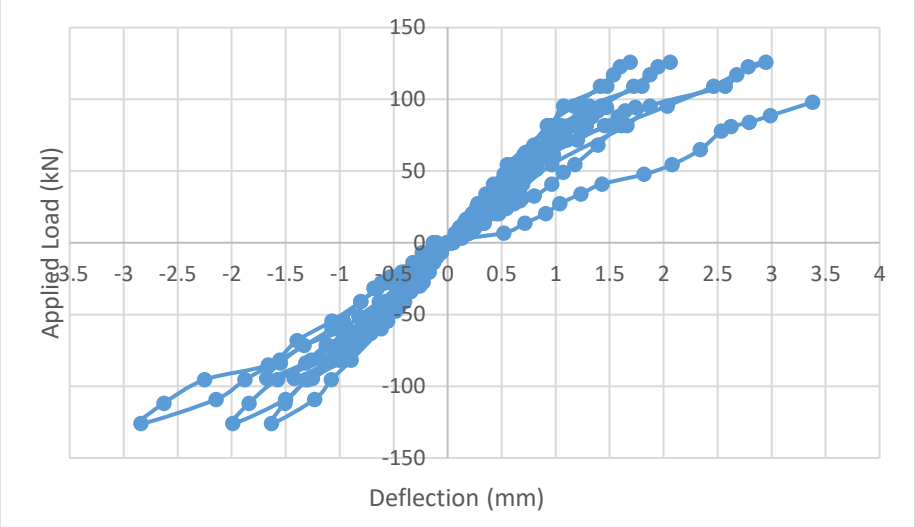

Figure 5.15. C.G30 Applied cyclic loading

After the cycles, the CDBs are loaded monotonically till failure as explained in Figure 5.16. The slope of curves decreases gradually after each percentage of rubber replacement, due to the changing of concrete mix behavior from brittle to ductile. It is noted that, the replacement method (sand or gravel) has no essential significant effect, because S10 and G10 data almost approached, as well as the same curves data. It's clear to notice that from Table 5.3, the CDBs losses between

34 to 45 % of its capacity after the ten rainfall cycles. It is a logical result and matched with a decreasing occurrence at [164].

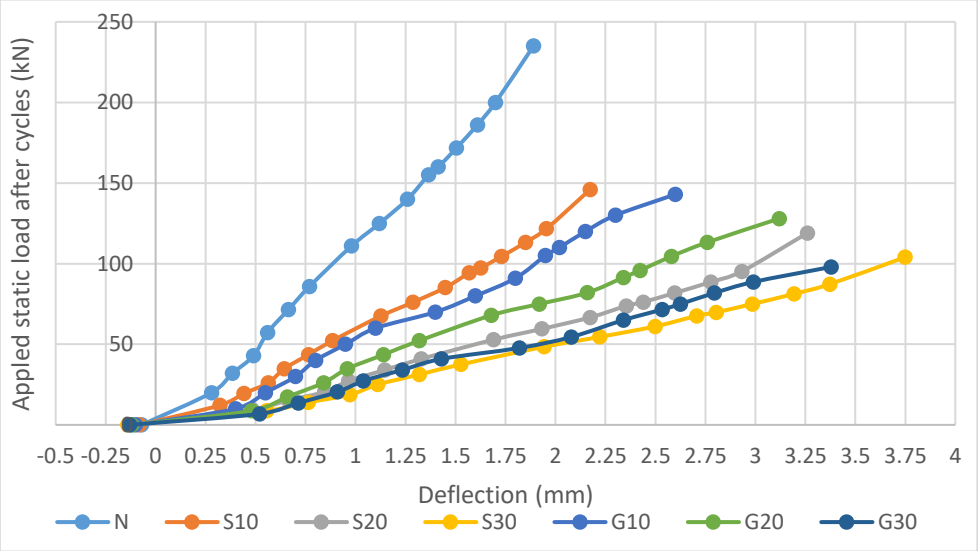

Figure 5.16. Numerical load-deflection curves at the final stage of reverse loading

Table 5.3. Decrement percentages of beams capacity after reverse cycles

Sample	Static test (kN)	Static after cycles of reverse loads (kN)	Dropping strength (%)
ST.0	378	235	37.83
ST.S10	230	146	36.52
ST.S20	180	119	33.89
ST.S30	165	104	36.97
ST.G10	264	143	45.83
ST.G20	230	128	44.35
ST.G30	180	98	45.56

CHAPTER SIX: CONTINUOUS DEEP BEAMS UNDER HARMONIC LOAD

6.1. Introduction

Concrete deep beams largely exposed to dynamic loads in different intensities and since the concrete is a brittle material, then the researches nowadays towards to enhance the concrete energy absorption to dynamic loads. The published researches confirmed that, replacing scrapped tire rubber by a percentage of aggregate (or even adding it into the mix) provides an excellent energy absorption (but decreases the mechanical properties of concrete)[32], [41], [113], [180]–[186]. The enhancement in impact energy of rubberized concrete (rubcrete) mixes reached to (138-185-300-396)% for 5, 10, 15, 20% volumetric sand replacement, While (150-204-326-426) % for the same percentages of volumetric gravel replacement [187]. Too many types of dynamic loads may the CDBs exposed to, such as impact, seismic and moving vehicles load.

The simple form of harmonic load may occur by unbalanced rotating machines in building. Also, it may cause by hydrodynamic pressure which is generated due to propeller at the stern of a ship or by inertial effects in reciprocating machinery, and this types is more complex. It is worth to mention that the harmonic wave may come in different types which are: fundamental wave, 3rd harmonic wave and the distorted wave.

CDBs may exposed to harmonic loads at bridges due to vehicle collision and that will cause sin or cosine wave load on it. Adding rubber into concrete mix leads mainly to develop the concrete energy absorption of the bridges and enhance the overall dynamic properties. It can be noted from the next section that, there is no cutting-edge studying results gives us an indication about the CDBs response

under harmonic loading. So, the study consists of three parts, the first one is deriving a theoretical solution for analyzing the CDBs under harmonic loads. While the second involved the theoretical solution for checking the accuracy of numerical analysis. The third part studied the effect of adding rubber to concrete mix on the behavior of CDBs under harmonic load, using ANSYS V.15.0 software program.

6.2. Methods

The problem has been solved by three solutions. The first two are theoretical analyses which depend on deriving new equations for simulating the deflection of concrete continuous deep beams under sinusoidal loads. These two methods comprised the dynamic general equation and the Timoshenko beam analysis. While the third solution involved a simulation of concrete beam by ANSYS software and comparing gotten results with the theoretical results then investigates some case studies to get the full description of parameter effect on the CDBs. Figure 6.1 shows a block diagram of the complete work and Figure 6.2 shows the selected CDBs model.

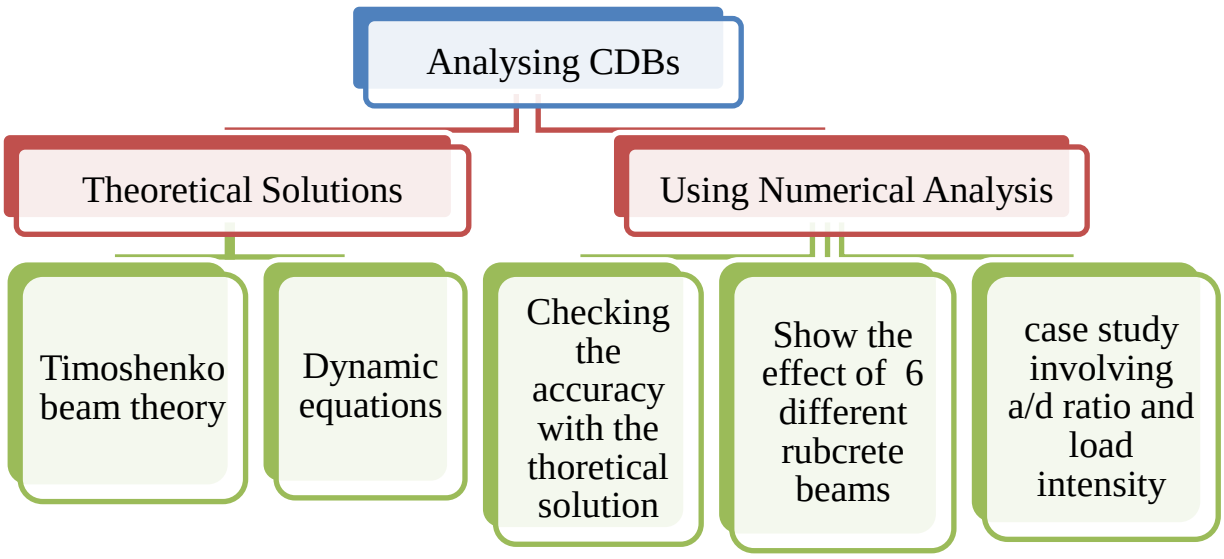

Figure 6.1. The adopted study plane of harmonic load

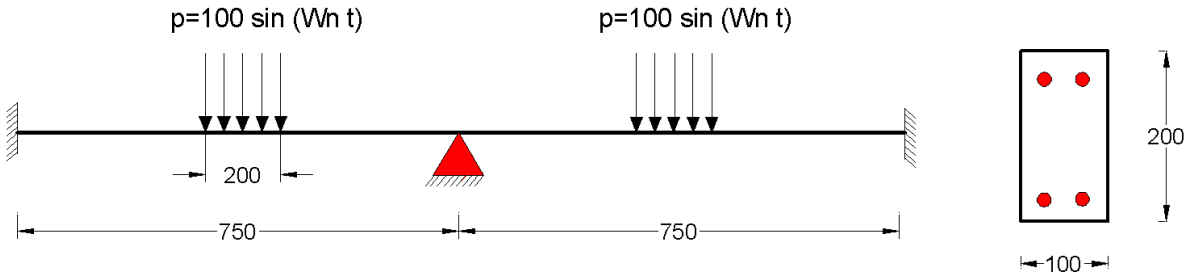

Figure 6.2. Studied beam details

6.2.1. Timoshenko Beam Solution

It is difficult to get a plastic theoretical solution for CDBs under the effect of harmonic load. So, an elastic solution has been derived and adopted. Timoshenko beam theory [149] has been used which satisfied the requirement of deep beams, which are

- The plane section does not remain plane after bending.
- The normal to the neutral plane after bending will not remain normal to the neutral but have an additional rotation due to high transverse shear deformation.
- Neglecting normal strain along the width.The deriving equation of deep beam deflection shown in equation (6-1).

$$\frac{d^4w}{dx^4} = \frac{q}{EI} - \frac{1}{c^2GA} \times \frac{d^2q}{dx^4} \tag{6-1}$$

Let $w(m) = \sum_{m=1}^{n} sin(\frac{2m\pi x}{l})$ to satisfy the boundary conditions of continuous deep beam. Substitute in equation (6-2), to get the final equation of CDB deflection under harmonic load (Equation

$$w_{at\ mid\ span} = 0.09752\, sin(w_n\, t) \tag{6-2}$$

6.2.2. Dynamic Equation Solution

In general, the structural members resist the dynamic load by its mass, stiffness and the magnitude of damping which depend on the material itself [20]. The damping ratio ignored in most structural calculations for safety. For concrete, the damping factor does not exceed 6%. For solving the CDBs under sinusoidal loads, the dynamic equation response of structures has been derived with ignoring the effect of deep beams, as listed below (Equation (6-3))

$$m\ddot{y} + c\dot{y} + ky = F(t) \tag{6-3}$$

Applying the same details of beam at Figure 6.2, to get the time deflection equation for the given beam (Equation (6-4)). The details of all solutions can be found at **Appendix G**.

$$y = \frac{\frac{F(t)}{m}}{\frac{k}{m} - w_n^2} \tag{6-4}$$

6.2.3. Numerical Simulation

Beam 188 element has been used for simulating the CDB in ANSYS software [179] (As shown in Figure 6.3). After trying some meshing sizes, it was found that, 20 mm meshing length gives a good agreement with the theoretical model in such fast-rendering time. External supports were selected to be fixed while the internal was of single vertical reaction.

Seven concrete mixes has been simulated depending on Topcu's tested mixes [42], three percentages has been used which are (15, 30, 45) % for sand and gravel replacement besides the ordinary conventional mix. All concrete properties has been considered from reference [42] results. Compressive strength, tensile strength, concrete unit weight and young's modulus for all mixes were inserted at Table 6.1. The inputted stress versus strain curve shown at Figure 6.4. Young's modulus has been considered using the ACI 318- 19 (Equation (5)) which is proportional to rubcrete weight (and as adopted for rubcrete mixes at reference [44]).

Table 6.1 Shows details of elastic modulus values for all selected mixes. The analysis was displacement control with a tolerance factor equals 6%.

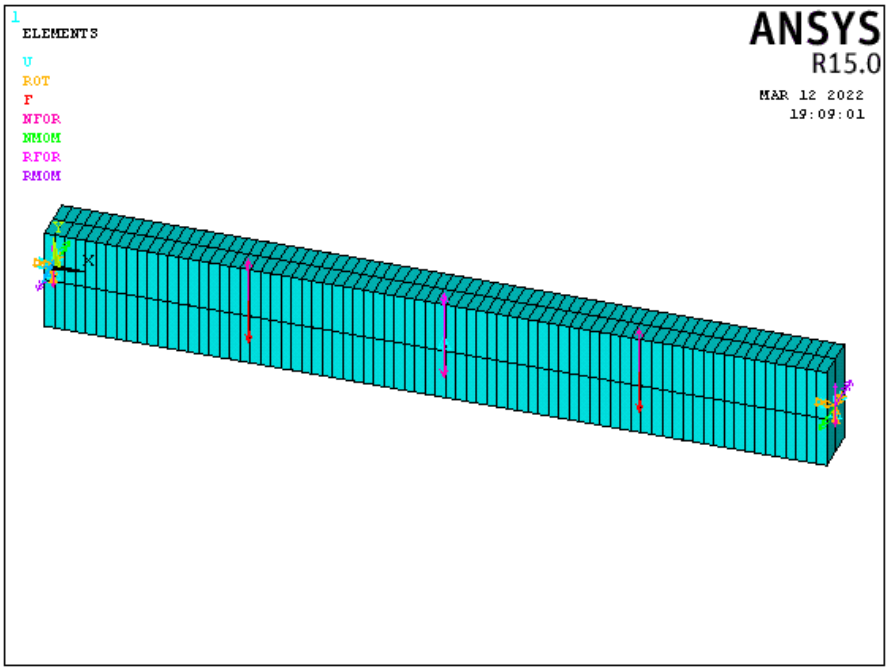

Figure 6.3. CDB modelling at ANSYS software for harmonic load

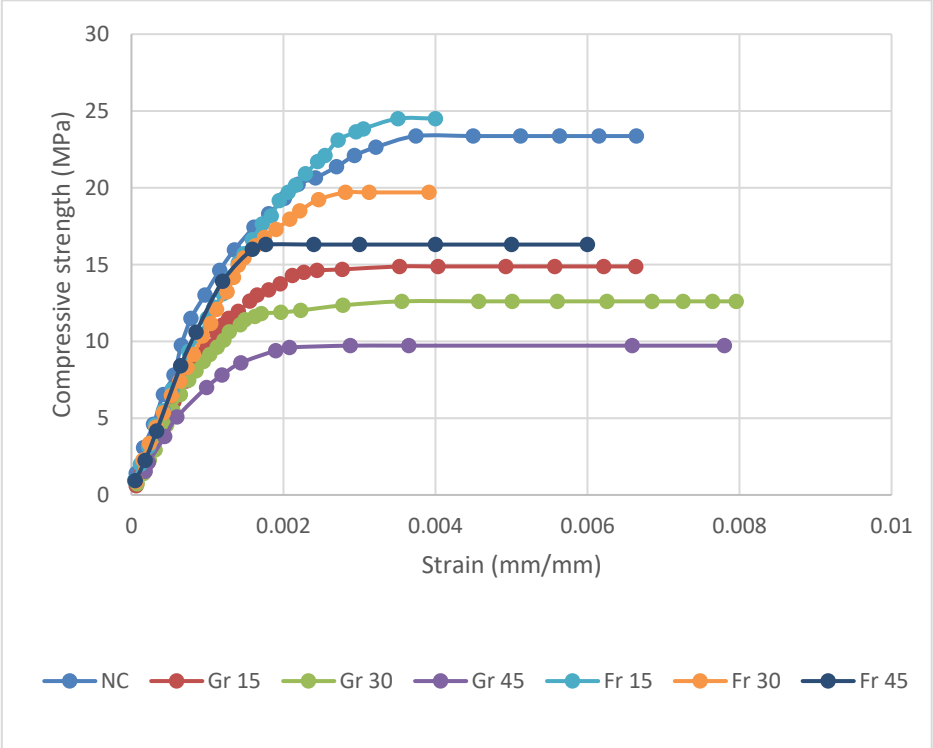

Figure 6.4. Inserted stress-strain curve into program [42]

Table 6.1. Mechanical concrete properties [42]

Mix	w_c (Kg/ m^3)	f_c' (MPa)	f_t (MPa)	Ec (MPa)
NC	2300	23.48	3.21	22983
G15	2220	16.18	1.50	18092
G30	2140	12.62	1.06	15122
G45	2010	9.9	0.82	12192
S15	2220	24.22	2.17	22135
S30	2140	19.7	1.53	18894
S45	2010	14.77	1.13	14892

6.3. Results

6.3.1. Comparison Between the Theoretical and Numerical Results

The validation between numerical and theoretical solutions have been investigated as illustrated in Figure 6.5. A good match in beam response between the numerical and the Timoshenko beam solutions with slight difference in the amplitude between them caused due to that, the nonlinear simulation gives more accurate results because it simulates the problem as it is in the nature in a matter accurate than the theoretical solutions. This nonlinear model has been considered to use for simulating a parametric study for rubcrete beams. While, the solution using the general dynamic equation also gives the same response but with less accurate due to ignore the effect of deep beam effect, the same cause make it in difference with the Timoshenko equation solution. It causes an error in deflection magnitudes but the good point, it also gives the same response.

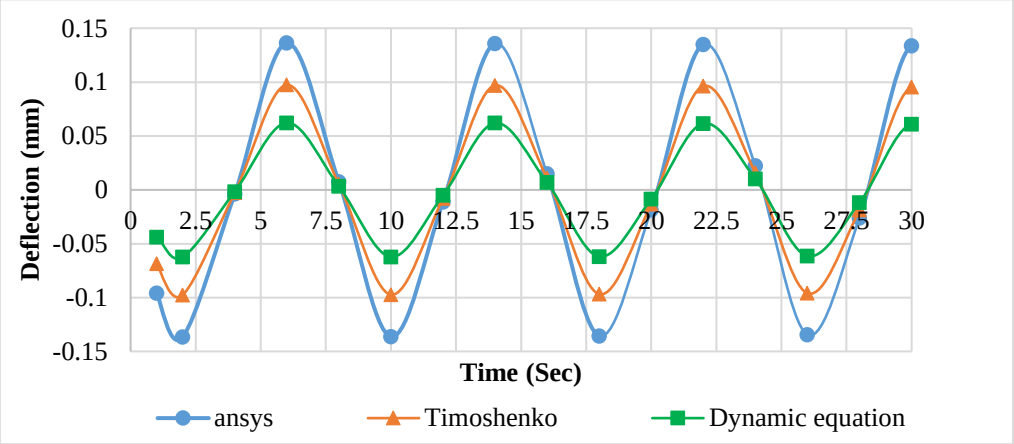

Figure 6.5**.** Verification of deflection by theoretical and analytical solutions

6.3.2. Rubberized CDBs Results

Nonlinear solution has been investigated to study the effect of sinusoidal harmonic load for seven beams. One beam was simulated without any rubber replacement in order to be the reference model, the first group was of three beams with 15, 30, 45% of gravel replacement (GR) and the second group is of the same percentages of fine aggregate replacement (FR). The results for the seven beams as illustrated in Figure 6.6 to Figure 6.8, the displacement, velocity and acceleration have been discussed. From Figure 6.6, it can be noting that, the beam of normal concrete (NC) deflects in the less magnitude than the other beam due to its higher compressive strength and low elasticity. Beam GR45 shows the maximum values of displacement due to the sinusoidal load because of its low compressive strength, elastic property, and large ability to absorb energy. Also, the negative values of deflection were higher than the positive, which refers to that the beam approaches from cracking. In another word, if the all-deflection points were in negative zone, then the beam is fully cracked. For all beams, the time period does not change in contract with the amplitude. Velocity of beams have been also investigated in Figure 6.7. The velocity wave formed as distorted wave (the latter is a combination between fundamental and the third harmonic wave). The same arrangement of amplitude appears at acceleration responses, as shown in Figure 6.8.

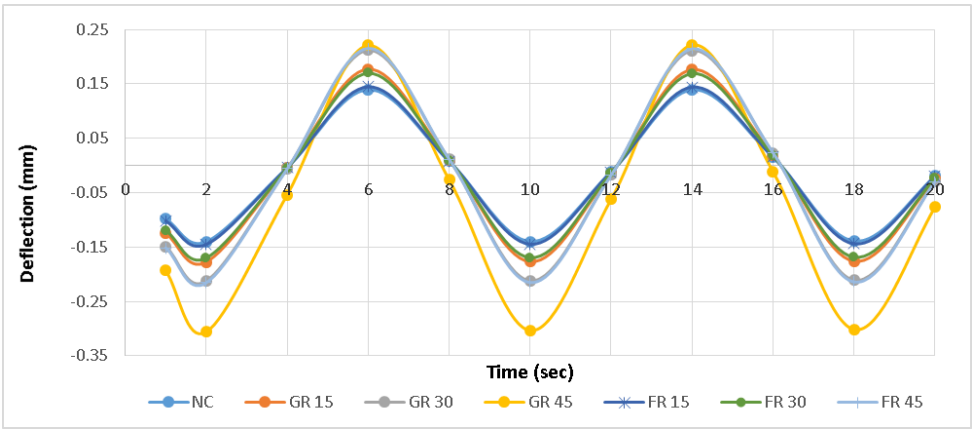

Figure 6.6. Deflections- time curves for rubcrete beams

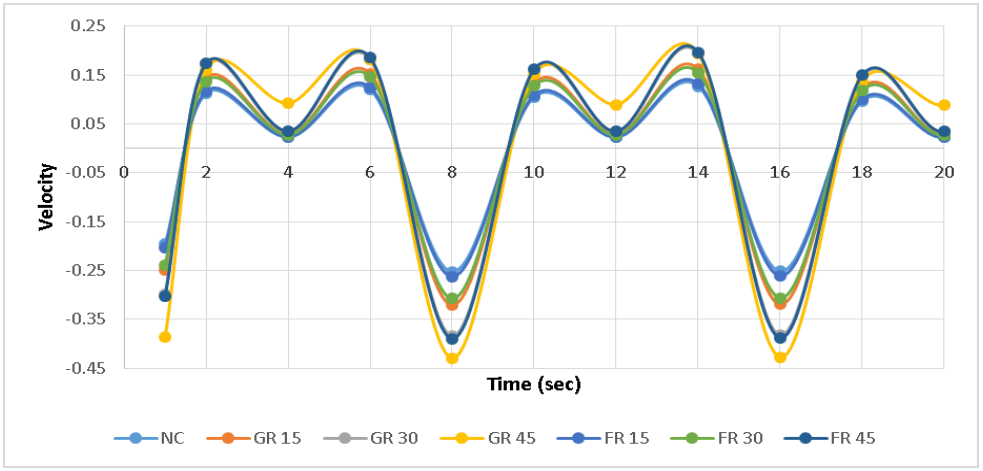

Figure 6.7**.** Velocity-time curves for different rubberized beams (mm/sec)

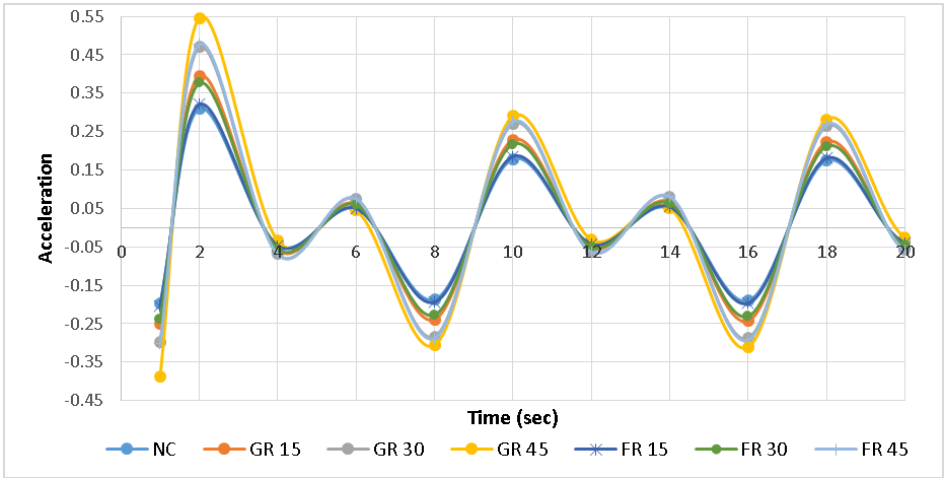

Figure 6.8. Acceleration versus time curves (mm/sec^2)

6.3.3. Case Studies' Results

6.3.3.1. a/h Ratio Influence

The beam GR 45 showed the weakest model due to its low compressive strength and its high elasticity, so it has been considered for modelling the effect of changing a/h ratio because it represents the more dangerous case of rubcrete. Theoretically, the CDB behavior approaches to be flexural with a smaller a/h ratio, and its shear strength capacity increases linearly with a/h reduction [19]. The smaller a/h ratio shows minimum deformation capacity of CDB also ductility and beam load capacity [20], [21]. This fact has been also noticed in the dynamic analysis of the rubcrete beams. The model of a/h=0.5 shows less displacement against the same load and rubcrete properties. The time durations of waves were still deposit, but there is a visible difference in beams' amplitudes for all the given deep beams due to a/h difference, as shown in Figure 6.9.

But in case of using a shallow beam (a/d=3), the velocity and acceleration amplitudes and periods changed (Figure 6.10 and Figure 6.11). The time periods shift to the left with staying on the overall general wave shape. While the deflection (Figure 6.9) of shallow beam still keeps the periods and the overall general wave shape, but with a significant large displacement comparing with the deep beams due to its higher bending capacity.

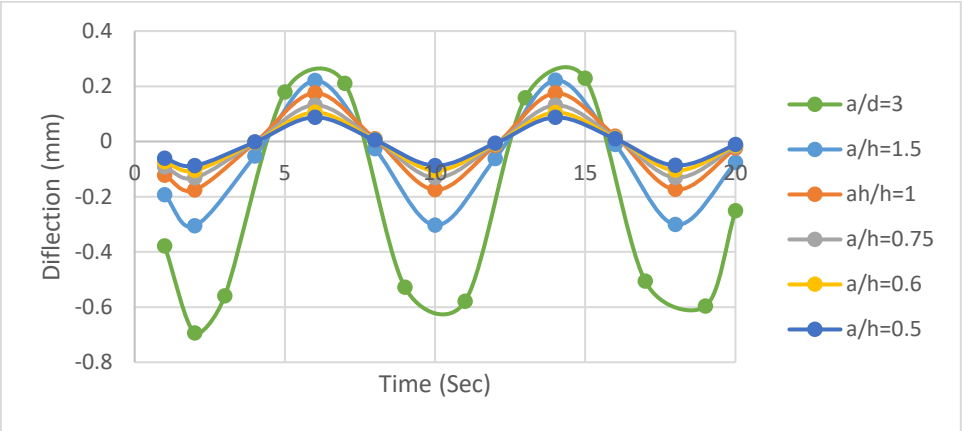

Figure 6.9. Influence of a/h ratio on rubcrete beams' deflection

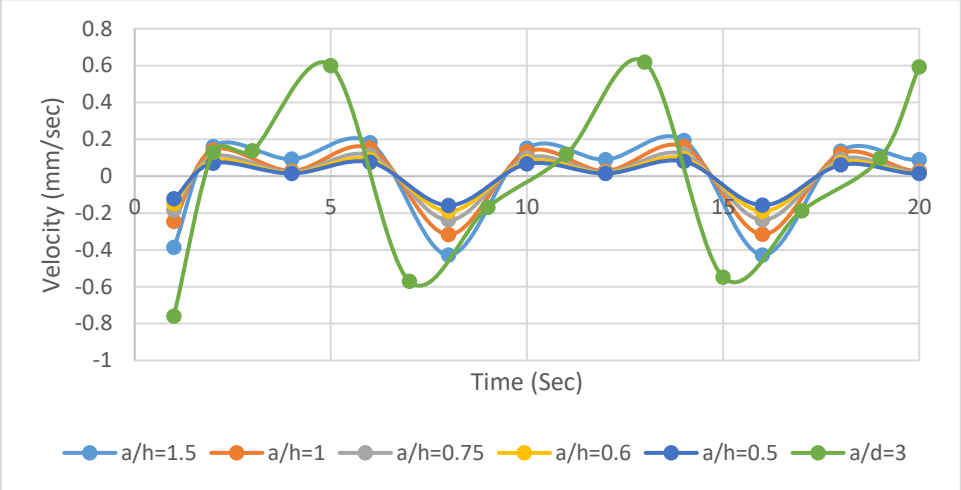

Figure 6.10. Velocity of CDBs of different beams depth

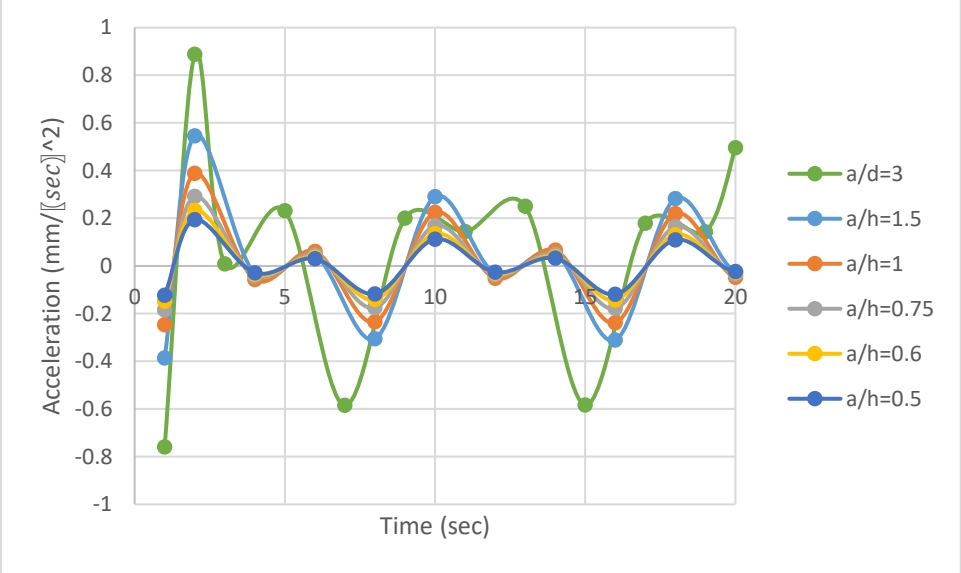

Figure 6.11. Acceleration of CDBs of different depths (mm/sec^2)

6.3.3.2. Load Intensity

The specimen GR45 has been selected to study the influence of incrementing load intensity. The original selected load has been doubled, tripled, quadruple and quintuple. It can be seen that, the relatively low loads vibrate the beam about the original zero displacement axis but the higher ((300 and 400) × $sin\, W_n t$) product the same wave shape occurs with high negative displacement only. Quintuple load forces the rubcrete model to a plastic flow. Also, from curves at Figure 6.12, it can be

concluded that, the vibration amplitude of rubcrete CDBs depends in the first degree on a/h ratio, beams' natural frequency and the load intensity. The last conclusion also matches with reference [22] discussions.

The higher displacement occurs when quadrupling the load, the beam deflects more by 92%.

Figure 6.13 to Figure 6.17 show the stress versus time for CDBs. It can be noting that, the stress waves gets bigger when increasing harmonic load intensity on beams.

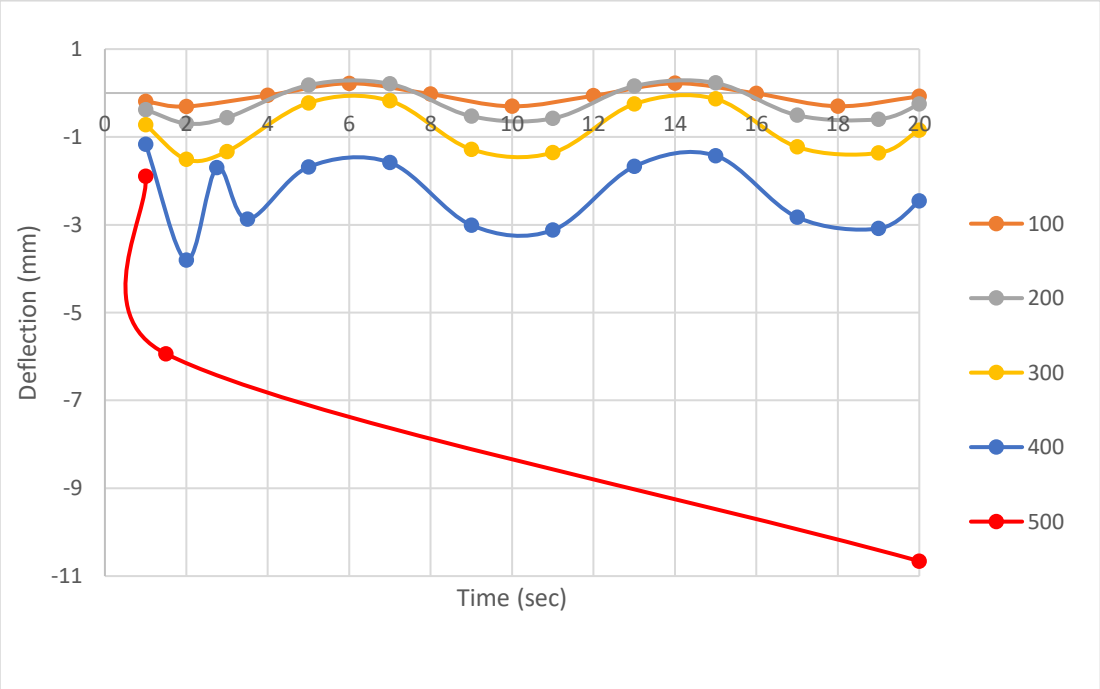

Figure 6.12**.** Effect of load increment on CDB deflection response

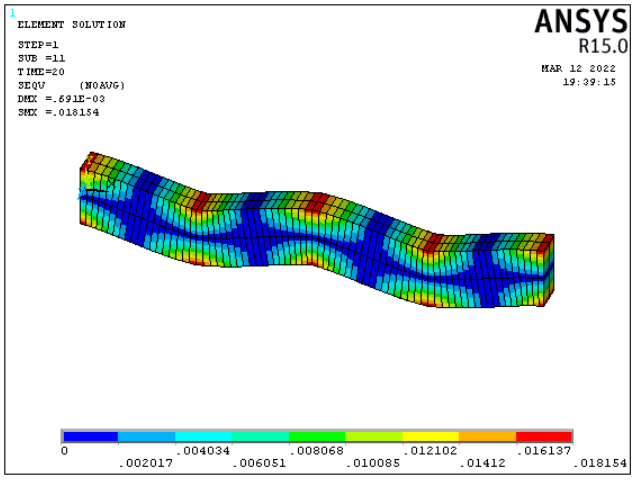

Figure 6.13. Von-Misses Stress for 100 $sin\, W_n t$ loading

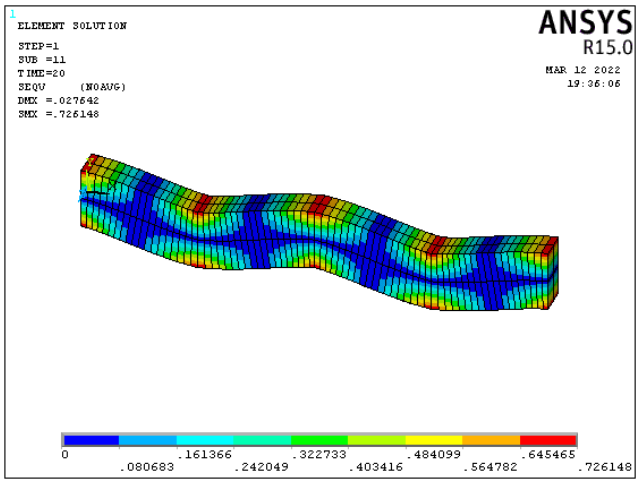

Figure 6.14. Von-Misses Stress for 200 $sin\, W_n t$ case

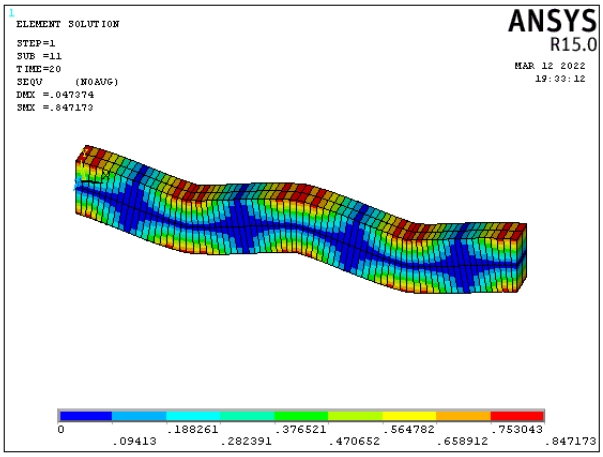

Figure 6.15. Von-Misses Stress for 300 $sin\, W_n t$ case

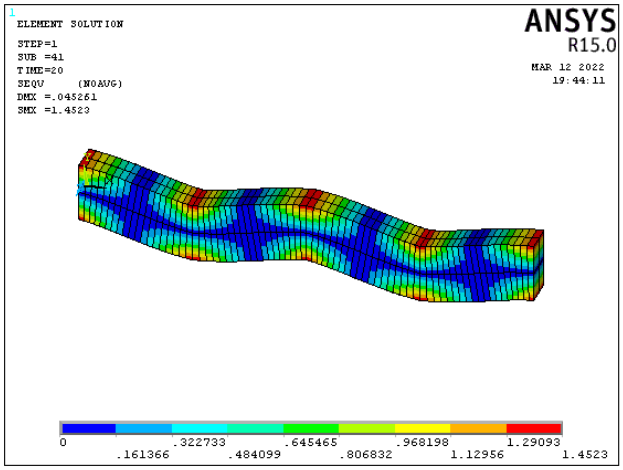

Figure 6.16**.** Von-Misses Stress for 400 $sin\, W_n t$

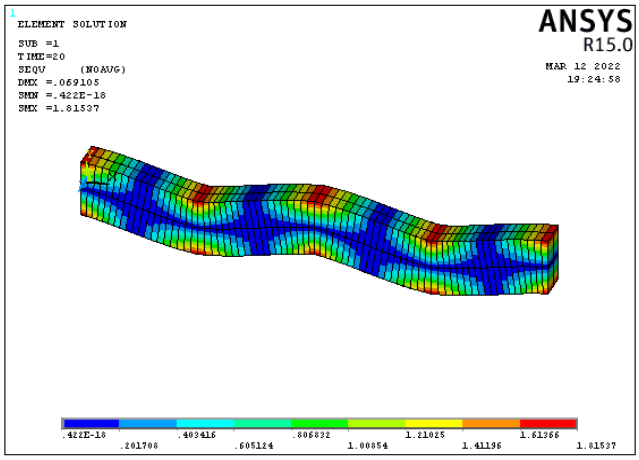

Figure 6.17. Stress for 500 $sin\, W_n t$ loading

CHAPTER SEVEN: CONCLUSIONS AND RECOMMENDATIONS

7.1. Rubberized Concrete Mixes Conclusions

1. The converting factor (CF) from rubberized cubes to rubcrete cylinders is found to be ranged from 0.82 to 0.76 which matches the normal converting factor, and it is recommended to be used for rubcrete mixes.
2. Converting the rubcrete compressive strength from 100*200 cylinder to 150*300 cylinder ranges from (0.86 to 0.94) for 10%, 20% and 30 rubber replacement.
3. Replacing 30% of gravel by chips and 30% of sand by crumb, leads to decrease the concrete tensile strength by 46% and 52% respectively.
4. The impact resistance develops to 662.5% and 1350% when replacing30% rubber by sand and gravel respectively.

7.2. Monotonic, Impacted and Retested Rubberized CDBs Conclusions

1. STM is more suitable and accurate for rubcrete than the conventional concrete CDBs.
2. Conventional concrete beams losses capacity equals 39%, 52% and 56% when replacing sand-crumb by 10%, 20% and 30%, while losing 30%, 39% and 52% respectively for the same percentages of gravel-chips replacement. One can conclude that, gravel replacement is better than the sand replacement according to the ultimate strength.
3. References continuous deep beams which impacted by 30kg and 40 kg loss capacity equal 23.81% and 36.51% respectively.

4. Rising the intensity of impact from 30 to 40 kg for G30 beams lead to rising the amount of losses from 33.33% to 43.89%, Also, for S30, the magnitude of losses in beam capacity rises from 35.45% to 46.67%.
5. The beams in spite of its deepness, is still has the capacity to cumber and behave as a continuous beam.
6. The value of conventional concrete strains (I30 and I40) do not accede the logical strain 0.003.
7. The effect of rubber allows the CDBs to absorb more energy, replacing sand versus crumb by 10%, 20% and 30% leads to rise all G2 strains by 2.3%, 10.7% and 10.97% respectively.
8. Rubcrete allows the beams to deform more due to its flexibility when comparing with the conventional concrete and gravel replacement product CDBs more flexible than the sand replacement.
9. The conventional CDBs after hit lost 9.25% and 12.5% for 30 kg and 40 kg respectively. While for 30% sand replacement, the CDBs loss 2.12% and 2.42% respectively, and for 30% gravel replacement, the decrement is 2.77% and 3.33%, respectively.
10. Adding 10% of chip replacement decreases the negative strains G1 and G3 by 21% and 28% respectively and 29% decrement for the impacted tie zone.
11. Due to 30kg of impact, the CDBs loss 42% and 37% for 10% sand and gravel replacement respectively, while the decrements of impact are 39% and 30%. Thus, the effect of impact on rubber on CDBs decreases by 3% and 7% respectively.
12. For the 30kg beams, replacing sand versus crumb by 10%, 20% and 30% leads to rising all G2 strains by 2.3%, 10.7% and 10.97% respectively, while decreasing G3 strains by 25.6%, 4.2% and 63.1% respectively.
13. Comparing between sand and gravel replacement beams (30kg), it can be observed that, the most strains at crumb impacted spans are larger than the

impacted strains at chips beams. For G1 points, the presence of 10%, 20% and 30% of crumb increases the strain by 18.7%, 0% and 16.7% when comparing with the same percentages of replacement with chips, respectively.

14. Static load after impact develops the impact cracking and causes to collapse the beam by strut shear failure.
15. In discussing the effect of discontinuity of the beams (I30.G30 and I30.G30.SS), it can be concluded that, The simply supported beam prefer to bent that to overcome the load by shear, G2 is larger simply by 15% than the continuous beam.

7.3. Repeated and Reverse Rubberized CDBs Conclusions

1. The ultimate strength of the beams decreases when comparing with the static loads by 18%, 8% and 4% for conventional, gravel and sand replacement respectively. Ultimate load capacity of R.G10 larger than R.S10 due to the higher compressive strength of the first, while deflection values for sand replacing beam are slightly larger than the R.G10 due the higher flexural capacity of S.R.10.
2. The rubcrete is more suitable for repeated loads, as well as the sand replacement is better than the gravel replacement according to the result of repeated load.
3. The dropping in CDBs after many cycles of loading ranged (33% to 37%) for sand replacement and (44% to 46%) for gravel replacement.
4. The rubberized CDBs losses 35 to 45% of their capacity when comparing with the monotonically loading beams.
5. For the reverse cyclic load, each load (positive or negative) make its own strut, till it’s crossed together.

6. CDBs which contains 10%,20% and 30% of rubber, their ultimate strength dropped due to the repeated reverse loading which exposed on them by 36%, 33%, 37% for sand replacement, and 45%, 44%, 45.5% for gravel replacement.

7.4. Harmonically Loading Rubberized CDBs Conclusions

1. Timoshenko beam theory can be used for harmonic loaded with a significant degree of exact to obtain the elastic response of CDBs.
2. When solving the beam by using the general dynamic equations gives a correct estimation for the beam response but error values of displacement due to ignoring the deep beam effect.
3. Beam element 188 (in spite of its nonlinearity and it is a 2D model) offers a good degree of validation and the exactly same response with the theoretical method.
4. The sensitive of concrete deep beams towards a/h ratio stills considerable for harmonic loads, i.e. minimizing the ratio leads to decrementing the deflection wave amplitudes.
5. The vibration amplitude of rubcrete CDBs depends in the first degree on a/h ratio, beams natural frequency and the load intensity.

7.5. Recommendations for Future Work

1. Study the effect of fatigue on rubberized concrete beams.
2. Discuss the water preventing of rubberized concrete.
3. Simulate the impact load numerically in order to study extra cases.
4. Study the case of equaling the rubcrete compressive strength under different rubber contain.

REFERENCES

[1] O. M. Makki and H. M. K. Al-Mutairee, “Continuous Deep Beams Behavior under Static Loads: A Review Study,” *IOP Conf. Ser. Earth Environ. Sci.*, 2022.

[2] A. C. I. Committee, *318-19 Building Code Requirements for Structural Concrete and Commentary*. 2019.

[3] T. Park, R. and Paulay, *Reinforced Concrete Structures*. John Wiley and sons, 1975.

[4] “Deep beams.” [Online]. Available: eurocode6.org.

[5] M. Chemrouk and F. Kong, *Reinforced concrete deep beams*. 1998.

[6] T. Manual, *Ansys Trining Manual Dynamics 7.0*. SAS IP, Inc., 2003.

[7] J. Radović, Andrija and Radovanović, “DYNAMIC ANALYSIS AND RESPONSE OF SYSTEMS UNDER IMPACT LOADS,” *Conf. Proc. Int. Conf.*, vol. 34, no. April, pp. 173–182, 2018, doi: 10.14415/konferencijagfs2018.015.

[8] T. M. P. and H. Hao, “Plastic hinges and inertia forces in RC beams under impact loads,” *Int J Impact Eng*, 2017.

[9] K. Fujikake, B. Li, and S. Soeun, “Impact Response of Reinforced Concrete Beam and Its Analytical Evaluation,” *J. Struct. Eng.*, vol. 135, no. 8, pp. 938–950, 2009, doi: 10.1061/(asce)st.1943-541x.0000039.

[10] R. P. Kennedy, “A review of procedures for the analysis and design of concrete structures to resist missile impact effects,” *Nucl. Eng. Des.*, vol. 37, no. 2, pp. 183–203, 1976, doi: 10.1016/0029-5493(76)90015-7.

[11] S. C. Chaikaew, Piti, “Properties of concrete pedestrain block mixed with crumb rubber,” *Constr. Build. Mater.*, vol. 20, no. 7, pp. 450–457, 2006.

[12] Mohamed Elchalakani, “High strength rubberized concrete containing silica

fume for the construction of sustainable road side barriers.," *Structures*, vol. 1, pp. 20–38, 2015.

[13] P. V Elchalakani M, Hassanein M, Karrech A, Fawzia S, Yang B, "Experimental tests and design of rubberised concrete-filled double skin circular tubular short columns," *Structures*, 2016.

[14] S. M. Soleimani and N. Banthia, "A novel drop weight impact setup for testing reinforced concrete beams," *Exp. Tech.*, vol. 38, no. 3, pp. 72–79, 2014, doi: 10.1111/j.1747-1567.2012.00810.x.

[15] I. I. R. Damasceno, M. de P. Ferreira, and D. R. C. de Oliveira, "RC beams with steel fibers under impact loads," *Acta Sci. - Technol.*, vol. 36, no. 1, pp. 23–31, 2014, doi: 10.4025/actascitechnol.v36i1.17561.

[16] M. E. K. and M. F. Ayaho Miyamoto, "Non-linear dynamic analysis and design concepts for RC beam under impulsive loads," *Bull. New Zeal. Natl. Soc. Earthq. Eng.*, vol. 22, 1989.

[17] *https://www.ensonhaber.com/samsunda-damperi-acilan-kamyon-ust-gecitte-takildi- 2015-05-02.html*. .

[18] "https:// www.posta.com.tr/kamyon-eve-carpti-mutfak-coktu-2-yarali-haber-fotograf- 2083547." .

[19] "http://www.imo.org.tr/resimler/ dosya_ekler/ 16c33bc24136a9d_ek.pdf (accessed 09 Feb. 2019)." .

[20] RayW. Clough and Joseph Penzien, *DYNAMICS OF STRUCTURES*, Third edit. Computers & Structures, Inc, 1995.

[21] J. Biggs, *Structural Dynamics*. USA: McGrew-Hill, Inc., 1964.

[22] S. H. U. Q. Chowdhury, "Damping Characteristics of Reinforced and Partially Prestressed Concrete Beams," *Engineering*, no. April, 1999.

[23] "Anil_K_Chopra_Dynamics_of_Structures_Theory_anBookZZ_org.pdf." Prentice- Hall, Inc., USA, 1995.

[24] F. Aslani, "Mechanical Properties of Waste Tire Rubber Concrete," *J.*

Mater. Civ. Eng., vol. 28, no. 3, p. 04015152, 2016, doi: 10.1061/(asce)mt.1943-5533.0001429.

[25] "Aljarida magazine," 2015. https://www.aljarida.com/articles/1479573124876400300/.

[26] S. P. S. Kumar, N. Manodeepan, S. Arulkesavan, "An Experimental Investigation on Rubberized Concrete," *Int. J. Innov. Researc Sci. Technol.*, vol. 2, no. 07/013, pp. 82–88, 2015.

[27] K. B. Najim and M. R. Hall, "Workability and mechanical properties of crumb-rubber concrete," *Proc. Inst. Civ. Eng. Constr. Mater.*, vol. 166, no. 1, pp. 7–17, 2013, doi: 10.1680/coma.11.00036.

[28] F. Liu, L. Y. Meng, G. F. Ning, and L. J. Li, "Fatigue performance of rubber-modified recycled aggregate concrete (RRAC) for pavement," *Constr. Build. Mater.*, vol. 95, pp. 207–217, 2015, doi: 10.1016/j.conbuildmat.2015.07.042.

[29] . S. K. G., "Fundamental Properties of Self-Compacting Concrete Utilizing Waste Rubber Tires-a Review," *International Journal of Research in Engineering and Technology*, vol. 05, no. 01. pp. 254–261, 2016, doi: 10.15623/ijret.2016.0501051.

[30] F. Hernández-Olivares, G. Barluenga, M. Bollati, and B. Witoszek, "Static and dynamic behaviour of recycled tyre rubber-filled concrete," *Cem. Concr. Res.*, vol. 32, no. 10, pp. 1587–1596, 2002, doi: 10.1016/S0008-8846(02)00833-5.

[31] A. Abdulameer and H. M. K. Al-mutairee, "An Experimental Study on Behavior of Sustainable Rubberized Concrete Mixes," vol. 6, no. 7, pp. 1273–1285, 2020.

[32] S. Shah, S. Shrestha, N. Karki, and R. Shrestha, "Evaluation of Performance of Rubber Concrete," no. April, pp. 599–603, 2020.

[33] J. Al Adwan, "Impact of rubber crumb fraction and grain size on concrete

strength," *ARPN J. Eng. Appl. Sci.*, vol. 14, no. 13, pp. 2333–2337, 2019.

[34] S. Y. Esraa Emam, "Experimental Study on Enhanced Crumb Rubber Concrete," *Int. J. Sci. Eng. Res.*, vol. 9, no. February, pp. 1240–1247, 2018.

[35] G. Girskas and D. Nagrockienė, "Crushed rubber waste impact of concrete basic properties," *Constr. Build. Mater.*, vol. 140, pp. 36–42, 2017, doi: 10.1016/j.conbuildmat.2017.02.107.

[36] A. M. Almaleeh, S. M. Shitote, and T. Nyomboi, "Use of waste rubber tyres as aggregate in concrete," *J. Civ. Eng. Constr. Technol.*, vol. 8, no. 2, pp. 11–19, 2017, doi: 10.5897/JCECT2016.0421.

[37] G. M. Siringi, A. Abolmaali, and P. B. Aswath, "Properties of Concrete With Crumb Rubber Replacing Fine Aggregates (Sand)," *Adv. Civ. Eng. Mater.*, vol. 2, no. 1, p. 20120044, 2013, doi: 10.1520/acem20120044.

[38] E. N. and S. A., "Engineering properties of rubberized concrete," *Can. J. Civ. Eng.*, vol. 19, pp. 912–923, 1992.

[39] S. Somerville, R. Dhanasekar, T. Frame, and T. G. Suntharavadivel, "An investigation into the techniques for improving the properties of crumb rubber concrete," *ISEC 2015 - 8th Int. Struct. Eng. Constr. Conf. Implement. Innov. Ideas Struct. Eng. Proj. Manag.*, pp. 613–618, 2015, doi: 10.14455/isec.res.2015.79.

[40] M. K. Batayneh, I. Marie, and I. Asi, "Promoting the use of crumb rubber concrete in developing countries," *Waste Manag.*, vol. 28, no. 11, pp. 2171–2176, 2008, doi: 10.1016/j.wasman.2007.09.035.

[41] S. Khan and A. Singh, "Behavior of Crumb Rubber Concrete," *Int. J. Res. Eng. IT Soc. Sci.*, vol. 08, no. 2, pp. 86–92, 2018, [Online]. Available: https://www.researchgate.net/publication/333044437_Behavior_of_Crumb_Rubber_Concrete.

[42] I. B. Topçu, "The properties of rubberized concretes," *Cem. Concr. Res.*, vol. 25, no. 2, pp. 304–310, 1995, doi: 10.1016/0008-8846(95)00014-3.

[43] F. Liu, W. Zheng, L. Li, W. Feng, and G. Ning, “Mechanical and fatigue performance of rubber concrete,” *Constr. Build. Mater.*, vol. 47, pp. 711–719, 2013, doi: 10.1016/j.conbuildmat.2013.05.055.

[44] K. Bisht and P. V. Ramana, “Evaluation of mechanical and durability properties of crumb rubber concrete,” *Constr. Build. Mater.*, vol. 155, pp. 811–817, 2017, doi: 10.1016/j.conbuildmat.2017.08.131.

[45] F. N. Shib, “Punching shear strength of rubberized concrete flat plates,” 2020.

[46] S. binti Salehuddin, N. L. Rahim, N. Mohamad Ibrahim, S. A. N. Tajri, and M. Z. Zainol Abidin, “The Behaviour of Rubber Tyre as Fine Aggregate in Concrete Mix,” *Appl. Mech. Mater.*, vol. 754–755, pp. 427–431, 2015, doi: 10.4028/www.scientific.net/amm.754-755.427.

[47] M. R. Wakchaure and P. A. Chavan, “Waste Tyre Crumb Rubber Particle as A Partial Replacement to Fine Aggregate in Concrete,” *Int. J. Eng. Res. Technol.*, vol. 3, no. 6, pp. 1206–1209, 2014.

[48] R. Aggregates, K. S. Atif, N. Ahmed, N. Hasan, and S. Barua, “A Comparative Study on Compressive Strength of Concrete Mix Containing A Comparative Study on Compressive Strength of Concrete Mix Containing Plastic , Glass and Rubber Aggregates,” no. November, 2020, doi: 10.11648/j.aas.20200504.11.

[49] A. O. Atahan and A. Ö. Yücel, “Crumb rubber in concrete: Static and dynamic evaluation,” *Constr. Build. Mater.*, vol. 36, pp. 617–622, 2012, doi: 10.1016/j.conbuildmat.2012.04.068.

[50] A. B. Senouci and A. Member, “By Nell N . Eldin , ~ Member , ASCE , TABLE 1 . Control-Mix Proportions Material Quantity (kg / m 3) Coarse aggregate Sand Cement Water FIG . 1 . Typical Size and Shape of Rubber Aggregates Each group consisted of several batches , in which the mineral ,” *J. Mater.*, vol. 5, no. 4, pp. 478–496, 1994.

[51] American Society of Testing and Materials, “C293 - 15 Flexural Strength of Concrete (Using Simple Beam With Center-Point Loading),” *ASTM Int.*, pp. 1–3, 2015, doi: 10.1520/C0293.

[52] L. Zheng, X. S. Huo, and Y. Yuan, “Strength, Modulus of Elasticity, and Brittleness Index of Rubberized Concrete,” *J. Mater. Civ. Eng.*, vol. 20, no. 11, pp. 692–699, 2008, doi: 10.1061/(asce)0899-1561(2008)20:11(692).

[53] G. Li, Y. Hu, and X. L. Zang, “Design and analysis of offset printing press plate cylinder using finite element method,” *Proc. 2nd Int. Conf. Model. Simulation, ICMS2009*, vol. 7, pp. 537–540, 2009.

[54] E. Ganjian, M. Khorami, and A. A. Maghsoudi, “Scrap-tyre-rubber replacement for aggregate and filler in concrete,” *Constr. Build. Mater.*, vol. 23, no. 5, pp. 1828–1836, 2009, doi: 10.1016/j.conbuildmat.2008.09.020.

[55] BenazzoukO.DouzaneT.LangletK.MezrebJ.M.RoucoultM.Quéneudec, “Physico-mechanical properties and water absorption of cement composite containing shredded rubber wastes,” *Cem. Concr. Compos.*, vol. 29, no. 10, pp. 732–740, 2007.

[56] W. H. Yung, L. C. Yung, and L. H. Hua, “A study of the durability properties of waste tire rubber applied to self-compacting concrete,” *Construction and Building Materials*, vol. 41. pp. 665–672, 2013, doi: 10.1016/j.conbuildmat.2012.11.019.

[57] W. S. Ya Mei Zhang, Shen-Xia Chen, Bo Chen, “Dry Shrinkage, Frost Resistance and Permeability of Rubber Included Concrete,” *scientific.net*, pp. 120–124, 2006.

[58] M. Bravo and J. De Brito, “Concrete made with used tyre aggregate: Durability-related performance,” *Journal of Cleaner Production*, vol. 25. pp. 42–50, 2012, doi: 10.1016/j.jclepro.2011.11.066.

[59] R. Si, S. Guo, and Q. Dai, “Durability performance of rubberized mortar and concrete with NaOH-Solution treated rubber particles,” *Constr. Build.*

Mater., vol. 153, pp. 496–505, 2017, doi: 10.1016/j.conbuildmat.2017.07.085.

[60] P. and R. K. D. K. A. Paine BEng, "Research on new applications for granulated rubber in concrete," *Constr. Mater.*, vol. 163, no. 1, pp. 7–17, 2009.

[61] E. D. Alan Richardson*, Kathryn Coventry, Vikki Edmondson, "Crumb rubber used in concrete to provide freezeethaw protection (optimal particle size)," *J. Clean. Prod.*, vol. 112, pp. 599–606, 2015.

[62] H. Liu, X. Wang, Y. Jiao, and T. Sha, "Experimental investigation of the mechanical and durability properties of crumb rubber concrete," *Materials (Basel).*, vol. 9, no. 3, pp. 1–12, 2016, doi: 10.3390/ma9030172.

[63] A. J. Bigaj, "Bond behaviour of deformed bars in NSC and HSC," vol. Report 25., 1995.

[64] C. Wang, Y. Zhang, and A. Ma, "Investigation into the Fatigue Damage Process of Rubberized Concrete and Plain Concrete by AE Analysis," *J. Mater. Civ. Eng.*, vol. 23, no. 7, pp. 953–960, 2011, doi: 10.1061/(asce)mt.1943-5533.0000257.

[65] Y. M. Zhang and Z. Zhao, "Internal Stress Development and Fatigue Performance of Normal and Crumb Rubber Concrete," *J. Mater. Civ. Eng.*, vol. 27, no. 2, pp. 1–10, 2015, doi: 10.1061/(asce)mt.1943-5533.0001000.

[66] L. Zheng, X. Sharon Huo, and Y. Yuan, "Experimental investigation on dynamic properties of rubberized concrete," *Constr. Build. Mater.*, vol. 22, no. 5, pp. 939–947, 2008, doi: 10.1016/j.conbuildmat.2007.03.005.

[67] N. D. S. and C. A. Z. D. M. Cotsovos, "Behavior of RC Beams Subjected to High Rates of Concentrated Loading," *J Struct Eng*, vol. 134, no. 12, pp. 1839–1851, 2008.

[68] E. M. White T, Soudki K, "Response of RC beams strengthened with CFRP laminates and subjected to a high rate of loading," *J. Compos. Constr.*, vol.

5, no. 3, pp. 153–162, 2001.

[69] S. H. Tang T, “Analytical and experimental studies of fiber-reinforced polymer-strengthened concrete beams under impact loading,” *ACI Struct. J.*, vol. 102, no. 1, pp. 139–149, 2005.

[70] E. M. and M. U, “Impact loading of concrete beams externally strengthened with CFRP laminates,” *J. Compos. Constr.*, 1999.

[71] P. H. B. and S. H. P. Perry, “Compressive behaviour of concrete at high strain rates,” *Mater. Struct.*, vol. 24, no. 1, pp. 425–450, 1991.

[72] L. J. M. and C. A. Ross, “Review of strain rate effects for concrete in tension,” *ACI Mater. J.*, vol. 95, no. 6, pp. 735–739, 1998.

[73] N. P. Banthia, S. Mindess, and A. Bentur, “Impact behaviour of concrete beams,” *Mater. Struct.*, vol. 20, no. 4, pp. 293–302, 1987, doi: 10.1007/BF02485926.

[74] N. B. and S. M. S. M. Soleimani, “Behavior of RC beams under impact loading,” *Concr. Concr. Struct*, 2007.

[75] J. Guo, J. Cai, and W. Chen, “Inertial Effect on RC Beam Subjected to Impact Loads,” *Int. J. Struct. Stab. Dyn.*, vol. 17, no. 4, pp. 1–23, 2017, doi: 10.1142/S0219455417500535.

[76] S. M. and N. B. A. Bentur, “The behaviour of concrete under impact loading: Experimental procedures and method of analysis,” *Mater. Struct*, 1986.

[77] S. Saatci and F. J. Vecchio, “Effects of shear mechanisms on impact behavior of reinforced concrete beams,” *ACI Struct. J.*, vol. 106, no. 1, pp. 78–86, 2009, doi: 10.14359/56286.

[78] T. M. Pham, W. Chen, M. Elchalakani, A. Karrech, and H. Hao, “Experimental investigation on lightweight rubberized concrete beams strengthened with BFRP sheets subjected to impact loads,” *Eng. Struct.*, vol. 205, no. 1, pp. 1–16, 2020, doi: 10.1016/j.engstruct.2019.110095.

[79] W. S. and S. P. Shah, “Inertial effects in the instrumented impact testing of cementitious composites,” *Cem. Concr. Aggr*, 1981.

[80] M. C. Yilmaz, Anil, B. Alyavuz, and E. Kantar, “Load displacement behavior of concrete beam under monotonic static and low velocity impact load,” *Int. J. Civ. Eng.*, vol. 12, no. 4, pp. 488–503, 2014.

[81] B. A. Barr B, “A repeated drop-weight impact testing apparatus for concrete,” *Mag Concr Res*, 1988.

[82] P. M. Breen C, Guild F, “Impact of thick CFRP laminates: the effect of impact velocity.,” *Compos. Part A Appl. Sci. Manuf.*, vol. 36, no. 2, pp. 205–211, 2005.

[83] F. F. Zhang R, Zhi XD, “Plastic behavior of circular steel tubes subjected to lowvelocity transverse impact,” *Int J Impact Eng*, 2018.

[84] M. K. AndoT, Kishi N, Mikami H, Sato M, “Experimental study on impact resistance of bending failure type RC beams,” *Proc. Seventh East Asia-Pacific Conf. Struct. Eng. Constr.*, 2001.

[85] N. Kishi, H. Mikami, K. G. Matsuoka, and T. Ando, “Impact behavior of shear-failure-type RC beams without shear rebar,” *Int. J. Impact Eng.*, vol. 27, no. 9, pp. 955–968, 2002, doi: 10.1016/S0734-743X(01)00149-X.

[86] D. M. Cotsovos, “A simplified approach for assessing the load-carrying capacity of reinforced concrete beams under concentrated load applied at high rates,” *Int. J. Impact Eng.*, vol. 37, no. 8, pp. 907–917, 2010, doi: 10.1016/j.ijimpeng.2010.01.005.

[87] G. Dok, N. Caglar, A. Ilki, and C. Yilmaz, “Effect of impact loading on residual flexural capacity of high-strength reinforced concrete beams,” *Structures*, vol. 27, no. 2019, pp. 2466–2480, 2020, doi: 10.1016/j.istruc.2020.08.054.

[88] S. D. Hughes G, “An investigation on the beam impact problem,” *Tech. Rep. 546. London Cem. Concr. Assoc.*, 1982.

[89] Y. and I. M. Chen, “Reinforced concrete members under drop-weight impacts,” *Struct. Constr. Build.*, vol. 162(1): 45, pp. 415–428, 2009.

[90] M. Johansson, “Residual Capacity of RC Beams Subjected to Impact Loading Residual Capacity of RC Beams Subjected to Impact Loading,” no. November 2019, 2020.

[91] B. X. and X. Zeng, “Experimental study on the behaviors of reinforced concrete beams under impact loadings,” *China Civ. Eng*, 2014.

[92] H. O. and S. G. Nomachi, “Dynamic response and local rupture of reinforced concrete beam and slab under impact loading,” *rans. 8th Int. Conf. Struct. Mech. React. Technol*, 1985.

[93] AASHTO, “Guide specications and commentary for vessel collision design of highway bridges, American Association of State Highway and Transportation ocial,” 1990.

[94] M. A. K. and D. Bonyun, “Ship collision against the sunshine skyway bridge,” *IABSE Colloq. Sh. Collis. with Bridg. O®shore Struct.*, 1983.

[95] D.-B. Zhao, W.-J. Yi, and S. K. Kunnath, “Shear Mechanisms in Reinforced Concrete Beams under Impact Loading,” *J. Struct. Eng.*, vol. 143, no. 9, p. 04017089, 2017, doi: 10.1061/(asce)st.1943-541x.0001818.

[96] X. X. Zhang, G. Ruiz, and R. C. Yu, “A new drop-weight impact machine for studying fracture processes in structural concrete,” *Strain*, vol. 46, no. 3, pp. 252–257, 2010, doi: 10.1111/j.1475-1305.2008.00574.x.

[97] Y. Fu *et al.*, “Investigating the failure behaviors of RC beams without stirrups under impact loading,” *Int. J. Impact Eng.*, vol. 137, p. 103432, 2020, doi: 10.1016/j.ijimpeng.2019.103432.

[98] J. E. Akin, “Impact Load Factors for Static Analysis,” in *Rice University*, p. 13.

[99] H. Ohnuma, C. Ito, and S. G. Nomachi, “Dynamic Response and Local Rupture of Reinforced Concrete Beam and Slab Under Impact Loading.,”

International Conference on Structural Mechanics in Reactor Technology, vol. J 5/3. pp. 179–184, 1985.

[100] A. T. Kishi N, Mikami H, Matsuoka KG, "An empirical impact resistant design formula of RC beams with statically bending failure mode," *JSCE*, 2000.

[101] A. Q. Bhatti, N. Kishi, and H. Mikami, "An applicability of dynamic response analysis of shear-failure type RC beams with lightweight aggregate concrete under falling-weight impact loading," *Mater. Struct. Constr.*, vol. 44, no. 1, pp. 221–231, 2011, doi: 10.1617/s11527-010-9621-9.

[102] S. Kumar and H. J. Petroski, "Plastic response to impact of a simply supported beam with a stable crack," *Int. J. Impact Eng.*, vol. 3, no. 1, pp. 27–40, 1985, doi: 10.1016/0734-743X(85)90023-5.

[103] D. S. C. and H. F. B. P. E. Duwez, "The behavior of long beams under impact loading," *J. Appl. Mech.*, 1950.

[104] S. Das Adhikary, B. Li, and K. Fujikake, "Strength and behavior in shear of reinforced concrete deep beams under dynamic loading conditions," *Nucl. Eng. Des.*, vol. 259, pp. 14–28, 2013, doi: 10.1016/j.nucengdes.2013.02.016.

[105] W. L. Zhang Q, Zhang J, "Impact and energy absorption of long fiber-reinforced thermoplastic based on two-phase modeling and experiments," *Int. J. Impact Eng.*

[106] C. W. Hazizan MA, "The low velocity impact response of an aluminium honeycomb sandwich structure.," *Compos. Struct.*, vol. 34, no. 8, pp. 679–687, 2003.

[107] H. H. Pham TM, "Prediction of the impact force on RC beams from a drop weight," *Adv. Struct. Eng.*, pp. 1–13, 2019.

[108] Abrate S., "impact of composite structures," *Cambridge Univ. Press*, 2005.

[109] "Buiding Code requirements for structural concrete ACL 318M-14 and commentary." .

[110] C. S. Gupta T, Sharma RK, "Impact resistance of concrete containing waste rubber fiber and silica fume.," *Int. J. Impact Eng.*, 2015.

[111] B. J. Donga PD, Shah D, "impact resistance of waste rubber fiber silica fume concrete.," *J. Civ. Eng. Constr. Technol.*

[112] F. Liu, G. Chen, L. Li, and Y. Guo, "Study of impact performance of rubber reinforced concrete," *Constr. Build. Mater.*, vol. 36, pp. 604–616, 2012, doi: 10.1016/j.conbuildmat.2012.06.014.

[113] H. M. K. Al-mutairee and O. M. Makki, "Rubberized concrete mix – discussions for literature review," 2021, doi: 10.1088/1742-6596/1895/1/012011.

[114] M. and S. Y. O. David M., Rogowsky, James G., "Tests of Reinforced Concrete Deep Beams," *ACI J.*, 1986.

[115] B. Singh and S. K. Kaushik, "Design of a deep beam using the strut-and-tie method," *J. Struct. Eng.*, vol. 33, no. 5, pp. 429–434, 2006.

[116] M. Schlaich, J., Schafer, K. and Jennewin, "Toward a Consistent Design of Structural Concrete," *PCI J.*

[117] D. M. Rogowsky, "continuous deep beams," 1990.

[118] H. Chen, W. J. Yi, Z. J. Ma, and H. J. Hwang, "Shear strength of reinforced concrete simple and continuous deep beams," *ACI Struct. J.*, vol. 116, no. 6, pp. 31–40, 2019, doi: 10.14359/51718003.

[119] I. O. P. C. Series and M. Science, "Shear behaviours of hybrid continuous deep beams strengthened with carbon fibre reinforced polymer Shear behaviours of hybrid continuous deep beams strengthened with carbon fibre reinforced polymer," pp. 0–14, 2018, doi: 10.1088/1757-899X/433/1/012027.

[120] B. I. Mihaylov, B. Hunt, E. C. Bentz, and M. P. Collins, "Three-parameter

kinematic theory for shear behavior of continuous deep beams," *ACI Struct. J.*, vol. 112, no. 1, pp. 47–58, 2015, doi: 10.14359/51687180.

[121] A. Nihad, "EFFECT OF WEB REINFORCEMENT ON SELF-COMPACTING REINFORCED on self compacting reinforced concrete continuous deep beams," no. July, 2018, doi: 10.13140/RG.2.2.27821.74726.

[122] mac G. J. . and O. s>Y. rogowsky D.M., "test of reinforced concrete deep beams," *ACI J.*, 1986.

[123] K. H. Yang and A. F. Ashour, "Load Capacity of Reinforced Concrete Continuous Deep Beams," *J. Struct. Eng.*, vol. 134, no. 6, pp. 919–929, 2008, doi: 10.1061/(asce)0733-9445(2008)134:6(919).

[124] F. Beshara, I. G. Shaaban, and T. S. Mustafa, "Behaviour and Analysis of Reinforced Concrete Continuous Deep Beam," no. January 2016.

[125] K. H. Yang, H. S. Chung, and A. F. Ashour, "Influence of section depth on the structural behaviour of reinforced concrete continuous deep beams," *Mag. Concr. Res.*, vol. 59, no. 8, pp. 575–586, 2007, doi: 10.1680/macr.2007.59.8.575.

[126] A. A. Yang KH, "Structural behaviour of reinforced-concrete continuous deep beams with web openings," *Mag. Concr. Res.*, 2007.

[127] G. Rodriguez, "Numerical modeling of reinforced concrete continuous deep beams," no. February, 2018.

[128] A. N. N. Adnan Falih Ali, "EXPERIMENTAL STUDY OF SELF-COMPACTING REINFORCED CONTINUOUS DEEP BEAMS," *J. Eng. Sustain. Dev.*, no. February, 2021.

[129] A. M. Jalil, K. S. Abdul-razzaq, and A. H. Mohammed, "STM EXPERIMENTAL VERIFICATION FOR REINFORCED CONCRETE CONTINUOUS DEEP," no. February, 2019.

[130] K. H. Yang and A. F. Ashour, "Aggregate interlock in lightweight concrete

continuous deep beams," *Eng. Struct.*, vol. 33, no. 1, pp. 136–145, 2011, doi: 10.1016/j.engstruct.2010.09.026.

[131] M. Zargarian and A. Rahai, "Theoretical and Experimental Studies of Two-Span Reinforced Concrete Deep Beams and Comparisons with Strut-and-Tie Method," *Adv. Civ. Eng.*, vol. 2021, no. 2010, pp. 5–7, 2021, doi: 10.1155/2021/8880067.

[132] H. N. Abbas and S. By, "Behavior of Reinforced Concrete Continuous Deep Beams with Opening Strengthened Using CFRP Strips." 2020.

[133] A. Abdulameer Kadhim, "Experimental_Behavior_of_Rubberized_Reinforced_Concrete.pdf." 2020.

[134] R. K. H., "Model for structural concrete members without transverse reinforcement," *Proc. IABSE Colloq. Struct. Concr.*, 1991.

[135] T. HPJ, "Investigation of forces carried across cracks in reinforced concrete beams in shear by interlock of aggregate," *Cem. Concr. Assoc.*, 1970.

[136] P. T. Fenwick RC, "Mechanisms of shear resistance of concrete beams," *J. Struct. Eng.*, 1968.

[137] L. N. Walraven J, "Size effects in short beams loaded in shear," *ACI Struct. J.*

[138] S. H. Bažant ZP, "Size effect in diagonal shear failure: influence of aggregate size and stirrups.," *ACI Mater. J.*, 1987.

[139] K. D. Collins MP, "How safe are our large, lightly reinforced concrete beams, slabs, and footings?," *ACI Struct. J.*, 1999.

[140] T. H.P., "Shear strength of large beams," *J. Struct. Eng.*, 1972.

[141] M. S. Sandeep, P. Nagarajan, and A. P. Shashikala, "Behaviour of Steel Fibre Reinforced Rubberized Continuous Deep Beams," *IOP Conf. Ser. Mater. Sci. Eng.*, vol. 330, no. 1, 2018, doi: 10.1088/1757-899X/330/1/012125.

[142] A. A. Kadhim and H. M. Kadhim, “Loading Capacity Prediction of Rubberized Reinforced Concrete Continuous Deep Beams,” *IOP Conf. Ser. Mater. Sci. Eng.*, vol. 1090, no. 1, p. 012031, 2021, doi: 10.1088/1757-899x/1090/1/012031.

[143] L. WY, “Shear strength prediction for steel reinforced concrete deep beams,” *J. Constr. Steel Res.*, 2006.

[144] (EC9) E C for S 2000 EUROCODE, “Design of aluminum structures - Part 1-I: General rules and rules for building DD ENV 1999-1-12000, Final Draft Oct. 2000, CEN.”

[145] A. A. F, “Tests of reinforced concrete continuous deep beams,” *ACI Struct. J.*, 1997.

[146] A. M. Abd and W. D. Salman, “ANN and Statistical Modelling to Predict the Deflection of Continuous Reinforced Concrete,” no. March 2016, 2015.

[147] M. A. T. Khatab, A. F. Ashour, T. Sheehan, and D. Lam, “Experimental investigation on continuous reinforced SCC deep beams and Comparisons with Code provisions and models,” *Eng. Struct.*, vol. 131, pp. 264–274, 2017, doi: 10.1016/j.engstruct.2016.11.005.

[148] Ali Sabah Mahdi, “Response of Two- way bubble deck reinforced concrete slabs to harmonic load,” University of Baghdad/College of Engineering, 2021.

[149] I. O. P. C. Series and M. Science, “Vibration analysis of the simply supported R / C beam Vibration analysis of the simply supported R / C beam,” 2021, doi: 10.1088/1757-899X/1141/1/012036.

[150] G. D. Chen, H. M. Mu, and X. B. Yang, “DYNAMIC RESPONSES OF RC BEAMS UNDER SLOWLY SWEPT HARMONIC LOADS,” pp. 444–450, 2000.

[151] T. Kocat, “Dynamic Analysis of Eccentrically Prestressed Damped Beam under Moving Harmonic Force Using Higher Order,” no. December, pp.

1733–1741, 2007.

[152] N. Sushmitha and M. N. Hegde, “Harmonic Analysis of Cantilever Beam with and without Cracks,” pp. 692–695, 2019.

[153] S. Mohammadzadeh, M. Esmaeili, and M. Mehrali, “Dynamic response of double beam rested on stochastic foundation under harmonic moving load,” no. September 2013, pp. 572–592, 2014, doi: 10.1002/nag.

[154] Y. Chen and Y. Song, “beams under distributed harmonic load,” vol. 12, 2018.

[155] C. Eng, M. Antalya, C. Eng, M. Nigde, C. Eng, and S. Bal, “Nonlinear Transient Dynamic Response of Clamped Rectangular Plates on Two-Parameter Foundations by the Algorithm of the Singular Convolution,” vol. 2, no. 2, pp. 165–177, 2007.

[156] E. Aydin, M. Dutkiewicz, B. Öztürk, and M. Sonmez, “Optimization of elastic spring supports for cantilever beams,” no. Marcelin 2001, 2020.

[157] B. Civalek, Omer and Ozturk, “Free vibration analysis of tapered beam-column with pinned ends embedded in Winkler-Pasternak elastic foundation,” *Geomech. Eng.*, 2010.

[158] M. The MathWorks, Inc., Natick, *MATLAB and Statistics Toolbox Release 2018b*. United States, 2018.

[159] A. M. Mohamed, K. Mahmoud, and E. F. El-Salakawy, “Behavior of Simply Supported and Continuous Concrete Deep Beams Reinforced with GFRP Bars,” *J. Compos. Constr.*, vol. 24, no. 4, p. 04020032, 2020, doi: 10.1061/(asce)cc.1943-5614.0001039.

[160] M. R. Khalaf and A. H. A. Al-Ahmed, “Effect of Large Openings on the Behavior of Reinforced Concrete Continuous Deep Beams under Static and Repeated Load,” *E3S Web Conf.*, vol. 318, p. 03012, 2021, doi: 10.1051/e3sconf/202131803012.

[161] M. K. Ali, “BEHAVIOR OF HYBRID REINFORCED CONCRETE

DEEP," vol. 23, no. 04, pp. 52–75, 2019.

[162] S. Muhaison, W. Abd, and M. Alwan, "Behaviour of Reactive Powder Rectaingular Deep Beam With Shear Zone Opening Subjected To Repeated Load," *J. Eng. Sustain. Dev.*, vol. 2018, no. 01, pp. 77–94, 2018, doi: 10.31272/jeasd.2018.1.7.

[163] A. A. N.K. Subedi, "Some experimental results for reinforced concrete deep beams with fixed-ended supports," *Struct. Eng. Rev.*, vol. 6, no. 2, pp. 105–128, 1994.

[164] A. Aarabzadeh and R. Hizaji, "Failure Mechanism in Fixed-Ended Reinforced Concrete Deep Beams under Cyclic Load," vol. 11, no. 4, pp. 562–566, 2017.

[165] "MasterGlenium 54 - High performance concrete superplasticiser based on modified polycarboxylic ether." https://www.master-builders-solutions.com/en-ae/products/masterglenium/masterglenium-54.

[166] ASTM A615/A615M, "Standard Specification for Deformed and Plain Carbon-Steel Bars for Concrete Reinforcement," *ASTM Int.*, no. March, pp. 1–8, 2015, doi: 10.1520/A0615.

[167] ASTM C143M, "Standard test method for slump of hydraulic-cement concrete," *ASTM Int. i(Reapproved)*, 2012, doi: 10.1520/C0143_C0143M-12.

[168] ASTM International, "Standard Test Method for Compressive Strength of Cylindrical Concrete Specimens 1 This standard is for EDUCATIONAL USE ONLY .," *Annu. B. ASTM Stand.*, no. C, pp. 1–7, 2010, doi: 10.1520/C0039.

[169] ASTM C469-11, "Standard Test Method for Splitting Tensile Strength of Cylindrical Concrete Specimens," *Man. Hydrocarb. Anal. 6th Ed.*, vol. i, pp. 545-545–3, 2008, doi: 10.1520/C0496.

[170] C133-97, "Standard test methods for cold crushing strength and modulus of

rupture of refractories (C133-97)," *Annu. B. ASTM Stand*, vol. 97, no. Reapproved 2008, pp. 1–6, 2015, doi: 10.1520/C0133-97R15.2.

[171] T. J. Mohammed and K. M. Breesem, "Enhancement of the Shear-flexural Strength of the Rubberized Concrete Prism Beam by External Reinforcement," *Int. J. Eng. Trans. B Appl.*, vol. 35, no. 5, pp. 1017–1023, 2022, doi: 10.5829/ije.2022.35.05b.17.

[172] ACI Committee, *544.4R-18: Guide to Design with Fiber-Reinforced Concrete*. 2018.

[173] J.-J. Michael A. Sutton, Hubert W. SchreiernOrteu and Image, *Image Correlation for Shape, Motion and Deformation Measurements*. 2009.

[174] H. A. Al-Salman, "Experimental Investigation of The Impact Resistance And Behavior Of Polypropylene Fiber Reinforced Slabs," Jordan University of Science and technology, 2015.

[175] "TML PFL-30-11-3LJCT-F Concrete Strain Gauge." https://shop.elkome.com/en/pfl-30-11-3ljct-f-concrete-material-strain-g.

[176] "PFL Series Strain Gauges for Concrete Material," [Online]. Available: https://www.althensensors.com/sensors/strain-sensors-strain-gauges/concrete-material-use-straingauges/4448/pfl-series-strain-gauges-for-concrete-material/.

[177] M. Nelkon, *Principles of physics*, 6th ed. St Albans : Hart-Davis, 1975.

[178] O. M. Makki, "Mechanical and Dynamical Properties of Structural Rubcrete Mixes," *Int. J. Eng.*, vol. 35, no. 09, pp. 1744–1751, 2022.

[179] A. library Help, "ANSYS Help," *Version 15*, 2015.

[180] A. Raj, P. Nagarajan, and A. P. Shashikala, "Behaviour of Fibre-Reinforced Rubcrete Beams Subjected to Impact Loading," *J. Inst. Eng. Ser. A*, vol. 101, no. 4, pp. 597–617, 2020, doi: 10.1007/s40030-020-00470-4.

[181] K. B. Najim and M. R. Hall, "Mechanical and dynamic properties of self-compacting crumb rubber modified concrete," *Constr. Build. Mater.*, vol.

27, no. 1, pp. 521–530, 2012, doi: 10.1016/j.conbuildmat.2011.07.013.

[182] P. Sukontasukkul, “Use of crumb rubber to improve thermal and sound properties of pre-cast concrete panel,” *Constr. Build. Mater.*, vol. 23, no. 2, pp. 1084–1092, 2009, doi: 10.1016/j.conbuildmat.2008.05.021.

[183] F. Elshazly, S. Mustafa, and H. Fawzy, “Rubberized concrete properties and its structural engineering applications – An overview,” *Egypt. J. Eng. Sci. Technol.*, vol. 30, no. 1, pp. 1–11, 2020, doi: 10.21608/eijest.2020.35823.1000.

[184] G. Tanwar, “Enhancing the Properties of Crumb Rubber Modified Concrete with Synthetic Resin,” pp. 2857–2860, 2020.

[185] A. Grinys, A. Augonis, M. Daukšys, and D. Pupeikis, “Mechanical properties and durability of rubberized and SBR latex modified rubberized concrete,” *Constr. Build. Mater.*, vol. 248, p. 118584, 2020, doi: 10.1016/j.conbuildmat.2020.118584.

[186] A. A. H. Beiram and H. M. K. Al-Mutairee, “Effect of using Waste Rubber as Partial Replacement of Coarse Aggregate on Torsional Strength of Square Reinforced Concrete Beam,” *Int. J. Eng. Trans. B Appl.*, vol. 35, no. 2, pp. 397–405, 2022, doi: 10.5829/ije.2022.35.02b.16.

[187] Ali Abdulameer Kadhim and Hayder M.K. Al-Mutairee, “Experimental Investigation of Rubberized Reinforced Concrete Continuous Deep Beams,” *J. King Saud Univ.*, 2021.

[188] ASTM C136, “ASTM C136/C136M Standard Test Method for Sieve Analysis of Fine and Coarse Aggregates,” *ASTM Stand. B.*, pp. 3–7, 2019, doi: 10.1520/C0136.

[189] A. A. H. Beiram and H. M. K. Al-Mutairee, “The effect of chip rubber on the properties of concrete,” *Mater. Today Proc.*, no. February, 2022, doi: 10.1016/j.matpr.2022.01.209.

[190] E. and G. I. Madenci, *The finite element method and application in civil*

engineering using ANSYS. The University of Arizona.

[191] M. A. Attiya, "Behavior of reinforced concrete corbels strengthened with carbon fiber reinforced polymer strips," university of Basrah, Iraq, 2010.

[192] C. L. Wang and Y. Huang, "Refined model for analysis of plates on elastic foundations," *Yantu Lixue/Rock Soil Mech.*, vol. 29, no. 1, pp. 52–57, 2008, doi: 10.1061/(asce)0733-9399(1991)117:12(2830).

[193] W. . Chen, *Plasticity in Reinforced Concrete*. McGraw-Hill Book Company, 1985.

[194] S. Desayi, P., and Krishnan, "Equation for the Stress-Strain Curve of Concrete," *J. Am. Concr. Inst.*, vol. 61, pp. 345–350, 1964.

[195] E. P. Willam, K. J. and Warnke, "Constitutive Model for the Triaxial Behavior of Concrete," *Proceedings, Int. Assoc. Bridg. Struct. Eng.*, vol. 19, 1975.

A. APPENDIX A: TRIAL MIX

Six concrete mixes of three percentages of replacement (10, 20 and 30%) of sand and the same percentages of gravel and the seventh mix is considered to be reference mix without any replacement. Chip versus gravel replacement also chosen to be fully graded and matches the same specifications. A full graded crumb versus sand replacement was selected and the grades classified in accordance to the ASTM C33-10 [188] and as shown in Figure A.8.2. All seven mixes were casted with the same mix proportions (1:1.5:3) with 0.48 w/c ratio. Three cubes of 100 mm cubic meter and three 100*200 mm cylinders were casted for each mix (Plate A.8.1). Mixes percentages for single cubic meters were listed in Table A.1.

Table A.1. Mixes weights in kg/m^3

Mixes	Cement	Sand	Gravel	Rubber	water
NC	394	651	1343	0	189.12
S10	394	625	1343	26	189.12
S20	394	599	1343	52	189.12
S30	394	573	1343	78	189.12
G10	394	651	1208.7	134.7	189.12
G20	394	651	1074.4	268.6	189.12
G30	394	651	940.1	402.9	189.12

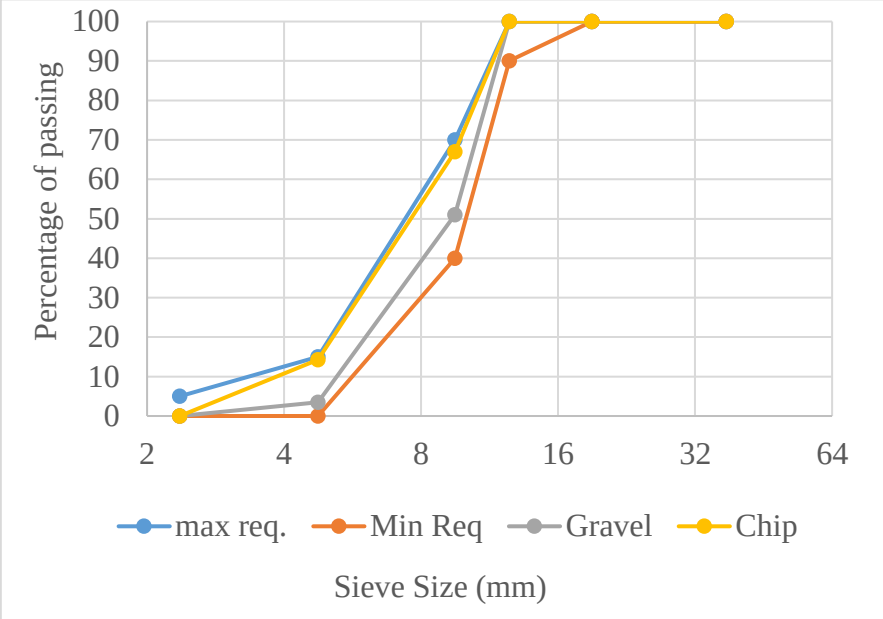

Figure A.8.1. Course aggregate sizes

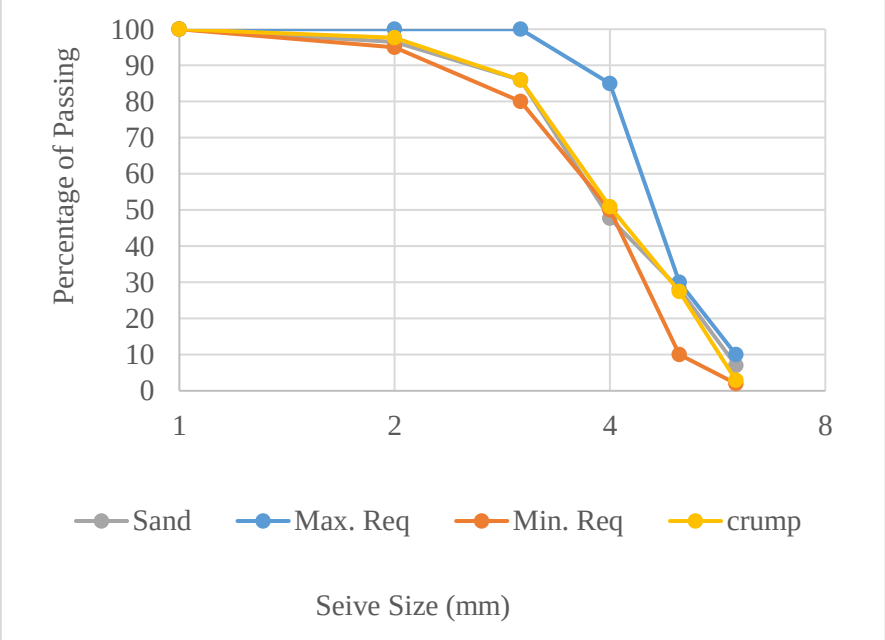

Figure A.8.2. Fine aggregate sieve analysis

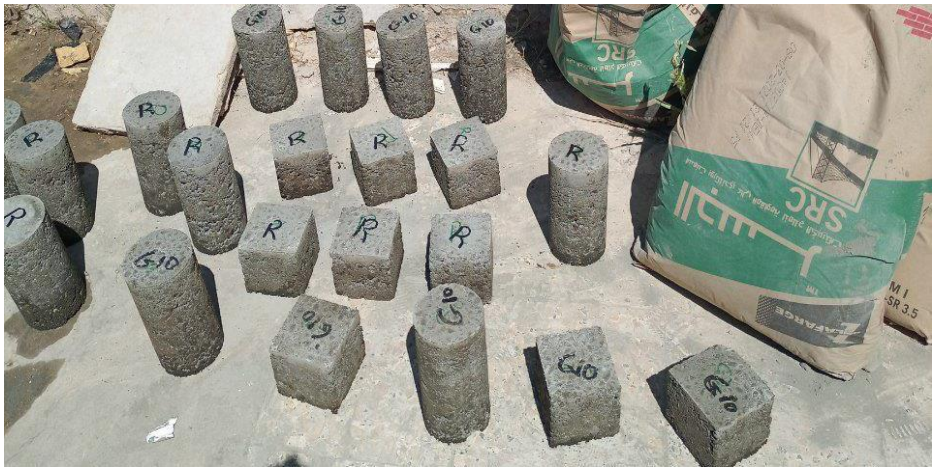

Plate A.8.1. First mix samples before curing

1. Workability

Bar chat ,Figure A.8.3, shows the effect of replacement on fresh concrete workability using slump test (Plate A.8.2) in accordance to ASTM 143M-12 [167]. One maybe noting that, slump values drops gradually after each raising in replacing percentage due to the rubber particles shape. The irregular shape of rubber confines water upon it and avoids to be flow into the paste which will cause the low workability.

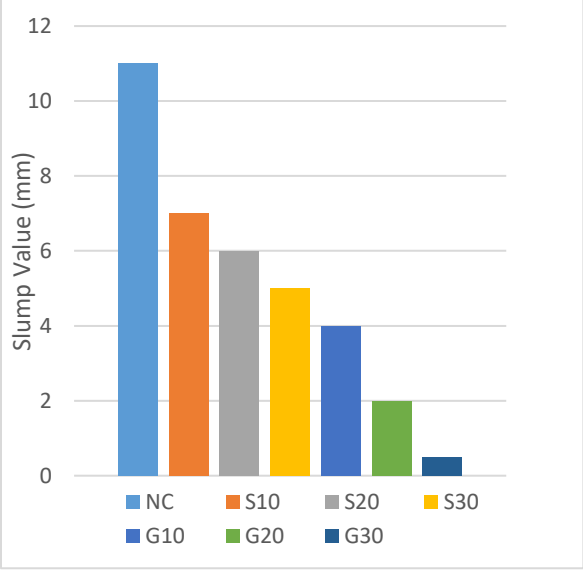

Figure A.8.3. Rubcrete workability

Plate A.8.2. Slump test for G10 mix

2. Unit weight

Logically, replacement rubber by aggregate leads to minimizing concrete unit weight due to the low density of rubber. Rubcrete with sand replacement by 10, 20 and 30% weight replacement loses (2.52, 4.91 and 11.1%) of its unit weight. Gravel replacement for the same percentages causes to larger drop in unit weight than sand replacement (6.25, 13.83, and 17.85%) respectively for the three percentages.

3. Compressive strength

The average of three cubes and cylinders were tested to investigate British and cylinder concrete compressive strength for rubcrete mixes. Table A.. lists the average values after 28 day of curing. It can be noting that, the drop in concrete strength rises gradually for every incrementing depending on rubber percentages. Furthermore, the strengths of sand replacement mixes' are better than gravel replacements. The converting factor from cube to cylinder was concluded to be in the range between (0.8- 0.87) and such result agrees with reference [189].

Table A.2. Mixes compressive strength

Type	Fcu (100 mm size) (MPa)	$f'c$ (MPa)	$f'c$ drop %	Convert factor
NC	35	28.6	------	0.82
S10	32	27.3	4.6	0.85
S20	29	23.5	17.8	0.81
S30	20	17.3	39.5	0.87
G10	30	25	12.6	0.83
G20	22	18	37.1	0.82
G30	18	14.5	49.3	0.80

4. Stress-strain curves

For more accuracy, three cylinders for each concrete mix have been tested using universal static compression machine and recording stress versus strain at every loading stage. Figure A.8.5 shows the results of one cylinder data for each mix. The tested NC stress strain curve found to be matched with the empirical code equations as explained in Figure A.8.4

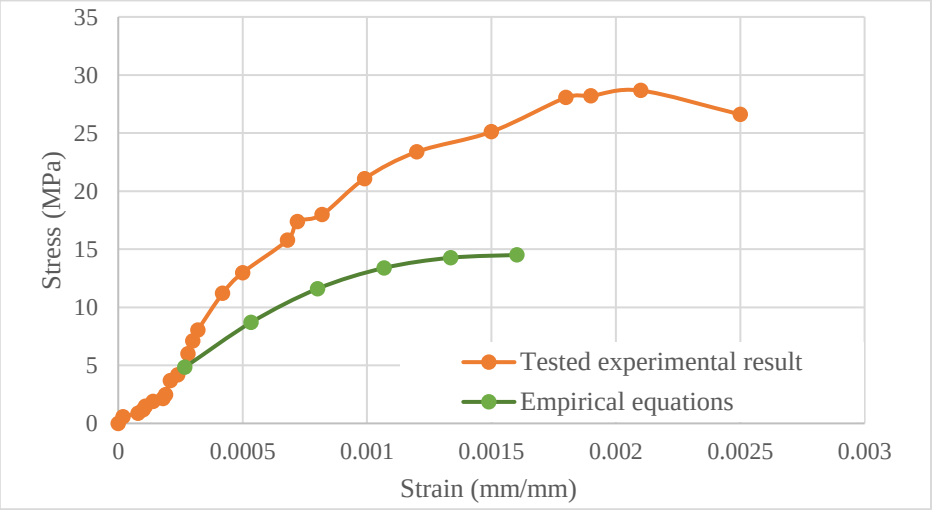

Figure A.8.4. Conventional concrete stress-strain curves experimentally and empirically

Figure A.8.5 allows to be concluded that, the rubcrete mixes have strains larger than the conventional concrete by 3 or 4 times depending on the rubber type and amount. The more rubber the more strain but the less compressive strength. Furthermore, the behavior of rubcrete differs gradually for every incrementing in replacement percentage. Sand replacement showed likeness curves in comparing with conventional concrete even for high replacements. In contrast with gravel curve at high rubber amounts.

Also, one could be noting that (by thinking in Figure A.8.6.), the behavior of high percent's replacement differs from the normal concrete mix. In another word, the

empirical equations of normal concrete are not correct to be used for rubcrete mixes.

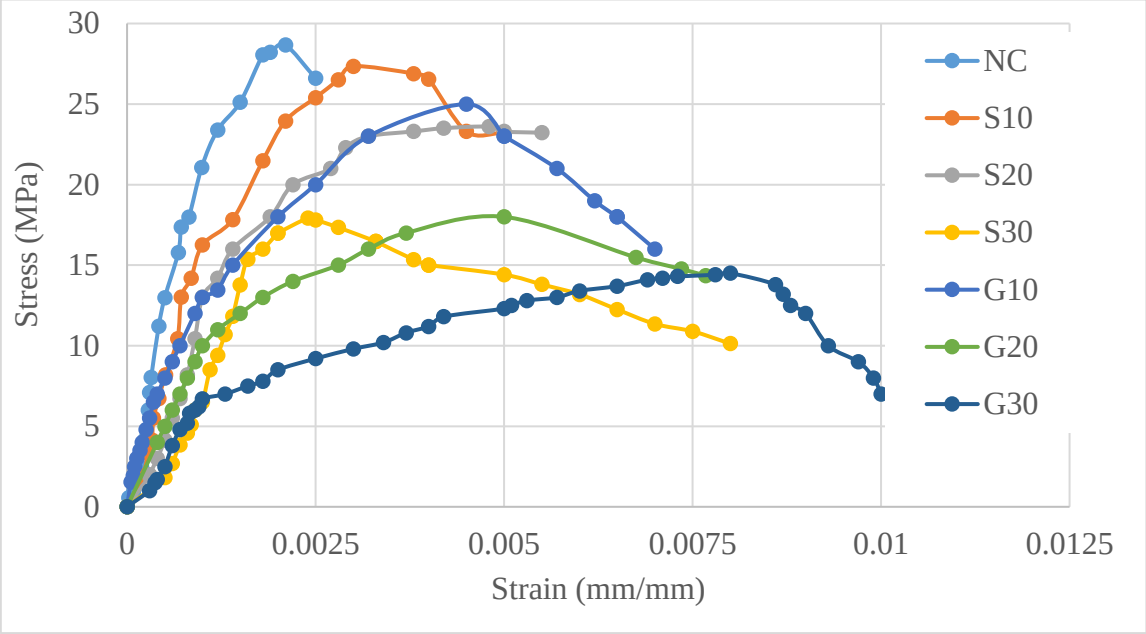

Figure A.8.5. Stress versus strain curves for one cylinder for each mix

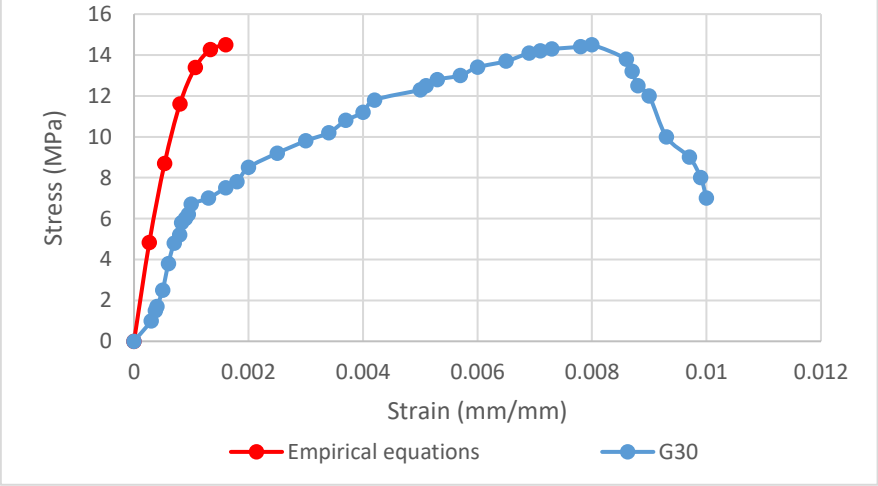

Figure A.8.6. Verifying rubcrete result with empirical equations of NC

The Time between failure and collapse also has been recorded for each specimen as illustrated in Table A.2. It can be clearly seen that, the higher rubber percentage the longer collapse time needed. Rubcrete records a longer time than conventional concrete because its capacity to still deform after failure. This mechanism

occurred due to rubber particles which worked as small micro springs resist load and the great ability of rubber straining.

Table A.2. Resisting time of rubcrete

No.	Time between failure to collapse (Sec)
NC	0
S10	5
S20	12
S30	28
G10	9
G20	14
G30	42

The failure mode of all samples occurs within the standard expected failure types listed in [168] specification for type 3 (i.e. columnar vertical cracks from both ends) as shown in Plate A. 8.3. Such type of failure indicates a well stress distributed over the top and bottom faces of specimens.

Plate A. 8.3. Types of failure

BASF
The Chemical Company

GLENIUM® 54

A high performance concrete superplasticiser based on modified polycarboxylic ether

Description
GLENIUM® 54 has been primarily developed for applications in the ready mixed and precast concrete industries where the highest durability and performance is required.

GLENIUM® 54 is free from chlorides and complies with ASTM C494 Types A and F.

GLENIUM® 54 is compatible with all Portland cements that meet recognised international standards.

Chemistry and mechanism of action of GLENIUM® 54
Conventional superplasticisers, such as those based on sulphonated melamine and naphthalene formaldehyde condensates, at the time of mixing, become absorbed onto the surface of the cement particles. This absorption takes place at a very early stage in the hydration process. The sulphonic groups of the polymer chains increase the negative charge on the surface of the cement particle and dispersion of the cement occurs by electrostatic repulsion.

GLENIUM® 54 is differentiated from conventional superplasticisers in that it is based on a unique carboxylic ether polymer with long lateral chains. This greatly improves cement dispersion. At the start of the mixing process the same electrostatic dispersion occurs as described previously but the presence of the lateral chains, linked to the polymer backbone, generate a steric hindrance which stabilises the cement particles capacity to separate and disperse.

This mechanism provides flowable concrete with greatly reduced water demand.

Typical applications
The excellent dispersion properties of GLENIUM® 54 make it the ideal admixture for precast and readymixed concrete where low water cement ratios are required. This property allows the production of very high early and high ultimate strength concrete with minimal voids and therefore optimum density. Due to the strength development characteristics the elimination or reduction of steam curing in precast works may be considered as an economical option.

GLENIUM® 54 can be used to produce very high early strength floor screeds. For screed mix designs consult BASF Technical Services.

- high workability without segregation or bleeding
- less vibration required
- can be placed and compacted in congested reinforcement
- reduced labour requirement
- improved surface finish

GLENIUM® 54 may be used in combination with RheoMATRIX for producing Smart Dynamic Concrete (SDC). The technology produces advanced self compacting concrete, without the aid of vibration. For economic, ecological and ergonomic ready-mix / precast concrete production.

Adding Value to Concrete

B.1. Glenium data sheet

BASF

The Chemical Company

GLENIUM® 54

Packaging

GLENIUM® 54 is available in 208 litre drums and in bulk tanks upon request.

***Typical properties**

Form	Whitish to straw coloured liquid
Relative density	1.07
pH	5-8

Effect on hardened concrete properties

- increased early and ultimate compressive strengths
- increased flexural strength
- higher E modulus
- improved adhesion to reinforcing and stressing steel
- better resistance to carbonation
- lower permeability
- better resistance to aggressive atmospheric conditions
- reduced shrinkage and creep
- increased durability

Compatibility of GLENIUM® 54

GLENIUM® 54 must not be used in conjunction with any other admixture unless prior approval is received form BASF Technical Services.

GLENIUM® 54 is suitable for mixes containing:

- microsilica
- pulverised fuel ash
- ground granulated blast furnace slag cement

Dosage

The normal dosage for GLENIUM® 54 is between 0.5 and 2.5 litres per 100 kg of cement (cementitious material). Dosages outside this range are permissible subject to trial mixes.

Directions for use

GLENIUM® 54 is a ready to use admixture that is added to the concrete at the time of batching.

The maximum effect is achieved when the GLENIUM® 54 is added after the addition of 50 to 70 % of the water. GLENIUM® 54 must not be added to the dry materials.

Thorough mixing is essential and a minimum mixing cycle, after the addition of the GLENIUM® 54, of 60 seconds for forced action mixers is recommended.

Storage

GLENIUM® 54 should be stored in original containers and at above 5 Centigrade. If frozen gradually thaw and agitate until completely reconstituted.

Failure to comply with the recommended storage conditions may result in premature deterioration of the product or packaging. For specific storage advice consult BASF's Technical Services Department.

Safety precautions

GLENIUM® 54 contains no hazardous substances requiring labelling. For further information refer to the Material Safety Data Sheet.

B.2. Supperplasticizer data sheet

APPENDIX C: STM BEAMS DESIGN PROCEDURE

Estimating CDB capacity may determine using strut and tie method STM, in which it depends on the plastic theory, balance theory and yielding state theory. The discontinuous regions considers as a truss where tension and compression forces transfer to support by struts and ties as shown in Figure C. 1.

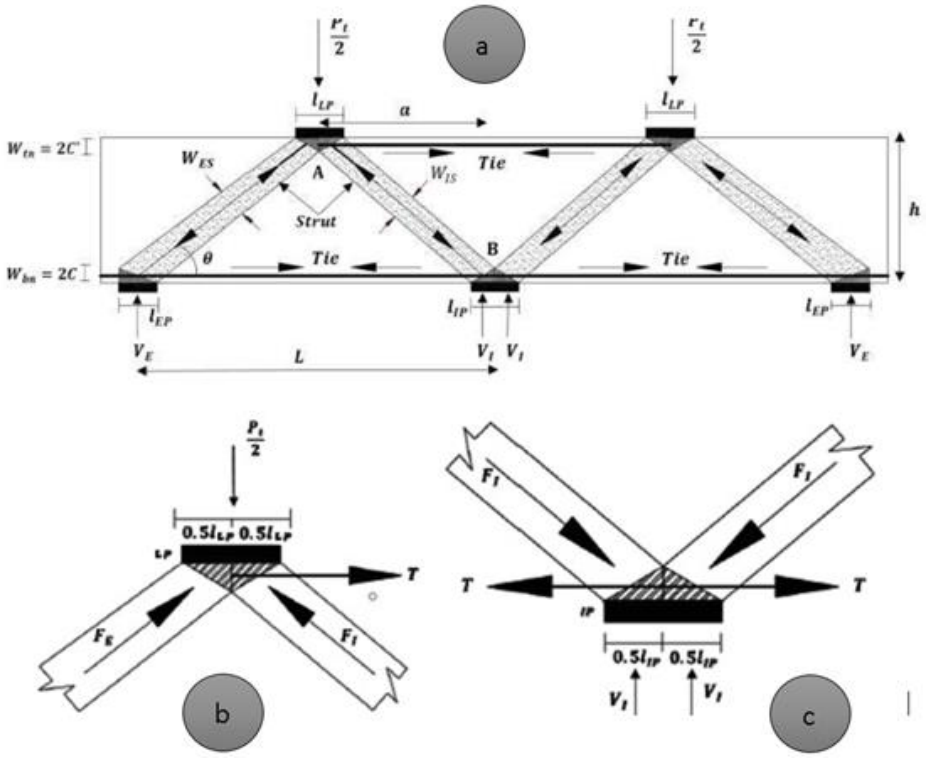

Figure C. 1. STM of CDB, a-Truss model, b-loading joints, c-intermediate supporting joint [142]

Total span to overall depth =0.6/0.2=3

Shear span to depth ratio = 0.3/0.2=1.5

Flexural steel reinforcement requirement checking:

$$\rho = \frac{As}{bd} = \frac{2 * \frac{3.14}{4} * 12^2}{100 * (200 - 40)} = 0.014$$

Assume f'c=43.2 MPa & Fy =432 MPa

$$\rho_{min} = Max\ of \begin{bmatrix} \frac{1.4}{fy} = 0.0033 \\ \frac{\sqrt{f_c'}}{4fy} = 0.0037 \end{bmatrix} \text{Checked}$$

$$\rho_{max} = \frac{3}{8} * 0.85 * \beta_1 * \frac{f_c'}{fy} = 0.025 \quad \text{Checked}$$

Spacing requirements:

$$S = \frac{100 - 25 * 2 - 2 * 12}{2 - 1} = 26\ mm \qquad > db \quad > 12 \quad Checked.$$

Effective depth of top (W_{tn}) and bottom (W_{bn}) tie equals:

$$W_{tn} = W_{bn} = c + c' + Steel\ diameter = 40 + 40 + 12 = 92\ mm$$

External loading bearing plate width (L_{Ep}) = The internal one (L_{Ip}) = 100 mm.

The effective width of the strut can be estimated from the following equations. It's clear to noting that it depended on bearing plate's width, depth of ties, and angle degree.

$$\theta = tan^{-1}\left[\frac{h - c - c'}{a}\right] = 21 < 25 \quad Checked$$

$$W_{ES_t} = 0.5 LIP\ sin\theta + Wtn \cos\theta = 104$$

$$W_{ES_b} = LEP \sin\theta + Wbn \cos\theta = 122$$

$$W_{1S_t} = 0.5 LLP\ sin\theta + Wtn\ cos\theta = 104$$

$$W_{1S_b} = 0.5\ LIP \sin\theta + Wbn \cos\theta = 104$$

The failure load of beam can be determined by evaluating the average of lower and upper strut width:

$$W_{ES} = \frac{W_{ES_t} + W_{ES_b}}{2} = 113$$

$$W_{1S} = \frac{W_{1S_t} + W_{1S_b}}{2} = 104$$

Assuming $f_c' = 40\ Mpa\ , and\ v\ from\ the\ table.2.$

Table C.1. ACI 318-19 requirements for Concrete effectiveness factor

Codes name	Effectiveness factor for struts (υ)		
ACI 318-19	υ=0.85βs (State of Bottle-shaped only)	Reinforcement satisfy the clues ACI 318-19	βs =0.75
		Reinforcement does not satisfy ACI 318-19	βs =0.60

$v = 0.85 * 0.6 = 0.51$

The nodes collect struts and ties. The CDB shear capacity represented by both internal and external reactions (VE & VI) and it can be determined as the following:

$F_E = \upsilon\ f_c'\ b\ W_{Es}$ =248.8 kN

$V_E = F_E \sin\theta = 94$ kN

$F_1 = \upsilon\ f_c'\ b\ W_{Is} = 248.8$kN

$V_I = F_I \sin\theta = 94$ kN

$P_t = 2(V_1 + V_E)$ =377.2 kN.

Checking bending failure:

Moment at mid span=$0.156 * p * clear\ span$ = 0.156* 319*0.6= 35.3 kN.m

$$a = \frac{A_s\ f_y}{0.85\ f_c'\ b} = \frac{2 * \frac{3.14}{4} * 12^2 * 432}{0.85 * 43.2 * 100} = 26.6\ mm$$

$$Mn = A_s\, f_y \left(d - \frac{a}{2}\right) * 10^{-6} = 14.3\ kN.m$$

The normal strength of Tie $F_{nt} = A_{st}\, f_y = 2 * \frac{3.14}{4} * 8^2 * 350 = 35168\ kN$

Appendix D: Strain gage tool

STRAIN GAUGE TEST DATA

GAUGE TYPE	: PFL-30-11	TESTED ON	: SS 400
LOT NO.	: A802611	COEFFICIENT OF THERMAL EXPANSION	: 11.8 $\times 10^{-6}$/°C
GAUGE FACTOR	: 2.09 ±1%	TEMPERATURE COEFFICIENT OF G.F.	: +0.15±0.05 %/10°C
ADHESIVE	: P-2	DATA NO.	: DB0014

THERMAL OUTPUT (ε app : APPARENT STRAIN)

$\varepsilon app = -1.65 \times 10^{1} + 2.09 \times T^{1} - 7.56 \times 10^{-2} \times T^{2} + 6.64 \times 10^{-4} \times T^{3} - 2.43 \times 10^{-6} \times T^{4}$ (μm/m)

TOLERANCE : ±0.85 [(μm/m)/°C], T : TEMPERATURE(°C)

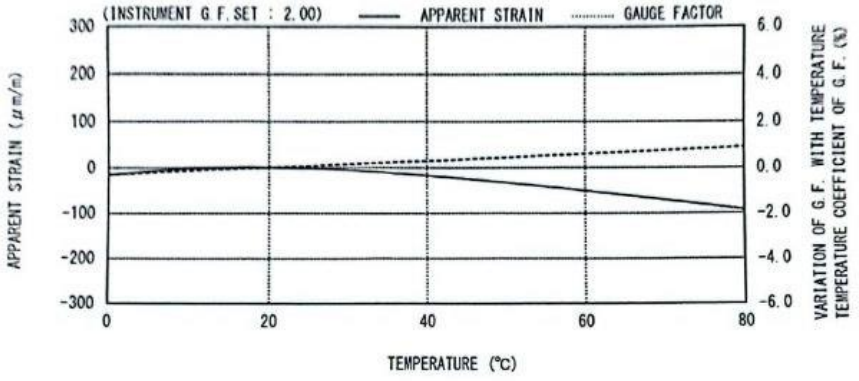

ひずみゲージ取扱いの注意事項

・上記の特性データは、リード線の取付けによる影響を含んでおりません。裏面記載のリード線の測定値への影響に従って補正してください。
・ひずみゲージの使用温度は、接着剤の耐熱温度などにより変わります。
・絶縁抵抗などの点検は、印加電圧を50V以下にしてください。
・ゲージリードに無理な力を加えないでください。
・ひずみゲージの裏面に接着剤を塗布して接着してください。
・ひずみゲージの裏面は脱脂洗浄してありますので、汚さないように取扱いしてください。
・ゲージの包装を開封後は、乾燥した場所で保管してください。
・ご使用に際して、ご不明な点などがございましたら、当社までお問い合わせください。

CAUTIONS ON HANDLING STRAIN GAUGES

- The above characteristic data do not include influence due to lead wires. Correct the data in accordance with the influence of lead wires on measured values described overleaf.
- The service temperature of strain gauge depends on the operating temperature of adhesive, etc.
- Check of insulation resistance, etc. should be made at a voltage of less than 50V.
- Do not apply an excessive force to the gauge leads.
- Apply an adhesive to the back of a strain gauge and stick the gauge to a specimen.
- As the back of strain gauge has been degreased and washed, do not contaminate it.
- After unpacking, store strain gauges in a dry place.
- If you have any questions, please feel free to contact us or your local agent.

株式会社東京測器研究所
〒140-8560 東京都品川区南大井6-8-2
TEL 03-3763-5611
URL http://www.tml.jp

Tokyo Measuring Instruments Laboratory Co.,Ltd.
8-2, Minami-Ohi 6-Chome, Shinagawa- Ku,
Tokyo 140-8560, JAPAN
URL http://www.tml.jp/e

Tokyo Measuring Instruments Lab.

MADE IN JAPAN
3rd ed. Oct. 2018

HANDLING METHOD OF STRAIN GAUGES

Basic Bonding Procedures

1. **Select adhesive**
   Select an adhesive most suitable for test conditions.
2. **Surface treatment**
   Remove grease, rust, paint, etc. from the bonding surface of a specimen, lightly polish with an abrasive paper of #120 ~ 180 (#240 ~ 320 for aluminium), wipe with acetone, etc. and mark gauge installation position.
3. **Gauge installation**
   Refer to the operation manual of adhesive.
4. **Adhesive curing**
   Refer to the operation manual of adhesive.
5. **Gauge installation check**
   Check gauge resistance and insulation resistance.
6. **Lead wire attachment**
   Solder lead wires to the strain gauges through connecting terminals.
   - If necessary, apply waterproof coating.

Influence of Lead Wires on Measured Values

● **Influence of temperature variation of lead wires (3-wire system is independent of temperature.)**

$$\varepsilon l = \frac{r \cdot L \cdot \alpha \cdot \Delta T}{K\,(R + r \cdot L)} \qquad \text{<Equation1>}$$

where
- εl = thermal output of lead wires
- r = total resistance per meter of lead wires (Ω/m)
- L = length of lead wires (m)
- α = temperature coefficient of resistance of lead wires (copper wire = 3.9×10^{-3}/℃)
- ΔT = temperature variation
- K = gauge factor
- R = gauge resistance

● **Gauge Factor Correction due to Lead Wire Attachment**

- **In case of 2-wire system**

$$Ko = \frac{R}{R + r \cdot L} \cdot K \qquad \text{<Equation2>}$$

- **In case of 3-wire system**

$$Ko = \frac{R}{R + \frac{r \cdot L}{2}} \cdot K \qquad \text{<Equation3>}$$

where Ko = corrected gauge factor

リード線1m当りの往復抵抗値
Total Resistance per Meter of Lead Wires

構成(心数/線径) Lead wires(Core/Diameter)	ポリイミド線 Polyimide		7/0.12	7/0.16	7/0.18	10/0.12	12/0.18	20/0.18
リード線の直径または断面積 Diameter or cross sectional area of lead wires	φ0.14mm	φ0.18mm	0.08mm²	0.24mm²	0.2mm²	0.11mm²	0.3mm²	0.5mm²
1m当りの往復抵抗 Total resistance per meter	2.5Ω/m	1.5Ω/m	0.44Ω/m	0.24Ω/m	0.2Ω/m	0.32Ω/m	0.12Ω/m	0.07Ω/m

Tokyo Measuring Instruments Lab.

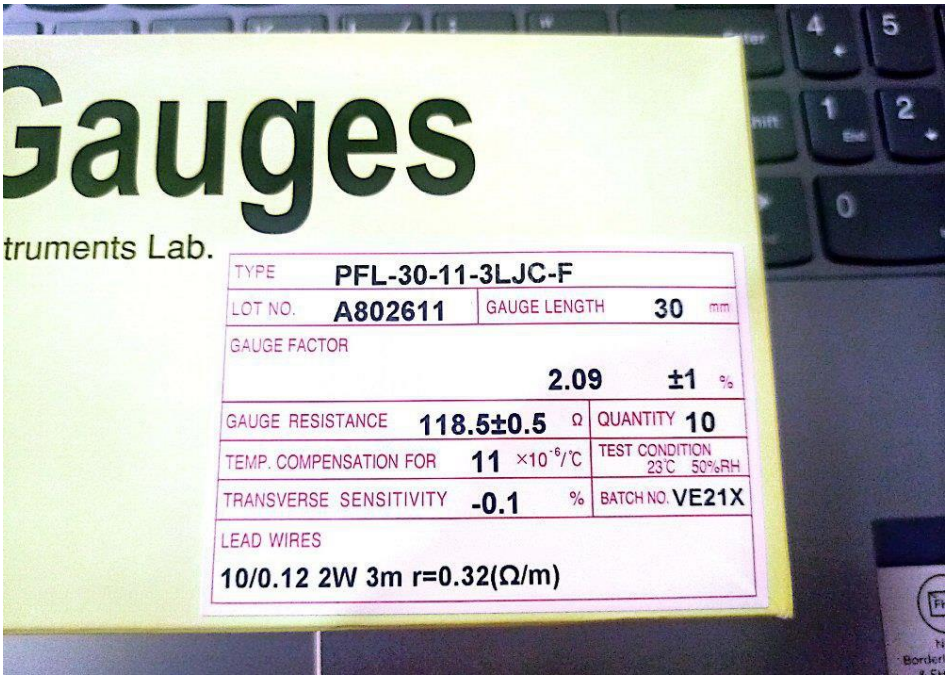

APPENDIX E: STM BEAMS SOLUTIONS

The reference beam was selected as a sample to mention the theoretical solution for the CDBs by STM. The beam details are:

b= 100 mm

h= 200 mm

Clear span =600 mm

C= 40 mm

c' = 40 mm

Diameter of steel =12 mm

Angle = 22 ° < 25° Checked

f'c =43.3 MPa

Wtn=Wbn=$C + C' + \emptyset = 92$

Wes_t = $W1s_t$ = $W1s_b$= $0.5\ LIP \sin\theta + Wbn \cos\theta = 104.25$

Wes_b = $LEP \sin\theta + Wbn \cos\theta = 123.2$

Wes = $\frac{W_{ES_t} + W_{ES_b}}{2} = 113.72$

Interior and exterior struts loading capacities

Bs = 0.65

FE= $\upsilon\ f_c'\ b\ W_{Es}$= 249.41

VE=$F_E \sin\theta$ = 94.51 kN

F1= $\upsilon\ f_c'\ b\ W_{Is} = 249.41$ kN

VI=$F_I \sin\theta$ = 94.51 kN

pt=$2(V_1 + V_E)$ = 378.06 kN

APPENDIX F: DETAILS OF FINITE-ELEMENT METHOD

F.1. Introduction

Finite-element method (FEM) is a famous powerful tool used for obtaining an approximate solution to a wide range of engineering problems, which is one of them is the structural analysis problems. This method works on replacing the continuum by multiple finite elements jointed by a finite number of nodal points.

All the phenomena are nonlinear in solid mechanics. Whilst, for many applications, it is practical and suitable way to use the linear formulation for some problems for obtaining the engineering solutions. On the other hand, a lot of problems absolutely need necessarily a nonlinear analysis when most reality results are to be found just like the post yielding case and the large deflection behavior of the structures analysis. The finite element programs can be used to solve problems involving linear material behaving and nonlinear behavior.

It has been believed that the use of full three-dimensional analysis provides better representation of material nonlinearity and cracking[190].

In the present study, the ANSYS V.15 software program has been used to simulate the problem. Three-dimensional isoperimetric finite element model was used to analyze concrete beams . The finite element formulation, material idealization and the material model were used in the analysis are discussed.

F.2. Constitutive Relationships of Materials

Any loaded structure responses and reacts with loading in accordance to type material built with. In a more accurate word, its response to load in keeping with material stress-strain relationship. In this research, three composite material

(concrete, rebars, bearing plate) will take shape and work as a reclusive system. The stiffness matrix of the total system will be built by exploiting the material relationships and properties of each material. The followings are the details of relationships behavior of each material [191].

F.3. Concrete

It is the most widely construction material. As all known, this material consists of sand and gravel amassed by cement but surly in the help of water. After chemical reaction stopped, capillary pores will be formed due to shrinkage. Also, the additional water evaporating from the mix, by moving from core member to the surface of it bring about capillary paths. Also, a micro cracks will be form especially between gravel particles and mortar. These (capillary pores, capillary paths, micro cracks) touch on the concrete's mechanical behavior because it can be stretch and linkup during loading. It is insufferable to get rid of these weakness points in concrete because it's formed by thermal expansion, segregation, and shrinkage of mortar, and that cannot be avoided. So, these factors should be taken in consideration during studying concrete's behavior [179], [191]. All there micro cracks did not found in ANSYS simulation model, so that the value of failure load and maximum deflection in numerical analysis, becomes larger than the experimental work.

Concrete at the first stages of loading acts linearly, but in the procedure of the loading stages behaves nonlinearly. In more exactly conformity, the uniaxial stress- strain curve behaves linearly from (0 to 30%) of uniaxial compressive strength ($f'c$). overhead of (30) %, the nonlinearity stage starts. The increment in the non-linearity evidences in the level of stress ranging from (0.75 $f'c$) to (0.9 $f'c$). From this limit (0.9 $f'c$) onward, a sharp convexity curvature occurs till reaches the peak stress ($f'c$) [192].

Up to stress stage of about (0.8 $f'c$), the magnitude of Poisson's ratio noticed to be constant approximately and ranging from (0.15 to 0.22). after this limit (0.8 $f'c$), the amount of Poisson's ratio starts in suddenly increment [193].

F.3.1. Stress–Strain Relationship of Concrete Comparison

Usually, the concrete assumed to be a homogenous and isotropic material. The adopted stress- strain relation is based on Desayi and Krishnan work [194].

The compression uniaxial concrete stress strain relationship has been obtained by the use of the following equations in order to compute the multi-linear isotropic stress- strain curve. [42]

$$f'c = \varepsilon E_c \quad for \quad 0 \leq \varepsilon \leq \varepsilon_1 \qquad \text{Eq.F.1}$$

$$fc = \frac{\varepsilon E_c}{1+\left(\frac{\varepsilon}{\varepsilon_\circ}\right)^2} \quad for \quad \varepsilon_1 \leq \varepsilon \leq \varepsilon_\circ \qquad \text{Eq.F.2}$$

$$fc = f'c \quad for \quad \varepsilon_\circ \leq \varepsilon \leq \varepsilon_{cu} \qquad \text{Eq.F.3}$$

$$\varepsilon_1 = \frac{0.3\, f'c}{E_c} \qquad \text{Eq.F.4}$$

$$\varepsilon_\circ = \frac{2\, f'c}{E_c} \qquad \text{Eq.F.5}$$

Where:

fc : stress at any strain, ε (MPa)

Ec : the elastic modulus of concrete (MPa).

ε : stain at stress fc

$\varepsilon_\circ$: strain at ultimate compressive strength $f'c$

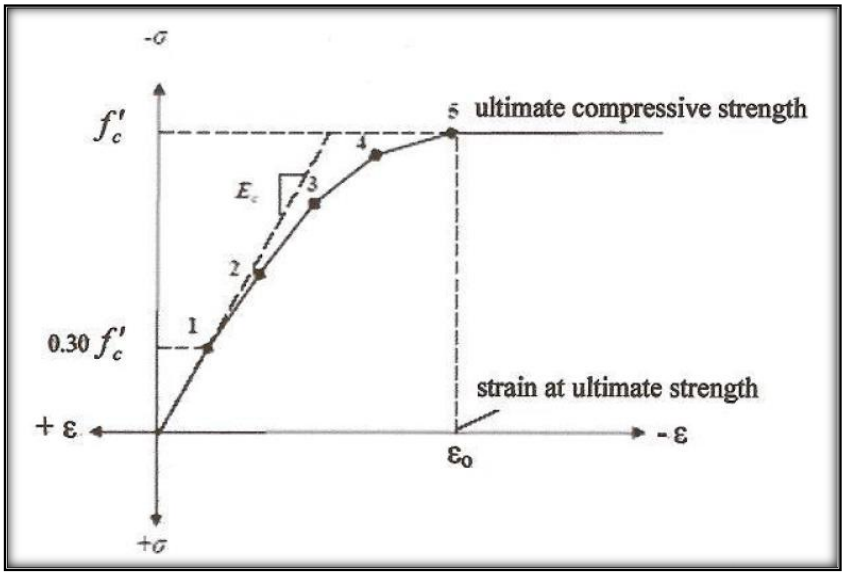

Figure F. 1. Concrete uniaxial stress- strain curve [195]

As shown in Figure F. 1, the point number (1) represented the stress at (0.3 f'c) and the curve is linear till this point. The last point is defined as (f'c). The concrete modulus of elasticity (Ec) is defined as "the slope of the line drawn from a zero of stress to a compressive strength of (0.3 f'c)". The equation is discussed in ACI committee 318M-2014. This equation has been used in this research to identify the amount of this parameter [194]

$E_c = 4700\sqrt{f'c}$ Eq.F.6

F.3.2. Concrete in Tension

The uniaxial tensile stress- strain curve shape does not differ from the uniaxial compressive stress-strain curve. The limits of elasticity in tension minimizes the uniaxial tensile strength (ft) by about (40%) of the total uniaxial tensile strength. The ratio between uniaxial tensile and compressive strength may change a lot but usually range from 0.05 to 0.10. The modulus of elasticity under uniaxial tension is somewhat higher and the Poisson's ratio somewhat lower is than in uniaxial compression [195].

According to above information, the concrete stress-strain curve in tension is usually drawn using the same modulus of elasticity, and using (ft) instead of ($f'c$).

In this study, the amount of (ft) is taken as:

ft = 0.1 * ($f'c$) Eq.F.7

F.4. Finite Element Idealization

The modeling denoted choosing a suitable element type, real material's constant, an accurate inserting of the material properties, an exact representation of loadings and supports boundary conditions as well as choosing sufficient number of the finite elements and selecting a proper integration technique.

F.4.1. Concrete Idealization

Concrete is usually simulated by a hexahedral brick element (SOLID65). It is an eight-node isoperimetric brick element. Each node in this element contains three translation degrees of freedom u, v and w respectively in the x, y and z coordinates. As shown in Figure F. 2.

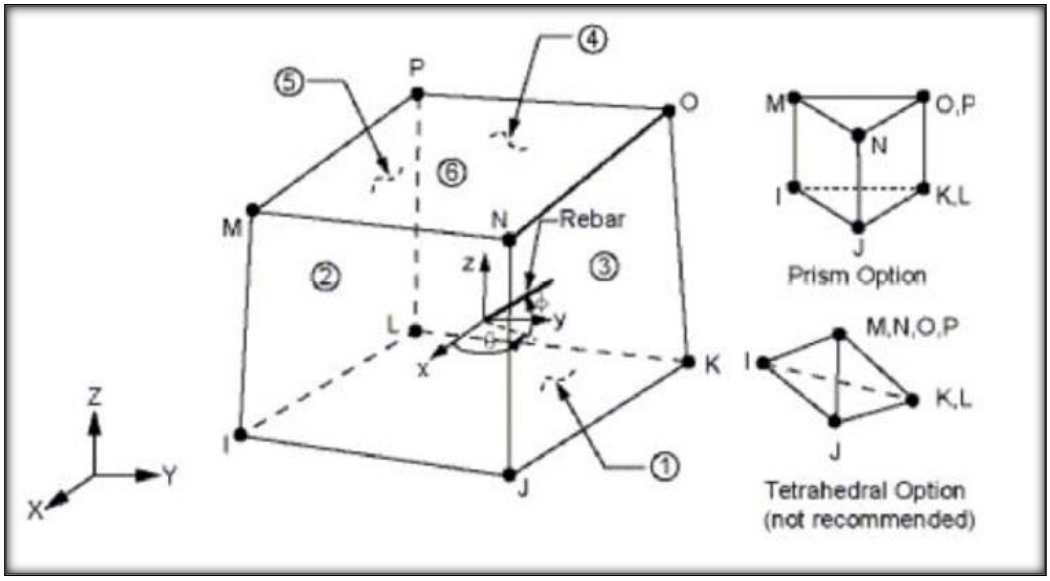

Figure F. 2. Geometry of SOLID 65 element[179]

The most important property of this element is that how it deals with the nonlinearity of the material. The most important properties of concrete are:

1. Capability of cracking in 3-direction orthogonally
2. Crushing and creep.
3. Plastic deformation.

This element (SOLID65) is capable to simulate these properties accuracy, so that it is used in this research for simulating concrete.

F.4.2. Reinforcement Idealization

Steel wires, in this research, are represented in two nodes (as shown in Figure F. 3) element which is (LINK180) and included within the properties of (SOLID65) element.

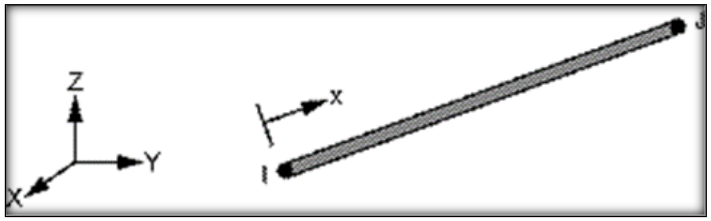

Figure F. 3. LINK 180 element [179]

Link180 is a wedge or truss element, "uniaxial tension- compression element of three degrees of freedom at each node". Creep, plasticity, stress stiffening, swelling, and large deformation capacity are included.

There are three different ways to represent the reinforcement in concrete members, they were: distributed representation, embedded representation, and distributed representation (Figure F. 4). In discrete representation, the steel bars assumed to be spread over the element of concrete. In the embedded representation, the steel bars are considered as members built within the concrete element so that the amount of displacements are still consistent between the two materials. The third representation, the discrete representation, one-dimensional

steel bar contacted with concrete by using the same nodes of concrete mesh, the third representation has been used in this study. (LINK 180) is defined by material properties, cross sectional area and initial strain value [179].

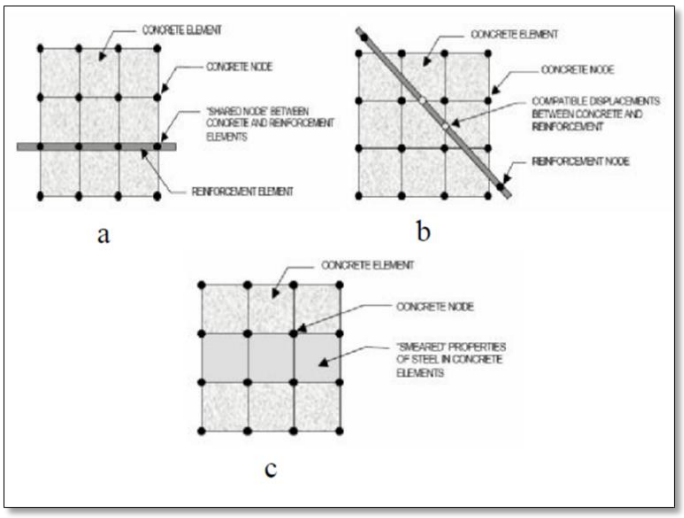

Figure F. 4. Steel reinforcement method of idealization [179]

In the finite element programing, the steel bars simulated to behaves by a bilinear behavior, which is represented in bilinear stress-strain curve. The initial value (which represents the initial slope) is taken as the steel modulus of elasticity. The second slope is represented by the point of yield stress. The uniaxial stress- strain curve for the steel bar is shown in Figure F. 5 typically [191].

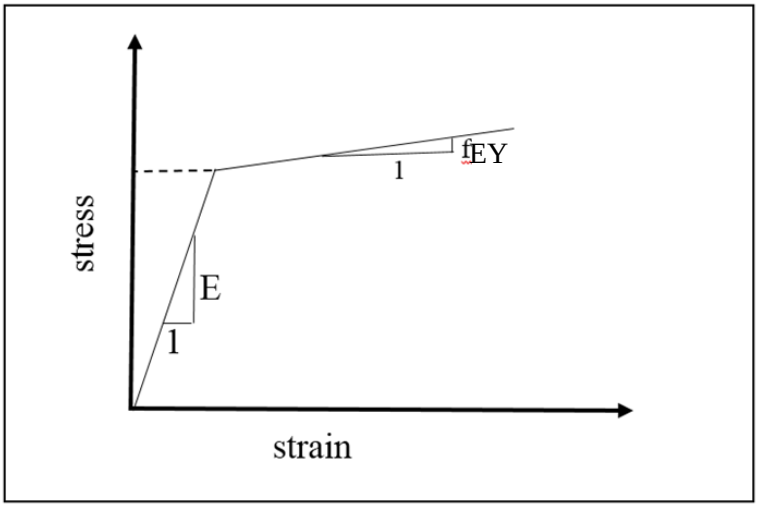

Figure F. 5. Stress strain curve of steel wire

F.5. Finite Element Modelling and Materials Properties

For simulating the experimental models in the finite element program, element types, real constant of each element, material properties, and the models' geometry should be defined.

F.5.1. Element Type

In this study, five different element types were used. They were for concrete, steel wires, and bearing plate. Each material has an element type. They are: SOLID65, LINK180 and SOLID185. Concrete element was defined as SOLID65, it is also having eight nodes with three degrees of freedom at each translation in nodal x, y, and z, but it differs from SOLID185 by its capability of cracking in three orthogonal direction, plastic deformation, and crushing. It is defined as an isotropic material. LINK180 has been used to represent the main reinforced steel wire mesh. The volume ratio, which is meant the ratio between the wire volume to the total element volume, is taken equal to zero (for plain concrete).

Steel plate is also represented as SOLID185 but defined as linear elastic isotropic material. Supplementary data of concrete material are described in Table C.1, like coefficient of shear transfer, tensile and compressive strength.

Table F.1. Concrete details

Constant	meaning
1	Uniaxial tensile stress of cracking.
2	Uniaxial tensile stress of crashing.
3	Biaxial crashing stress.
4	Shear transfer coefficients(open crack).
5	Shear transfer coefficients(closed crack).
6	crack factor of tension.

Exemplary coefficient of shear transfer is ambit from 0.0 to 1.0. The smallest value represents small cracks (i.e. the complete losing in shear transfer is considered) and the largest range represents the rough cracks (i.e. there is no losing in shear transfer). This detailing could be used for closed and shear cracks. But, in most, open shear crack coefficient is smaller than the close coefficient.

LINK180 is a one-dimensional bar element. It is an element with two nodes and three degrees of freedom for each node, translations in the nodal x, y, and z directions. The element eligible for plastic deformation, it can be defined by inserting its requirements which are: two nodes, the area cross- section, and material properties [179].

F.5.2. Real Constant

In such modelling cases, and such material used, two sets of real constants have to be defined. The first set is set 1 which is associated with SOLID65 element. For reinforced concrete beams, the amount of volume ratio has been determined.

Set2 represented steel wire requirements, area of wires defined in this set. Table F.2 shows the details of real constant values.

Table F.2. Real constant sets

Set 1	SOLID 65 element	Volume ratio	0.014
Set2	LINK 180 element	Steel section area	113 mm^2

F.5.3. Material Properties

The ANSYS program works on formulate a stiffness matrix for the structure form its inputted properties information, where elastic modulus of material, moment of inertia, Poisson's ratio, etc. All of them form structures' stiffness matrix. But it is efficient to undefined the parameters which has a little or no-effect because the

stiffness matrix of the structure gets bigger and that will increase the speed of rendering.

Material model number 1 points out to concrete material element (SOLID65), where this element defined as linear, isotropic, and multilinear isotropic in the addition to the parameters of concrete itself.

Material model number 2 refers to LINK180 element for reinforced steel wires. A linear isotropic and bilinear isotropic information has been discussed in this material model.

Material model number 3 shows the information of SOLID185 element which is for steel plate details. The plate defined as an elastic- isotropic material with high elastic modulus fit with steel.

F.6. Nonlinear Solution Technics

Material response under loading is one of the major aims of the finite- element analysis for members. The load deflection response of reinforced concrete member consists of linear and nonlinear stages. The first linear response is found at early stages below a limit point. After this point, a nonlinear load deflection response happens. The main sources of material non-linearities are the cracking of concrete, yielding of reinforcement and plastic deformation of concrete and steel reinforcement. In general, for any structural problem, applying the finite element method required passing by a set of algebraic equations as follows [191].

$$[K]\{u\} = \{F\} \qquad \text{Eq.F.8}$$

where:

[K] = system matrix of stiffness.

{u}= nodal displacements vector.

{F}= applied loads vector.

In the linear elastic problems equation above, it can directly to be solved to obtain the unknown displacement vector {u}. In the case of nonlinear system, the stiffness matrix [K] represents the function of the unknown displacements {u} (or their derivatives). The solution of nonlinear problems by the (FE) method is usually have a try by three basic techniques, which are:

F.6.1. Incremental Technique

For this technique, loads are applied on the structure as a series of an equal on unequal load increments and the change in deformation is obtained using a linear analysis. Before appling the next increment step, the values of the material properties corresponding to the previous load are showed. The convergence can be achived easily by insreting a very small load increment. Figure F. 6 explained a scatch for this technique.

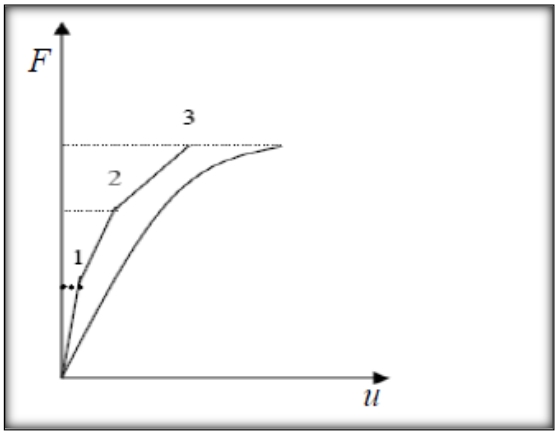

Figure F. 6. Increment technique

F.6.2. Iterative Technique

The total load, in this technique, at the first iteration, is applied in one increment and the out of balance forces are computed and used for the next iteration so as to obtain a gradually improved solution. The iterate solution continues until vanishing the difference between the last two iterative results or becomes within the acceptable tolerance, and then the final converged solution has been obtained. Figure F. 7 showed the progress.

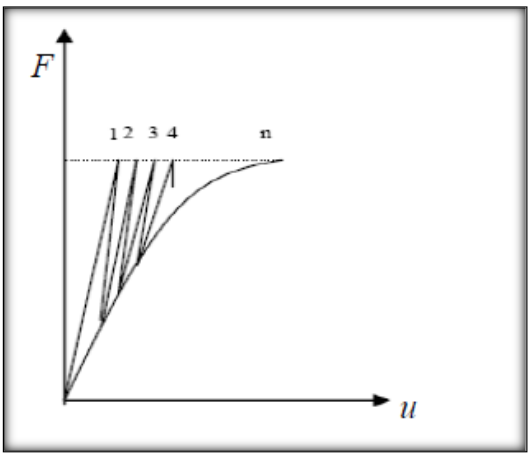

Figure F. 7. Iterative technique

F.6.3. Incremental-Iterative Technique.

This technique utilizes a combination of incremental and iterative techniques, it implies sub-divisions of the external total load into smaller increments. “Within each increment of loading, iterative cycles are performed in order to obtain a converged solution corresponding to the stage of loading under consideration”. This technique has widely been used for nonlinear analyzing reinforced concrete structures. This is due to its ability to trace the history of the structural response and to provide information with regard to cracking of concrete that occurs at different load levels, yielding of reinforcement, crushing of concrete and load-deflection curve. This technique is adopted in the present work.

ANSYS computer program utilizes the "Newton-Raphson" approach for solving the nonlinear problems. By this approach, the load is sub-divided into many series of load increments. The load increments can be applied over several load steps. Figure F. 8 illustrates the use of Newton-Raphson equilibrium iterations for single DOF nonlinear analysis.

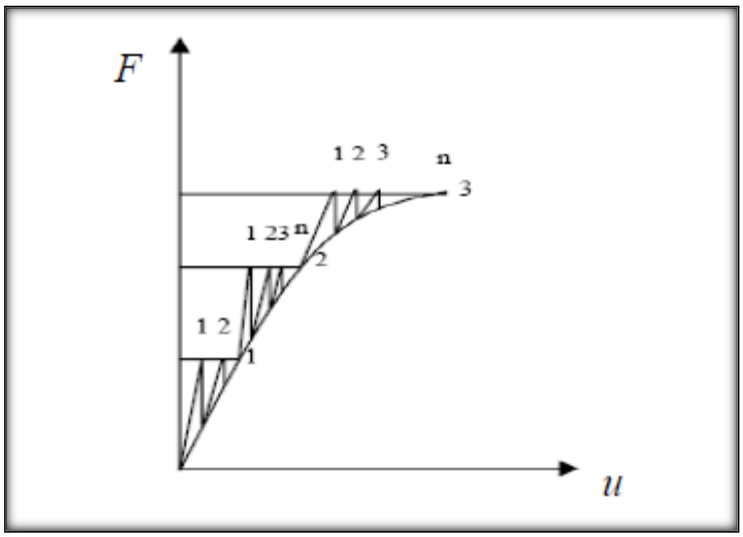

Figure F. 8. Incremental iterative technology

Appendix F References:

[198] E. and G. I. Madenci, *The finite element method and application in civil engineering using ANSYS*. The University of Arizona.

[199] M. A. Attiya, "Behavior of reinforced concrete corbels strengthened with carbon fiber reinforced polymer strips," university of Basrah, Iraq, 2010.

[200] C. L. Wang and Y. Huang, "Refined model for analysis of plates on elastic foundations," *Yantu Lixue/Rock Soil Mech.*, vol. 29, no. 1, pp. 52–57, 2008, doi: 10.1061/(asce)0733-9399(1991)117:12(2830).

[201] W. . Chen, *Plasticity in Reinforced Concrete*. McGraw-Hill Book Company, 1985.

[202] S. Desayi, P., and Krishnan, "Equation for the Stress-Strain Curve of Concrete," *J. Am. Concr. Inst.*, vol. 61, pp. 345–350, 1964.

[203] E. P. Willam, K. J. and Warnke, "Constitutive Model for the Triaxial Behavior of Concrete," *Proceedings, Int. Assoc. Bridg. Struct. Eng.*, vol. 19, 1975.

APPENDIX G: THEORETICAL HARMONIC LOAD SOLUTIONS

G.1. Timoshenko beam theory solution

$$q_m = \frac{2}{L}\int_{0.33L}^{0.6L} P * \sin\frac{2m\pi x}{L}\, dx = -0.213P$$

$$q_x = -0.213\, P \sin\frac{2m\pi x}{L}$$

$$\frac{\partial^4 w}{\partial x^4} = \frac{q}{EI} - \frac{1}{c^2 GA} * \frac{\partial^2 q}{\partial x^2}$$

$$w(x) = \sum w_m \sin\frac{2m\pi x}{L}$$

$$w_m * \sin\frac{2m\pi x}{L} * (\frac{2m\pi}{L})^4$$

$$= -0.213\, P\, \sin\frac{2m\pi x}{L} - \frac{1}{c^2 GA} * (-0.213P\, \sin\frac{2m\pi x}{L} ** (\frac{2m\pi}{L})^2$$

$$w(x) = 0.097524 \sin w_m t$$

G.2. Solving using dynamic equations

$$m\ddot{y} + ky + c\dot{y} = F(t)$$

$$2 * 66\, \ddot{y} + 5570398\, y = 100 \sin w_n t$$

$$\ddot{y} + 42200y = 91 \sin w_n t$$

$$y = A \sin w_n t + B \cos w_n t$$

$$\ddot{y} = (-A \sin w_n t - B \cos w_n t)\, w_n^2$$

By solving the last two equations after substituting them into the general equation, gets the value of A, where:

$$A = \frac{91 \sin w_n t}{(42200 - w_n^2)}$$

الخلاصة

تحرت الدراسة سلوك العتبات الخرسانية العميقة المطاطية المستمرة والمعرضة الى احمال ديناميكية نظرا لكثرة تعرض العتبات العميقة المستمرة الى الاحمال الديناميكية في الواقع العملي. تم اضافة المطاط الى الكونكريت كأسلوب من اساليب زيادة مطيليته و تحسين امتصاصه للطاقة وخصوصا ان مخلفات المطاط هي من المواد غير القابلة للتحلل البايلوجي في الطبيعة وبالتالي فإن مخلفاته تسبب زيادة كبيرة في التلوث البيئي.

تم اضافة المطاط باستبدال حجمي من حجم الرمل مرة ومن حجم الحصى مرة اخرى وبثلاثة مقادير وهي 10% و20% و30%. على هذه النسب، تم صب 21 عتبا خرسانيا مسلحا وتم تصنيفه وفق ثلاثة مموعات تبعا لطريقة فحصه. المجموعة الاولى تم فحص العينات فيها فحصا ستاتيكيا اعتياديا وتمت مقارنة النتائج بالنتائج النظرية لطريقة STM. اما المجموعة الثانية وهي عباره عن 11 عتبا فقد تم فحصها بواسطة الحمل الصدمي وبوزنين مختلفين وهما 30kgو 40kg. هذه المجموعة تمت اعادة فحص عيناتها مرة اخرى بواسطة الحمل السكوني الاعتيادي وتتمت مقارنتها بالعينات غير المضروبة. اما المجموعة الاخيرة فهي تتكون من 3 عتبات خرسانية تم فحصها بواسطة الحمل السكوني المتكرر وتمت مقارنة النتائج مع نتائج نظرية اجريت بواسطة برنامج التحليل العددي ANSYS APDL V.15.0 وتمت نمذجة العتب لدراسة الحمل الدوري نظريا. تشمل الدراسة ايضا تحليلا نظريا اخر يتعلق بالحمل التوافقي وتمت مقارنته مع نتائج نظرية لمعادلات مشتقة للعتب المفحوص.

نستنتج من الدراسة ان مقاومة انضغاط الخرسانة لاسطوانات بقياس 200*100ملم تساوي مايعادل 0.86-0.94 من مقاومة انضغاط الاسطوانات الاكبر بقياس 300*150 ملم. وأن العتب الخرساني المسلح المستمر المعرض الى حمل صدمي سيستمر يتصرف وفق طريقة STM . إن اكثر تشقق مؤثر ضهر في العينات المضروبة هو في مواقع الوتد الداخلي وفي منطقة العزم الموجب وكذلك تشققات نتيجة عن احديداب الفضاء غير المضروب. يمكن ايضا ان نستنتج ان اعادة فحص العينات المضروبة بفحص ستاتيكي ان التشققات سوف تندمج وتتصل وتكبر تحت تأثير الحمل السكوني وان العتبين المضروبين ب 30kgو 40kg سيفقدان حوالي 35.5%و 46.7% من قابليتهما بسبب الحمل الصدمي.

كما وجد ان العتب العميق المستمر اذا سلطت عليه احمال متكررة فإنه يفقد مايقارب 14% و 8% و 9% للعينة اللامطاطية وللاستبدال المطاطي بالحصى والرمل بالتتابع. كما وتم التوصل الى ان التحليل العددي اعطى نتائج مقاربة للواقع العملي وفق النمذجة المدخلة اليه.

جمهورية العراق
وزارة التعليم العالي والبحث العلمي
جامعة بابل
كلية الهندسة
قسم الهندسة المدنية

الإستجابة الديناميكية للأعتاب العميقة المستمرة الخرسانية المطاطية المسلحة المستدامة

اطروحة

مقدمة الى جامعة بابل / كلية الهندسة

كجزء من متطلبات الحصول على درجة الدكتوراه في اختصاص الهندسة المدنية/الانشاءات

بواسطة

عُلا مازن مكي علي

(بكلوريوس في الهندسة المدنية 2015)

(ماجستير في الهندسة المدنية 2019)

بإشراف :

أ.د. حيدر محمد كاظم المطيري